

# Guide to Storm Surge Forecasting



**World  
Meteorological  
Organization**

WMO-No. 1076

**Weather • Climate • Water**



# Guide to Storm Surge Forecasting

WMO-No. 1076



**World  
Meteorological  
Organization**  
Weather • Climate • Water

2011 edition

WMO-No. 1076

© World Meteorological Organization, 2011

The right of publication in print, electronic and any other form and in any language is reserved by WMO. Short extracts from WMO publications may be reproduced without authorization, provided that the complete source is clearly indicated. Editorial correspondence and requests to publish, reproduce or translate this publication in part or in whole should be addressed to:

Chairperson, Publications Board  
World Meteorological Organization (WMO)  
7 bis, avenue de la Paix  
P.O. Box No. 2300  
CH-1211 Geneva 2, Switzerland

Tel.: +41 (0) 22 730 84 03  
Fax: +41 (0) 22 730 80 40  
E-mail: [publications@wmo.int](mailto:publications@wmo.int)

ISBN 978-92-63-11076-3

#### NOTE

The designations employed in WMO publications and the presentation of material in this publication do not imply the expression of any opinion whatsoever on the part of the Secretariat of WMO concerning the legal status of any country, territory, city or area, or of its authorities, or concerning the delimitation of its frontiers or boundaries.

Opinions expressed in WMO publications are those of the authors and do not necessarily reflect those of WMO. The mention of specific companies or products does not imply that they are endorsed or recommended by WMO in preference to others of a similar nature which are not mentioned or advertised.

# CONTENTS

Page

|   |            |
|---|------------|
| <b>FOREWORD .....</b>   | <b>vii</b> |
| <b>ACKNOWLEDGEMENTS.....</b>  | <b>ix</b>  |
| <b>CHAPTER 1. INTRODUCTION AND GENERAL CONSIDERATIONS .....</b>   | <b>1-1</b> |
| 1.1 Oceanographical aspects of storm surges .....   | 1-1        |
| 1.2 Meteorological aspects of storm surges .....  | 1-3        |
| 1.3 Methods of storm surge prediction – an overview .....   | 1-3        |
| 1.4 Empirical methods for surge prediction .....  | 1-4        |
| 1.5 Statistical methods .....   | 1-5        |
| 1.6 Storm surge prediction through artificial neural networks.....  | 1-6        |
| 1.6.1 Artificial neural networks.....   | 1-6        |
| 1.6.2 Optimal ANN modelling.....  | 1-7        |
| 1.6.3 Regional real-time storm surge prediction system for three stations in the<br>Republic of Korea ..... | 1-8        |
| 1.7 Numerical methods.....  | 1-9        |
| <b>CHAPTER 2. STORM SURGE PHYSICS.....</b>  | <b>2-1</b> |
| 2.1 Meteorological effects .....  | 2-1        |
| 2.2 Oceanographical effects .....   | 2-3        |
| 2.3 Hydrographical effects.....   | 2-3        |
| 2.4 Seiches.....  | 2-4        |
| 2.5 Tide–surge interaction .....  | 2-5        |
| 2.6 Surge–river interaction .....   | 2-6        |
| 2.7 Interaction between surge, wind waves and wave set-up .....   | 2-6        |
| 2.8 Influence of sea ice on storm surges .....  | 2-6        |
| 2.9 Bottom friction.....  | 2-8        |
| <b>CHAPTER 3. BASIC EQUATIONS AND SOLUTIONS .....</b>   | <b>3-1</b> |
| 3.1 Formulation of the storm surge equations .....  | 3-1        |
| 3.2 Finite differencing of the time derivative.....   | 3-2        |
| 3.3 Computational stability and CFL criterion.....  | 3-3        |
| 3.4 Staggered and non-staggered grid schemes.....   | 3-3        |
| 3.5 Treatment of the non-linear advective terms.....  | 3-4        |
| 3.6 Treatment of open boundaries .....  | 3-5        |
| 3.7 Treatment of complex coastal boundaries .....   | 3-5        |
| 3.8 Moving-boundary models, inclusion of tidal flats and coastal inundation .....                           | 3-6        |
| 3.9 Unstructured grids (finite element and finite volume models).....                                       | 3-7        |
| 3.9.1 Finite element methods .....  | 3-7        |
| 3.9.2 Finite volume methods .....   | 3-8        |
| 3.10 Mesoscale forcing.....   | 3-8        |
| 3.11 Remote forcing .....   | 3-9        |
| <b>CHAPTER 4. INPUT AND OUTPUT PARAMETERS .....</b>   | <b>4-1</b> |
| 4.1 Introduction .....  | 4-1        |
| 4.2 Model set-up.....   | 4-1        |
| 4.2.1 Bathymetry and geometry.....  | 4-1        |
| 4.2.2 Tidal boundaries .....  | 4-1        |
| 4.2.3 Data for tuning and calibration.....  | 4-2        |

|   | <i>Page</i>   |
|---|---|
| 4.3   | Using the model..... 4-3  |
| 4.3.1   | Meteorological input ..... 4-3  |
| 4.3.1.1   | Meteorological input for a tropical cyclone ..... 4-3   |
| 4.3.1.2   | Interpolation issues for numerical models..... 4-4  |
| 4.3.2   | Hydrological input..... 4-4   |
| 4.4   | Validation and verification ..... 4-5   |
| 4.5   | Output parameters..... 4-5  |
| 4.5.1   | Time series..... 4-5  |
| 4.5.2   | Fields ..... 4-6  |
| 4.5.3   | Output from other models ..... 4-6  |
| 4.5.4   | Example of a forecast result ..... 4-6  |
| <br>  |   |
| <b>CHAPTER 5. STORM SURGE PREDICTION MODELS..... 5-1</b>      |   |
| 5.1   | Operational two-dimensional storm surge prediction models ..... 5-1   |
|   | The rationale of the forecasting system ..... 5-1   |
| 5.2   | Setting the initial state for the forecast ..... 5-1  |
| 5.3   | Nesting higher resolution storm surge models ..... 5-2  |
| 5.4   | Operational products and requirements ..... 5-2   |
| 5.5   | Data assimilation ..... 5-3   |
| 5.5.1   | Ensemble forecasts ..... 5-3  |
| 5.5.2   | The Cressman scheme ..... 5-3   |
| 5.5.3   | Statistical (optimal) assimilation ..... 5-4  |
| 5.5.4   | Kalman filter ..... 5-4   |
| 5.5.5   | Three- and four-dimensional variational analysis ..... 5-5  |
| 5.5.6   | The United Kingdom system..... 5-5  |
| 5.5.7   | The system in the Netherlands..... 5-5  |
| <br>  |   |
| <b>CHAPTER 6. OPERATIONAL FORECAST VERIFICATION ..... 6-1</b> |   |
| 6.1   | Introduction ..... 6-1  |
| 6.2   | Routine verification of the United Kingdom operational storm surge model ..... 6-1  |
| 6.3   | Routine verification of the Danish storm surge model..... 6-2   |
| 6.4   | Routine verification of the German BSH storm surge model..... 6-4   |
| 6.5   | Routine verification of the Netherlands DCSM98 storm surge model..... 6-5   |
| 6.6   | Total forecast verification – an example from the United Kingdom Coastal Monitoring and Forecasting (UKCMF) service ..... 6-5 |
| <br>  |   |
| <b>CHAPTER 7. REGIONAL FORECAST SCENARIOS ..... 7-1</b>       |   |
| 7.1   | Storm surges generated by tropical cyclones..... 7-1  |
| 7.1.1   | North-western Pacific ..... 7-1   |
| 7.1.2   | South-western Pacific..... 7-4  |
| 7.1.3   | The Gulf of Mexico and United States Caribbean coastline ..... 7-6  |
| 7.1.4   | French Caribbean ..... 7-10   |
| 7.1.5   | Western and Northern Australia ..... 7-13   |
| 7.1.6   | Bay of Bengal and Arabian Sea..... 7-14   |
| 7.2   | Storm surges generated by extra-tropical cyclones (mid-latitude depressions) ..... 7-19                                       |
| 7.2.1   | North Sea (a typical mid-latitude shelf sea)..... 7-19  |
| 7.2.2   | Argentina – an example of smaller-scale estuarine forecasting..... 7-21   |
| 7.2.3   | Baltic Sea (enclosed sea with low tidal range) ..... 7-24   |
| 7.3   | Storm surges in the Arctic seas and seas covered by ice..... 7-25   |
| <br>  |   |
| <b>CHAPTER 8. INUNDATION MAPPING ..... 8-1</b>                |   |
| 8.1   | Developments in the United States..... 8-1  |

|  |  |                 |
|--|--|-----------------|
| 8.2  | A case study: the Indian coast at Andhra Pradesh .....         | 8-3             |
| 8.2.1  | Maps of physical vulnerability for the coastal districts ..... | 8-4             |
| 8.2.2  | Social vulnerability.....                                      | 8-5             |
| <b>CHAPTER 9. STORM DISASTER PREPAREDNESS: FINDINGS OF THE JCOMM ETWS SURVEY OF NATIONAL AGENCIES.....</b> |  | <b>9-1</b>      |
| 9.1  | Introduction.....  | 9-1             |
| 9.2  | Basic information on storm surges.....                         | 9-1             |
| 9.2.1  | Observational data .....                                       | 9-1             |
| 9.2.2  | Hindcast databases .....                                       | 9-2             |
| 9.3  | Operational and pre-operational numerical models.....          | 9-2             |
| 9.3.1  | Model characteristics.....                                     | 9-2             |
| 9.3.2  | External forcing .....   | 9-2             |
| 9.3.3  | Products and dissemination .....                               | 9-2             |
| 9.3.4  | Verification procedures .....                                  | 9-2             |
| <b>APPENDIX I. REFERENCES.....</b>   |  | <b>App.I-1</b>  |
| <b>APPENDIX II. ACRONYMS.....</b>  |  | <b>App.II-1</b> |





## FOREWORD

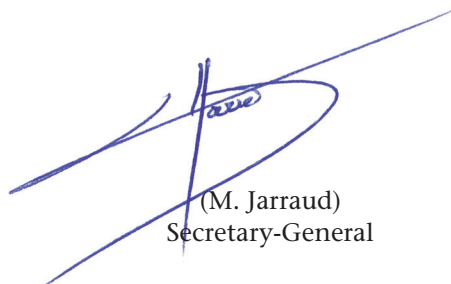
For many years, the National Meteorological and Hydrological Services (NMHSs) of an increasing number of maritime countries have actively engaged in the provision of storm surge forecast services for a wide range of maritime and coastal activities; in particular for coastal defense, shipping, fisheries, offshore mining, commerce, coastal engineering, construction and recreation, among others.

Recognizing this key issue, the 1st session of the WMO/IOC Joint Technical Commission for Oceanography and Marine Meteorology (JCOMM-I; Akureyri, June 2001) agreed that it would be most appropriate to transform the existing WMO Wave Programme into a new JCOMM Wind Wave and Storm Surge Programme.

Importantly, the Commission noted that the provision of storm surge predictions was already included in the mandated JCOMM terms of reference and, furthermore, that considerable overlapping existed between those systems providing wind wave and storm surge predictions. The Commission therefore agreed to establish its Expert Team on Wind Waves and Storm Surges (ETWS), building upon the success of the Subgroup on Wave Modelling and Forecasting of the former WMO Commission for Marine Meteorology (CMM).

Four years later, JCOMM-II (Halifax, September 2005) recognized the potential value for WMO Members/IOC Member States, of a guide to storm surge analysis and forecasting, and in so doing, it urged the ETWS to provide the relevant technical advice and guidance for its preparation, while additionally noting that the future guide should also contribute to draw attention on vulnerabilities in coastal areas exposed to storm surges by also focusing on risk forecasting, in addition to hazard forecasting.

In response to the JCOMM mandate, the ETWS established an ad-hoc group of storm surge experts under the chairmanship of V. Swail (Canada), which immediately set out to work on these objectives. I am indeed confident that the Guide to Storm Surge Forecasting will prove to be an invaluable asset in support of the various marine services currently being provided by WMO and IOC maritime Members/Member States.



(M. Jarraud)  
Secretary-General



## ACKNOWLEDGEMENTS

The development of this *Guide to Storm Surge Forecasting*, produced under the guidance of JCOMM ETWS, has been a team effort, involving a number of experts in various aspects of storm surge modelling and forecasting from several countries, many of whom are Members of ETWS.

The overall responsibility for the final version of the Guide, including the final synthesis and editing, has been undertaken by Kevin Horsburgh (National Oceanography Centre, United Kingdom of Great Britain and Northern Ireland) and Hans de Vries (Royal Netherlands Meteorological Institute). Individual chapters were produced with contributions from one or more of the co-authors listed below:

- Kevin Horsburgh (United Kingdom);
- Hans de Vries (the Netherlands);
- Paula Etala (Argentina);
- Tad Murty (Canada);
- Jang-Won Seo (Republic of Korea);
- Shishir Dube (India);
- the late Igor Lavrenov (Russian Federation);

- Martin Holt (United Kingdom);
- Pierre Daniel (France);
- Masakazu Higaki (Japan);
- Graham Warren (Australia);
- Regina Cabrera (United States of America);
- Niru Nirupama (Canada);
- Denis Paradis (France);
- Philippe Dandin (France).

The sources of illustrations used in this Guide are indicated in the captions in the event that the figures have not been specially prepared for this edition.

Contact with contributors can be made through the Ocean Affairs Division of the WMO Secretariat. The Secretariats of both WMO and IOC, in particular Boram Lee and Alice Soares, assisted greatly in the guidance and preparation of this publication. Mikhail Entel and Peter Otto (both of Australia) provided a very thorough peer review of the manuscript prior to its final publication.



# CHAPTER 1

## INTRODUCTION AND GENERAL CONSIDERATIONS

### 1.1 OCEANOGRAPHICAL ASPECTS OF STORM SURGES

Storm surges are oscillations of the water level in a coastal or inland body of water in the time range of a few minutes to a few days, resulting from forcing from atmospheric weather systems. According to this definition, the so-called wind waves, which have durations on the order of several seconds, are excluded (Murty, 1984).

That storm surges can occur over short periods on the order of a few minutes is generally well understood and recognized. However, the situations in which high water levels associated with storm surge events can last for two to three days are not. Figure 1.1 shows modelled storm surges at Sagar Island and the Pussur River entrance in the Bay of Bengal following a major storm surge event on 13 November 1970.

It can be seen from Figure 1.1 that the tidal oscillations are superimposed on the elevated water levels due to the storm surge. It may be noted that the contribution from the storm surge is several metres and that the surge event lasted from two to three days.

The ocean wave spectrum is shown in Figure 1.2. Tides, storm surges and tsunamis belong to the class of long gravity waves (Gonnert et al., 2001).

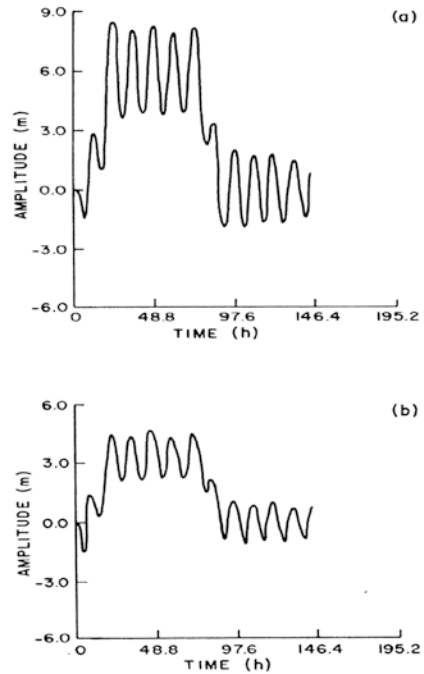


**Figure 1.1. Calculated water level (tide plus surge) at (a) Sagar Island and (b) the Pussur River entrance in the Bay of Bengal for a hypothetical storm modelled after the storm of 13 November 1970**

The ocean wave spectrum is shown in Figure 1.2. Tides, storm surges and tsunamis belong to the class of long gravity waves (Gonnert et al., 2001).

Storm surges are centred at about  $10^{-4}$  cycles per second (cps, or hertz, Hz), which gives a period of

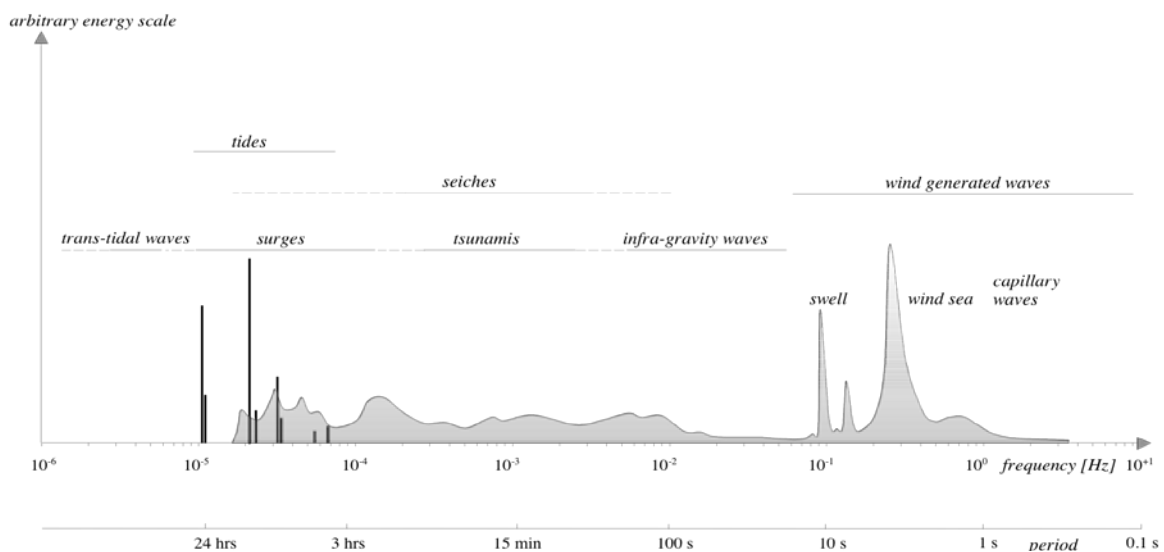


**Figure 1.2. Frequencies and periods of the vertical motions of the ocean surface**

approximately three hours. However, the periods in oscillations of water level may vary considerably. This depends mainly on the topography of the body of water, but also, to a lesser extent, on other parameters such as the direction of movement of the storm, the strength of the storm, the stratification of the water body, the presence or absence of ice cover and the nature of tidal motion in the water body. Even within the same body of water, storm surge records for different locations indicate different periods.

Storm surges occur due to meteorological forcing fields from synoptic-scale (large) weather systems (cyclones) and also from mesoscale (medium) systems (squall lines). Tides arise due to the gravitational attraction of the moon and sun on the ocean waters. Tsunamis are generated mainly by earthquakes under the ocean (Murty, 1977), although they can also be generated by volcanic island eruptions, submarine land slides, nuclear or large chemical explosions in the oceans and asteroid strikes on the ocean surface.

The main characteristic of a long gravity wave is that its wavelength is much greater than the depth of the water over which it is travelling. For all practical purposes, one can use the following simple formula for the speed of a long gravity wave:

$$c = \sqrt{g \cdot D} \quad (1.1)$$

where:

- $c$  = the speed of a long gravity wave;
- $g$  = acceleration due to gravity = 9.8 metres per second squared;
- $D$  = the depth of water.

However, it should be noted that slight corrections to the above equation are necessary if dispersion is taken into account.

While storm surges, astronomical tides and tsunamis are all classed as long waves, there are at least two important differences between the former and the two latter types. First, whereas tides and tsunamis occur on the oceanic scale, storm surges are predominantly a coastal phenomenon. Second, significant tsunamis and tides cannot occur in a completely enclosed small coastal or inland body of water, but storm surges can occur in completely enclosed lakes, canals and rivers.

Figure 1.3 illustrates how a storm surge built up in the Bay of Bengal during the highly destructive event of November 1970.

As illustrated in Figure 1.3, in the deeper part of the bay, the amplitude of the storm surge was zero. Over deep water, the storm surge propagates much faster than the speed at which the weather system travels in the atmosphere. However, in the gradually shallowing waters towards the head of the bay, the gravity wave slows down and its speed gradually matches the speed of movement of the weather system. When both these speeds match, resonance coupling takes place and energy is transferred from the weather system to the ocean surface, leading to the development of a storm surge.

In water bodies in higher latitudes, ice cover can have a substantial influence on the storm surge. Studies of Canadian water bodies have shown that ice cover can clip the crest of the storm surge, but leave the trough unaffected, as shown in Figure 1.4.

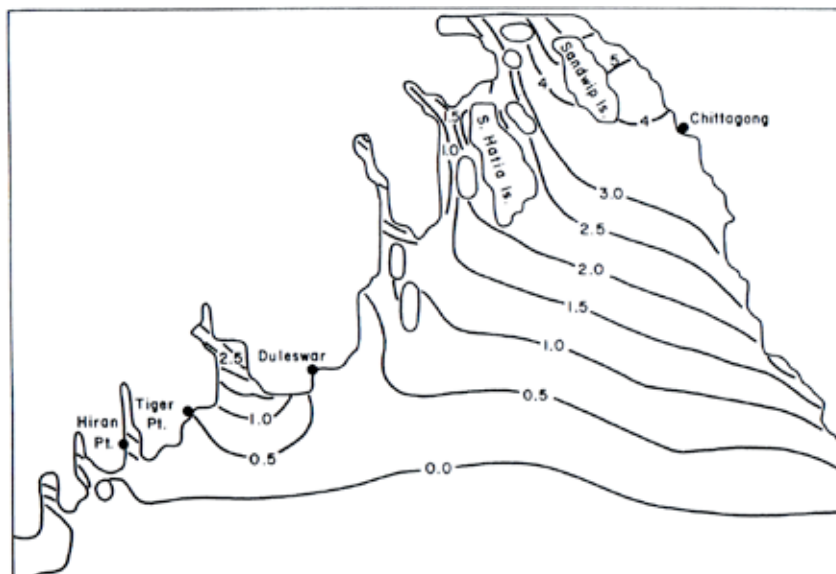


Figure 1.3. Storm surge heights (metres) in the northern part of the Bay of Bengal from a hypothetical storm modelled after the storm of November 1970

A more detailed analysis of the influence of surface ice cover on storm surges will be provided in 2.8.

**1.2 METEOROLOGICAL ASPECTS OF STORM SURGES**

Storm surges are phenomena that arise from an interaction between air and sea, that is, the atmosphere forces the body of water, which responds by generating oscillations with periods ranging from a few minutes to a few days. When a weather system moves over a water body, there are essentially two forcing fields. The first is the atmospheric pressure gradient normal to the ocean surface. For every reduction in pressure of 1 hectopascal (hPa) at the centre of the weather system, the sea level rises temporarily by approximately 1 centimetre. This phenomenon is referred to as the “inverse barometer effect” and is also called “static amplification” or the static part of the storm surge. The static part usually contributes from 10 to 15 per cent of the magnitude of the storm surge. The second and dominant part of the storm surge, termed the dynamic amplification, is caused by the tangential wind stress (associated with the wind field of the weather system) acting over the ocean surface, which pushes the water towards the coast, thereby causing a pile-up of water at the coast.

The dynamic amplification  $A_D$  can be related to the static amplification  $A_S$  through the following simple relationship (Proudman, 1953):

$$A_D = A_S \cdot \frac{1}{\left(1 - \frac{v_w^2}{c^2}\right)} \tag{1.2}$$

where:

- $v_w$  = the speed of movement of the weather system;
- $c$  = the speed of propagation of the storm surge as defined in Equation (1.1).

Over deep water,  $c$  is much greater than  $v_w$ , hence  $A_D$  is only slightly greater than  $A_S$ . On the other hand, in shallow water,  $c$  is close to  $v_w$  in value, the denominator in Equation (1.2) becomes small and  $A_D$  becomes much greater than  $A_S$ . Theoretically at least, when  $c$  and  $v_w$  are equal,  $A_D$  becomes infinite, but in practice, due to friction and some other parameters,  $A_D$  has an upper limiting value.

It can be shown that:

$$S = K \cdot \frac{w^2}{D} \tag{1.3}$$

where:

- $S$  = the storm surge amplitude;
- $w$  = the wind speed;
- $D$  = the depth of water;
- $K$  = a constant encompassing several other factors, such as bottom stress, stratification of the water body, atmospheric stability, nature of the ocean surface (rough versus smooth) and the angle at which the wind is blowing.

However, the most important parameters in determining the storm surge amplitude are the wind speed and the water depth. The surge amplitude is directly proportional to the square of the wind speed (Pugh, 1987). Hence, if the wind speed doubles, the surge height increases fourfold. In addition, the surge amplitude is inversely proportional to the water depth. Thus, the shallower the water, the greater the surge amplitude. This is because, as shallow waters are entered, approximately the same energy is compressed into a shorter, vertical column of water.

Other factors that can increase the storm surge amplitude include interaction with tides, wind waves or river flow and also the effects of precipitation on surges in rivers, lakes and estuaries.

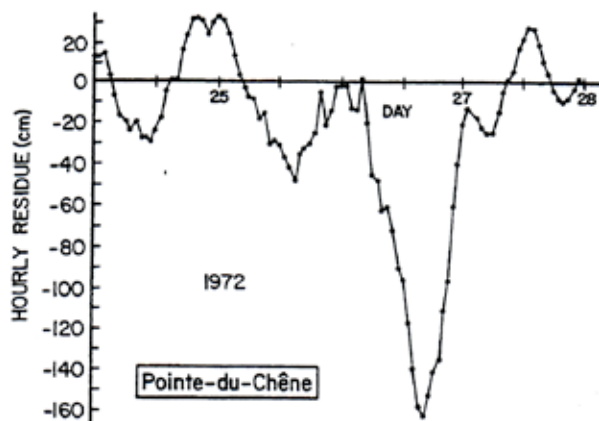


Figure 1.4. Observed storm surge at Pointe-du-Chêne, Canada

**1.3 METHODS OF STORM SURGE PREDICTION – AN OVERVIEW**

Before the computer era, the techniques used for storm surge prediction were analytical, empirical, graphical (nomograms) and statistical (regression relations). Electrical analog methods were also occasionally used. However, with the advent of computers, numerical models have gradually taken over and numerical methods are now used almost exclusively. However, for the sake of simplicity, simple analytical and graphical methods are still used occasionally. For site-specific purposes, empirical and statistical methods are also used.

Until recently, the majority of numerical models for storm surge prediction consisted of vertically integrated two-dimensional models with three independent variables, namely, the two horizontal coordinates (east–west and north–south) and time. The dependent variables are usually the surge amplitude and the x and y components of the vertically averaged horizontal current.

#### 1.4 EMPIRICAL METHODS FOR SURGE PREDICTION

Empirical methods are those techniques that are derived from simple analytical theories and experience, and are usable more or less directly for practical situations. Silvester (1971) considered an enclosed body of water, such as a rectangular lake, to develop the following relationship:

$$\frac{S}{d} = \frac{K_{10} U_{10}^2 L}{2gd^2} \quad (1.4)$$

where:

- $d$  = the (uniform) depth of the lake;
- $U_{10}$  = the wind speed 10 metres above the water surface;
- $L$  = the length of the lake (or wind fetch);
- $S$  = the surge amplitude at the downwind end;
- $K_{10} = 3.3 \times 10^{-6}$  (wind drag coefficient).

Note that this equation is dimensionless.

For non-rectangular shapes,  $S/d$  must be multiplied by a form factor  $N$ .

For storm surges on a continental shelf, Silvester assumed a uniform variation from a depth  $d_1$  at the shelf edge to  $d_2$  near the coast. If  $L$  is the width of the shelf and  $F$  the length of the wind fetch, then the depth ratio  $d_2/d_1$  can be expressed in terms of  $L/x$ , where  $x$  is the theoretical distance inland at which the plane of the bed would meet the mean water level. For extra-tropical cyclones,  $F$  is generally greater than  $L$ . However, it is necessary to allow that  $F$  equals  $L$ , as only the portion of the fetch over the shallow zone is effective at producing surge. On the other hand, for tropical cyclones,  $F$  is usually less than  $L$ . Allowing  $V$  to be the speed of movement of the wind field, then if  $V$  is equal to zero, the wind field is referred to as a static wind field.

For the case in which a wind field is static, the surge  $S$  is given by Bretschneider (1966) as:

$$\frac{S}{d_1} = \frac{KU^2L}{gd_1^2 \left(1 - \frac{d_1}{d_2}\right)} \ln \left(\frac{d_1}{d_2}\right) \quad (1.5)$$

Reid (1956) expressed the surge amplitude as:

$$\frac{S}{d_1} = \frac{KU_{\max}^2 L}{gd_1^2} \left[ \frac{1.12}{1 + \sqrt{\frac{d_2}{d_1}}} \left(\frac{d_1}{d_2}\right)^{1/4} \right] \quad (1.6)$$

When a wind field is moving across the shelf towards the shore, the forward part of the surge wave system is being reflected as the later waves are still approaching the shore. Reid considered the interaction between these two wave systems and included graphs for the ratio  $R$  of the maximum surge  $S_{\max}$  to that of static storm situations. Silvester (see Equation 1.4) gave the following formula for the surge  $S_a$  due to a reduction in the atmospheric pressure:

$$S_a = (1013 - P_c) 0.033 \quad (1.7)$$

where:

- $S_a$  = the surge amplitude in feet;
- $P_c$  = the pressure at the storm centre in hectopascals.

As already mentioned in 1.2, this relation is known as the inverse barometer effect and, as usually expressed, indicates that a decrease of 1 hectopascal in atmospheric pressure gives rise to an increase of 1 centimetre in the water level.

Rao and Mazumdar (1966) expressed the storm surge  $S$  as:

$$S = B + P + X + F \quad (1.8)$$

where:

- $B$  = the static rise due to atmospheric pressure deficiency towards the centre of the storm;
- $P$  = the rise due to piling up of water against the coast caused by offshore winds;
- $X$  = the height of crests of individual waves (wind-generated waves) superimposed on the general rise of the water level;
- $F$  = the effect of forerunners.

Of these,  $P$  and  $X$  are the most important. Rao and Mazumdar combined the effects of  $B$ ,  $P$  and  $X$ , and gave the formula for the surge as:

$$S = \frac{5}{3} \times 4.5 \times 10^{-9} \bar{W}^2 \sum_{d_1, D_1}^{d_n, \Delta D_n} \frac{\Delta D}{D} + \frac{5 \Delta P_a}{3g} \times 10^{-3} \quad (1.9)$$

where:

- $W$  = the sustained speed of the onshore component of the wind;
- $\Delta D$  = the horizontal length of a section;
- $d$  = the depth of the water column;
- $\Delta P_a$  = the pressure deficiency (in hectopascals) at the point under consideration.



Bretschneider (cited above) equally provided a convenient classification of water bodies for developing empirical methods for storm surge prediction, shown in Table 1.1.

**Table 1.1. A convenient classification of water bodies for developing empirical relations for engineering design problems**

Source: Bretschneider, 1966

- 
- A. Enclosed lakes and reservoirs
    1. Rectangular channel, constant depth
    2. Regular in shape
    3. Somewhat irregular in shape
    4. Very irregular in shape
  - B. On coast or continental shelf
    1. Bottom of constant depth
    2. Bottom of constant slope
    3. Slightly irregular bottom profile
    4. Irregular bottom profile
  - C. Coastline
    1. Smooth coastline
    2. Coastline somewhat irregular
    3. Jagged coastline
  - D. Behind coastline
    1. Low natural barriers
    2. Medium-high natural barriers
    3. High natural barriers
  - E. Open bays and estuaries
    1. Entrance backed by long estuary and with tidal flow moving freely past entrance
    2. Entrance backed by short estuary and with tidal flow moving freely past entrance
    3. Entrance obstructed sufficiently to prevent free movement of tidal flow past entrance
- 

## 1.5 STATISTICAL METHODS

Harris (1962) appears to be among the first to have suggested the relevance of statistical methods for storm surge prediction. Venkatesh (1974) developed statistical regression models for storm surge prediction at several stations in Lakes Ontario, Erie, Huron (including Georgian Bay) and Saint Clair. He mentioned that storm surges are not important in Lake Superior. Using data for the period 1961–1973, regression relations in terms of sea-level pressures and air–water temperature differences with lag times of zero to six hours were developed for Lakes Ontario, Erie, Huron, and Georgian Bay. For Lake Saint Clair the sea-level pressures were replaced by local winds.

The grid points used by Venkatesh, shown in Figure 1.5, are the same as those used in the

Canadian Meteorological Centre numerical weather forecast models, so the sea-level pressures forecast could be used directly. The input data were divided into two parts, namely dependent and independent storms. The data from the dependent storms were used to develop the regression relations and the data from the independent storms were used to verify the models. The portion of the variance in the storm surges accounted for by the statistical method is between 55 and 75 per cent. The model best fits the observed data for Lake Saint Clair. The standard error of the estimate for all lakes except Erie is between 0.2 and 0.3 feet (0.06–0.09 metres), whereas for Lake Erie it is approximately 0.6 feet (0.18 metres).

The following equation gives the storm surge  $S$  at Belle River on Lake Saint Clair:

$$S = 0.0189 + 0.0007511V^2 - \quad (1.10)$$

$$0.0000446 (T_A - T_W)_0 V^2 + 0.0000149 (T_A - T_W)_{-1} V^2$$

where:

$S$  = the surge in feet from the mean water level;

$V^2$  = the component of effective wind speed in the north–south direction;

$(T_A - T_W)_0$  and  $(T_A - T_W)_{-1}$

= the air–water temperature differences at lag times of zero and one hour, respectively.

As an example, the storm surge equations at Collingwood on Georgian Bay are listed below. Prediction equations for other locations on the

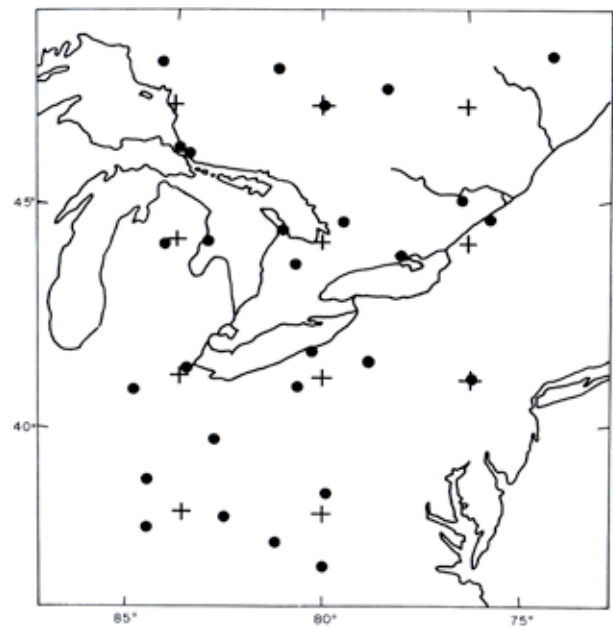


**Figure 1.5. Locations of grid points (+) and observing stations (•) for the Great Lakes area used by Venkatesh (1974)**

Great Lakes are given in the publication by Venkatesh cited above:

$$\begin{aligned}
 S_0 &= 10.903050 + 0.01097P_{(4,-6)} - 0.03517P_{(10,-6)} - 0.02183P_{(3,0)} + 0.04691P_{(6,0)} \\
 &\quad - 0.01164P_{(10,0)} - 0.004680(T_A - T_W)_0 \\
 S_1 &= 9.890630 + 0.01580P_{(4,-6)} - 0.02339P_{(9,-6)} - 0.01110P_{(10,-6)} - 0.003700(T_A - T_W)_{-6} \\
 &\quad - 0.02271P_{(3,0)} + 0.06267P_{(6,0)} - 0.02559P_{(7,0)} + 0.0548P_{(9,0)} - 0.02093P_{(0,0)} - 0.001740(T_A - T_W)_0 \\
 S_2 &= 8.069170 - 0.01213P_{(5,-6)} + 0.03338P_{(7,-6)} - 0.01754P_{(9,-6)} - 0.01323P_{(10,-6)} - 0.01314P_{(3,0)} \\
 &\quad + 0.05873P_{(6,0)} - 0.03047P_{(7,0)} + 0.02644P_{(9,0)} - 0.04000P_{(10,0)} - 0.004320(T_A - T_W)_0 \\
 S_3 &= 8.389940 + 0.02566P_{(7,-6)} - 0.02229P_{(9,-6)} - 0.00598P_{(10,-6)} + 0.0117P_{(3,0)} \\
 &\quad + 0.05529P_{(6,0)} - 0.03541P_{(7,0)} + 0.02561P_{(9,0)} - 0.03940P_{(10,0)} - 0.005040(T_A - T_W)_0 \\
 S_4 &= 9.677820 - 0.01089P_{(3,-6)} + 0.03688P_{(7,-6)} - 0.01901P_{(10,-6)} + 0.06540P_{(6,0)} - 0.05273P_{(7,0)} \\
 &\quad - 0.02922P_{(10,0)} - 0.003790(T_A - T_W)_0 \\
 S_5 &= 9.393110 - 0.02087P_{(3,-6)} + 0.04418P_{(7,-6)} - 0.02025P_{(9,-6)} - 0.0128P_{(10,-6)} + 0.01087P_{(3,0)} \\
 &\quad + 0.05780P_{(6,0)} - 0.0566P_{(7,0)} + 0.01208P_{(9,0)} - 0.02615P_{(10,0)} - 0.004380(T_A - T_W)_0
 \end{aligned}
 \tag{1.11}$$

where:

- S = surge (feet), with the subscript representing the number of hours after the time of the pressure forecast;
- $P_{(N, T)}$  = pressure (hectopascals) at grid point number N (see Figure 1.5) and lag time T (hours).

**1.6 STORM SURGE PREDICTION THROUGH ARTIFICIAL NEURAL NETWORKS**

Recently, artificial neural network (ANN) models have been applied to storm surge and tide prediction. Tsai and Lee (1999) and Lee and Jeng (2002) used ANNs for tide forecasting based on field data. Lee (2004, 2008) proposed the application of back-propagation ANN for the prediction of long-term tidal level and short-term storm surge. Moreover, Lee (2006), Sztobryn (2003) and Tissot et al. (2003) demonstrated the application of ANNs for forecasting storm surge directly by incorporating it into an operational storm surge forecast. This section sets out how ANN storm surge prediction models may be used operationally.

**1.6.1 Artificial neural networks**

Human brain biology has provided the basis for the development of ANNs. They can be represented by a network diagram with three components: an input layer, a hidden layer and an output layer

(Figure 1.6). This model contains many interconnected units (neurons) that can extract linear and non-linear relationships in the data. In this model, input units correspond to input variables and each variable is usually normalized. Combination functions combine input units or hidden units and the multilayer perception (MLP) structure mainly applies a linear combination function. Linear combinations of input units create hidden units and the output unit is modelled as a function of linear combinations of these hidden units. Activation functions are usually chosen to be the sigmoid functions, such as logistic hyperbolic tangent functions. These can extract linear and non-linear relationships from the combination input or hidden units. The output function allows a final transformation of linear combinations of



**Figure 1.6. Multilayer perception structures with one hidden layer and a hidden unit**

hidden units. The identity function would normally be selected for regression. Here we present a feed-forward ANN architecture, which includes an input layer and a broadcasting output layer, with one or more hidden layers in between. In a feed-forward ANN model, the units in one layer are connected uniquely to the units in the next layer.

### 1.6.2 Optimal ANN modelling

The optimal structure of an ANN model must be determined by basing it on the data. This modelling stage involves four main problems (Hastie et al., 2001):

- Starting values: The starting values for weights are selected randomly from values near zero, so the model starts out nearly linear and becomes non-linear as weights increase.
- Overfitting: ANNs often have too many weights and will overfit the data at the global minimum of errors (the sum of squared errors) contained in the training data. It is therefore important to train the model for only a short period and stop well before approaching the global minimum.
- Number of hidden units and layers: Large numbers of hidden units can reduce the extra weights towards zero if appropriate

regularization is used. It is most common to select a reasonably large number of units, train them with regularization and then choose the number of hidden units.

- Selection of input variables: Appropriate lags and input variables of the model must be selected.

Many experiments were conducted to select the optimal model for the Jeju and Yeosu Stations in the coastal regions of the Republic of Korea, using different training datasets, input variables (variable and lag selection of observed storm surge height, wind stress and sea-level pressure) and model structure (Lee et al., 2005). Table 1.2 outlines several experimental set-ups and Tables 1.3–1.6 list the results of these model experiments. The results indicate the accuracy of the ANN model forecasts. The root mean square error (RMSE) between MLP and radial basis function (RBF) models differed only slightly, but MLP was more stable. The best results were obtained when MLP training involved three hidden units and previous input data to an RMSE of approximately 20 centimetres, which is approximately 5 per cent of the tidal range at Jeju and Yeosu. Table 1.7 presents the performance of model 2 for data from Yeosu Station for forecasting times of 3, 6, 12, and 24 hours. For 24-hour forecasts,

**Table 1.2. Summary of experiments used to determine optimal ANN model structure**

| Experiment | Training dataset (years)   | Lags included in input data   | Model structure | Period for validation       |
|------------|--|---|-----------------|-----------------------------|
| 1          | 2000/2001/2002   |   | MLP             | 2003                        |
| 2          | 2000/2001/2002   |   | RBF             | 2003                        |
| 3          | 1990–2002  |   | MLP             | 2003                        |
| 4          | 2002   | Storm surge: –6 to –1 hours<br>Atmospheric elements: –3 to –1 hours | MLP             | Typhoon <i>Maemi</i> (2003) |
| 5          | Stormy situations (1990–2003) with the exception of Typhoon <i>Maemi</i> | Storm surge: –6 to –1 hours<br>Atmospheric elements: –3 to –1 hours | MLP             | Typhoon <i>Maemi</i> (2003) |

**Table 1.3. Root mean square error of the MLP models from experiment 1 and harmonic forecast at the Jeju and Yeosu Stations of the Republic of Korea (centimetres)**

| Station | Harmonic forecast | Year for training | MLP<br>(hidden = 2) | MLP<br>(hidden = 3) | MLP<br>(hidden = 4) | MLP<br>(hidden = 5) |
|---------|-------------------|-------------------|---------------------|---------------------|---------------------|---------------------|
| Jeju    | 7.80              | 2002              | 7.86                | 7.40                | 7.51                | 7.43                |
|         |                   | 2001              | 8.75                | 7.94                | 7.56                | 7.56                |
|         |                   | 2000              | 8.29                | 8.27                | 7.94                | 8.94                |
| Yeosu   | 7.98              | 2002              | 7.20                | 7.18                | 7.18                | 7.30                |
|         |                   | 2001              | 7.21                | 7.32                | 7.35                | 7.39                |
|         |                   | 2000              | 7.30                | 7.27                | 7.36                | 7.30                |

**Table 1.4. Root mean square error of the RBF models from experiment 2 and harmonic forecasts at the Jeju and Yeosu Stations (centimetres)**

| Station | Harmonic forecast | Year for training | MLP<br>(hidden = 2) | MLP<br>(hidden = 3) | MLP<br>(hidden = 4) | MLP<br>(hidden = 5) |
|---------|-------------------|-------------------|---------------------|---------------------|---------------------|---------------------|
| Jeju    | 7.80              | 2002              | 7.67                | 18.75               | 7.99                | 7.64                |
|         |                   | 2001              | 8.41                | 8.92                | 8.19                | 8.00                |
|         |                   | 2000              | 7.97                | 8.21                | 9.61                | 7.92                |
| Yeosu   | 7.98              | 2002              | 7.18                | 7.22                | 7.18                | 61.18               |
|         |                   | 2001              | 7.20                | 7.21                | 7.50                | 7.73                |
|         |                   | 2000              | 7.29                | 7.35                | 7.47                | 7.30                |

**Table 1.5. Root mean square error of the models from experiments 1 and 3 and harmonic forecasts (centimetres)**

| Station | Harmonic forecast | Experiment 1 | Experiment 3 |
|---------|-------------------|--------------|--------------|
| Jeju    | 7.80              | 7.40         | 7.54         |
| Yeosu   | 7.98              | 7.18         | 7.25         |

**Table 1.6. Comparison of observed sea levels and forecasts from HA and experiments 4 and 5 at Yeosu Station during Typhoon *Maemi* (centimetres)**

| Model performance | Harmonic forecast | 1-hour forecast |              | 24-hour forecast |              |
|-------------------|-------------------|-----------------|--------------|------------------|--------------|
|                   |                   | Experiment 4    | Experiment 5 | Experiment 4     | Experiment 5 |
| RMSE              | 41.23             | 11.21           | 11.63        | 19.82            | 19.25        |
| Correlation       | 0.9307            | 0.9948          | 0.9937       | 0.9825           | 0.9867       |

**Table 1.7. Performance of model 2 for typhoons at Yeosu Station for forecasting times of 3, 6, 12 and 24 hours (centimetres)**

| Forecast time (hours) | RMSE               |                      |                    |
|-----------------------|--------------------|----------------------|--------------------|
|                       | <i>Olga</i> (1999) | <i>Saomai</i> (2000) | <i>Rusa</i> (2002) |
| 3                     | 10.15213           | 12.83874             | 12.62161           |
| 6                     | 11.07748           | 14.61391             | 15.62709           |
| 12                    | 11.43110           | 14.74966             | 15.43273           |
| 24                    | 12.10389           | 15.07784             | 15.53923           |
| Harmonic forecast     | 13.67884           | 22.97632             | 39.52742           |

RMSE improves from 13–39 to 12–15 centimetres. Figure 1.7 shows results from experiment 5, comparing observed levels to those obtained from harmonic analysis (HA) and ANN for five different typhoons. Figure 1.8 presents the results of ANN model 1 for Busan Station using the data predicted by the Mesoscale Model 5 from the Republic of Korea Meteorological Administration (MM5–KMA) for 12–13 September 2003.

### 1.6.3

#### **Regional real-time storm surge prediction system for three stations in the Republic of Korea**

Regional real-time storm surge prediction systems have been constructed based on the previous ANN model experiments at Busan, Yeosu and Wando Stations. Figure 1.9 presents results from the ANN model for the three stations. Input values were

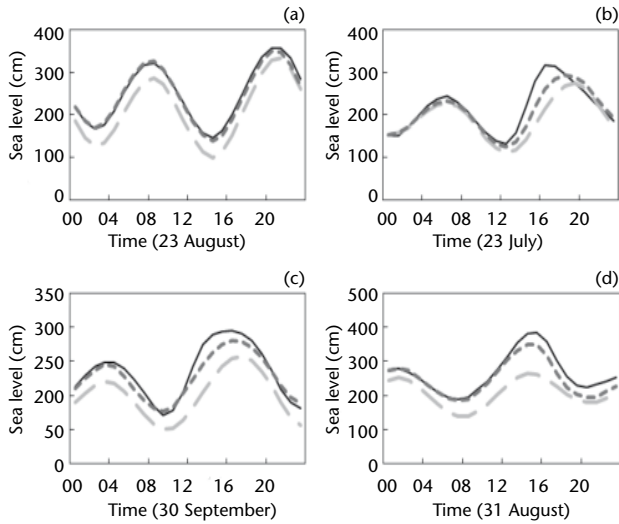


**Figure 1.7. Results of experiment 5. The observed (solid line) and predicted sea levels from HA (dashed line) and ANN (dotted line) models at Yeosu Station during the passage of typhoons (a) Gladys in 1991, (b) Faye in 1995, (c) Yanni in 1998 and (d) Rusa in 2002**

updated hourly, and newly updated values were continuously applied to the model. These results indicate that it is possible to apply an ANN model for each cluster to the regional storm surge forecasting system and to extend this into all coastal regions. Extension into all coastal regions requires continual updates of typhoon meteorological data. In addition, model accuracy can be improved by

correcting predicted air pressure and wind stress, which use model input variables. Future research will include construction of an autonomous modelling system incorporating a model for real-time training and optimization that will include the present meteorological state as well as past typhoon information.

**1.7 NUMERICAL METHODS**

Numerical methods are now the most widely used approach for storm surge prediction (for a review of such methods, see Gonnert et al., 2001). Until the 1980s, finite difference models with rectangular or square grids were traditionally

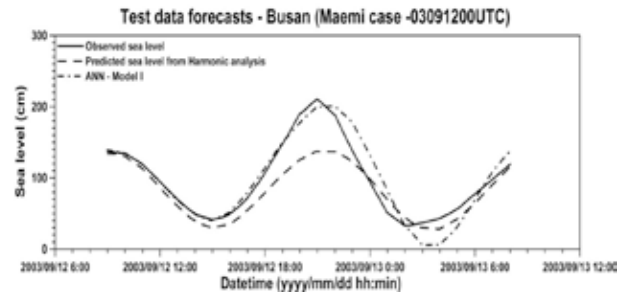


**Figure 1.8. Observed sea levels and those predicted by HA and ANN model 1 for Busan Station in the Republic of Korea for the period 12–13 September 2003**

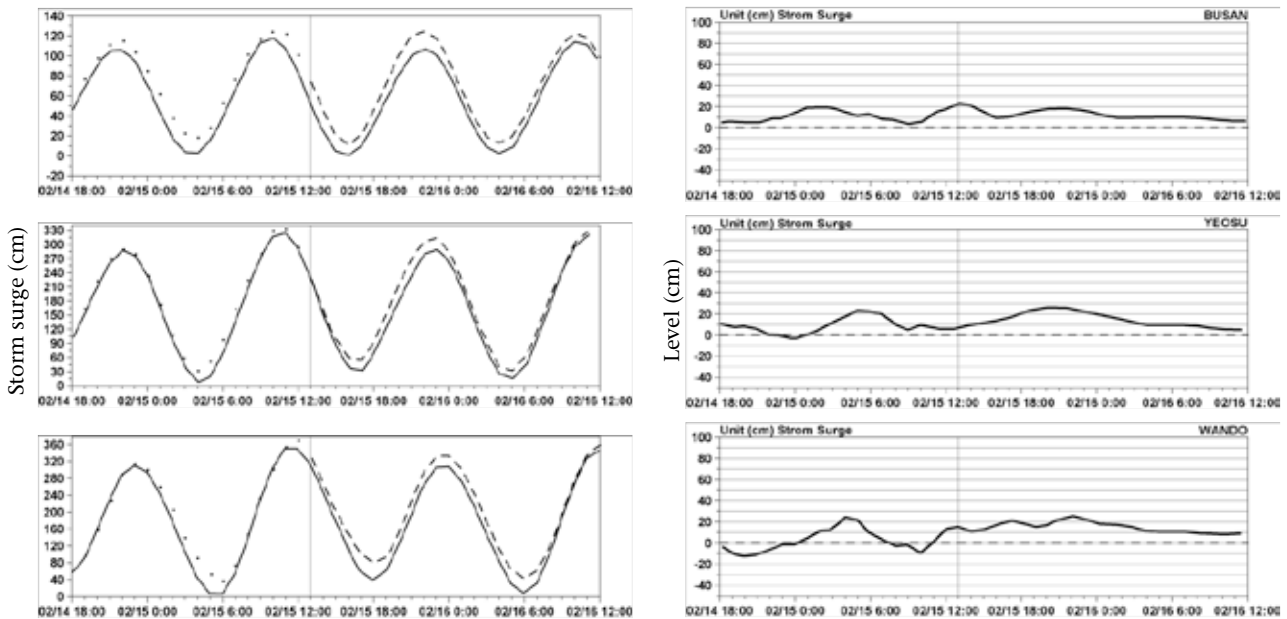


**Figure 1.9. Real-time storm surge prediction using the ANN model at Busan, Yeosu and Wando Stations. Left panels: observed levels (dotted line); levels predicted by the ANN model plus tides predicted by HA (dashed line); tides predicted by HA (continuous line); the vertical line indicates the time when prediction began. Right panels: storm surge levels observed (before the vertical line) and predicted by the ANN model (after the vertical line)**

used to improve resolution near the coastlines. The grids may have been telescoped, such as shown in Figure 1.10 for the Bay of Fundy (Greenberg, 1979).

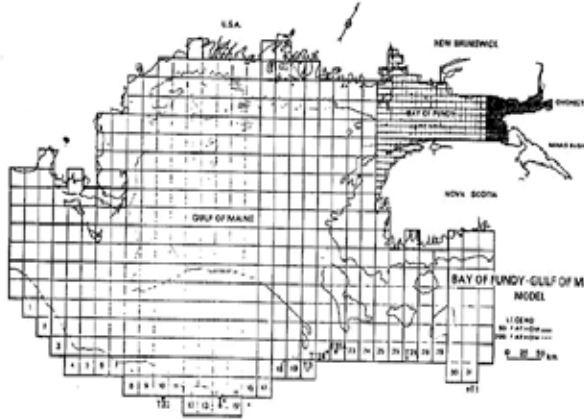


**Figure 1.10. Telescoped rectangular grids for modelling tides in the Bay of Fundy**

Source: Greenberg, 1979

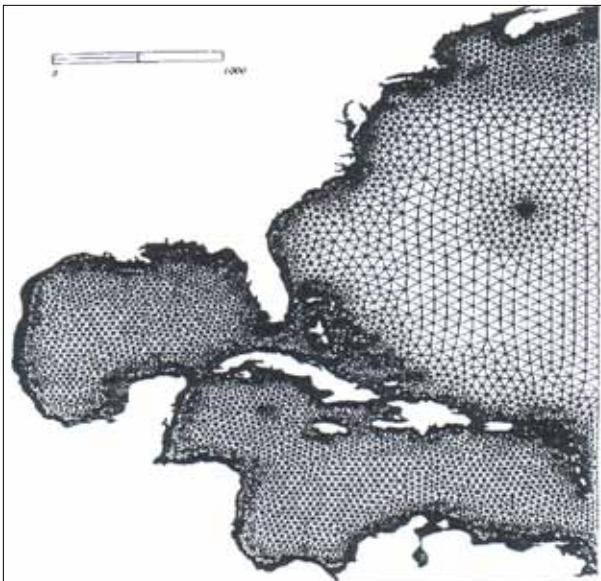


**Figure 1.11. The East Coast of the United States, Gulf of Mexico and Caribbean Sea computational domain (bar scale in kilometres)**

Source: Scheffner et al., 1994

The fundamental drawback of rectangular grids is that the coastline of a body of water can only be represented as a staircase in orthogonal coordinates. In reality, coastlines are highly irregular and are oriented in all directions. Forcing coastlines to conform in only two perpendicular directions thus creates artificial sub-basins. These sub-basins will have their own normal modes (free oscillations) that may contaminate the computation of the storm surge in the main basin.

To avoid these problems, as well as to provide better resolution of the coastal geometry and the shallow-water bathymetry, finite element models with irregular triangular grids were developed from the late 1970s. The advantage of such grids is that in deep water, where there is little or no surge, the grid can be coarse, while in the main area for the development of storm surge in shallow water, smaller triangles can provide better resolution. Examples of such grids for a continental coastline and for an island system are shown in Figures 1.11 and 1.12, respectively.

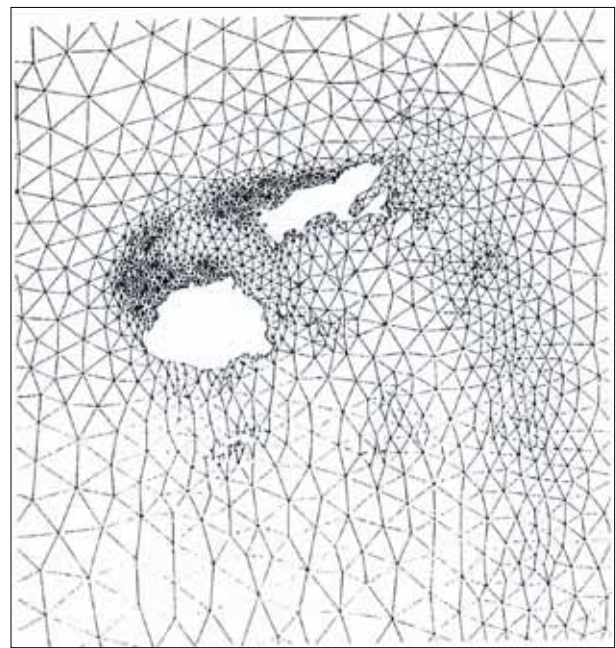


**Figure 1.12. A detailed view of an irregular triangular grid for the Fiji area**

Source: Luick et al., 1997

## CHAPTER 2

### STORM SURGE PHYSICS

#### 2.1 METEOROLOGICAL EFFECTS

Storm surge is directly connected with the dynamic processes developing in the atmosphere. Due to the “inverse barometer effect”, as stated in Chapter 1, a pressure change of 1 hectopascal causes a sea-level change of approximately 1 centimetre. When pressure systems are moving with a definite speed, the sea level at that point does not necessarily correspond to the static value, and under certain conditions the level can be significantly increased due to resonance. Spectral density analysis of atmospheric pressure, wind and sea level reveals the connection between these parameters and the frequency of the pressure oscillation. Its limiting value is the inverse barometer effect. When the limiting oscillation frequency of atmospheric pressure is exceeded, the reaction of the sea level to it is considered random.

In reality, the atmospheric pressure field is non-stationary and acts simultaneously with the wind field. Wind waves are formed on sea surfaces by the wind field, but they are not directly related to long-period oscillations in sea level. Surface currents theoretically deviate from the wind direction by an angle of 45 degrees in the deep ocean, this reducing to practically zero in shallow-water areas. In the deep ocean, the depth-averaged current in the layer affected by wind is directed transversally to the acting wind direction. As a result, surges are generally greatest when the winds are directed parallel to a coastline in the deeper part of the ocean and transversally to the coastline in shallow waters.

Oscillations in water level occur predominantly at the fundamental natural period of the basin, which depends on its length and depth, and less on the temporal scale of the weather system. When forcing exceeds the natural period of the system, oscillations in water level (with various natural frequencies and uniform distribution of energy in the perturbation spectrum) are observed when an external impulse of short duration is applied. The speed of movement of the weather system, together with the ocean bathymetry, mainly determines at which points disastrous coastal inundations may occur from a storm surge.

Winds blowing over a sea create tangential stress on its surface. As for the wind-generated current, only the shear forces at the sea surface as they influence the subsurface water layer are considered (that is, pressure perturbations on the deformed surface are

not taken into account). The work done by the tangential stress of the wind field is partially spent on wave generation. In turn, a part of the wave momentum is transferred to the wind-generated current due to wave breaking. The wind field also influences the tangential stress in another way, as it determines the effective surface roughness. All these factors must be taken into consideration to determine the tangential stress of the wind field acting on a sea surface.

There has been considerable progress in the modelling of air–sea fluxes of momentum, heat, moisture and gases, following a better understanding of how wind generates waves and how breaking waves play a role in the exchange processes between atmosphere and ocean. This understanding of air–sea interaction has been introduced into both wave and storm surge modelling. As an example, the wave model used by the European Centre for Medium-Range Weather Forecasts (ECMWF) uses a parameter dependent on sea state in its drag formulation (Charnock, 1955) (see: <http://www.ecmwf.int/research/ifsdocs/CY31r1/WAVES/IFSPart7.pdf>). The “wind-over-waves” coupling theory developed by Kudryavtsev and Makin (Makin, 2003) has been used to develop parameterizations for the sea drag that include these effects. Such parameterizations can also be used in storm surge modelling.

The tangential stress  $\tau$  of the wind per unit area is usually expressed through an average wind speed  $W$ , together with air density  $\rho_a$  and air turbulence coefficient  $k_a$ , as:

$$\tau = k_a \rho_a \frac{\partial W}{\partial z} \quad (2.1)$$

The turbulence coefficient  $k_a$  can be expressed as a function of the height  $z$ :

$$k_a = \theta v_* z \quad (2.2)$$

where:

$\theta$  = the von Karman constant;  
 $v_*$  = the dynamic velocity.

In this relation, for a logarithmic profile of the wind,  $v_*$  is given by:

$$v_* = \sqrt{\tau / \rho_a} \quad (2.3)$$

The invariability of  $\sqrt{\tau / \rho_a}$  over the height within the limits of the lowest 30–50 metres allows the integration of Equation (2.2) over  $z$ , thus

generating the general expression for determining the tangential stress:

$$\tau = c' \rho_a (W - V) |W - V| \tag{2.4}$$

where the friction coefficient  $c'$  is given by:

$$c' = \left( \frac{\theta}{\ln z / z_0} \right)^2 \tag{2.5}$$

in which:

- $\theta = 0.4$  (the von Karman constant);
- $z_0$  = aerodynamic roughness of the underlying surface;
- $V$  = transverse speed of the underlying surface;
- $W$  = surface wind speed;
- $\rho_a$  = air density.

In practical situations, the speed of water (or ice) is usually neglected when determining the tangential stress of the wind on the sea surface, since the surface current or speed of the ice drift is approximately two orders of magnitude less than the wind speed.

Thus, the tangential stress of the wind field on the sea surface is normally expressed by a quadratic drag law:

$$\tau = C_D \rho_a W |W| \tag{2.6}$$

where:

$C_D$  = the drag coefficient.

In general,  $C_D$  is not a constant coefficient, but is a varying function depending on the degree of surface roughness, atmosphere stratification and other wind parameters. There are many good reviews that discuss the determination of the drag coefficient (see, for example, Parker, 1975; Smith and Banke, 1975), and more recent papers address constraints on drag coefficients at the very high wind speeds found in tropical cyclones (see, for example, Powell et al., 2003). Nevertheless,  $C_D$  is

often taken as constant in many models of storm surges. Such an approach may be valid when modelling surges of short duration covering relatively small areas of the coast (that is, where the tangential stress of the wind field on the sea surface has little variability in space and time). However, for storm surges of longer duration over extensive stretches of a coastline one should take into consideration the spatial and temporal variability of the drag coefficient. Figure 2.1 illustrates examples of calculations of the friction coefficient over a water surface at different wind speeds and stratifications.

In coastal areas, estuaries or lakes, wind speeds from an atmospheric model are, on average, lower over land than over water. This physical fact, coupled with resolution of the atmospheric and surge models, can give an underestimate of the wind speed used for surge modelling. The speeds of winds up to 10 metres above the surface are usually derived in a post-processing step after running the atmospheric model itself. The wind profile of a boundary layer between the surface and the lowest model level is determined. Where the surface type changes within a grid box, some averaging has to be applied.

To overcome this problem without increasing the resolution of the atmospheric model, a technique called downscaling can be used (Verkaik et al., 2003; Verkaik, 2006). The technique uses a high-resolution roughness map and a simple two-layer model of the planetary boundary layer. The roughness map is determined from a map of land use and a footprint model to account for upstream properties of the surface. The roughness lengths are hence dependent on the wind direction. The planetary boundary layer model is first used to calculate the wind at the top of the planetary boundary layer from the surface wind of the atmospheric model with the roughness length that is used by the atmospheric model. In a second step, the surface wind is recalculated with the high-resolution roughness map.

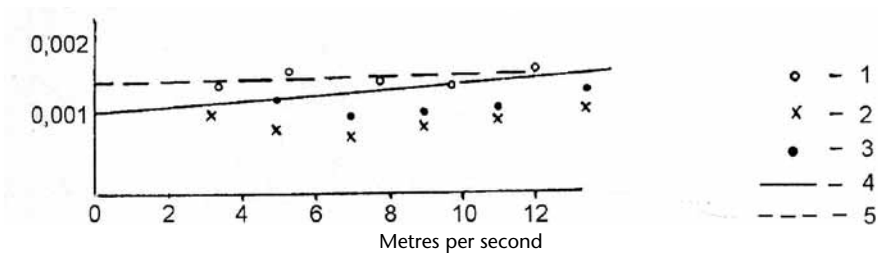


**Figure 2.1.** Examples of calculations of friction coefficients for different wind speeds over a water surface and measured at different stratifications. 1: Brox (Roll, 1968); 2 and 3: Deacon (Deacon, 1962; Deacon and Webb, 1962); 4: Deacon's formulae  $c^s = (1.1 + 0.04W) \times 10^{-3}$ ; 5:  $c^s = (1.5 + 0.01W) \times 10^{-3}$



2.2 OCEANOGRAPHICAL EFFECTS

Changes of sea level due to variations in atmospheric pressure are considerably less than those caused by the influence of winds and currents both along coastlines and in an open sea. On the basis of an approximate dependence, Zubov (1947) concluded that:

Dynamic reduction in sea level caused by winds and currents under the influence of atmospheric pressure distribution in the area of reduced pressure is ten times higher than static rise in level produced with the same pressure distribution without taking into consideration the influence of winds, currents and deflecting force of the Earth's rotation (Coriolis forces).

However, subsequent verification showed that the influence of wind on sea level was not ten but only two times more in comparison to that of atmospheric pressure.

In regions of strong freshwater influence, stratification near the coast is also affected by wind action. Surges may cause displacement of lighter surface waters into a coastal area resulting in an increase of sea level. The increase is somewhat intensified due to the reduced density of the waters displaced. Conversely, if offshore winds move lower density water away from a coastline then denser, upwelled bottom waters are raised along a continental slope to replace them. The level in these areas is then reduced due to the water outflow. It is known that non-periodic oscillations in sea level on the West Coast of the United States are almost completely dependent upon water density in a 500-metre surface layer and that these density changes are dynamically driven.

2.3 HYDROGRAPHICAL EFFECTS

Tides propagate as long gravity waves affected by the rotation of the Earth and their particular features are determined by the depth and shape of the ocean basins. Similarly, the behaviour of storm surges in a certain region is modified by the bottom topography and coastal complexity. The adjustment required to account for rigid boundaries produces Kelvin-type waves near the coasts up to a certain distance from the shore (the Rossby radius of deformation). The most significant storm surges are produced in the coastal zone where depth-limited conditions enhance the wind forcing. As they propagate along the shore or onto the coast, they are modified by bottom topography and the coastal geometry.

Observations of tides and storm surges are limited to relatively few locations where measurements of water level can be made (for example, with tide gauges). As coastal altimetry algorithms improve, remotely sensed sea-level data may eventually provide a better observational basis, but at the present numerical modelling is the most widely used tool for understanding the relevant physical processes for storm surge.

On the scale of continental shelves, the bottom topography steers the behaviour of long gravity waves. When evaluating bathymetric datasets, the best solution is one that produces the most accurate representation of known wave systems, for example tides. Extremely shallow areas may strongly influence the circulation in complex topographies or estuaries. In all cases, the concept of the "hydrodynamic definition" of a model's bathymetry should be considered (Schwiderski, 1978). This refers to the realistic consideration of islands and coastal features that, even on a lower scale, may influence water circulation.

Drift current generated by tangential stresses of wind on a water surface does not lead to changes of level in an open sea away from coasts. Drift currents that move water masses into coastal areas can, according to the continuity equation (see Chapter 3), cause changes to surface level and, as a consequence, gradient currents. In the case of a boundless, rectilinear, open ocean coast the largest surges are observed when the wind is blowing transversely to the coastline. If the wind is blowing parallel to the coastline no significant surge will develop. In these situations, the bathymetry plays a very dominant role.

The process of cumulative water flows caused by drift and gradient currents at various wind vector orientations relative to the coastline is presented in Figure 2.2. In favourable conditions, a drift current carrying water mass in the direction transverse to

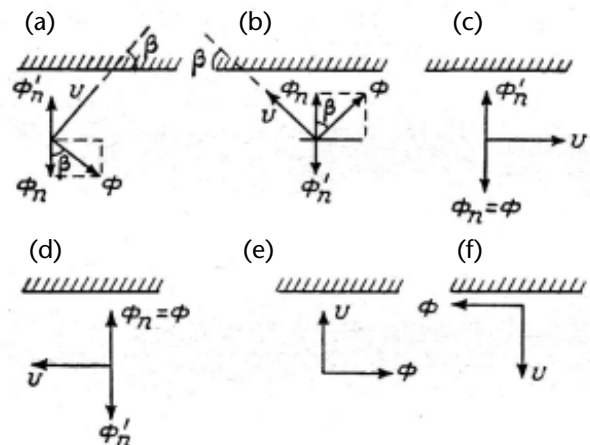


Figure 2.2. Positive and negative surge in deep water offshore

the wind action appears initially to be under the influence of the wind. If the wind is blowing at a sharp angle to a coastline, the drift flow constituent that causes positive surge/negative surge is equal to  $\Phi_n = \Phi \cos \beta$ .

The presence of the drift flow component normal to the coast line causes a slope of sea level, and hence, a geostrophic current. However, when a geostrophic current appears, frictional forces can result in a mass flow away from the coast, with an opposite direction to the original drift. If the wind and drift were to remain constant, then eventually a balance would be reached and the sea-level slope would not change (the circulation would then be in equilibrium). As depth decreases, surface drift currents become more aligned with the wind direction. This explains why the largest surges occur with the wind blowing transversely to a coastline in a shallow-water area. Current flow in a bottom boundary layer is transverse to the coastline, opposite to the wind action and dependent on the geostrophic current.

## 2.4 SEICHES

Seiches are sea-level oscillations at the resonant frequency of enclosed bodies of water. They are usually observed in long narrow bays or harbours with narrow entrances. A number of such examples can be observed on the coasts of Japan and the Kurile Islands, in the Euripus Strait (Greece), in the Bay of Algeria (Labzovsky, 1971) and on the Shan Dung Peninsula of China, where the largest oscillation reported was 2.9 metres (Wang et al., 1987) (see Figure 2.3). In some locations seiches are sufficiently well recognized that there are unique words for them in the local language or dialect. For instance, in Nagasaki Bay, where, on 31 March 1978, oscillations with amplitude of more than 4.5 metres were registered (Akamatsu, 1982), the term "abiki" is used. In the Balearic Islands the oscillations are called "rissaga" (for more detail, see 3.10) where, in Suedadela Bay on the island of Minorca, amplitudes of 3–3.5 metres in height have been observed (Gomis et al., 1993; Tintore et al., 1988). Whatever the term used, these events are routine natural disasters that can cause considerable destruction. There is evidence that the occurrence of seiches correlates with the passage of atmospheric disturbance (Gomis et al., 1993; Hibiya and Kajiura, 1982; Monserrat et al., 1991; Rabinovich, 1993; Rabinovich and Monserrat, 1996; Gonnert et al., 2001). Furthermore, Giese et al. (1990) and Chapman and Giese (1990) proposed a model explaining the appearance of seiches on the coasts of Puerto Rico due to the influence of internal tidal waves formed during spring tides. These authors suggested that a similar

mechanism may contribute to the generation of extreme seiches in other areas, including the abiki and rissaga phenomena.

The process of seiche generation in closed basins and in basins with open outer boundaries differs significantly. In the first case, the seiche excitation occurs due to outer atmospheric disturbance directly. This phenomenon is considered in detail by Wilson (1972). The excitation in many open bays and gulfs occurs in two stages. First, a long-wave disturbance is formed in the area exterior to the defined area of water; second, that disturbance causes seiche oscillations in the interior area. The most extreme examples of such exterior phenomena are tsunami waves: having appeared in the open ocean under the influence of a seismic source, on reaching coastline they cause standing oscillations in bays and gulfs. Similar processes occur with waves generated by atmospheric sources. There are three main conditions for the generation of strong seiche oscillations: first, strong long-wave disturbance is present in the outer area; second, matching of resonance frequency parameters

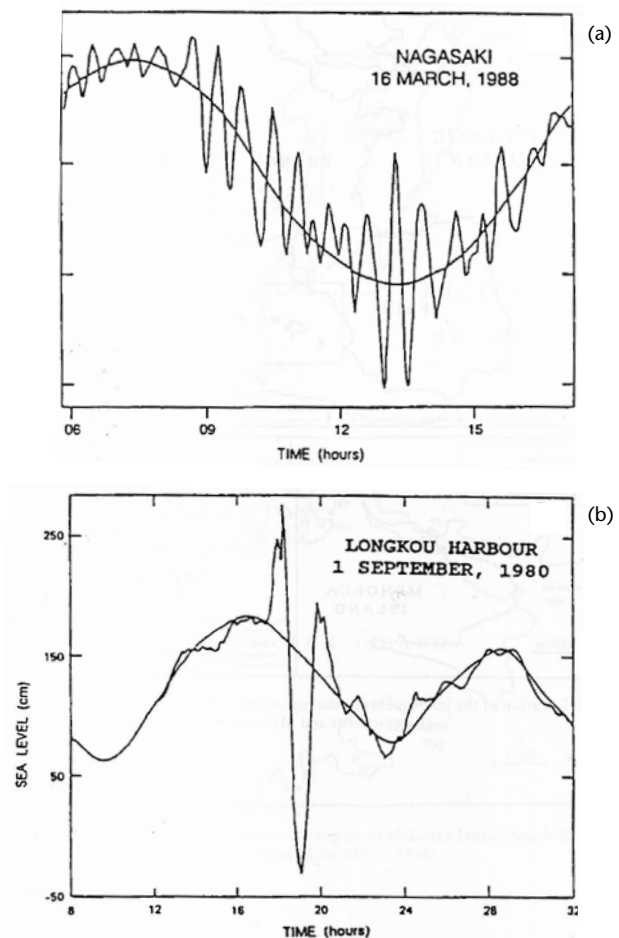
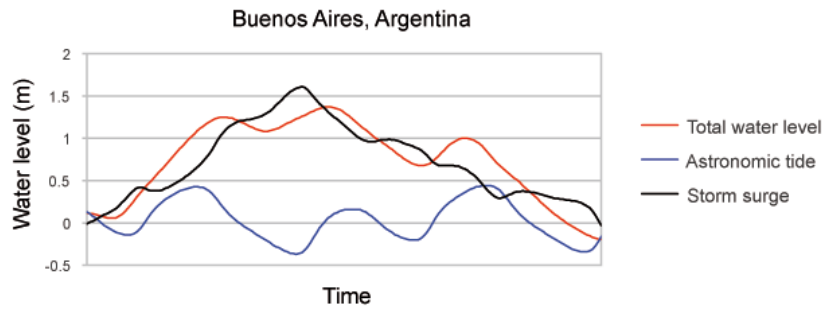


Figure 2.3. Seiche-type oscillations: (a) Nagasaki, Japan; (b) Langkou Harbour, China



**Figure 2.4. Interaction between tide and surge due to shallow water. The combined wave (red line) is advanced with respect to the normal tide (blue line). The resulting peak of the storm surge (black line) occurs during the flood tide.**

occurs between the outer and interior areas of water; third, there is low damping of the seiche in the interior area.

## 2.5 TIDE–SURGE INTERACTION

Storm surges and tidal waves interact. That is, the storm surge modifies the tide while the tidal cycle produces alterations in the storm surge. The main causes that produce these interactions are the effects of bottom friction and the variation of the wave propagation speed (which is dependent on total depth). The action of wind stress giving rise to surge is theoretically inversely proportional to depth, which varies significantly with the tide in shallow waters. Advective effects in the velocity field are also responsible for some interactions, although even in very shallow waters this is not as significant (see, for example, Gill, 1982). According to Horsburgh and Wilson (2007), the phase shift of the tidal signal represents the effect of the surge on the tide, whilst the modulation of surge production by the wind represents the effect of the tide on the surge.

Interaction in shallow water produces a phase shift of the tidal wave. A positive storm surge increases the speed of the tidal wave, so advancing the high and low tides. The result is the increase of

the non-tidal residual during the flood tide, as shown in Figure 2.4. The interaction alternately diminishes and increases the residual, especially for large tidal ranges. Many properties of the residual time series are thus an artefact of small changes in the timing of predicted high water, combined with the fact that wind stress is most effective at generating surge around low water. A better measure of storm surge is the “skew surge”, which is simply the difference between the elevation of the predicted astronomical high tide and the nearest experienced high water. It is the preferred surge diagnostic for the Dutch operational system (see, for example, de Vries et al., 1995) and is of far greater practical significance than the maximum residual. An indication of the improved statistical usefulness of skew surge over non-tidal residual is given by Howard et al. (2010).

Many authors identify bottom friction as having the largest effect on surge–tide interaction (see, for example, Tang et al., 1996). Frictional interaction is certainly very important in strong tidal or storm surge currents, or when both are of the same order of magnitude. This latter case is illustrated in Figure 2.5. After a certain time, increased friction tends to reduce the growth of the combined wave and, therefore, of the storm surge. In this case, the general effect is to delay the combined wave with respect to the predicted tide.

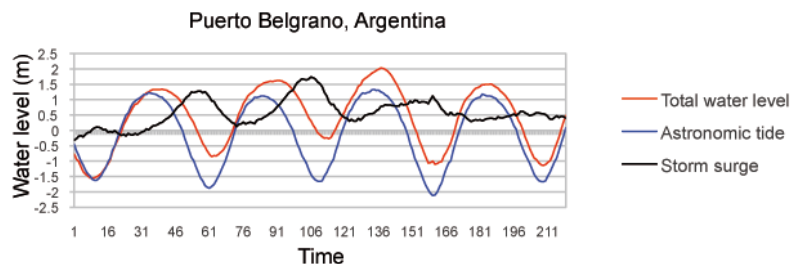


**Figure 2.5. Interaction between tide and surge due to bottom friction when surge and tidal currents are of the same order of magnitude. The combined wave (red line) is retarded with respect to the normal tide (blue line). The resulting peak of the storm surge (black line) occurs during ebb tide.**

If the local wind forcing is very strong during a short period, then peak surge generation can take place at any time, even at high water, with insufficient time for interactions to take place (see, for example, Proctor and Flather, 1989).

## 2.6 SURGE-RIVER INTERACTION

River flows can influence considerably the development of storm surge in the mouth of a river, where pronounced temperature and salinity gradients are formed at the boundary between sea and river waters. Large horizontal and vertical density gradients are characteristic features of coastal waters. Density-driven forces interact with the motion caused by external forces, forming a complicated dynamic system. Surge-river interactions have been successfully modelled within a proper mathematical formulation of motion, involving momentum, heat and salt. The detailed solutions are highly mathematical and the interested reader is referred to the literature. Articles discussing shallow-water theory include Wolzinger and Pyaskovsky (1968) and Eremeev (1974). There are also many studies based on solutions to diffusion equations (Borishansky, 1958, 1964; Filippov, 1974; Shkudova, 1974). Methods of free turbulent streams (Abramovich, 1960) were used in a paper by Vulis and Masalov (1972). Numerical models of water circulation near river mouths, taking into consideration fluid motion and thermal and ionic flow effects, are put forward in a paper by Molchanov (1976). In this paper, the dynamic and diffusive elements are connected using an equation of state.

The influence of river runoff on water-level oscillations at the open coast is relatively small. Even in the event of very large river discharge, when water level is raised by several metres in the river, the influence on sea level is quickly reduced to no more than a few tens of centimetres with increasing distance from the river mouth. Conversely, storm surge propagation into estuaries and the distance of seawater penetration along a river depends on the bottom slope of the river. If the river bed is relatively flat, storm surges can propagate upstream for tens or, in extreme cases, hundreds of kilometres, causing saline intrusions and the flooding of riverbanks.

## 2.7 INTERACTION BETWEEN SURGE, WIND WAVES AND WAVE SET-UP

The contribution of the ocean waves to the roughness of the sea surface has been extensively studied (see, for example, Donelan et al., 1993). There is a

dependence of the drag coefficient on the state of development of the waves and various approaches have been developed (Johnson et al., 1998). These findings have consequences for the modelling of transient ocean phenomena such as storm surge. Traditional approaches to the determination of surface stress used for storm surge calculations (see 2.1) consider momentum transfer to be solely and directly from the atmosphere to the surface current. In models in which the effects of atmosphere, waves and surge are combined, the wave contribution to either total surface or wave-induced stress is explicitly included. The increased roughness of the sea surface due to wave growth during the active stage of the storm can enhance momentum exchange, so that water levels vary in a more physically realistic way in such a fully coupled model. Widely used wave models can provide parameters to facilitate wave-surge coupling through the surface stress (see, for example, Janssen and Bidlot, 2003; Tolman, 2002).

When waves break on a beach they produce a rise in the mean water level. This “wave set-up” is the additional water level due to the transfer of wave-related momentum during the wave-breaking process. As waves approach the shoreline they transport both energy and momentum in the direction of wave advance. When they break, wave energy is dissipated (as turbulence) but momentum is balanced so that the slope of the sea surface in the surf zone equates to the onshore component of momentum flux. The theoretical explanation of Longuet-Higgins and Stewart (1963) demonstrates how wave set-up equilibrates the gradient in the radiation stress directed across shore (that is, the pressure gradient of the sea surface balances the gradient of the incoming momentum). The contribution of wave set-up during extreme storm events can add up to 1 metre to the sea level. It is normally difficult to distinguish by measurement wave set-up from the larger-scale storm surge, since both cause sea levels to be higher than tidal predictions and both are due to meteorological effects. However, estimates of the set-up component can be made from a numerical modelling study: Brown et al. (2011) ran a fully coupled wave-surge model and then repeated the forcing without the radiation stress coupling. They were thus able to isolate wave set-up.

## 2.8 INFLUENCE OF SEA ICE ON STORM SURGES

The influence of sea ice on sea-level oscillations has not received a great deal of attention from storm surge modellers. Ice cover leads to considerable energy dissipation and acts as a barrier to the

meteorological forcing of the water mass. Some important effects of ice cover on the propagation of long waves include:

- The appearance of a sub-ice frictional boundary layer;
- The reflection of long waves from the ice–water interface, with energy loss due to elastic deformation;
- The decrease of long-wave speed, and damping as they propagate under the ice.

Drifting ice cover can alter the behaviour of surface currents in the Ekman layer and can also influence storm surge development and propagation. Floating ice has a weaker damping influence on waves than fast ice. Ice cover may not remain constant during a storm surge forecasting period, but in most cases it is possible to neglect thermal changes of ice cover when modelling short periods (of up to five days). Floe sizes are not explicitly taken into account in storm surge models, but it is advisable for the numerical grid size to be chosen such that it is significantly larger than the ice floes. Typical floe sizes vary greatly with the season. During the Arctic summer they can be from metres to kilometres in size, while consolidated floating ice with sizes from tens of metres up to 2 kilometres prevail in winter.

Ice cover parameters in surge models need to reflect the proportions of fast and drifting ice. Dissipation of long-wave energy under drifting ice is negligible. However, fast ice exerts considerable damping on long waves (so lessening storm surge height), reducing both phase speed and wave amplitude. The degree of influence on storm surges is determined by the fast-ice area and thickness. Locally, extremes of perturbation of sea level tend to occur at the boundary between fast and drifting ice. Practical ways of incorporating these effects into storm surge models include changing the configurations of calculation areas and altering the bed friction coefficient for fast-ice cells.

Ice concentration, its thickness and the variation of thickness (hummocking) determine the effective wind stress acting on the sea surface. Stress at the sea surface can be considered a simple combination of the stresses in the ice-covered and ice-free areas:

$$\bar{\tau}^s = (1 - C)\bar{\tau}^a + C\bar{\tau}^w \quad (2.7)$$

where:

$C$  = an ice concentration function (from zero to one);

$\bar{\tau}^a$  = stress at the air–sea interface;

$\bar{\tau}^w$  = stress at the ice–sea interface.

Stresses can be derived using the quadratic approach of Equation (2.6), and various papers

suggest typical values for the coefficient of friction. An average value for even ice is  $1.7 \times 10^{-3}$  and for hummocked ice  $2.2 \times 10^{-3}$ . Thus, the coefficient of wind friction on even ice is approximately equal to its value for the air–sea interface and it is approximately 1.5 times higher for hummocked ice. Ice thickness exerts considerable influence on the speed of drifting ice, with thick ice moving slower than thin ice under the influence of the same forces.

The main source of information about spatial distributions of ice concentration, its thickness and hummocking, is an ice map. Ice information is typically summarized from several sources for a particular period. Ice-cover parameters indicated in a map are gridded and then represented in a numerical model by their modal or average values within a grid cell. In many ice maps the development stage of the ice is used as a proxy for ice thickness. The following table presents general thicknesses corresponding to the developmental stage of the ice, which can be used as a rule-of-thumb guide.

**Approximate thicknesses of ice for different stages of development (centimetres)**

| <i>Developmental stage of ice</i> | <i>Thickness</i> |
|-----------------------------------|------------------|
| New ice                           | 3                |
| Nilas                             | 8                |
| Grey ice                          | 12               |
| Grey-white ice                    | 22               |
| Thin first-year ice               | 50               |
| Medium first-year ice             | 100              |
| Thick first-year ice              | 180              |
| Second-year ice                   | 250              |
| Multi-year ice                    | 300              |

The influence of ice cover on storm surges was studied by Belsky (1954), Skriptunov and Gan (1964) and Freidson et al. (1960). Their results demonstrate the impact of ice on surge magnitude. For example, surge height in the mouth of the Neva River in the ice-free period is generally greater than in the ice period. Mustafin (1970) also found that fast ice changes the formation and propagation of storm surges, shielding the water mass from the direct influence of the wind. Changes to sea level under fast ice are due to external long waves propagating under it and the energy of these oscillations is decreased due to friction both at the bed and the lower surface of the ice.

Various numerical models dealing with the influence of ice cover on water-level oscillations have

been developed by Sheng and Lick (1972), Liland (1975), Henry (1975), Lisitzin (1973, 1974), Murty and Polavarapu (1979), Murty et al. (1981) and Murty and Holloway (1985). This body of work shows that the influence of ice cover on storm surges is complex: ice cover can reduce the amplitude of positive surges while not influencing the amplitude of the negative surges. More advanced numerical models taking into account the full dynamic interaction between the ice cover and storm surges have been developed by Henry and Heaps (1976), Drabkin and Pomeranets (1978), Kowalik (1984), Johnson and Kowalik (1986), Gudkovich and Proshutinsky (1988), Proshutinsky (1993), Ashik (1995) and Ashik and Larionova (2003). Noteworthy features of these models include the incorporation of correction, due to ice, of the surface-wind stresses, of the shielding effect of the ice cover and of the three-dimensional nature of the problem, including the dynamics of the sub-ice layer.

Statistical methods relating storm surge amplitudes to ice cover have been developed by Kuprianova and Freidson (1977, 1981), Kuprianova and Tretyakova (1981), Proshutinsky and Uranov (1985) and Freidson et al. (1960). The drawback of statistical models is that they are relevant only to that local area for which they were developed and it is difficult to apply them to other areas.

## 2.9 BOTTOM FRICTION

Where fluid flow occurs along a rigid boundary such as the sea bed, the viscous influence on flow is usually concentrated in a boundary layer. This frictional layer needs to be correctly represented in numerical models (friction on lateral boundaries is usually neglected in numerical storm surge models).

One of two approaches is normally used to treat bottom friction. In the so-called "no-slip condition", horizontal components of flow at the sea bed ( $u_b$  and  $v_b$ ) are taken to be zero:

$$u_b = v_b = 0 \quad (2.8)$$

More commonly, in the "slip condition", the stress at the bottom boundary layer is assumed to depend in some way on flow speed near the bed. A linear relationship is occasionally employed but the most widely used approach is a quadratic parameterization (see, for example, Wolzinger and Pyaskovsky, 1968, 1977) of the following form:

$$\tau^b = k_1 \frac{U|U|}{H^2} \quad (2.9)$$

where:

$U$  = the near-bed current speed;

$H$  = the total water depth.

The coefficient  $k_1$  normally takes a value in the range from  $2.0 \times 10^{-3}$  to  $3.0 \times 10^{-3}$  (see, for example, Proshutinsky, 1993) and it has been shown that there is a weak dependence of the surge height on the value of this coefficient.

More complex functional relationships for bed friction have been explored (Kazakov, 1976):

$$\tau^b = f\left(\frac{\partial \xi}{\partial x}, \frac{\partial \xi}{\partial y}; \tau_x^s; \tau_y^s; H\right) \quad (2.10)$$

The more complicated formulation given by Equation (2.10) was shown to have some advantage in a series of channel flow experiments. Achieving the most effective empirical bottom friction parameterization is a key factor in the tuning process of any model.

## CHAPTER 3

### BASIC EQUATIONS AND SOLUTIONS

#### 3.1 FORMULATION OF THE STORM SURGE EQUATIONS

We will first consider the storm surge equations most commonly used, following Welander (1961). It is assumed that the water is homogeneous and incompressible, and that as a cause of friction, vertical shear is much more important than horizontal. Then the equations of motion in a right-handed Cartesian coordinate system can be written as follows:

$$\frac{\partial u}{\partial t} + u \frac{\partial u}{\partial x} + v \frac{\partial u}{\partial y} + w \frac{\partial u}{\partial z} - f v = -\frac{1}{\rho_0} \frac{\partial P}{\partial x} + \frac{1}{\rho_0} \frac{\partial \tau_x}{\partial z} \quad (3.1)$$

$$\frac{\partial v}{\partial t} + u \frac{\partial v}{\partial x} + v \frac{\partial v}{\partial y} + w \frac{\partial v}{\partial z} + f u = -\frac{1}{\rho_0} \frac{\partial P}{\partial y} + \frac{1}{\rho_0} \frac{\partial \tau_y}{\partial z} \quad (3.2)$$

$$\frac{\partial w}{\partial t} + u \frac{\partial w}{\partial x} + v \frac{\partial w}{\partial y} + w \frac{\partial w}{\partial z} = -\frac{1}{\rho_0} \frac{\partial P}{\partial z} - g \quad (3.3)$$

The continuity equation is:

$$\frac{\partial u}{\partial x} + \frac{\partial v}{\partial y} + \frac{\partial w}{\partial z} = 0 \quad (3.4)$$

where:

- $u, v, w$  = velocity fields in the  $x, y,$  and  $z$  directions;
- $f$  = the Coriolis parameter;
- $g$  = gravity;
- $\rho_0$  = the uniform density of water;
- $P$  = pressure;
- $\tau_x$  and  $\tau_y$  = the  $x$  and  $y$  components of the frictional stress.

With reference to the origin of the coordinate system located at the undisturbed level of the free surface ( $z = 0$ ), the free surface can be denoted by  $z = h(x, y, t)$  and the bottom by  $z = -D(x, y)$ . Let  $\tau_{sx}$  and  $\tau_{sy}$  denote the tangential wind stress components and let  $P_a$  be the atmospheric pressure on the water surface. Then the following boundary conditions must be satisfied. At the free surface  $z = h$ :

$$\tau_x = \tau_{sx}, \quad \tau_y = \tau_{sy} \quad (3.5)$$

$$P = P_a \quad (3.6)$$

Since the free surface has to follow the fluid, an additional condition is required, given by:

$$\frac{\partial h}{\partial t} + u \frac{\partial h}{\partial x} + v \frac{\partial h}{\partial y} = w, \text{ at } z = h \quad (3.7)$$

At the bottom, all the velocity components have to vanish. Thus:

$$u = v = w = 0, \quad \text{at } z = -D \quad (3.8)$$

The traditional storm surge equations are derived by performing two operations of vertical integration and linearization. To perform the vertical integration, the  $x$  and  $y$  components of horizontal transport are defined as follows:

$$M \equiv \int_{z=-D}^h u dz \quad \text{and} \quad N \equiv \int_{z=-D}^h v dz \quad (3.9)$$

The pressure terms can be evaluated as follows:

$$\frac{\partial P}{\partial x} = g \rho_0 \frac{\partial h}{\partial x} + \frac{\partial P_a}{\partial x} = 0 \quad (3.10)$$

Following vertical integration, this gives:

$$\int_{-D}^h \frac{\partial P}{\partial x} dz \sim g \rho_0 D \frac{\partial h}{\partial x} + D \frac{\partial P_a}{\partial x} \quad (3.11)$$

Note that, here,  $h$  relative to  $D$  is ignored, which is consistent with the above approximation.

$$\frac{\partial M}{\partial t} - f N = -g D \frac{\partial h}{\partial x} - \frac{D}{\rho_0} \frac{\partial P_a}{\partial x} + \frac{1}{\rho_0} (\tau_{sx} - \tau_{bx}) \quad (3.12)$$

$$\frac{\partial N}{\partial t} + f M = -g D \frac{\partial h}{\partial y} - \frac{D}{\rho_0} \frac{\partial P_a}{\partial y} + \frac{1}{\rho_0} (\tau_{sy} - \tau_{by}) \quad (3.13)$$

$$\frac{\partial h}{\partial t} + \frac{\partial M}{\partial x} + \frac{\partial N}{\partial y} = 0 \quad (3.14)$$

For convenience, hereafter the subscript on the density field will be omitted.

In these linear storm surge prediction equations, the dependent variables are the transport components  $M$  and  $N$  and the water level  $h$ . The forcing functions are the atmospheric pressure gradients given by  $\partial P_a / \partial x$  and  $\partial P_a / \partial y$  and the wind stress components  $\tau_{sx}$  and  $\tau_{sy}$ . The retarding force is the bottom stress. At this stage, there are more unknowns than the available equations. To obtain a closed system of equations, the bottom stresses in Equations (3.12) and (3.13) must be expressed (parameterized) in terms of known variables such as the current speed (see 2.9).

### 3.2 FINITE DIFFERENCING OF THE TIME DERIVATIVE

The time derivative terms in the storm surge equations are derivatives of the horizontal transport components  $M$  and  $N$  in the momentum equations, together with the time derivative of the free surface height  $h$  in the continuity equation. Since the terms  $\partial M/\partial t$ ,  $\partial N/\partial t$ , and  $\partial h/\partial t$  all have the same form, discussion will be based on a general relationship of the following form:

$$\frac{\partial U}{\partial t} = F(U, t), U = U(t) \quad (3.15)$$

In this section, liberal use will be made of the works of Mesinger and Arawaka (1976) and Simons (1980), in which more mathematical detail can be found.

Several time-differencing schemes are available and we begin with two-level schemes without iteration, the Euler (or forward), backward and trapezoidal schemes. In the Euler scheme, the time derivative is approximated as:

$$U_{n+1} = U_n + \Delta t \cdot F_n \quad (3.16)$$

$$F_n = F(U_n)$$

This is a first-order, accurate scheme with a truncation error of zero ( $\Delta t$ ) and it is an uncentred scheme because  $F$  is not centred in time.

In the backward scheme:

$$U_{n+1} = U_n + \Delta t \cdot F_{n+1} \quad (3.17)$$

$$F_{n+1} = F(U_{n+1})$$

This scheme, as written here, is implicit, because  $F$  depends on  $U_{n+1}$ , which must be determined. In the case of partial differential equations, this will require iteration because a set of simultaneous equations (one for each grid point) must be solved. The truncation error of this scheme is also of zero ( $\Delta t$ ).

In the trapezoidal scheme:

$$U_{n+1} = U_n + \frac{1}{2}\Delta t(F_n + F_{n+1}) \quad (3.18)$$

As can be seen, this is also an implicit scheme, but its truncation error is of zero ( $\Delta t$ )<sup>2</sup>.

Next, two iterative schemes will be discussed, still involving only two time levels. In the Matsuno or Euler backward scheme, the first step is the regular Euler scheme:

$$U_{(n+1)*} = U_n + \Delta t \cdot F_n \quad (3.19)$$

This value of  $U_{(n+1)*}$  is used to determine  $F_{(n+1)*}$ , through:

$$F_{(n+1)*} = F(U_{(n+1)*}) \quad (3.20)$$

This value of  $F_{(n+1)*}$  is used in a backward step to compute  $U_{n+1}$ :

$$U_{n+1} = U_n + \Delta t \cdot F_{(n+1)*} \quad (3.21)$$

As can be seen, this is a first-order accurate scheme and is explicit.

The Heun scheme is a development of the trapezoidal scheme and can be expressed as follows:

$$U_{(n+1)*} = U_n + \Delta t \cdot F_n \quad (3.22)$$

$$U_{n+1} = U_n + \Delta t/2 (F_n + F_{(n+1)*})$$

This is also an explicit scheme, but is of second-order accuracy.

The alternate direction implicit (ADI) method, described by Stelling (1984), is a two-step method with:

$$U_{n+\frac{1}{2}} = U_n + \frac{1}{2}\Delta t \cdot F_{n+\frac{1}{2}}^* \quad (3.23)$$

$$U_{n+1} = U_{n+\frac{1}{2}} + \frac{1}{2}\Delta t \cdot F_{n+1}^*$$

where  $F_{n+\frac{1}{2}}^*$  has taken the partial derivative  $\partial/\partial x$  at  $t + \frac{1}{2}\Delta t$  and the derivative  $\partial/\partial y$  in  $t$ , and  $F_{n+1}^*$  has taken the partial derivative  $\partial/\partial x$  at  $t + \frac{1}{2}\Delta t$  and the derivative  $\partial/\partial y$  in  $t + \Delta t$ . Hence, the first step is implicit in  $x$  and the second step implicit in  $y$ .

The method is second-order and unconditionally stable. The equations reduce to a tridiagonal matrix and can be efficiently solved, which makes it attractive for storm surge models.

The most common three-level scheme is the leap-frog scheme (also called the midpoint rule or step-over rule). This is second-order accurate and is given as:

$$U_{n+1} = U_{n-1} + 2\Delta t \cdot F_n \quad (3.24)$$

Another scheme, referred to as the Milne-Simpson scheme, involves fitting a parabola to the values of  $F_{n-1}$ ,  $F_n$  and  $F_{n+1}$ , which will lead to an implicit scheme. Young (1968) discussed 13 time-differencing schemes. A discussion on the conservation of the energy of low-frequency waves in iterative time integration schemes is given in Kondo et al. (1982).



**3.3 COMPUTATIONAL STABILITY AND CFL CRITERION**

The storm surge Equations (3.12)–(3.14) are transformed into finite difference forms before numerical integration can begin. However, the time step chosen for the computation must obey the so-called Courant-Friedrichs-Lewy (CFL) criterion, otherwise the computation will become unstable. The formal derivation of the CFL stability criterion for integration in time is as follows. Assuming a constant advecting velocity  $c$ , the equations of motion and continuity for the one-dimensional case are:

$$\frac{\partial u}{\partial t} + c \frac{\partial u}{\partial x} + g \frac{\partial h}{\partial x} = 0 \tag{3.25}$$

$$\frac{\partial h}{\partial t} + c \frac{\partial h}{\partial x} + D \frac{\partial u}{\partial x} = 0$$

where:

$D$  = the uniform water depth;

$h$  = the free surface height.

The second part of Equation (3.27) is multiplied by an arbitrary parameter  $\lambda$ , and to this is added the result to the Equation (3.25), to give:

$$\frac{\partial}{\partial t}(u + \lambda h) + (c + \lambda D) \frac{\partial u}{\partial x} + (g + \lambda c) \frac{\partial h}{\partial x} = 0 \tag{3.26}$$

Following Mesinger and Arakawa (1976),  $\lambda$  is chosen so that:

$$\frac{g + \lambda c}{c + \lambda D} = \lambda \tag{3.27}$$

This gives:

$$\lambda = \pm \sqrt{\frac{g}{D}} \tag{3.28}$$

Substitution of Equation (3.30) into Equation (3.28) gives:

$$\left[ \frac{\partial}{\partial t} + \left( c + \sqrt{gD} \frac{\partial}{\partial x} \right) \right] \left[ u + \sqrt{\frac{g}{D}} h \right] = 0 \tag{3.29}$$

$$\left[ \frac{\partial}{\partial t} + \left( c - \sqrt{gD} \frac{\partial}{\partial x} \right) \right] \left[ u - \sqrt{\frac{g}{D}} h \right] = 0$$

Equation (3.29) implies that the parameter  $(u + \sqrt{g/D} h)$  is advected with a velocity of  $c + \sqrt{g/D}$  and that the parameter  $(u - \sqrt{g/D} h)$  is advected with a velocity of  $c - \sqrt{g/D}$ , both in the positive  $x$  direction. Using a leapfrog scheme the following stability criterion is obtained:

$$(c + \sqrt{gD}) \frac{\Delta t}{\Delta x} \leq 1 \tag{3.30}$$

which is referred to as the CFL condition. As usual (in the atmosphere),  $c$  is an order of magnitude less than the phase speed of external gravity waves and is therefore often neglected, to give:

$$\sqrt{gD} \frac{\Delta t}{\Delta x} < 1 \tag{3.31}$$

In the two-dimensional case, assuming that  $\Delta y = \Delta x$ , it can be shown that the stability condition is:

$$\sqrt{2gD} \frac{\Delta t}{\Delta x} < 1 \tag{3.32}$$

The parameter  $(\sqrt{2g/D} \Delta t / \Delta x)$  is referred to as the Courant number.

**3.4 STAGGERED AND NON-STAGGERED GRID SCHEMES**

In many numerical solutions the physical variables (for example, current, transport and sea-level elevation) are staggered in space on the grid (see Figure 3.1). Away from the boundaries, central differencing is the most convenient manner of space discretization. At or near lateral boundaries, special attention is required. It is possible to place fictitious points outside the boundary or use one-sided difference schemes. One of the simplest central difference schemes is shown in Figure 3.1(a). However, this scheme is not convenient for the evaluation of either the advective or the Coriolis

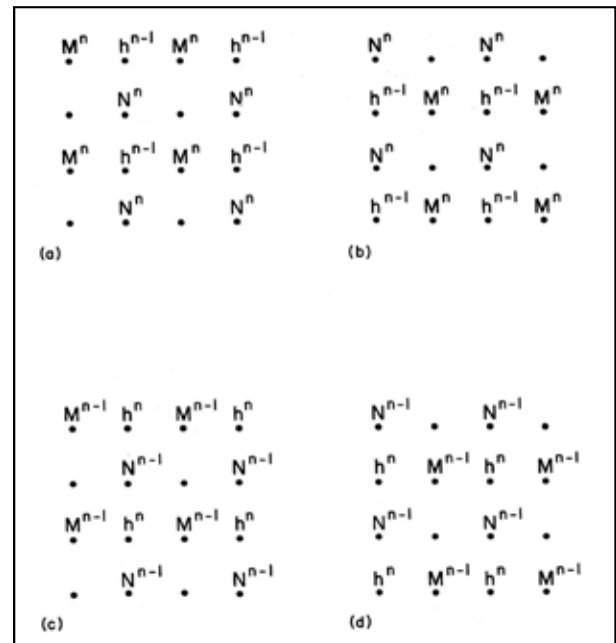


**Figure 3.1. Various grids staggered in time and space for the central difference scheme: (a) basic scheme; (b) space supplement of (a); (c) time supplement of (a); (d) space–time supplement of (a). Superscript n denotes the time step.**

terms. For convenient evaluation of these terms, multiple-lattice grids have been used. Simons (1980) suggested coupling the grid in Figure 3.1(a) with its space supplement (Figure 3.1(b)), its time supplement (Figure 3.1(c)), or its space-time supplement (Figure 3.1(d)). Note that the scheme in Figure 3.1(d) corresponds to the conjugate lattice developed by Platzman (1963).

In double-lattice grids, both of the transport variables are defined at the same location, which leads to a combination of conjugate lattices in Figure 3.1(a) and (d) as originally proposed by Eliassen (1956). Lilly (1961) used a time interpolation for the Coriolis terms for the space-supplemental lattices in Figure 3.1(a) and (d). Single-lattice grids are useful in situations in which Coriolis terms and non-linear advective terms are not important. For larger bodies of water in which rotational effects are important, the truncation errors due to spatial averaging on a single lattice need to be reduced.

It is possible to form double-lattice grids by combining the space-supplemental lattices in Figure 3.1(a) and (b) or the conjugate lattices in Figure 3.1(a) and (d) (Simons, 1980). The spatial representation of either of these is the same and is shown in Figure 3.2(a). The chief advantage of a double-lattice grid over a single-lattice grid is that no spatial averaging will be required for most of the terms in the equations of motion and continuity. The main

drawback of such a grid is that the surface gravity waves travel independently in each lattice and the lattices can become decoupled progressively with time. The Coriolis and non-linear advective terms will tend to keep the two lattices coupled. However, as was shown by Platzman (1958), some spurious results may be obtained in addition to computational instability.

The phenomenon of grid dispersion can become quite a serious hindrance in calculations with double-lattice grids, and various spatial smoothing operators have been developed. An alternative to space smoothing is the introduction of an artificial viscosity that operates in a similar manner to a horizontal eddy diffusion of momentum (Obukhov, 1957). Another attempt to couple the two lattices has been made through the rotation of the basic coordinate system to give a new system,  $x_r$  and  $y_r$  (see Figure 3.2(b)) followed by evaluation of the Laplacian operator for diffusion along the rotated coordinates (see, for example, Simons, 1980).

Several authors (see, for example, Lauwerier, 1962; Leith, 1965; Heaps, 1969) have used rotated coordinates and evaluated all the derivatives in the relevant equations along these coordinates. However, it should be pointed out that any improvements in the elimination of grid dispersion is due not only to the evaluation of all the derivatives along the rotated coordinates but also to the orientation of the grid relative to the boundaries of the water body.

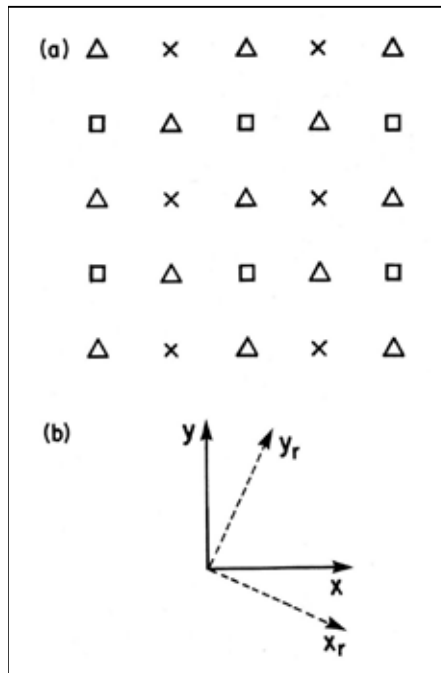


Figure 3.2. (a) Double-lattice grid;  $\Delta$ : locations where the transport components,  $M$  and  $N$ , are defined;  $\times$ : surface height field belonging to one lattice;  $\square$ : surface height field belonging to a second lattice. (b) Rotated coordinates

### 3.5 TREATMENT OF THE NON-LINEAR ADVECTIVE TERMS

This section serves as a complete example of how to discretize the non-linear transport equations. It is based on the form of governing equations used by Crean (1978):

$$\frac{\partial M}{\partial t} + \frac{\partial}{\partial x} \left( \frac{M^2}{H} \right) + \frac{\partial}{\partial y} \left( \frac{MN}{H} \right) - fN + v_H \left( \frac{\partial^2 M}{\partial x^2} + \frac{\partial^2 M}{\partial y^2} \right) + gH \frac{\partial h}{\partial x} + \frac{KM\sqrt{M^2 + N^2}}{H^2} = 0 \quad (3.33)$$

$$\frac{\partial N}{\partial t} + \frac{\partial}{\partial x} \left( \frac{MN}{H} \right) + \frac{\partial}{\partial y} \left( \frac{N^2}{H} \right) + fM + v_H \left( \frac{\partial^2 N}{\partial x^2} + \frac{\partial^2 N}{\partial y^2} \right) + gH \frac{\partial h}{\partial y} + \frac{KN\sqrt{M^2 + N^2}}{H^2} = 0 \quad (3.34)$$

$$\frac{\partial h}{\partial t} + \frac{\partial M}{\partial x} + \frac{\partial N}{\partial y} = 0 \quad (3.35)$$

where:

$H = D + h$ , the total water depth;  
 $D$  = the undisturbed water depth;

$K$  = a bottom friction coefficient;  
 $\nu_H$  = the horizontal eddy viscosity.

The grid is similar to that used by Flather and Heaps (1975) and Hansen (1962).

The finite difference form for the  $x$ -momentum equation is the following:

$$\begin{aligned} \frac{(M_{j,n+1} - M_{j,n})}{\Delta t} = & \bar{f}\bar{N}_{j,n} - \frac{g\bar{H}_j^x}{\Delta S}(h_{j+1,n+1} - h_{j,n+1}) - \frac{KM_{j,n}(M_{j,n}^2 + \bar{N}_{j,n}^2)^{1/2}}{(\bar{H}_j^x)^2} \\ & - \left[ \frac{(\bar{M}_{j,n}^x)^2}{2(\bar{H}_j^x + \bar{H}_{j+1}^x)} - \frac{(\bar{M}_{j-1,n}^x)^2}{2(\bar{H}_{j-1}^x + \bar{H}_j^x)} \right] \frac{1}{\Delta S} - \left( \frac{\bar{M}_{j,n}^y \bar{N}_{j-m,n}^x}{\bar{H}_j} - \frac{\bar{M}_{j+m,n}^y \bar{N}_{j,n}^x}{\bar{H}_{j-m}} \right) \frac{1}{\Delta S} \\ & + \frac{\nu_H}{(\Delta S)^2} (M_{j-m,n} + M_{j+m,n} + M_{j-1,n} + M_{j+1,n} - 4M_{j,n}) \end{aligned} \quad (3.36)$$

The finite difference form for the  $y$ -momentum equation is:

$$\begin{aligned} \frac{(N_{j,n+1} - N_{j,n})}{\Delta t} = & -\bar{f}\bar{M}_j - \frac{g\bar{H}_j^y}{\Delta S}(h_{j,n+1} - h_{j-m,n+1}) - KN_{j,n}(\bar{M}_{j,n}^2 + N_{j,n}^2)^{1/2} / (\bar{H}_{j,m}^y)^2 - \\ & \left( \frac{\bar{M}_{j+m,n}^y \bar{N}_{j,n}^x}{\bar{H}_{j+m}} - \frac{\bar{M}_{j-m-1,n}^y \bar{N}_{j-1,n}^x}{\bar{H}_{j-m-1}} \right) \frac{1}{\Delta S} \left[ \frac{(\bar{N}_{j,n}^y)^2}{2(\bar{H}_j^y + \bar{H}_{j+m}^y)} - \frac{(\bar{N}_{j+m,n}^y)^2}{2(\bar{H}_{j+m}^y + \bar{H}_{j+2m}^y)} \right] \frac{1}{\Delta S} \\ & + \frac{\nu_H}{(\Delta S)^2} (N_{j-m,n} + N_{j+m,n} + N_{j-1,n} + N_{j+1,n} - 4N_{j,n}) \end{aligned} \quad (3.37)$$

where:

$$\bar{M}_j^x = \frac{1}{2}(M_j + M_{j+1})$$

$$\bar{M}_j^y = \frac{1}{2}(M_j + M_{j-m})$$

$$\bar{H}_j = \frac{1}{4}(H_j + H_{j-m} + H_{j-m+1} + H_{j+1}) \quad (3.38)$$

$$\bar{M}_j = \frac{1}{4}(M_j + M_{j+m} + M_{j+m-1} + M_{j-1}) \quad (3.39)$$

$$\bar{N}_j = \frac{1}{4}(N_j + N_{j-m} + N_{j-m+1} + N_{j+1}) \quad (3.40)$$

The finite difference form for the continuity equation is given by:

$$\frac{(h_{j,n+1} - h_{j,n})}{\Delta t} = - \frac{(M_{j,n} - M_{j-1,n} + N_{j-m,n} - N_{j,n})}{\Delta S} \quad (3.41)$$

The stability criterion (CFL condition) is given by:

$$t \leq \frac{\Delta S}{\sqrt{2gH_{\max}}} \quad (3.42)$$

### 3.6 TREATMENT OF OPEN BOUNDARIES

Setting the surface elevation to zero at the boundary of open sea is not satisfactory because this amounts to perfect reflection at the boundary. A better approximation (see Heaps, 1974; Henry and Heaps, 1976) is to assume that all outward-travelling waves are normal to the boundary and to calculate the volume transports  $M$  (or  $N$ ) from the water level  $h$  at the nearest interior grid point, that is  $M = [g(D + h)]h^{1/2}$ . This is the so-called radiation condition. Bode and Hardy (1997), while giving a detailed review of open boundary conditions, conclude that, in spite of the effort devoted to the development of artificial open boundary conditions, model studies show that the ideal way to minimize the problem is to use as large a domain as possible.

### 3.7 TREATMENT OF COMPLEX COASTAL BOUNDARIES

Finite element models with irregular triangular grids are now the preferred way of dealing with complex coastal boundaries. Before finite element models began to be used routinely, a variety of other methods were used: nested and multiple grids, boundary-fitted coordinates, stretched

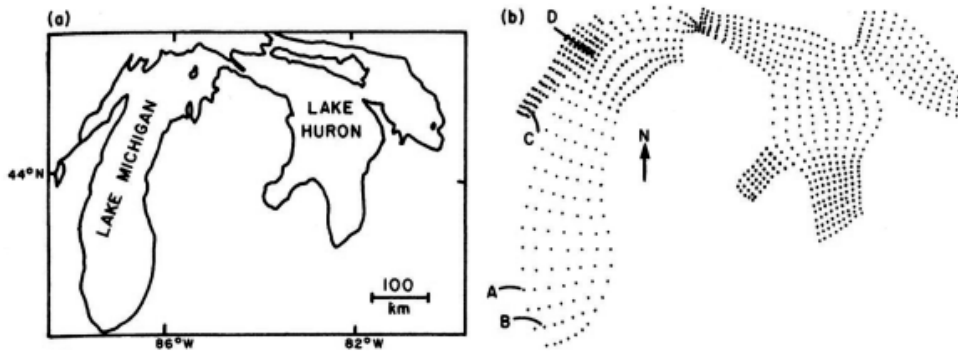


Figure 3.3. (a) Basins of Lakes Michigan and Huron joined at the straits of Mackinac. (b) Curvilinear mesh for the basins of Lakes Michigan and Huron. Note that the North Channel has been excluded. Points A, B, C, and D are special locations where observations were available to compare to theoretical results.

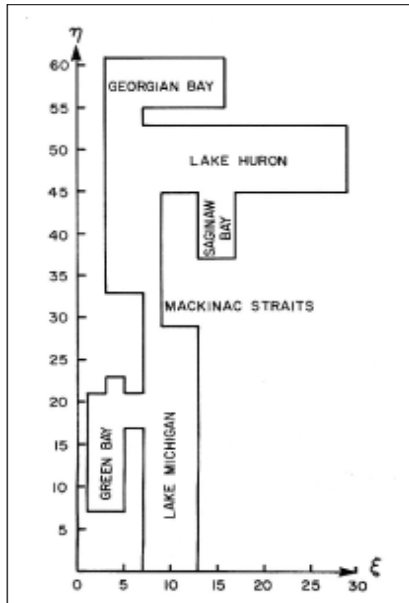


Figure 3.4. Basins of Lakes Michigan and Huron as arranged on the planes  $\xi$  and  $\eta$

coordinates and transformed grid systems. Birchfield and Murty (1974) used a system of stretched coordinates to study wind-generated circulation in the combined systems of Lake Michigan, the Straits of Mackinac and Lake Huron.

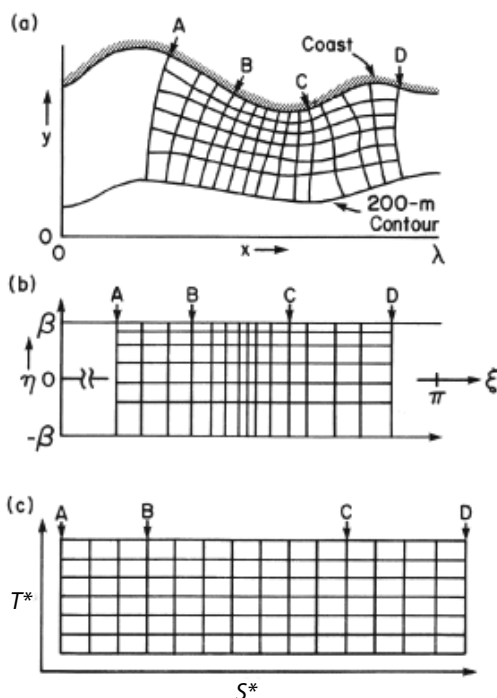


Figure 3.5. (a) The  $(x, y)$  space to be mapped by the transformation equations given in the text. (b) The transformed system represented in the  $(\xi, \eta)$  space. (c) The  $(\xi, \eta)$  space transformed to  $(S^*, T^*)$  space

Source: Reid et al., 1977

The system studied is shown in Figure 3.3(a) and the curvilinear grid used is shown in Figure 3.3(b). The curvilinear grid is mapped onto a plane in which the irregular basin is transformed into a series of connected rectangles, shown in Figure 3.4. An equally spaced grid was used in the connected rectangle system allowing all the calculations to be performed conveniently.

Reid et al. (1977) developed a transformed stretched-coordinate system to calculate storm surges on a continental shelf, illustrated in Figure 3.5(a)–(c). The principle underlying this scheme is to find a transformation involving mapping relations to maintain the orthogonality and to make sure that the new independent variables  $\xi$  and  $\eta$  are continuous monotonic functions of the original independent variables  $x$  and  $y$ . Furthermore, the transformation must map the coastline and seaward boundaries as isolines of the curvilinear coordinate  $\eta$ . A point  $(x, y)$  on the  $z$ -plane will be transformed to point  $(\xi, \eta)$  in a rectangular region on the  $\zeta$ -plane and will satisfy the above conditions provided the mapping relation is conformal.

### 3.8 MOVING-BOUNDARY MODELS, INCLUSION OF TIDAL FLATS AND COASTAL INUNDATION

Moving-boundary models allow for the wetting and drying of beaches and intertidal areas. Good numerical schemes for wetting and drying are essential if storm surges are to be correctly forecast in low-lying coastal areas. Reid and Bodine (1968) developed a technique for the inclusion of tidal flats that allowed for the flooding of dry land and submerged barriers. Empirical formulae based on the concept of flow over weirs were applied to storm surges in Galveston Bay, Texas, United States.

Leendertse (1970) and Leendertse and Gritton (1971) developed an alternating direction-implicit technique for wetting and drying tidal flats, with application to Jamaica Bay, New York. In this model, the boundary moves along grid lines in discrete steps. However, the condition for a dry area is more stringent than simply zero local water depth in order to suppress computational noise due to the moving boundary. Other works that dealt with this problem are those of Ramming (1972), Abbott et al. (1973), Backhaus (1976), Runchal (1975) and Wanstrath (1977, 1978).

Flather and Heaps (1975) created a wetting–drying scheme that took account of the local water depth and the slope of the sea surface. They found that using the sea surface slope suppressed unrealistic movements of the boundary. As in the models

developed by Reid and Bodine, and Leendertse and Gritton, cited above, the water-land boundary followed grid lines in discrete time steps. Before the calculation of currents  $u$  and  $v$  in the  $x$  and  $y$  directions, at each time step each grid point was tested to see if it was wet (that is, if water depth was positive) or dry (zero water depth). If the point was dry, then the current was prescribed as zero. For wet points,  $u$  and  $v$  were computed from the relevant equations.

Sielecki and Wurtele (1970) developed a moving-boundary scheme in which the lateral boundary of the fluid is determined as a part of the solution. They tested the validity of their scheme by comparing the results of some simple numerical experiments to the results from analytical solutions. Their scheme combined three different methods, namely the Lax-Wendroff scheme (Lax and Wendroff, 1960) as modified by Richtmeyer and Morton (1963), the principle of energy conservation as formulated by Arakawa (1966) and the quasi-implicit character of the difference equations. Comparative studies have been reported on modelling under fixed- or moving-boundary conditions, for example as reported by Yeh and Chou (1979) (Figure 3.6).

For some more recent work on wetting-drying techniques, the reader is referred to Flather and Huppert (1990) and Bolzano (1998).

### 3.9 UNSTRUCTURED GRIDS (FINITE ELEMENT AND FINITE VOLUME MODELS)

#### 3.9.1 Finite element methods

Brebbia and Partridge (1976) studied the tides and storm surges of the European shelf in the North Sea using finite element models based on vertically integrated equations and including tides, wind stress, atmospheric pressure gradients, bottom friction, Coriolis force and advective terms.

To develop the finite element model, the horizontal momentum equations and the continuity equation, together with their boundary conditions, are written in the following weighted-residual manner:

$$\iint \left( \frac{\partial u}{\partial t} + u \frac{\partial u}{\partial x} - B_x \right) \delta u dA = 0$$

$$\iint \left( \frac{\partial v}{\partial t} + u \frac{\partial v}{\partial x} + v \frac{\partial v}{\partial y} - B_y \right) \delta v dA = 0 \quad (3.43)$$

$$\iint \left[ \frac{\partial H}{\partial t} + \frac{\partial}{\partial x} (Hu) + \frac{\partial}{\partial y} (Hv) \right] \delta H dA = \int (HV_n - H\bar{V}_n) \delta H dS = \int H\bar{V}_n \delta H dS$$

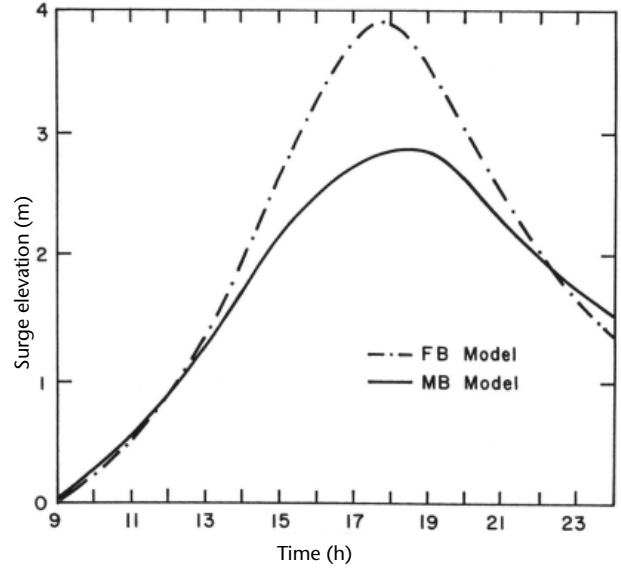


Figure 3.6. Computed storm surge at Eugene Island, United States, using fixed-boundary (FB) and moving-boundary (MB) models

Source: Yeh and Chou, 1979

where:

$n$  denotes the normal and  $V_n$  the component of velocity;

$B$  represents the sum of external forcing (pressure gradients, Coriolis, surface and bed stresses).

It is assumed that over an element, the same interpolation of the unknowns  $u$ ,  $v$ , and  $H$  exists. Thus:

$$u = \phi u^n$$

$$v = \phi v^n \quad (3.44)$$

$$H = \phi H^n$$

where:

$\phi$  = the interpolation function;

$u^n$ ,  $v^n$  and  $H^n$  = the nodal values of  $u$ ,  $v$ , and  $H$ .

A six-nodal triangular "isoparametric" grid was used by Brebbia and Partridge, cited above. The advantage of using curved elements is the suppression of the spurious forces generated on the boundaries by straight line segments joining at an angle (Connor and Brebbia, 1976).

From Equations (3.43) and (3.44):

$$M \frac{\partial u^n}{\partial t} + Ku^n - fMv^n + G_x H^n + F_x = 0$$

$$M \frac{\partial v^n}{\partial t} + Kv^n - fMu^n + G_y H^n + F_y = 0 \quad (3.45)$$

$$M \frac{\partial H^n}{\partial t} + C_x u^n - C_y v^n + F_H = 0$$

with the following definitions (superscript  $T$  denotes the transpose):

$$K = \int \frac{\partial}{\partial x} (\phi^T \phi) u dA + \int \frac{\partial}{\partial y} (\phi^T \phi) v dA + \frac{g}{C^2} \int \frac{\phi^T (u^2 + v^2)^{1/2}}{H} \phi dA$$

$$G_x = g \int \frac{\partial}{\partial x} (\phi^T \phi) dA$$

$$G_y = g \int \frac{\partial}{\partial y} (\phi^T \phi) v dA$$

$$M = \int \phi^T \phi dA$$

$$F_x = \int \phi^T \frac{\partial}{\partial x} \left( \frac{p}{\rho} \right) dA + \frac{\gamma}{\rho} \int \phi^T \frac{W_x}{H} (W_x^2 + W_y^2)^{1/2} dA$$

$$F_y = \int \phi^T \frac{\partial}{\partial y} \left( \frac{p}{\rho} \right) dA + \frac{\gamma}{\rho} \int \phi^T \frac{W_y}{H} (W_x^2 + W_y^2)^{1/2} dA$$

$$C_x = \int \frac{\partial}{\partial x} (\phi^T) H \phi dA$$

$$C_y = \int \frac{\partial}{\partial y} (\phi^T) H \phi dA$$

$$F_H = \int (H \bar{V}_n \phi^T) dA$$

$$\begin{bmatrix} M & . & . \\ . & M & . \\ . & . & M \end{bmatrix} \begin{bmatrix} \frac{\partial u^n}{\partial t} \\ \frac{\partial v^n}{\partial t} \\ \frac{\partial H^n}{\partial t} \end{bmatrix} + \begin{bmatrix} K & -M & G_x \\ -M & K & G_x \\ -C_x & -C_y & O \end{bmatrix} \begin{bmatrix} u^n \\ v^n \\ H^n \end{bmatrix} + \begin{bmatrix} F_x \\ F_y \\ F_H \end{bmatrix} = \begin{bmatrix} 0 \\ 0 \\ 0 \end{bmatrix} \quad (3.46)$$

or in the abbreviated form:

$$MQ + KQ = F \quad (3.47)$$

Brebbia and Partridge used two different procedures for time integration, but here we report only the implicit scheme involving the trapezoidal rule. Assuming that:

$$\begin{aligned} Q &= \frac{Q_T - Q_0}{\Delta t} \\ Q &= \frac{Q_T + Q_0}{2} \\ F &= \frac{F_0 + F_t}{2} \end{aligned} \quad (3.48)$$

then equation (3.47) becomes:

$$\left( \frac{2}{\Delta t} M + K \right) Q_t = (F_0 + F_t) + \left( \frac{2M}{\Delta t} - K \right) Q_0 \quad (3.49)$$

This can be written in the abbreviated form as:

$$K^* Q_t = F^* \quad (3.50)$$

The recurrence relationship is then given by:

$$Q = (K^*)^{-1} F^* \quad (3.51)$$

The  $K^*$  matrix, which must be inverted, will generally be a large asymmetrical banded matrix of a size approximately three times the number of nodes by six times the element band width (that is, the maximum difference between the element nodal point numbers plus one). The fourth-order Runge-Kutta method was used for the explicit time integration.

### 3.9.2 Finite volume methods

Various classes of numerical methods have been developed to deal with the difficulties of solving hyperbolic systems, most of which are finite volume methods (George and Le Veque, 2006). A finite volume numerical solution consists of a piecewise constant function  $Q_i^n$  that approximates the average value of the solution  $q(x, t^n)$  in each grid cell  $l_i = [x_{i-1/2}, x_{i+1/2}]$ . A conservative finite volume method updates the solution by differencing numerical fluxes at the cell boundaries:

$$\frac{(Q_i^{n+1} - Q_i^n) \Delta x}{\Delta t} + \left( F_{i+1/2}^n - F_{i-1/2}^n \right) = 0 \quad (3.52)$$

$$Q_i^{n+1} = Q_i^n - \frac{\Delta t}{\Delta x} (F_{i+1/2}^n - F_{i-1/2}^n)$$

where:

$$F_{i-1/2}^n \approx \frac{1}{\Delta t} \int_{t_n}^{t_{n+1}} f \left[ q(x_{i-1/2}, t) \right] dt$$

and:

$$Q_i^n \approx \frac{1}{\Delta x} \int_{x_{i-1/2}}^{x_{i+1/2}} q(x, t^n) dx \quad (3.53)$$

where we have assumed the grid cells are of fixed length  $\Delta x$ .

Note that Equation (3.53) is a direct discrete representation of the integral conservation law over each grid cell (neglecting source terms) using approximations to the time-averaged fluxes at the boundaries. The essential properties of the finite volume method, therefore, come from the approximation for the numerical fluxes.

### 3.10 MESOSCALE FORCING

In traditional storm surge computations, the pressure and wind forcing fields are associated with large-scale weather systems, such as tropical and extra-tropical cyclones. When the forcing terms are deduced from large-scale weather systems, these are referred to as the synoptic scale. Until now, most of the existing storm surge prediction is for synoptic-scale forcing. However, coastal flooding arising from weather systems on the mesoscale (10–100 kilometres) occurs quite frequently. Oscillations of water level in the Great Lakes of North America from squall and pressure-jump lines are well documented in the literature (Murty, 1984). At present, there is no system in place for the operational prediction of coastal flooding produced by mesoscale weather systems.

The reasons for the lack of such a forecasting system are twofold. First, there is no mesoscale weather network worldwide to observe these events and to provide the meteorological forcing for numerical models. Second, a complete understanding of the fundamental dynamics of these events is lacking. It should be noted that the system of standard global weather observations at the four synoptic hours of 0000, 0600, 1200 and 1800 Universal Time (UT) does not provide adequate temporal resolution for mesoscale systems, and that, furthermore, the spacing of currently existing weather station networks does not provide sufficient spatial resolution.

In the literature, mesoscale weather systems have been referred to variously as squall lines or pressure-jump lines. Here we propose that the terminology “squall lines” may be used to refer to mesoscale weather systems. For the coastal flooding events associated with mesoscale forcing, various terms such as seiche, “rogue waves”, “freak waves”, “giant waves” and, in local languages, “*rissaga*” and “*abiki*” have been used in the literature, as already discussed in 2.4.

*Rissaga* is a Spanish word meaning “high-amplitude sea-level oscillations”. The phenomenon was first described in Spain and was reported in a series of papers. Tintore et al. (1988) reported large sea level oscillations (up to 1 metre in amplitude and with an approximately 10-minute period) in various bays and harbours of the western part of the Mediterranean Sea. They showed that these oscillations arise due to a three-way resonant coupling among atmospheric gravity waves, coastally trapped edge waves and the normal modes of a harbour. The energy sources are atmospheric pressure fluctuations with a period of approximately 10 minutes and an amplitude of approximately 1.5 hectopascals. Every year from June to September these oscillations are observed on the north-east coast of Spain and in the Balearic Islands. The largest amplitudes usually occur in the town of Ciutadella (Jansa, 1986), which is an elongated harbour 1 kilometre long and 90 metres wide, situated on the west coast of Minorca. One of the largest oscillations observed was approximately 2 metres, on 21 June 1984.

Rabinovich and Monserrat (1996) presented characteristics of *rissaga* for the Balearic Islands and Catalina in Spain. From these data, one can note that the wave heights can reach up to 3 metres, the wave periods range from 3 to 30 minutes and the total duration of the events is usually between 2 and 48 hours, with a maximum reported value of 63.4 hours. Jansa et al. (2007) reported that, on 15 June 2006, a *rissaga* occurred in Ciutadella with amplitudes of between 4 and 5 metres and a period of about 10 minutes. Approximately one hundred

marine vessels were damaged, out of which 35 sank.

The recurrence of such events in the same places indicates that they are strongly related to the topography and geometry of the corresponding bays, inlets or harbours. Simultaneous sea-level measurements in the Ciutadella inlet and Palma Bay demonstrated that, during the same events, seiches in Ciutadella are approximately six times larger (Miles and Munk, 1961). The relative intensity of the phenomena can be explained in terms of the so-called Q-factor, a measure of wave damping in enclosed harbours. Reducing the harbour entrance by wave protection constructions increases the Q-factor and therefore the harbour oscillations. From this point of view it is quite understandable why the narrow inlet of Ciutadella has much stronger seiches than other more open-mouthed inlets and harbours of the Balearic Islands.

Rabinovich (1993) proposed that the extreme seiche oscillations observed in some locations are forced by a double resonance effect, for example by the coincidence of resonant frequencies of the shelf and the inner basin, or by the eigenfrequencies of the harbour and the outer bay. According to this theory, the relatively small probability of such coincidences is the main reason for the rareness of basins for which large-amplitude seiches are reported.

### 3.11 REMOTE FORCING

In terms of frequency of occurrence and local impact, there is one more type of coastal flooding, indirectly associated with weather systems, which should be considered. In the case of the Indian Ocean, the swell generated by storms near Antarctica propagates northward and, through interaction with the coastal currents, causes flooding on the coasts of the Bay of Bengal and the Arabian Sea in India (Baba, 2005; Murty and Kurian, 2006). Similar incidents are reported for the Atlantic and Pacific Oceans. Other types of remotely forced waves include the so-called topographically forced Rossby waves that are generated far outside the area of interest and that then propagate towards the coasts (Morey et al., 2006). These waves contribute to the augmentation of storm surges in the Bay of Bengal and also in the Gulf of Mexico.

The term “*kallakkadal*” is used by fishermen in the state of Kerala in south-west India to refer to coastal flooding provoked by swell from Arctic storms (Kurian et al., 2009). In Malayalam (the language spoken predominantly in the state of Kerala),

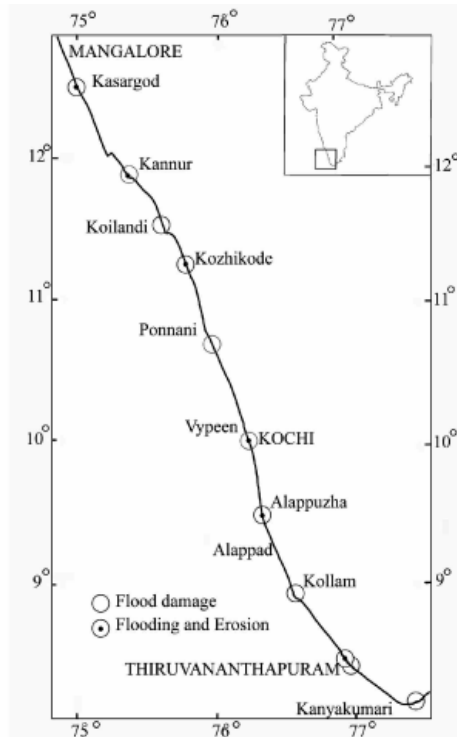


**Figure 3.7. The locations where *kallakkadal* occurred on the coast of Kerala and Tamil Nadu, India in May 2005**

Source: Baba, 2005

“*kallan*” means “thief” and “*kadal*” means “sea”. In the spoken language, both words are combined and pronounced as *kallakkadal*, meaning the ocean that arrives like a thief (unannounced). *Kallakkadal* occur on the southern coasts of India, mainly during the months of April and May (prior to the monsoon season) (see Figure 3.7). The swell generated in the Southern Ocean by storms near Antarctica propagates northward into the Arabian Sea and the Bay of Bengal. When it encounters a

coastal current directed southward, the swell can be amplified through interaction with this current. Due to the increased wave set-up, low-lying areas on the coast may be flooded. When *kallakkadal* occurs during a spring tide the flooding will be more severe. The flooding is not continuous all along the coast because of varying coastal topography. These flooding incidents appear to be more severe and more frequent on the southern Indian coasts than on the northern coasts. The main reason for this is the orientation of the coastline: towards the south the coast curves in such a manner that the swell waves meet it in a perpendicular direction. Though the occurrence of *kallakkadal* is not well documented in the scientific literature, according to fishermen it occurs almost every year.

The *kallakkadal* events of May 2005 (Figure 3.7) were the most intense in recent years and have been well documented (Narayana and Tatavarti, 2005; Baba, 2005; Murty and Kurian, 2006). Because of the memory of the Indian Ocean tsunami of December 2004, the inundations created panic and were well reported in the media. Almost all the low-lying areas of the Kerala coast and the southern coasts of Tamil Nadu were flooded. The following general observations can be made about the *kallakkadal* phenomenon observed along the Kerala coast:

- It occurs mostly during the pre-monsoon season (occasionally post-monsoon);
- It continues for a few days;
- Low-lying coasts are inundated;
- During high tide, the run-up can be as much as 3 to 4 metres above mean water level;
- The associated wave characteristics are typical of swells with moderate heights (2 to 3 metres) and long periods (approximately 15 seconds);
- The occurrence is more on the south-west coast of India than other coasts.



## CHAPTER 4

# INPUT AND OUTPUT PARAMETERS

### 4.1 INTRODUCTION

This section addresses the impacts of various input and output parameters for storm surge models both in the initial set-up, tuning and validation phase, and in the operational phase. Oceanographical data, which are needed in the set-up of the model, consist of bathymetry and tidal forcing data at the open boundary. The location of the open boundary may possibly be determined by the availability of tidal forcing. Tide-gauge data will be needed for tuning, validation and verification, and possibly data assimilation, together with HA of astronomical tides. Satellite altimeter data can be very useful for tuning and calibrating the model, but their availability is generally too low to be of much practical use in the operational running of the model, especially if it is not large. Any available data on currents might also prove useful for tuning the model. Meteorological input to the model consists of surface winds up to 10 metres above sea level or data on surface stress and mean pressures at sea level. This chapter will elaborate on the spatial resolution of the different available meteorological sources and input time intervals.

Hydrological inputs consist of data for river runoff and precipitation. Ice input is needed for modelling in areas where this is relevant. For all inputs, considerations of accuracy and timeliness will be addressed. Output parameters that can be considered include total water level and surge, either as fields or as time series for high and low tides. This chapter will also address the question of how to deal with the surge component of the total water level.

### 4.2 MODEL SET-UP

#### 4.2.1 Bathymetry and geometry

The first stage in the set-up of the model is the definition of the area. For that purpose, data on geometry and bathymetry are required that correspond to the required resolution of the storm surge model for the area under consideration. The open boundary of a two-dimensional storm surge model is best located in water deeper than 200 metres and requires available tidal forcing, either as currents or as levels. For shoreline data, the Global Self-consistent, Hierarchical, High-resolution Shoreline Database (GSHHS) (Wessel and Smith, 1996), with a

typical resolution of about 200 metres, is available in the public domain and can be downloaded from the University of Hawaii at the Website <http://www.soest.hawaii.edu/pwessel/gshhs/>.

Bathymetry data can be obtained from sea charts and satellite altimetry maps, and also from local measurement campaigns. The General Bathymetric Chart of the Oceans (GEBCO) project, which operates under the joint auspices of IOC and of the International Hydrographic Organization (IHO), provides global bathymetry datasets for the world's oceans. Their "One Minute Grid" is available for download from the British Oceanographic Data Centre (BODC) at [http://www.bodc.ac.uk/data/online\\_delivery/gebco](http://www.bodc.ac.uk/data/online_delivery/gebco). Furthermore, the United States National Oceanic and Atmospheric Administration (NOAA) National Geophysical Data Center (NGDC) has an extensive collection in the public domain that can be downloaded from <http://www.ngdc.noaa.gov/mgg/bathymetry/relief.html>. Local sources for such data include hydrographical institutes, which may be integrated within a country's naval administration or some other research institute structure.

When using bathymetry data one should verify the purpose for which the data were originally collected and used, which might influence their usefulness for storm surge modelling. For example, one principle use of sea charts is to prevent ships from running aground and, therefore, these charts tend to give a minimum depth rather than an average depth, although the latter is needed for modelling water movement. Such deficiencies can be corrected in the tuning phase to obtain proper astronomical tides inside the model domain.

#### 4.2.2 Tidal boundaries

The condition for the open boundary proposed by Davies and Flather (1978) is applied to the difference between the interior value and the prescribed value of the tide and the storm surge, so that the perturbation leaving the domain follows the expression:

$$q - \hat{q} - q_s = \frac{c}{H} (h - \hat{h} - h_s) \quad (4.1)$$

where:

$q$  = the current normal to the boundary;  
 $c \pm \sqrt{gH}$  = the speed of the external gravity waves leaving the model domain;

- $\hat{h}$  and  $\hat{q}$  = the water level and the depth-averaged current of the tide prescribed in the open boundary, respectively;
- $h$  = the height calculated in the interior point adjacent to the boundary;
- $h_s$  and  $q_s$  = the height and current, respectively, associated with the storm surge entering the domain obtained from other sources, such as a coarser grid model or an inverse barometer effect.

The tide is prescribed as a combination of several harmonic constituents, as follows:

$$h_{(\phi, \Theta, t)} = \sum_{i=1}^n F_{(t)}^{(i)} \Gamma_{(\phi, \Theta)}^{(i)} \cos\left(a^{(i)}t + V_{0_u}^{(i)} + p^{(i)}\Theta - G_{(\phi, \Theta)}^{(i)}\right) \quad (4.2)$$

where:

- $n$  = the prescribed number of tidal constituents;
- $F$  = the nodal factor;
- $a$  = the speed of the constituent;
- $t$  = the time starting from the beginning of the prediction in Greenwich mean time (GMT);
- $V_{0_u}$  = the equilibrium tide at the Greenwich meridian;
- $p$  = 1 for diurnal components and 2 for semi-diurnal;
- $\Gamma$  = the amplitude of the component;
- $G$  = the phase (expressed as epoch) of the tidal constituent.

The values of  $F$  and  $V_{0_u}$  depend on time and, according to usual practice, may be tabulated for each year, as well as being corrected for the month and day. These parameters should be calculated for every prescribed day and time of a run to establish the phase of the selected tidal components. For further details on tidal analysis, the reader is referred to the work of Schureman (1958).

In most cases, the constituents defined for the tidal current at the open boundaries are not known. In this case, the linear approach  $\hat{q} = \pm \sqrt{\frac{g}{H}} \hat{h}$  can be used, in which the sign corresponds to the normal component of the speed of a perturbation that enters into the domain.

The constituents used should be those available that are the most representative of the local tidal regime. The values of amplitude and epoch may be determined by local observations. At boundaries of open sea, amplitude and co-tidal fields from global tidal models or other sources can be interpolated and introduced into Equation (4.2). Blending this information with data from any oceanographic station located close to the boundary is appropriate. In other cases, such as semi-enclosed seas or estuaries, an adequate interpolation of coastal values at the open boundary, by following known patterns or prescribing a Kelvin wave shape, may be suitable.

Tidal constants can be calculated at selected points after an adequate spin-up period, that is, the time needed by the tidal waves to establish a steady state. The spin-up period depends on the local tidal regime and the area covered by the model domain. As a general rule, a run of one month is sufficient for the time series needed to obtain the tidal constituents (Foreman, 1979).

It is strongly recommended that the tidal part of the model (that is, the storm surge model applied to the tide only) should be calibrated with the available analysed tidal data. The tidal constituents and their distribution throughout the open boundaries may be used in the calibration process, together with other model parameters with their own ranges of uncertainty. These may include bottom friction or some critical depth for land flooding and drying in high-resolution coastal models. The modelled tidal wave may be more sensitive to the values at a particular boundary, depending on the incidence of the external wave. Occasionally, differences between various bathymetric sources may be sufficient to produce significant modifications in speed and direction of long gravity waves. An optimal solution must then be found to fit the observations, if necessary after reviewing the bathymetric information. The correct simulation of the tide will ensure the adequacy of the model for the representation of the local hydrodynamic processes and hence the storm surge.

The tidal constituents that are used in the United Kingdom Proudman Oceanic Laboratory (POL – part of the National Oceanographic Centre National Tidal and Sea Level Facility) model CS3X (POL, 2007) are Q1, O1, P1, K1, MNS2, 2N2,  $\mu$ 2, N2,  $\nu$ 2,  $\lambda$ 2, M2, L2, T2, S2, K2, MSN2, 2SM2, MO3, MK3, MN4, M4, MS4, M6, 2MS6, 2MK6 and 3M2S2. The Dutch Continental Shelf Model (DCSM) of the Royal Netherlands Meteorological Institute (KNMI) (KNMI, 2007) uses M2, S2, N2, K2, O1, K1, Q1, P1,  $\nu$ 2 and L2.

#### 4.2.3 Data for tuning and calibration

Once the model has been set up and tidal boundaries have been established, it has to be tuned and calibrated for the intended use.

A first step is to verify whether the astronomical tide that enters through the open boundaries is propagated correctly through the model. Data that are useful here include time series of observed water levels for quiet periods, during which the weather was calm with no significant surges. Tidal constituents determined by HA of long time series can also be used.

The model may then be run without meteorological input for a certain period to establish the equivalents of these constituents or the time series for the quiet periods. Discrepancies between the model and the observations will require adjustments to the bathymetry or the astronomical tide at the open boundaries. Satellite altimeter data might prove useful to obtain an overview of the spatial structure of the astronomical tide and help to identify regions where adjustments are necessary.

Calibration for surges is best based on periods during which there is much wind and should cover both positive and negative surges. Apart from the time series of observed water levels, meteorological input is also needed, preferably comparable to that which will be used for the forecast mode in the operational phase of the model. Any available current data are also useful during this phase to compare to results produced by the model.

### 4.3 USING THE MODEL

#### 4.3.1 Meteorological input

Meteorological input for two-dimensional storm surge forecasting usually consists of near-surface wind stress and sea-level pressure. For more sophisticated air–sea interaction schemes other parameters might come into play, such as temperature and wind at other levels (see, for example, Makin, 2003; Flather et al., 1991; Mastenbroek et al., 1993).

Accurate meteorological fields, especially wind fields, are crucial, since the magnitude of storm surges is at least proportional to the square of the wind speed. A natural source for these parameters is the atmospheric models that are used for weather forecasting. Global models, such as those from ECMWF, the United Kingdom Met Office (UKMO) and NOAA National Weather Service (NOAA NWS) have horizontal resolutions of 25–100 kilometres for 240–360 hours ahead, which makes them suitable for extra-tropical storms. However, for tropical storms and also for high-resolution current and water-level forecasts, these models are often not sufficient because the structure of tropical cyclones and other relevant details are not sufficiently resolved. In this case, limited area models (LAMs), as operated by many National Meteorological Services, are a better option. Currently, LAMs generally have resolutions in the order of 10 kilometres up to 48 hours in advance. The objective for the next generation of these models is 1 kilometre up to 24 hours ahead.

There are several ways to use meteorological data for storm surge forecasting. If used in a numerical model, the meteorological fields generally have to be interpolated from the grid, together with the time steps of the atmospheric model, into the storm surge model. The questions that must be addressed are the type of interpolation in space and time to be used and the handling of land–sea boundaries. Other methods use empirical formulas and need other, derived parameters, such as the maximum wind and pressure in the centre of a tropical cyclone.

#### 4.3.1.1 Meteorological input for a tropical cyclone

Because tropical cyclones are usually smaller but stronger than extra-tropical cyclones, the modelling of tropical storm surge requires wind fields of higher resolution (for example, from 5 to 10 kilometres) that are capable of resolving the most intense part of a tropical cyclone. State-of-the-art mesoscale numerical weather prediction (NWP) models can provide the required resolution, but they are currently available only in a limited number of meteorological centres, since they are computationally intense and require an advanced data-assimilation scheme that can generate realistic tropical cyclone fields. Therefore, simple empirical formulas of tropical cyclone pressure or wind are often used to create forcing fields for models of tropical storm surge. As a tropical cyclone has a nearly axisymmetric structure, its distribution can be reasonably represented with an empirical formula for the radial distribution of wind or pressure. Once the distribution of either wind or pressure is determined, the other variable can be calculated from the gradient wind balance:

$$\frac{v^2}{r} + fv = -\frac{1}{\rho} \frac{dp}{dr} \quad (4.3)$$

where:

- $v$  = the speed of gradient wind at the distance  $r$  from the storm centre;
- $f$  = the Coriolis parameter;
- $\rho$  = the density of air;
- $p$  = the atmospheric pressure at sea level.

Many researchers have suggested empirical formulas to calculate the sea-level pressure of a tropical cyclone as functions of  $r$ , the radial distance from the storm centre. The following forms are often used:

$$\text{Fujita (1952):} \quad p(r) = p_{\infty} - \frac{p}{\sqrt{1 + (r/r_0)^2}} \quad (4.4)$$

$$\text{Myers (1954):} \quad p(r) = p_c + \Delta p \exp(-r/r_0) \quad (4.5)$$

$$\text{Holland (1980):} \quad p(r) = p_c + \Delta p \exp(-A/r^B) \quad (4.6)$$

where:

- $p_c$  and  $p_\infty$  = the pressure at the storm centre and the ambient pressure, respectively;  
 $\Delta p$  = the pressure drop defined as  $\Delta p = p_\infty - p_c$ ;  
 $r_0$ ,  $A$  and  $B$  = empirical constants that control the storm size.

Usually,  $B$  has a value of between 1 and 2.5.

In the model Sea, Lake and Overland Surges from Hurricanes (SLOSH) of NOAA (Jelesnianski et al., 1992), the radial wind distribution is first determined by the following simple storm wind model:

$$v = V_r \frac{2Rr}{R^2 + r^2} \quad (4.7)$$

where:

- $V_r$  = the maximum wind speed;  
 $R$  = the radius of the maximum wind.

To synthesize meteorological fields by using these formulas, the unknown parameters they contain should be determined with analysed or forecast values such as:

- The minimum pressure at the storm centre;
- The maximum sustained wind speed and, if available, its radius;
- The radii for representative wind speeds (of, for example, 30 and 50 knots);
- The location (longitude and latitude) of the eye of the storm.

These values can be obtained from the tropical cyclone advisories or bulletins issued by the Regional Specialized Meteorological Centres (RSMCs) and Tropical Cyclone Warning Centres assigned by WMO, through the Internet and the Global Telecommunications System (GTS). For details of the RSMC bulletins, the reader is referred to <http://www.wmo.int/pages/prog/www/tcp/Advisories-RSMCs.html>. The above methods are also useful for ensemble storm surge forecasts in case of tropical cyclones. Even when an ensemble NWP system is not available, one can easily create an ensemble of forcing fields with one of the formulas by changing the track or intensity of the target tropical cyclone.

#### 4.3.1.2 Interpolation issues for numerical models

When using output from an NWP model as input for a storm surge model, several issues have to be addressed regarding interpolation of data. Generally, the grid of the NWP model is different from that of the storm surge model and the meteorological fields are not available on all the time steps of the storm surge model.

The interpolation of wind data can be performed in two ways, either on wind vector components or

on wind intensity and direction. The first method leads to a loss of energy that can be significant in case of strong wind rotation (Figure 4.1). More details can be found in Skandrani and Daniel (2001). Interpolation of the winds based on force and direction, rather than on zonal and meridian components, minimizes the energy loss and seems to be preferable in most meteorological conditions.

For interpolation in time there are also two choices. Generally, a linear interpolation between the two nearest points in time for which the meteorological fields are available can be applied. However, another possibility is to keep the meteorological forcing constant over a period of time around the NWP output step. An advantage of this second option may be that sharp gradients in the fields are better conserved.

Interpolation in space is usually performed bilinearly. Care should be taken with the interpolation of the wind field in the vicinity of land–sea boundaries. As the wind significantly decreases over land, the wind for a sea point in the storm surge model should not be directly interpolated from NWP points over land. If the grid of the NWP model is coarser than that of the storm surge model, this factor might be an important consideration in the coastal zone. Solutions to this involve changing the coefficients of the interpolation near the coast with the aid of the land–sea masks of both the atmospheric and the storm surge model. For example, the weights of the land points may be set to zero and the remaining weights renormalized.

#### 4.3.2 Hydrological input

River runoff can have a significant effect on storm surges and needs to be taken into account in detailed models, especially for areas near estuaries. Data may come from observations or hydrological models that are used to forecast the water levels and discharge of a river system. Another application of

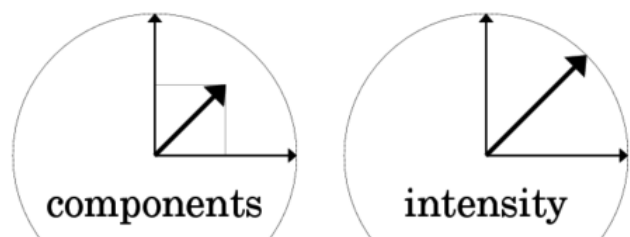


Figure 4.1. Two methods of interpolation of data on wind from an NWP to a storm surge model: vector components (left) or intensity (right)

hydrological data is the interaction of storm surge, river runoff and precipitation for the management of water levels inland. In the Netherlands this kind of information is used to optimize the use of pumps in case of expected heavy precipitation and to sluice water out of the country on low tides before the rains occur.

4.4 **VALIDATION AND VERIFICATION**

The terms “validation” and “verification” are not always clearly distinguished and defined. The meanings include the steps of making sure that the model does what it has been designed to do (model validation) and, in the operational phase, making a semi-permanent or permanent quantitative assessment of its performance (forecast verification). Validation and verification of the model are best performed on the primary output parameters of the forecasts. Nevertheless, for the assessment of the characteristics and the performance of the model in more general terms, other parameters and locations should be considered.

Observed water levels, as described for data assimilation, are an excellent base, especially for the ongoing forecast verification. However, any available current data, for example from cruises, or satellite altimetry data, could be helpful for the initial model validation.

4.5 **OUTPUT PARAMETERS**

Output from a storm surge model can be generated as time series for specific locations of interest, or as fields for a fixed time. Output from methods that do not directly involve a numerical storm surge model can be various and typically suited for the purpose of the method.

4.5.1 **Time series**

A time series of astronomical tide and meteorological surge for a specific location is typical output of a storm surge model. Very often, for these specific locations, astronomical tides are also available from HA of long time series. In particular, if the resolution of the model is moderate, HA is very often better than the astronomical tide from the model. The model can then be used to generate the surge alone, which is the output from a linear model, or the difference between runs with and without meteorological forcing from a non-linear model. The model surge added to the astronomical tide from HA then provides the most

accurate estimate of the total water level. Figure 4.2 illustrates an example of predicted and observed surge in Sheerness on the North Sea with data from the United Kingdom model CS3X (see 4.2.2).

A parameter that can be derived from the time series and that is especially important for storm surge situations is the skew surge for a high or low tide, defined in Figure 4.3. The skew surge quantifies the maximum deviation of the absolute water level with respect to the extreme of the astronomical tide. It can be used in combination with tables of the astronomical high and low tides. Due to possible time shifts, the skew surge is often different from the extreme of the non-tidal residual. To derive the skew surge from the model, the time series of the astronomical tide generated by the model itself should be used and not the series taken from HA.

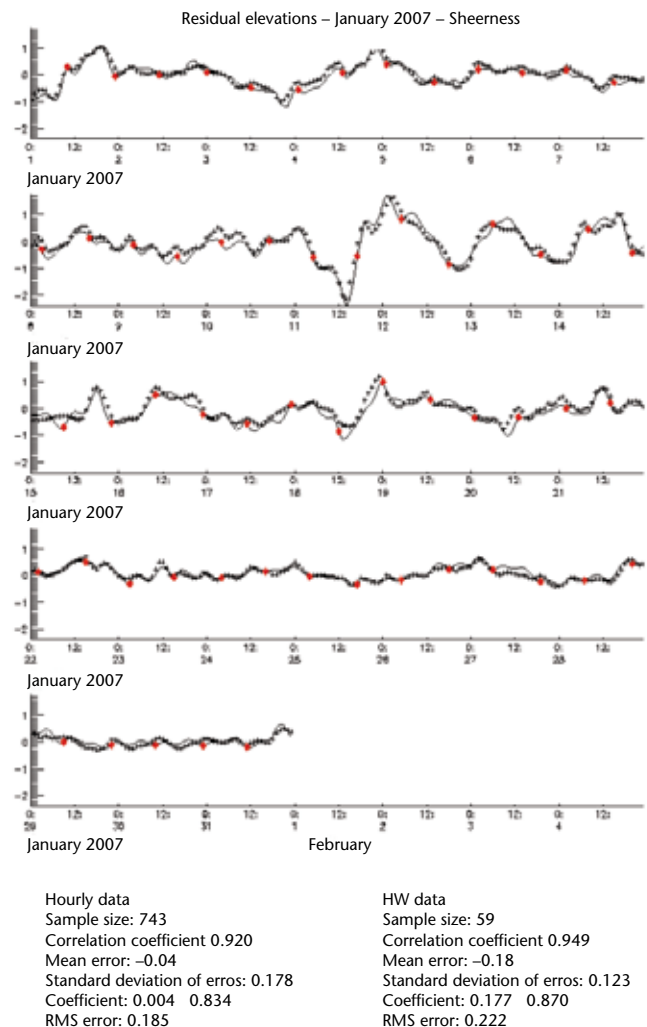


**Figure 4.2. Surge (metres) in Sheerness (North Sea) for January 2007 generated by the United Kingdom model CS3X (continuous line) together with observed surges (+) and markers for the high tides (HW: high water, red dots)**

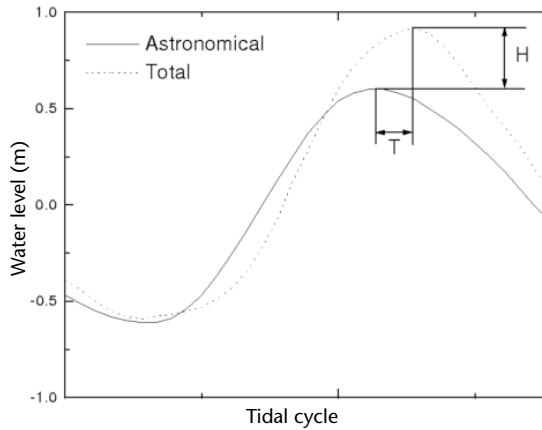


Figure 4.3. Skew surge indicating the parameters of time and height

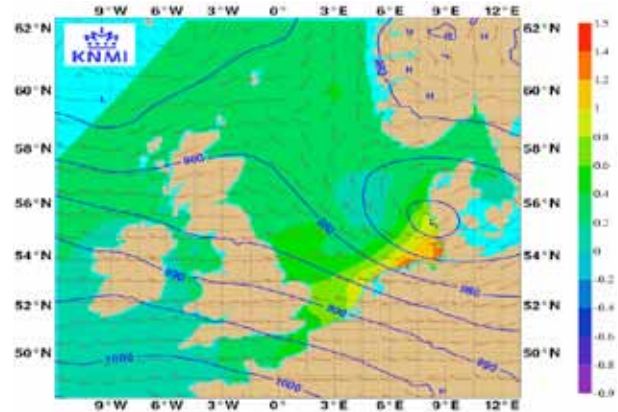


Figure 4.4. Surge (colour bar range in metres with reference to the astronomical tide) from the Netherlands DCSM model with wind and pressure input. Wind field is indicated as flags – speeds of 5 and 10 knots are represented by the shorter and longer bars, respectively. Pressure is contoured in hectopascals.

Source: KNMI, 2007

4.5.2 **Fields**

For a general overview of the situation at sea, fields of the astronomical tide and surge provide a useful tool. An example of the surge from the Netherlands storm surge model DCSM (see 4.2.2) together with the input wind and pressure fields is given in Figure 4.4. The wind field is indicated as flags with speeds of 5 and 10 knots represented by the shorter and longer bars, respectively. Pressure is contoured in hectopascals and the surge (in metres) is shown in colour code with reference to the astronomical tide.

4.5.3 **Output from other models**

An example of the output of the Japanese Meteorological Association (JMA) storm surge forecasting model is illustrated in Figure 4.5, showing the potential effect of a change in the path of a typhoon on storm surge for a region of Japan. The area and potential track are indicated in Figure 4.5(a). If the typhoon proceeds along a path to the north-west of the forecast track, a storm surge may occur in Osaka Bay, shown in Figure 4.5(b). Alternatively, if

the typhoon follows a track to the south-east, a surge may occur in Ise Bay, shown in Figure 4.5(c). To take into account the influence of the typhoon track on the occurrence of storm surge, five runs are normally conducted with the JMA model, each run being based on a different typhoon track. The five typhoon tracks are chosen at the centre and at four points on the indicated circle within which a typhoon is forecast to exist with a probability of 70 per cent, allowing the simulation of five meteorological fields with the empirical typhoon model mentioned.

4.5.4 **Example of a forecast result**

This section provides an example of results of the JMA storm surge forecasting system. Figure 4.6(a) shows the predicted positions of Typhoon *Chaba*

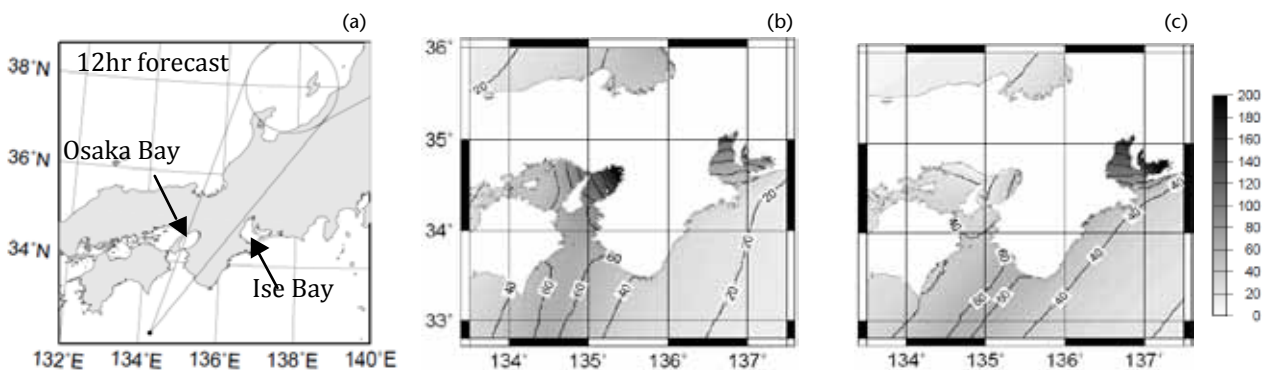
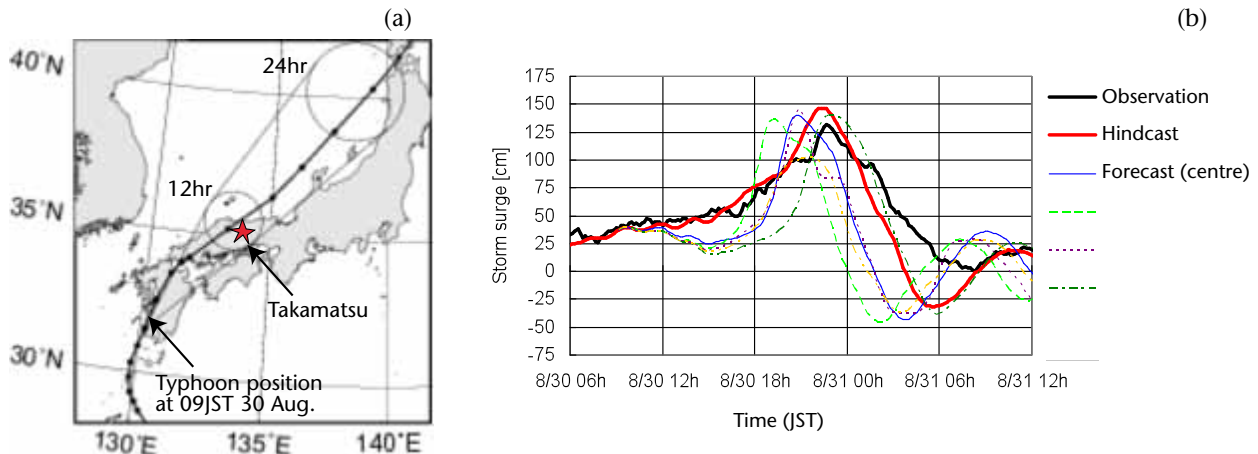


Figure 4.5. Maximum surge simulated with different typhoon tracks by the JMA storm surge forecasting model (bar units in centimetres). (a) Potential area of typhoon tracks used in the simulations. (b) Simulated surge for the case in which a typhoon takes the north-westerly path. (c) Simulated storm surge for the south-easterly path

(T0416) at 0900 hours Japan Standard Time (JST) on 30 August 2004, approximately 12 hours before the peak surge occurred. The two circles of 70 per cent probability were predicted by the 12-hour and 24-hour forecasts as indicated. The analysed track is also indicated. Figure 4.6(b) shows the time series of storm surge at the Takamatsu tide station on 30–31 August. The typhoon passed the north-western part of Japan, causing storm surge disasters in the coastal areas surrounding Seto Inland Sea. As described in 4.5.3, five forecast runs

were executed for five possible typhoon tracks and the results are denoted as lines in the figure. Although the time of the peak surges predicted by the model is slightly earlier than observed, the height is in good agreement with the observations. Based on this result, Takamatsu Local Meteorological Observatory issued storm surge warnings six hours before the sea level reached its maximum. This case can be considered to be an example that demonstrates the effectiveness of the forecasting system.



**Figure 4.6. Track of Typhoon *Chaba* (T0416) and the time series of the storm surge at Takamatsu. (a) Track of the typhoon – the thick line is the analysed track and the two circles indicate the typhoon positions predicted at a probability of 70% by the 12-hour and 24-hour forecasts. (b) The time series of observed and modelled storm surges for Takamatsu tide station**





## CHAPTER 5

# STORM SURGE PREDICTION MODELS

### 5.1 **OPERATIONAL TWO-DIMENSIONAL STORM SURGE PREDICTION MODELS**

An overview of operational practices regarding storm surge prediction compiled from the results of a worldwide survey is detailed in Chapter 9 and also included in the dynamic part of this Guide (<http://www.jcomm.info/SPA>). Analysis of the responses to the survey show that, without considering finer nested grids, approximately 75 per cent of the reported operational or pre-operational applications are two-dimensional models. Due to the essentially two-dimensional nature of the physical processes involved, as described in Chapters 2 and 3, the application of depth-averaged hydrodynamic models can produce accurate forecasts of storm surges for most practical purposes. They are transportable, adaptable and valid for a wide range of scales. They have proved to represent accurately the tides, the storm surge and the interaction between them.

Most of the operational applications referred to in the dynamic part of this Guide are forced by tides at the open boundaries. Estimation of surge at the boundary is used for two-dimensional models. For three-dimensional models, when atmospheric pressure data are available then inverse barometer corrections should be employed at the open boundary, otherwise non-tidal sea levels can be prescribed from climatological records, although this lacks accuracy.

An updated assessment of the state of the art in operational storm surge numerical models is detailed in the dynamic part of this Guide. International cooperation and the availability of data and models provide a favourable scenario for the development of such applications. Furthermore, these models provide a framework for the development and verification of other local products.

#### **The rationale of the forecasting system**

The main challenge for local and regional applications is to be accurate while practicable, ensuring that useful forecasts reach the public in a timely fashion. The role of the developer is to identify features of local or regional phenomena and to choose the approach and tools that best represent them, with the objective of achieving a sustained service.

The accuracy of the meteorological forcing required for storm surge modelling limits the forecast range in practice compared to the available meteorological forecasts. Experimental tests are therefore recommended to ascertain the accuracy required for the application. For phenomena requiring forecasts at very short range, the whole duration of processing time required for a given forecasting time should be taken into account, together with the frequency of successive runs. The former factor is composed of the delay required for meteorological fields, the acquisition process and the processing and dissemination time. The latter factor is usually called the data-assimilation cycle in NWP and will be referred to in Section 5.2.

The lifetime of the phenomena and/or the propagation speed of the waves in a coastal sea or into an estuary define the limits of the real-time use of data. On the other hand, the dynamics of propagation of waves in the basin to be considered determine the potential benefits of data assimilation for certain locations. There is a wide variety of uses of observations of sea level in real time in conjunction with numerical prediction, in operational or pre-operational applications, as described in Table 9.3, including the correction of forecast bias, assimilation of initial conditions, the blending of bulletins with the forecasts, the application of regression and empirical methods, and model validation.

The forcing winds used belong mostly to high-resolution national NWP models or hurricane predictions. The forecast ranges of most of the operational applications are from 36 to 72 hours, although a forecast range as long as 120 hours has been reported. The predictions of surges generated by tropical cyclones have shorter ranges, usually within 12 hours.

### 5.2 **SETTING THE INITIAL STATE FOR THE FORECAST**

The evolution of long gravity waves for short- and medium-range periods is highly dependent on the initial state. The period of time for which the regime is achieved is dependent on the specific local characteristics and is referred to as the spin-up period. For every individual forecast the initial fields should be as accurate as possible. For this reason the model is rerun from the starting time of the previous run (restart fields), up to the initial state (time zero) of

the current forecast. This is called the “hindcast” period of the run. During the hindcast period, the driving meteorological fields are diagnosed or analysed from observations. Figure 5.1 outlines the procedure for the storm surge (including tide) numerical model operation. Its frequency is related to the availability of the analysed meteorological fields, that is, the data-assimilation cycle, which is usually 6 or 12 hours. In addition, the update of forecast meteorological information depends on the output of the meteorological model, usually at one- or three-hour intervals. The model run corresponding to the isolated tidal component completes the forecasting procedure for the storm surge. Estimating the surge contribution to the total water level has been discussed in Chapter 4.

The direct assimilation of sea-level data in the hindcast period may improve the definition of the initial state of the forecast. Hindcasts are useful tools for model calibration and for the establishment of databases of regional storm surge climatology. Some of these bases are maintained from the hindcast part of operational runs. Consequently, their record length depends on the period of operation of the models. Case studies of extreme events are the most frequently encountered, usually performed for model assessment. With a few exceptions, the models used are the same as the operational ones. However, extensive hindcast databases are reported as the outcome of major projects.

### 5.3 NESTING HIGHER RESOLUTION STORM SURGE MODELS

Storm surges arriving at the coast have in general been generated and propagated according to particular local situations. A general case is the generation of the surge over shelf seas and its modification in estuaries, islands, bays and other restricted areas. These scenarios may require different parameterizations of subscale processes, such as bottom friction, to be incorporated during the model calibration process. The representation of local features of bottom topography also requires different resolution. Local modification of tides, such as amplification, may be poorly represented in coarse

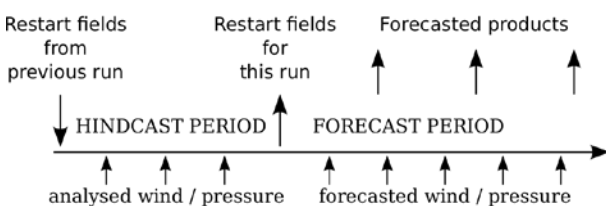


**Figure 5.1. Use of meteorological information for storm surge numerical forecasting**

grid models. This is also true for the surge component, which is modified locally even if it is not locally generated. The nesting technique is also appropriate to better represent the effects of remote perturbations in the area of interest, as modified by complex topography and local processes, such as flooding and drying, or tide–surge interaction in scenarios of either extremely shallow water or strong currents.

The nesting technique allows the consideration of the storm surge entering the domain of an LAM. The value of the storm surge given by the coarse model at the boundaries of the fine mesh model is extracted at time intervals, that is, from the estimated difference of values of water level and current between runs with and without the atmospheric effect. These values are then introduced to fulfil the conditions of external surge for the open boundaries of the fine mesh model when run with atmospheric forcing.

### 5.4 OPERATIONAL PRODUCTS AND REQUIREMENTS

The products derived from two-dimensional operational models are diverse. They include time-varying forecasts of sea level (usually of surge only) for specified locations, local peaks and maxima charts, and outputs for flooded areas and currents. There has been one report (see Chapter 9, which details the responses received to the ETWS survey) of the application of a statistically derived scale of the degree of risk for set-up (floods) as well as abatement (navigation risk). In response to an enquiry in the survey about additional requirements not considered by the model, other factors were mentioned by participants in the survey, such as the flooding of certain areas, the evolution of oil spills and surface currents.

The performance of operational and pre-operational storm surge models is monitored in most cases on a continuous basis. The sea level products considered for the validation can be either the full time series, the peaks or the levels at selected times, such as high and low waters. The statistical parameters obtained, usually for different forecast ranges, are varied. The bias, root mean square (RMS), standard deviation, average percentage error, linear regression (correlation coefficient) and the relation of standard error to mean square deviation are chosen by the different services. Statistics are provided either with a monthly or yearly frequency, or may be related to the occurrence of major storms. Examples of practices for operational model verification are summarized in Table 9.2, which also refers to model performance and some verification

results, as reported by several countries to the worldwide survey (see 5.1 and Chapter 9).

## 5.5 DATA ASSIMILATION

Data assimilation is a process enabling observational data to be integrated into a forecast model. This can be useful at a number of stages of development and application of the storm surge model. In forecasting mode it is important to correct boundaries and to account for processes not included in the model. In the initial calibration and tuning phase, data assimilation can be very useful to obtain optimal parameter settings. Methods for data assimilation are usually time-consuming and require a complex model set-up. During calibration and tuning, the cost aspects of data assimilation are much less critical than during the operational phase and elaborate and expensive but accurate methods, such as adjoint or inverse modelling, can be applied. During the operational phase, however, timely production of forecasts is essential and the data-assimilation method has to be cheap and fast enough to meet these requirements.

The crudest method of assimilation for operational forecasting would be the direct substitution of the observed values to replace the predicted values they represent. However, if the value at an observation point is changed in this way, it is possible that it will no longer agree with values at neighbouring grid points, thus introducing instability in the form of oscillations. Data-assimilation schemes, therefore, attempt to modify the original predictions around the observation point or on a larger scale so that they are consistent with the observations. Sequential data assimilation uses observations that precede the point of analysis, whereas non-sequential (or retrospective) data assimilation performs an analysis at an intermediate point in the time domain. Many assimilation approaches exist, most of which began in meteorology and were then integrated into oceanography.

An outline of several methods is given below, followed by a discussion of possible options for the operational implementation of a data-assimilation scheme. The techniques differ in their computational cost and their usefulness for real-time forecasting.

For a more complete review the reader is referred to Ghil and Malanotte-Rizzoli (1991) and also the lecture notes of Bouttier and Courtier (1999), obtainable at: [http://www.ecmwf.int/newsevents/training/lecture\\_notes/pdf\\_files/ASSIM/Ass\\_cons.pdf](http://www.ecmwf.int/newsevents/training/lecture_notes/pdf_files/ASSIM/Ass_cons.pdf).

### 5.5.1 Ensemble forecasts

Equally important as a forecast of the sea level itself is an estimate of the accuracy of the forecast. A traditional deterministic forecast of storm surge produces a single estimate of how the water level will evolve over time. A single forecast could thus fail to capture a particular non-linear combination of circumstances, consistent with a small change in model initial conditions, which could generate an extreme event. An ensemble modelling approach, already widely used in meteorology, addresses this by producing several simulations. Each simulation uses different initial conditions, boundary conditions and model physics, with the aim of sampling the range consistent with the uncertainty in both the observations and the model itself.

The variation in such an ensemble of forecasts contains information on the accuracy of the forecasts. This goes beyond a standard measure determined from verification of previous forecasts. However, interpretation of the ensemble forecasts is not always straightforward. Biases of the ensemble average or the width might require calibration before meaningful results are obtained. Further exploitation of the results of ensembles can lead to forecasts of the probability that certain critical levels will be exceeded.

A storm surge model can be forced with the output from the various members of a meteorological ensemble. The ensemble may consist of perturbations of one single model. Such ensemble surge systems are currently being run operationally in the United Kingdom (Flowerdew et al., 2009; Flowerdew et al., 2010) and in the Netherlands. Multimodel ensembles are also possible, in which the forecasts for certain parameters from a number of different models, very often from different institutes, are combined. Examples of this can be found in different atmospheric forecasting systems. Furthermore, the storm surge models operated by different agencies within the same area can also be exploited, as is shown in Chapter 7 for the case of the North Sea. Figure 5.2 shows a surge forecast based on the ECMWF ensemble model for the town of Den Helder (Netherlands). Skew surges from all individual members of the ensemble are shown, together with calibrated probabilities. The calibration has been derived from an earlier winter season of forecasts. Orange asterisks indicate the observed surges.

### 5.5.2 The Cressman scheme

One of the earliest and simplest successive correction schemes was published by Cressman (1959). It was used in the late 1950s for objective weather map analysis at the NWS (United States) and

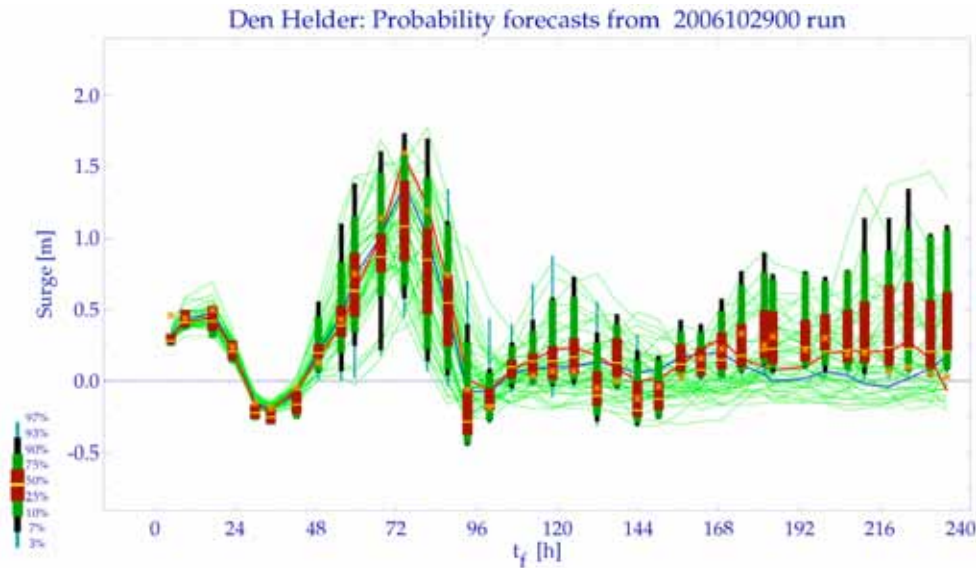


Figure 5.2. Forecasts of surge probabilities for the town of Den Helder (Netherlands), based on the ECMWF ensemble model. Skew surges from all individual ensemble members are indicated together with calibrated probabilities derived from an earlier winter season of forecasts. Orange asterisks indicate observed surges.

involved assimilating winds and pressure heights to a grid of the Northern Hemisphere. Values of a variable within a certain distance of each observation are corrected by adding them to some proportion of the error at the observation point (that is, the difference between the observation and the corresponding prediction). The size of the proportion for a given grid point will depend on its distance from the observation, as defined by a weighting function. The result will be consistent with the smoothed observations, but not necessarily consistent with model dynamics. One of the least satisfactory aspects of the Cressman scheme is the way in which the correction is relaxed as one moves away from the observation.

### 5.5.3 Statistical (optimal) assimilation

In optimal assimilation, large matrices of statistical information of forecast and observed errors are used to determine the model adjustment in space and time. In this scheme weights are applied to two measurements (that is, the model and observed values) to give a best estimate. The weights are based on the variances of the model and the observations, and are chosen so that the overall variance of the error of the best estimate is minimized (it is an optimal least-squares estimation). Unlike the Kalman filter, the background covariance matrix is assumed to have a time-invariant form; this is usually some function that depends on the distance between grid points and some assumed decorrelation length scale (inferred from existing physical knowledge, for example the Rossby deformation radius).

### 5.5.4 Kalman filter

Kalman filters (and the related extended Kalman filters) are approaches to the fundamental statistical method of least squares optimization that use the previous analysis to propagate a matrix of system errors forwards in time. This makes the method computationally expensive unless major assumptions are made. A matrix containing the filter at given times is dependent on the error covariances of the observations and of the model forcing. These error covariances are calculated at each time step and used to update the Kalman filter. The Kalman filter may be considered, therefore, to be a statistically optimal method of sequential assimilation of data into linear models. Optimal interpolation can be considered as an approximation to the Kalman filter, assuming the error covariances to be constant. Most commonly in oceanography, assumptions concern the form of the covariance matrix. Examples of efficient schemes based on reduced-rank approximations in two-dimensional shallow-water models are given by Canizares et al. (1998) and Heemink et al. (1997).

Steady-state Kalman filters can significantly improve operational forecasts in the North Sea with small extra costs or delays. With a fixed set of observations at each time step, a fixed Kalman filter proves to be a good approximation and the time-consuming step of calculating this can be done offline. The prerequisites are that there exist observations upstream from the locations for which the forecasts are needed and that these observations can be available fast enough to be assimilated.

In situ observations from tide gauges or platforms will in general be the best choice for data assimilation. Satellite altimeter products can in principle be used, but these data are generally so infrequent that one cannot rely on them and timely availability of the appropriate processed products might also be an issue.

Quality control of the observations is of crucial importance. A few erroneous observations can do more harm to the forecasts than many good observations can ever do to improve them. In general, if the model and the data assimilation have to run automatically, without human interference, quality control also has to be automated. Tide-gauge data are mostly not close enough together to have much practical value for correlations in space, but as the sea level tends to fluctuate on a time scale of minutes, observations are available with a high frequency, and correlations in time can be exploited fully. The combination of absolute values of the water level, the surge and the difference with previous model forecasts and their first and second derivatives in time prove to be a powerful tool to achieve this. All of these quantities should be restricted to “sensible” limits, which can be determined from historical data. The water level itself should be required to show a minimum variability to identify a hanging tide gauge. Furthermore, missing data should be dealt with sensibly: if too many observations are missing for a certain period, the data that are present might be rejected because the derivatives cannot be determined.

### 5.5.5 **Three- and four-dimensional variational analysis**

Variational analysis is a method of data assimilation using the calculus of variations. It was first devised by Sasaki (1958). Three-dimensional variational (3Dvar) analysis considers the method to be an approximate solution to a minimization problem. A “cost function” is found, consisting of quadratic expressions of the differences between observations and model variables and of their error covariances. Minimization methods (from optimization theory) are applied iteratively using an appropriate descent algorithm. Methods typically used are preconditioned conjugate-gradient or quasi-Newton techniques. An initial guess is used, which is normally the uncorrected model fields. The major difficulty with 3Dvar concerns the expression of the matrix for the covariance of model error, since it is this matrix that determines how assimilated increments spread out through the grid. Four-dimensional variational (4Dvar) analysis is a generalization for observations that are distributed either side of an analytical step in time. The method has the additional advantage that dynamical constraints (based on governing equations) can

be placed on the sequence of model states that result. For more details the reader is referred to Talagrand (1981).

### 5.5.6 **The United Kingdom system**

The atmospheric input to the surge ensemble in the United Kingdom is provided by the Met Office Global and Regional Ensemble Prediction System (MOGREPS), which is described by Bowler et al. (2007*a, b*). The perturbations are calculated using an ensemble transform Kalman filter (ETKF). Twenty four alternative fields of sea-level pressure and 10-metre winds are produced at hourly intervals. Surge ensemble runs are triggered by completion of the MOGREPS regional forecasts. The initial condition for all ensemble members is taken from the corresponding time step of the deterministic surge simulation.

The surge model is post-processed to produce a variety of graphical outputs, based on the requirements of the United Kingdom operational Storm Tide Forecasting Service. Some examples are shown in Figures 5.3–5.5 (see also Flowerdew et al., 2009; Flowerdew et al., 2010). Figure 5.3 shows a set of “postage stamps”, which is simply the surge residual predicted by each ensemble member. An animation of postage stamps would display all the information contained within the ensemble output, and would be useful as a tool to study the evolution of a particular ensemble member (for example, one that predicts an extreme event). In many cases, however, all the members look very similar, and this plot type can fail to highlight important differences or support definitive decision making. Figure 5.4 shows a “mean and spread” chart for the same time step of the same forecast. The mean is depicted by the contour lines, and the spread by the colour shading. The colours in this example indicate that the greatest uncertainty (spread) is along the German coast, which also has the largest mean surge prediction. This plot type is good for indicating regions of uncertainty and how they relate to the mean surge prediction. Figure 5.5 displays the fraction of ensemble members predicting a surge residual greater than 0.6 metres at a given time step. This example indicates the virtual certainty of such a surge along the German coast, risks of between 40 and 60 per cent along the Norfolk coast of the United Kingdom and negligible risk elsewhere. This type of plot allows a quick appreciation of the level of risk of the specified event across different sections of the coast.

### 5.5.7 **The system in the Netherlands**

The system in the Netherlands uses input from the ECMWF Ensemble Prediction System (EPS). This has a deterministic forecast and an ensemble of

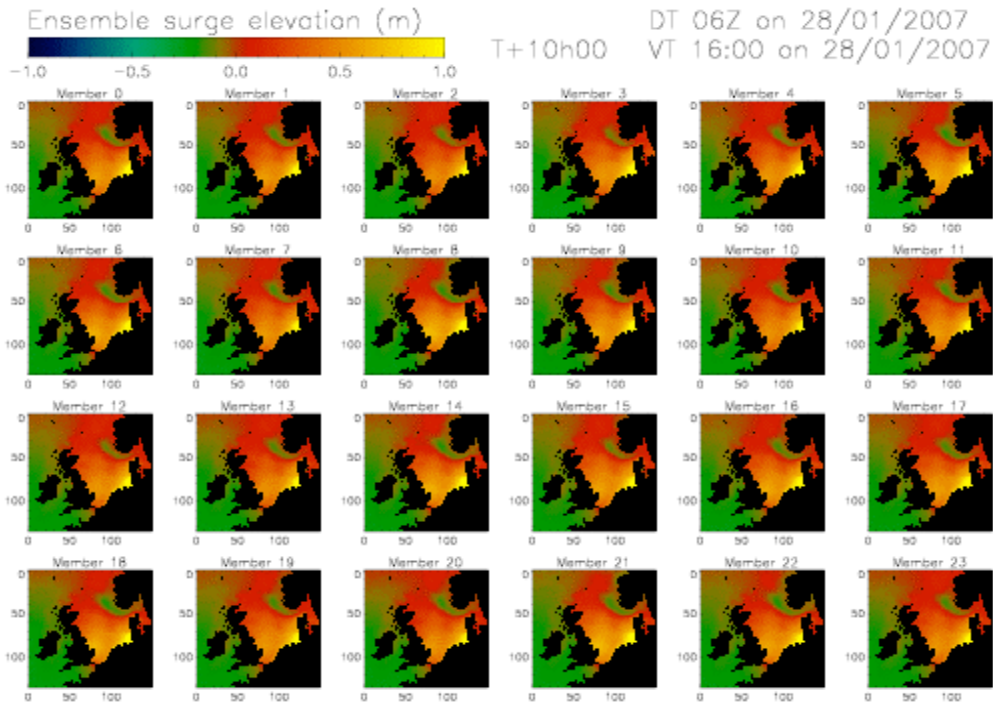


Figure 5.3. “Postage stamps” of residual surge elevation showing the surge residual predicted by each ensemble member

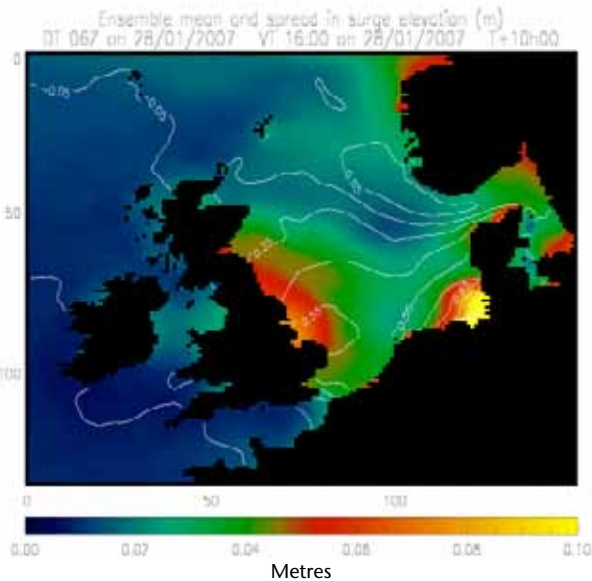


Figure 5.4. A “mean and spread” chart for the same time step and forecast as that illustrated in Figure 5.3. Mean (contours) and spread (colours) of residual surge elevation (metres)

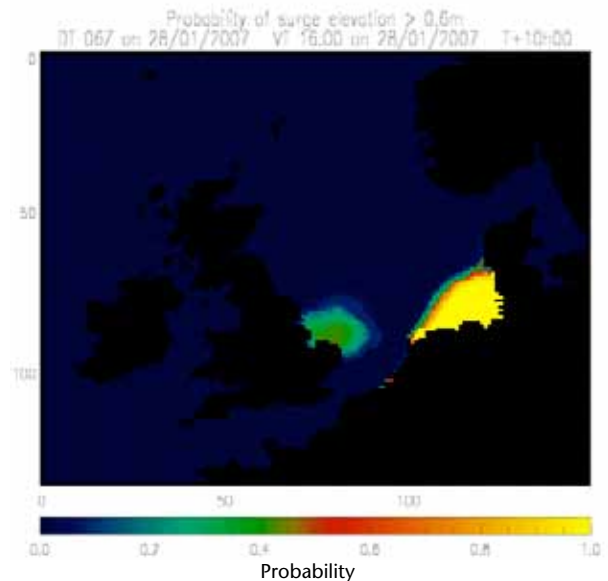


Figure 5.5. Forecast probability displaying the fraction of ensemble members predicting a surge residual greater than 0.6 metres at a given time step. This example indicates the virtual certainty of such a surge along the German coast, risks of between 40 and 60 per cent along the Norfolk coast of the United Kingdom and negligible risk elsewhere.

lower resolution with a control forecast and 50 perturbed members. All members are used to drive the storm surge model. The output is mainly used for forecasts of skew surge for coastal locations in the Netherlands. The individual forecasts are transformed into probability forecasts with a calibration derived from an earlier winter season of forecasts. Figure 5.6 shows an example of a surge

forecast for Vlissingen in the south of the country. Skew surges from all individual members are shown together with calibrated probabilities. Orange asterisks indicate the observed surges.

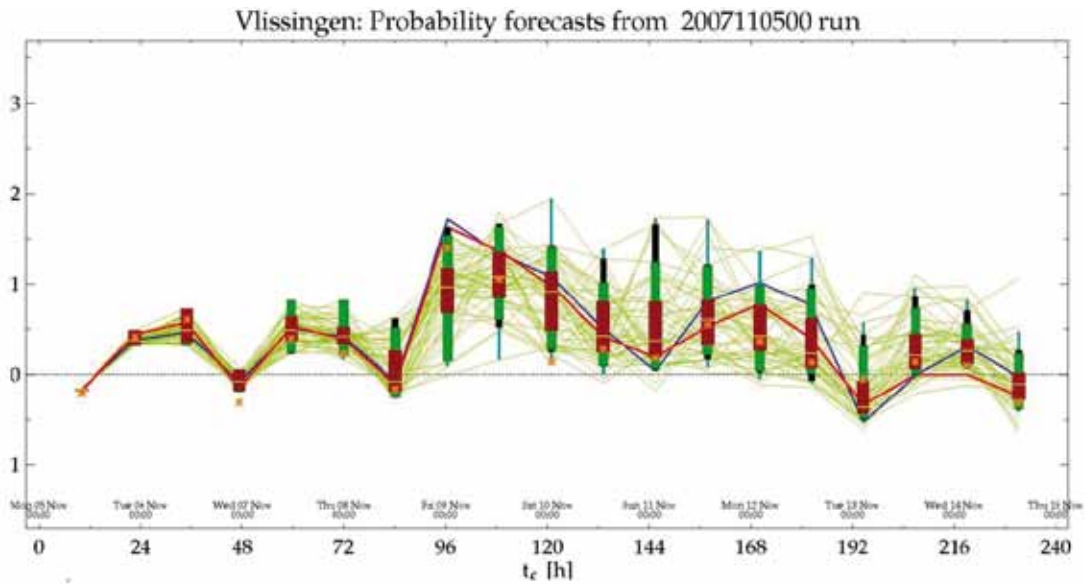


Figure 5.6. Probability surge forecast based upon the ECMWF ensemble for Vlissingen in the south of the Netherlands. Skew surges from all individual members are shown together with calibrated probabilities. Orange asterisks indicate the observed surges.





## OPERATIONAL FORECAST VERIFICATION

### 6.1 INTRODUCTION

This chapter reviews the various approaches to forecast verification that are applied to operational surge models. These methods concern routine permanent or periodic analyses of model output with some observed quantity. The primary purpose of verification is to monitor the consistency of outputs and to identify steps that may be taken to improve the quality of a forecast. In practice, the most commonly compared variable is total sea level or sea-level residual and the observational data are obtained from tide-gauge networks. Although not a routine choice, the verification of horizontal currents is also feasible using data from modern instruments such as acoustic Doppler current profilers (ADCP). Indeed, verification of model performance away from the coast in areas where tide-gauge data are not available is an area of monitoring that demands further investment. In the future, observations of sea level from satellite altimetry may be available for verification, but this is not the case at the time of writing.

When comparing observed and modelled sea levels, the differing nature of the two datasets must be taken into account. The majority of finite difference surge models are based on a C-grid (Arakawa and Lamb, 1977), which implies that the model elevation point is distant by half a grid cell from the modelled representation of the physical coastline. For models of medium or coarse resolution this may necessitate extrapolation of the model variable. Since the model output represents average conditions over several time periods, then some averaging of observations over time may also be required. As noted in Chapter 4, in many operational systems a modelled surge (plus tide–surge interaction) is generated by running the simulation with and then without meteorological forcing and subtracting the two. Unfortunately, as well as representing the results of surge and also of tide–surge interaction, the observed non-tidal residual may also contain errors of instrument timing and harmonic prediction (Horsburgh and Wilson, 2007). As shown in this paper, small errors of phase in harmonic predictions can cause significant oscillations in the calculated residual. The annual variability of tidal constituents is discussed in Pugh (1987, page 133). Although tides can be predicted to great accuracy, the combined error over 60–100 constituents can amount to several centimetres of amplitude, or phase errors equating to several minutes. These errors are typically largest in

regions of high tidal amplitude. Bearing all this in mind, it is good practice to use the word “surge” only when implying a genuine meteorological contribution to sea level.

Comparisons with observational data will usually take the form of a set of statistics, calculated monthly. The parameters of interest for sea levels are the correlation, the mean error (which can reveal model biases), the maximum error and RMSE. More concise verifications can be obtained via a specified skill score (see, for example, Bogden et al., 1996), which normally takes the form of a ratio between the instantaneous model error and the departure from a reference or background value:

$$Skill = 1 - \frac{\sum_{i=1}^N (O_i - M_i)^2}{\sum_{i=1}^N (O_i - C_i)^2} \quad (6.1)$$

where:

$O_i$  = the series of observed values;

$M_i$  = the modelled value;

$C_i$  = background (often climatic) value at that location.

Comparisons of several variables (for example, surface elevation and currents) can be combined in a weighted sum or cost function. For a thorough guide to oceanographic skill assessment see Lynch and Davies (1995).

If possible, the process of verification should be applied to the entire forecast suite. This includes the meteorological forcing and all components of the marine forecast delivered to the customer of the operational system. There is a long history of forecast verification in meteorology, and an excellent overview can be found at the Website <http://www.cawcr.gov.au/projects/verification/>. All of these techniques are equally applicable to storm surge forecasting. Examples of verification procedures from several regional operational models are given below.

### 6.2 ROUTINE VERIFICATION OF THE UNITED KINGDOM OPERATIONAL STORM SURGE MODEL

The National Oceanography Centre (NOC) develops and maintains the tide–surge models used to forecast storm surges around the United Kingdom

coast on behalf of the Environment Agency. Archived port data generated by the United Kingdom Tide Gauge Network (see Figure 6.1) are transferred back to NOC at regular intervals to assess model performance. Monthly plots of time series for each port are also available on the Internet ([https://www.bodc.ac.uk/data/online\\_delivery/ntslf/](https://www.bodc.ac.uk/data/online_delivery/ntslf/)). Additionally, simple statistics are calculated based on the difference between the hourly model and the observations (the model residual minus the observed residual). From this, mean, standard deviation, correlation coefficient, RMSE, maximum error and the time at which that occurred are calculated. Importantly, these parameters are calculated for the hour closest to model high water for each month, as these have the most practical relevance for flood forecasting. An example statistical table for these parameters is shown in Table 6.1.

Meteorological Institute (DMI) database, where all online Danish tide-gauge data are routinely stored. The data providers are DMI, the Coastal Authorities, the Royal Danish Administration of Navigation and Hydrography, and a number of local authorities. Positions of stations are indicated in Figure 6.2.

Predictions of sea level are compared with tide-gauge data on an annual basis and monthly forecast errors are calculated as annual running means. The mean error, RMSE, explained variance and

**6.3 ROUTINE VERIFICATION OF THE DANISH STORM SURGE MODEL**

The Danish storm surge model, Mike21, was developed by the Danish Hydraulic Institute (DHI). Tide-gauge data are retrieved from the Danish



Figure 6.2. The Danish tide-gauge network



Figure 6.1. The United Kingdom National Tide Gauge Network (see: <http://www.pol.ac.uk/ntslf/networks.html> for more details)

Table 6.1. Surge statistics for the United Kingdom model based on hourly values for January 2005

Column headings indicate:

**Size:** Sample size (where there exists both a model and observed value)

**Corr:** Correlation coefficient

**Mean:** The arithmetic mean of the series (metres)

**S.D.:** The standard deviation from the mean (metres)

**RMSE:** The root mean square error (metres)

**Max err:** The maximum difference between model and observation occurring in the series (metres)

**Date:** Hour and day of the month at which the maximum difference occurs

| <i>Port</i>   | <i>Size</i> | <i>Corr</i> | <i>Mean</i> | <i>S.D.</i> | <i>RMSE</i> | <i>Max err</i> | <i>Date</i> |
|---------------|-------------|-------------|-------------|-------------|-------------|----------------|-------------|
| Stornoway     | 595         | 0.98        | 0.10        | 0.06        | 0.12        | 0.33           | 3z 20th     |
| Wick          | 743         | 0.97        | 0.10        | 0.07        | 0.13        | -0.35          | 12z 12th    |
| Aberdeen      | 743         | 0.96        | 0.07        | 0.08        | 0.10        | 0.33           | 19z 5th     |
| North Shields | 743         | 0.95        | -0.01       | 0.09        | 0.09        | -0.42          | 16z 12th    |
| Whitby        | 297         | 0.95        | -0.08       | 0.08        | 0.12        | -0.38          | 20z 23rd    |
| Immingham     | 743         | 0.92        | -0.03       | 0.13        | 0.14        | -0.83          | 14z 8th     |
| Cromer        | 743         | 0.95        | 0.02        | 0.12        | 0.12        | -0.43          | 18z 12th    |
| Lowestoft     | 743         | 0.96        | -0.01       | 0.10        | 0.10        | -0.44          | 21z 12th    |
| Felixstowe    | 743         | 0.95        | 0.03        | 0.11        | 0.11        | -0.41          | 23z 12th    |
| Sheerness     | 743         | 0.94        | -0.01       | 0.13        | 0.13        | -0.52          | 0z 13th     |
| Ilfracombe    | 709         | 0.88        | -0.01       | 0.09        | 0.09        | -0.34          | 14z 11th    |
| Hinkley Point | 743         | 0.88        | 0.06        | 0.14        | 0.15        | 0.60           | 1z 18th     |
| Avonmouth     | 107         | 0.83        | 0.05        | 0.15        | 0.15        | -0.38          | 6z 30th     |
| Mumbles       | 743         | 0.92        | 0.01        | 0.11        | 0.14        | 0.40           | 9z 2nd      |
| Milford Haven | 743         | 0.92        | 0.10        | 0.07        | 0.07        | -0.42          | 13z 11th    |
| Fishguard     | 743         | 0.96        | 0.00        | 0.08        | 0.09        | -0.32          | 15z 11th    |
| Holyhead      | 743         | 0.94        | -0.05       | 0.07        | 0.09        | 0.35           | 18z 18th    |
| Llandudno     | 743         | 0.96        | 0.05        | 0.10        | 0.15        | 0.52           | 20z 18th    |
| Liverpool     | 743         | 0.97        | 0.12        | 0.10        | 0.11        | -0.58          | 19z 11th    |
| Heysham       | 743         | 0.96        | -0.04       | 0.10        | 0.12        | -0.58          | 16z 11th    |
| Workington    | 743         | 0.87        | -0.06       | 0.11        | 0.25        | 0.70           | 3z 12th     |
| St. Marys     | 743         | 0.83        | 0.22        | 0.06        | 0.06        | 0.23           | 23z 18th    |
| Newlyn        | 743         | 0.88        | 0.02        | 0.07        | 0.08        | 0.27           | 15z 18th    |
| Plymouth      | 371         | 0.84        | -0.03       | 0.06        | 0.08        | 0.19           | 18z 8th     |
| Weymouth      | 743         | 0.85        | 0.05        | 0.08        | 0.08        | 0.42           | 14z 18th    |
| Portsmouth    | 743         | 0.89        | 0.01        | 0.10        | 0.1         | 0.43           | 13z 18th    |
| Newhaven      | 743         | 0.93        | 0.04        | 0.09        | 0.09        | 0.37           | 17z 18th    |
| Dover         | 743         | 0.69        | 0.02        | 0.10        | 0.11        | 0.36           | 13z 8th     |
| Jersey        | 743         | 0.97        | 0.01        | 0.14        | 0.14        | 0.64           | 12z 18th    |
| Port Erin     | 743         | 0.97        | 0.00        | 0.07        | 0.26        | 0.48           | 19z 18th    |
| Portpatrick   | 743         | 0.97        | 0.25        | 0.08        | 0.11        | 0.33           | 15z 2nd     |
| Islay         | 743         | 0.98        | 0.08        | 0.08        | 0.12        | 0.37           | 5z 12th     |
| Tobermory     | 743         | 0.98        | 0.09        | 0.07        | 0.13        | 0.34           | 5z 8th      |
| Ullapool      | 743         | 0.98        | 0.11        | 0.06        | 0.17        | 0.50           | 21z 11th    |
| Kinlochbervie | 743         | 0.97        | 0.16        | 0.07        | 0.19        | 0.43           | 17z 12th    |
| Lerwick       | 743         | 0.74        | 0.18        | 0.06        | 0.11        | 0.31           | 12z 2nd     |
| Newport       | 743         | 0.84        | 0.09        | 0.20        | 0.20        | 0.82           | 15z 11th    |
| Bournemouth   | 743         | 0.82        | 0.01        | 0.03        | 0.10        | 0.41           | 12z 18th    |

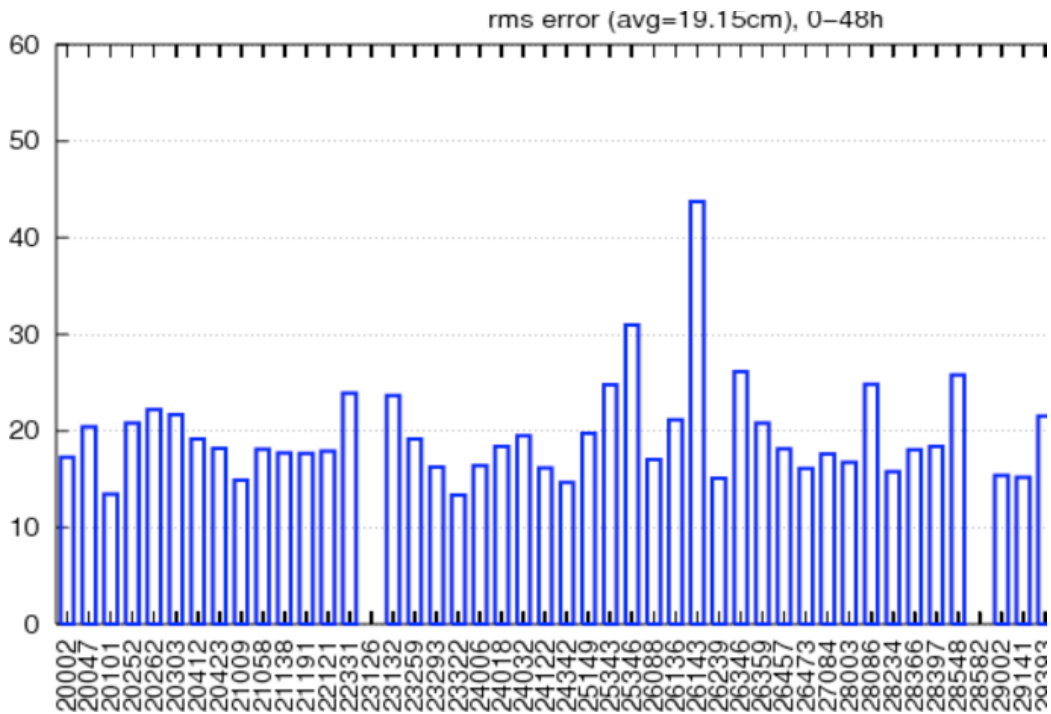


Figure 6.3. Root mean square error (centimetres) for all Danish stations for 2006

correlation coefficient are calculated for each station. This is done as a function of forecast range. Another parameter verified is the peak error (skew surge), previously illustrated in this Manual in Figure 4.3. Finally, a quality parameter, Q, is defined as the mean absolute peak percentage bias of the three highest peaks at 18 selected stations. This parameter is calculated once every month and reported as a running 12-month average. These results are shown in Figures 6.3 and 6.4.

6.4

**ROUTINE VERIFICATION OF THE GERMAN BSH STORM SURGE MODEL**

High- and low-water predictions for the German Baltic and North Sea stations are evaluated on an annual basis. Biases and standard deviations of high-water predictions are calculated at all stations. The examples shown in Table 6.2 are for the ports of Borkum and Cuxhaven for the years 2000 to 2005, produced by the BSH operational model. Higher bias values are typically found for differences

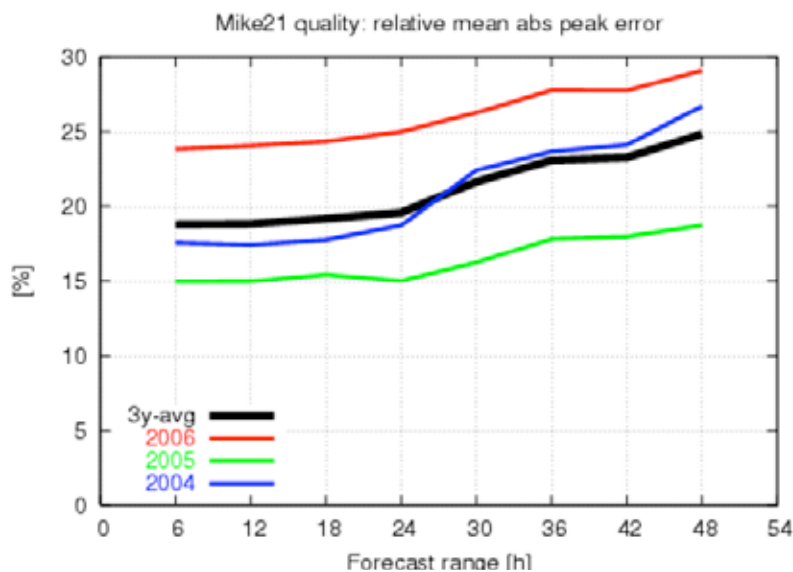


Figure 6.4. Quality factor, Q, for the Danish operational model Mike21 for years 2004 to 2006

**Table 6.2. Example frequency distributions of high- and low-water errors from the German BSH storm surge model for the ports of Borkum and Cuxhaven (centimetres)**

| Year | Borkum     |      |           |      | Cuxhaven   |      |           |      |
|------|------------|------|-----------|------|------------|------|-----------|------|
|      | High water |      | Low water |      | High water |      | Low water |      |
|      | Bias       | SD   | Bias      | SD   | Bias       | SD   | Bias      | SD   |
| 2000 | -0.6       | 16.2 | 11.2      | 23.3 | 6.1        | 18.5 | 18.1      | 20.8 |
| 2001 | -5.5       | 16.0 | 8.7       | 16.2 | 4.7        | 18.2 | 19.0      | 18.4 |
| 2002 | -5.5       | 16.7 | 7.1       | 16.8 | 2.7        | 19.1 | 24.8      | 19.1 |
| 2003 | -4.6       | 16.1 | 8.5       | 16.8 | 3.9        | 18.3 | 20.5      | 19.1 |
| 2004 | -2.1       | 17.6 | 11.5      | 17.4 | 10.7       | 21.8 | 24.6      | 18.8 |
| 2005 | -2.7       | 15.2 | 9.5       | 16.3 | 8.2        | 18.2 | 23.7      | 19.4 |

at low water because the complex topography of the Wadden Sea and German estuaries has a stronger effect on low than on high water, even for a model resolution of 1 nautical mile.

### 6.5 ROUTINE VERIFICATION OF THE NETHERLANDS DCSM98 STORM SURGE MODEL

The Netherlands storm surge model DCSM, run operationally by KNMI, is verified against observational data from the Rijkswaterstaat network. Skew surges are routinely evaluated at the ports of Vlissingen, Roompot Buiten, Hoek van Holland, Ijmuiden, Den Helder, Harlingen and Delfzijl. The examples in Figure 6.5 show 30-day averages of the RMSE, bias and standard deviation of the high-water skew surge for Hoek van Holland for the years from 1997 to 2007. It should be noted that the version of the model with data assimilation (Kalman filter, indicated by a red line) exhibits improved performance. The data assimilation reduces all the error parameters and removes seasonal signals from the verification plots.

### 6.6 TOTAL FORECAST VERIFICATION – AN EXAMPLE FROM THE UNITED KINGDOM COASTAL MONITORING AND FORECASTING (UKCMF) SERVICE

Ideally the whole forecasting system should be verified, including both the local winds and wind conditions in the generating region of the storm surge, the modelled surge and the timeliness and accuracy of issued alerts. Depending on how the system is structured, it may be possible for a forecaster to judge that the modelled atmospheric forcing is inaccurate and to modify the predicted surge value. If this occurs it is useful to verify both the raw model and the forecaster's values to judge the effectiveness of the intervention. The example

verification products shown in this section are taken from the annual report for the period 2004–2005 of the UKCMF Service.

The system is judged annually on three principal measures – performance, skill score and timeliness. The performance measure is an overall metric that assesses the timeliness of the issue of an alert and the significance of the observed sea level in relation to some predefined alert levels (which are prescribed for each region). The general principle is that the more significant the event is, the larger will be the reward, but also the penalty if no alert is issued (or if it is late). Table 6.3 shows the number of events in each category for the period from April 2004 to March 2005 for ports in England and Wales.

The performance is measured by multiplying the number of occurrences in a category by the weighting for that category (see Table 6.4) and then summing all components. This actual score is divided by the perfect score to give a percentage figure. For the period shown here the performance measure was 87 per cent. Reporting the forecast system performance with a single indicator is often useful when communicating to non-scientific stakeholders (for example policy makers or local planners).

**Table 6.3. Table of events for all ports in England and Wales from April 2004 to the end of March 2005. This information was used to generate the performance measure in the example cited in the text.**

| Alert issued?<br>(Alert time in hours) | Alert level reached? |     |                |        |
|--|----------------------|-----|----------------|--------|
|  | Major                | Yes | No – near miss | No     |
| Yes: $\geq 12$                         | 1                    | 22  | 42             | 26     |
| Yes: $\geq 8$ and $< 12$               | 1                    | 14  | 45             | 12     |
| Yes: $< 8$ and $\geq 4.5$              | 0                    | 0   | 1              | 0      |
| Yes: $< 4.5$                           | 0                    | 0   | 0              | 0      |
| No                                     | 0                    | 0   | 10             | 18 182 |

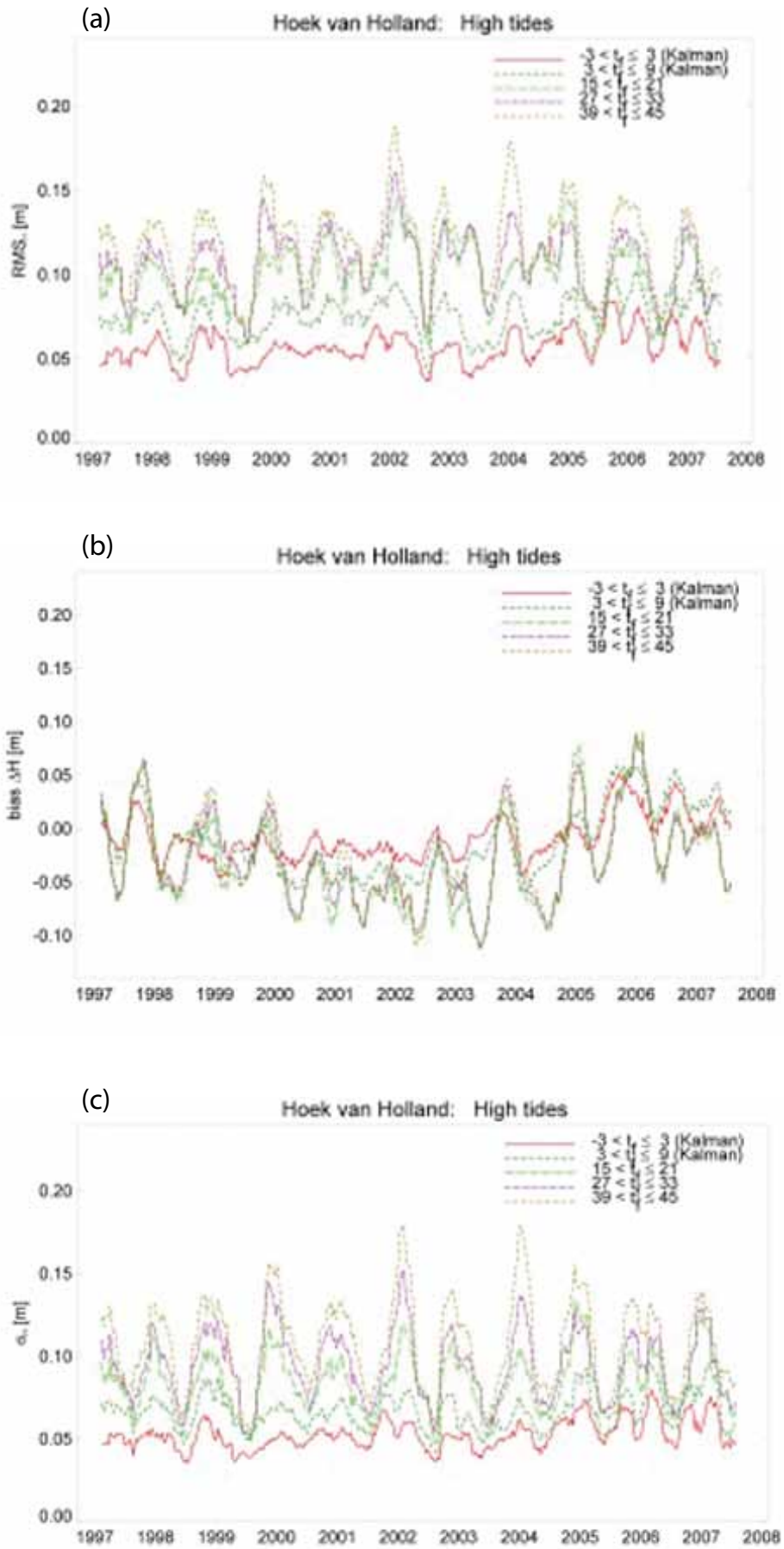


Figure 6.5. Thirty-day averages of (a) RMSE, (b) bias and (c) standard deviation (in metres) of the skew surge for the DCSM model. Colours denote different forecast periods as indicated in the captions.

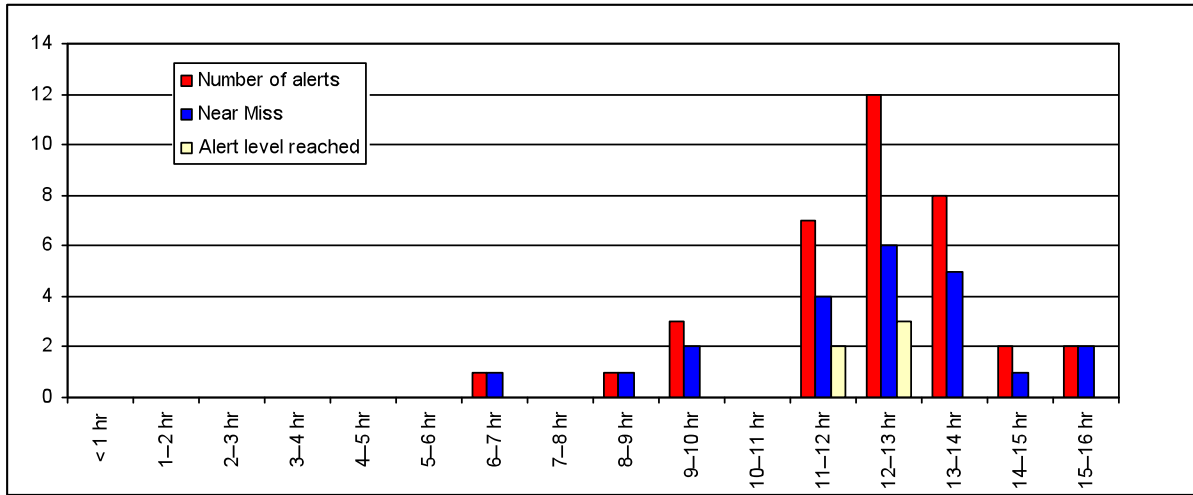


Figure 6.6. Distribution, as a function of lead time, of the total number of alerts issued and numbers of alerts for which near misses of levels or levels actually reached were recorded

Table 6.4. The weightings used for the calculation of the performance measure

| Alert issued?<br>(Alert time in hours) | Alert level reached? |     |                |       |
|--|----------------------|-----|----------------|-------|
|  | Major                | Yes | No – near miss | No    |
| Yes: $\geq 12$                         | 100                  | 10  | 5              | -2    |
| Yes: $\geq 8$ and $< 12$               | 85                   | 10  | 5              | -2    |
| Yes: $< 8$ and $\geq 4.5$              | 50                   | 6   | 4              | -4    |
| Yes: $< 4.5$                           | 10                   | 1   | 0              | -15   |
| No                                     | -20                  | -15 | 0              | 0.002 |

The skill score is calculated from the dataset of events used for the performance measure, but excludes tides that did not reach a significant alert level (that is, those in the no alert/near miss category). Skill scores are typically higher than the performance measures.

Timeliness is self explanatory. Figure 6.6 shows the distribution of lead time for all alerts emitted. For the reporting period shown, the average time for the issue of alerts was 12 hours 17 minutes, with the shortest being 6 hours 50 minutes. The average lead time for those alerts for which the sea level actually exceeded the alert threshold was 12 hours 6 minutes, with the shortest lead time in this case being 11 hours 31 minutes.





## CHAPTER 7

### REGIONAL FORECAST SCENARIOS

#### 7.1 **STORM SURGES GENERATED BY TROPICAL CYCLONES**

##### 7.1.1 **North-western Pacific**

In recent years natural maritime disasters, such as storm surges, increases in sea level and tsunamis have all caused serious loss of life and extensive economic damage along the coasts of this region. Storm surges are more important in the spring and summer since they are primarily influenced by typhoons. In 1997, Typhoon *Winnie* combined with perigean spring tides to cause serious flood damage in western coastal areas of the Korean Peninsula. There were 849 fatalities and the total value of property damage was estimated at over US\$ 22 million. In this instance the flooding was not caused by the primary storm surge associated with Typhoon *Winnie*. The tidal forcing was

enhanced due to the resonance coupling of this surge with the natural period of the Yellow Sea, about 37 hours (Moon et al., 2003). More recently, in 2003 Typhoon *Maemi* passed through the Korean Peninsula. It was especially devastating, leaving approximately 130 people dead and causing property damage worth more than US\$ 4 781 million (Seo et al., 2006).

The history of major storms around the Korean Peninsula during the years 1904–2005 is detailed in Table 7.1. Tropical storms and associated surges occur predominantly in the months of July, August and September. During surge events, coastal inundation is usually worst along the south coast where there is a broad, gently sloping shelf. There is less inundation along the steeper continental shelf of the east coast of the Peninsula, although large breaking waves still present major

**Table 7.1. Monthly distribution of the major storms around the Korean Peninsula for the period 1904–2005**

Source: Seo et al., 2006

| Year | Month |      |      |      |      |      | Total | Year | Month |      |      |      |      |      | Total |
|------|-------|------|------|------|------|------|-------|------|-------|------|------|------|------|------|-------|
|      | May   | June | July | Aug. | Sep. | Oct. |       |      | May   | June | July | Aug. | Sep. | Oct. |       |
| 1904 |       |      |      | 2    |      |      | 2     | 1956 |       |      |      | 1    | 3    |      | 4     |
| 1905 |       |      | 1    | 1    | 1    |      | 3     | 1957 |       | 1    |      | 1    |      |      | 2     |
| 1906 |       |      |      | 1    | 1    | 1    | 3     | 1958 |       |      |      |      | 1    |      | 1     |
| 1907 |       |      | 2    |      | 1    |      | 3     | 1959 |       |      | 2    | 1    | 4    |      | 7     |
| 1908 |       |      |      | 1    |      |      | 1     | 1960 |       |      | 1    | 2    |      |      | 3     |
| 1909 |       |      |      | 2    |      |      | 2     | 1961 | 1     |      | 1    | 1    | 1    | 1    | 5     |
| 1910 |       |      | 1    |      |      |      | 1     | 1962 |       |      | 1    | 2    | 1    |      | 4     |
| 1911 |       |      | 2    | 1    | 1    | 1    | 5     | 1963 |       | 1    | 1    | 1    |      |      | 3     |
| 1912 |       |      | 1    |      |      |      | 1     | 1964 |       |      | 3    | 1    |      |      | 4     |
| 1913 |       |      | 1    |      |      |      | 1     | 1965 |       |      | 1    | 2    |      |      | 3     |
| 1914 | 1     | 2    | 1    | 2    |      |      | 6     | 1966 |       |      |      | 2    | 1    |      | 3     |
| 1915 |       |      | 1    | 1    | 1    |      | 3     | 1967 |       |      | 1    |      |      |      | 1     |
| 1916 |       |      |      | 1    | 1    |      | 2     | 1968 |       |      | 1    | 1    | 1    |      | 3     |
| 1917 |       |      |      | 1    | 2    |      | 3     | 1969 |       |      |      |      | 1    |      | 1     |
| 1918 |       |      | 1    | 2    |      |      | 3     | 1970 |       |      | 2    | 2    |      |      | 4     |
| 1919 |       |      |      | 3    | 1    |      | 4     | 1971 |       |      |      | 2    | 1    |      | 3     |
| 1920 |       |      |      |      |      |      | 0     | 1972 |       |      | 2    | 1    | 1    |      | 4     |
| 1921 |       |      |      |      | 2    |      | 2     | 1973 |       |      | 2    | 1    |      |      | 3     |
| 1922 |       |      | 2    |      | 2    | 1    | 5     | 1974 |       |      | 2    | 1    | 1    |      | 4     |
| 1923 | 1     | 1    | 2    |      |      |      | 4     | 1975 |       |      | 1    | 1    |      |      | 2     |

(Table 7.1 continued)

| Year | Month |      |      |      |      |      | Total | Year    | Month |      |      |      |      |      | Total |
|------|-------|------|------|------|------|------|-------|---------|-------|------|------|------|------|------|-------|
|      | May   | June | July | Aug. | Sep. | Oct. |       |         | May   | June | July | Aug. | Sep. | Oct. |       |
| 1924 |       |      | 1    | 3    |      |      | 4     | 1976    |       |      | 3    | 2    | 1    |      | 6     |
| 1925 |       |      | 3    | 1    | 1    |      | 5     | 1977    |       |      |      | 1    | 1    |      | 2     |
| 1926 |       |      | 1    | 2    |      |      | 3     | 1978    |       | 1    |      | 2    | 1    |      | 4     |
| 1927 |       |      |      | 1    | 1    |      | 2     | 1979    |       |      |      | 2    |      |      | 2     |
| 1928 |       |      |      |      | 2    |      | 2     | 1980    |       |      | 1    | 1    | 1    |      | 3     |
| 1929 |       |      |      | 1    |      |      | 1     | 1981    |       | 2    | 1    |      | 2    |      | 5     |
| 1930 |       |      | 2    | 1    |      |      | 3     | 1982    |       |      |      | 3    | 1    |      | 4     |
| 1931 |       |      | 2    | 1    |      |      | 3     | 1983    |       |      |      |      | 1    |      | 1     |
| 1932 |       |      |      | 2    |      |      | 2     | 1984    |       |      | 1    | 1    | 1    |      | 3     |
| 1933 |       |      | 3    | 1    | 2    |      | 6     | 1985    |       | 1    |      | 3    |      | 1    | 5     |
| 1934 |       |      | 1    | 1    | 1    |      | 3     | 1986    | 1     | 1    |      | 1    | 1    |      | 3     |
| 1935 |       |      |      | 1    | 1    |      | 2     | 1987    |       |      | 2    | 1    |      |      | 3     |
| 1936 |       |      | 1    | 2    | 1    |      | 4     | 1988    |       |      |      |      |      |      | 0     |
| 1937 |       |      | 1    |      | 1    |      | 2     | 1989    | 1     | 1    |      |      |      |      | 2     |
| 1938 |       |      |      | 1    | 1    |      | 2     | 1990    |       | 1    | 1    |      | 2    |      | 4     |
| 1939 |       |      | 1    | 1    |      |      | 2     | 1991    |       |      | 1    | 2    | 2    |      | 5     |
| 1940 |       |      | 2    | 1    | 2    |      | 5     | 1992    |       |      |      | 1    | 1    |      | 2     |
| 1941 |       |      | 1    | 2    |      |      | 3     | 1993    |       |      | 2    | 1    | 1    |      | 4     |
| 1942 |       |      | 1    | 3    |      |      | 4     | 1994    |       |      | 2    | 2    |      | 1    | 5     |
| 1943 |       |      | 3    | 1    |      |      | 4     | 1995    |       |      | 1    | 1    | 1    |      | 3     |
| 1944 |       |      |      | 1    |      |      | 1     | 1996    |       |      | 1    | 1    |      |      | 2     |
| 1945 |       |      | 1    | 2    | 1    |      | 4     | 1997    | 1     | 1    | 1    | 2    | 1    |      | 5     |
| 1946 |       |      | 1    | 2    |      |      | 3     | 1998    |       |      |      |      | 1    | 1    | 2     |
| 1947 |       |      |      |      |      |      | 0     | 1999    |       |      | 1    | 2    | 2    |      | 5     |
| 1948 |       |      | 1    | 1    | 2    |      | 4     | 2000    |       |      | 2    | 2    | 1    |      | 5     |
| 1949 |       | 1    | 2    | 1    |      |      | 4     | 2001    |       |      |      | 1    |      |      | 1     |
| 1950 |       | 2    | 1    | 3    | 2    |      | 8     | 2002    |       |      | 3    | 1    |      |      | 4     |
| 1951 |       |      |      | 1    | 1    | 1    | 3     | 2003    | 1     | 1    |      | 1    | 1    |      | 4     |
| 1952 |       | 1    | 1    | 1    | 1    |      | 4     | 2004    |       |      | 1    | 3    | 1    |      | 5     |
| 1953 |       | 1    | 1    | 1    |      |      | 3     | 2005    |       |      |      | 1    |      |      | 1     |
| 1954 |       |      |      | 1    | 2    |      | 3     | Total   | 2     | 18   | 92   | 121  | 79   | 8    | 320   |
| 1955 |       |      | 2    |      | 1    |      | 3     | Average | 0.02  | 0.18 | 0.90 | 1.19 | 0.77 | 0.08 | 3.14  |

problems. The west coast is one of the strongest tidal areas in the world. The tidal range is 4 metres on the southern coast increasing to about 10 metres on the northern part of the west coast. These regions are exposed to hazardous conditions when high tides coincide with the passage of typhoons.

The majority of typhoons affecting the Korean Peninsula tend to affect the southern coast, then passing through the East Sea/Sea of Japan. The tracks of tropical storms during these critical months are shown in Figure 7.1.

Countries bordering the north-western Pacific have recognized the importance of exchanging observational data and information on the prediction of storm surges. This has enabled the development of comprehensive storm surge prediction and sea-level monitoring systems. Since the establishment of the first tidal monitoring station at Mokpo in 1952, 34 tidal stations have been operationally observed by the Republic of Korea National Oceanographic Research Institute (NORI). Real-time tidal data have been provided by NORI to the Republic of Korea Meteorological Administration (KMA) for storm

surge forecasting through the automatic online system since 2003.

Storm surge prediction is carried out by KMA using the operational model for atmospheric input data, the Regional Data Assimilation and Prediction System (RDAPS). Wind stress and mean sea-level pressure fields from this model are fed into a two-dimensional barotropic surge and tide version of the Princeton Ocean Model. This storm surge model of medium resolution (based on a grid of

approximately 8 kilometres) encompasses the East China Sea and the East Sea/Sea of Japan, defined by 115 to 150 degrees east and 20 to 52 degrees north (see Figure 7.2). The operational model uses eight

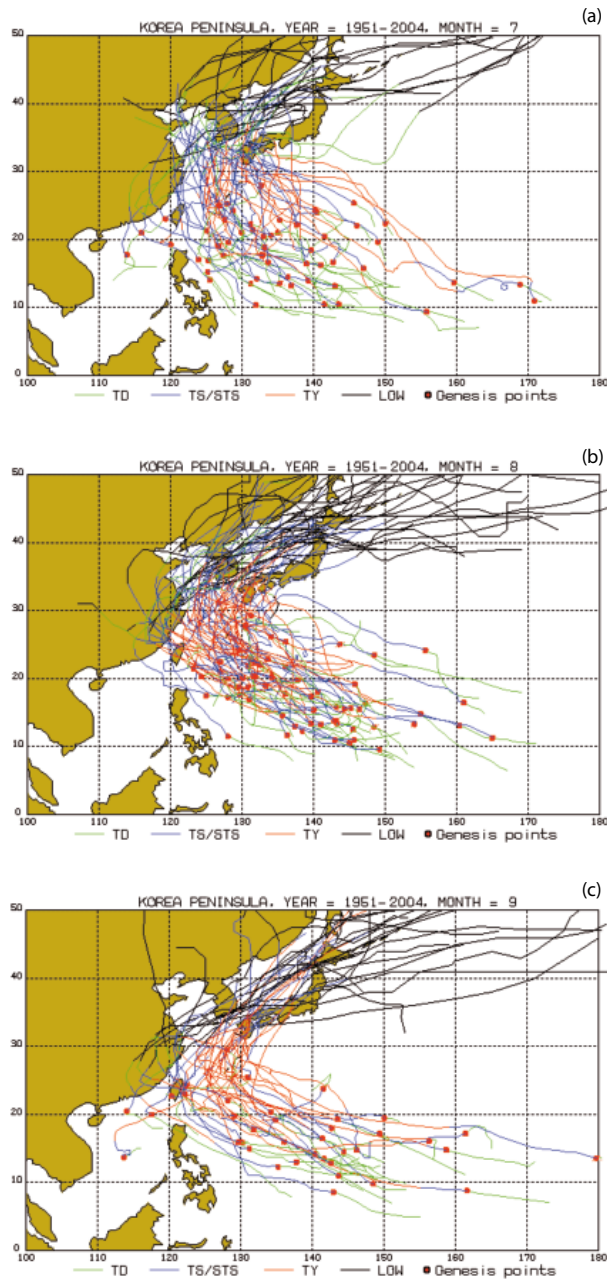


Figure 7.1. Tracks of typhoons in the north-western Pacific in (a) July, (b) August and (c) September from 1951 to 2004. Genesis points are indicated by red squares.

Source: Seo et al., 2005

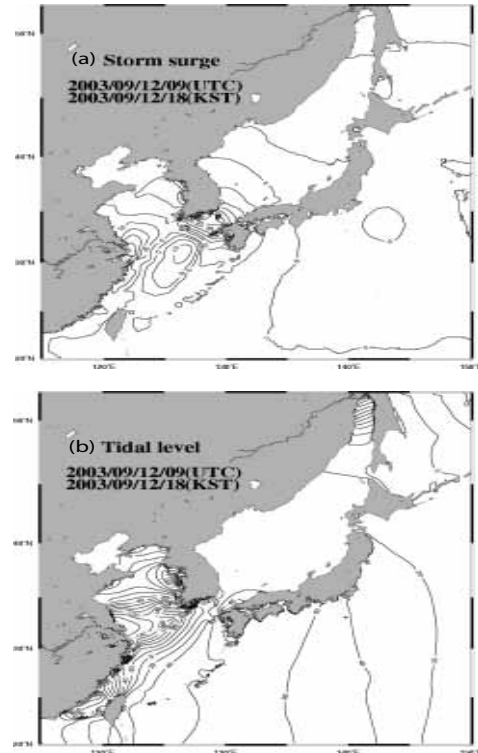


Figure 7.2. The spatial distributions of (a) storm surge and (b) tidal level obtained by the Regional Tide/Storm Surge Model (RTSM) of KMA. (Contours levels in centimetres)

Source: Seo et al., 2006

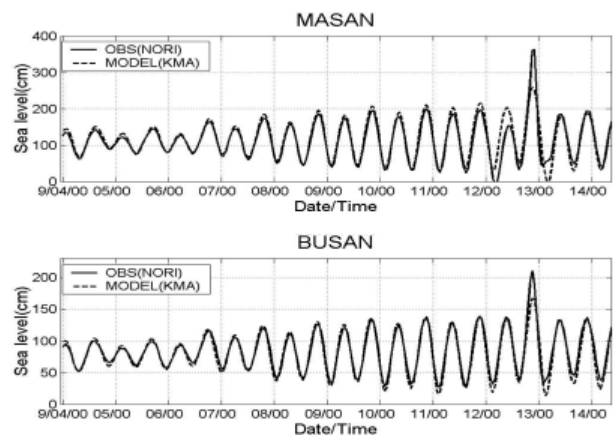


Figure 7.3. The time series of predictions obtained by the KMA model RTSM compared to tidal observations at Masan and Busan during Typhoon Maemi on 12 September 2003

Source: Seo et al., 2006

tidal components for lateral boundary conditions, runs twice each day and produces horizontal fields of surge.

Figure 7.3 compares sea-level observations from tidal stations with model predictions during Typhoon *Maemi*. There were severe impacts due to storm surge at both Masan and Busan. Note that *Maemi* coincided with high tide along the south coast of the Republic of Korea. In Masan, the maximum sea level reached was 3.6 metres, the highest level ever recorded. Even though the model under-predicted the surge magnitude at these two sites considerably the timing of peak surge was well represented. Table 7.2 provides more comprehensive observations for this event. In the open-sea stations (Jeju, Seogwipo and Wando) the predicted maximum surge heights agreed well with the observed ones, but in the complex coastal regions (Masan and Tongyeong) agreement was less satisfactory. It seems, therefore, that the current model resolution of one twelfth of a degree is not high enough to correctly simulate surge height along the southern coasts. To correct these deficiencies, alternative methods such as ANNs may be used to predict storm surge more exactly for a specific area. The ANN model used in this region is composed of an input layer, a hidden layer and an output layer (Hastie et al., 2001). The subject of ANNs has been treated in 1.6, previously.

The reader is also referred to previous Figures 4.5 and 4.6, and the discussion in 4.5.4, which illustrate the operational storm surge forecasting system used by JMA. In this region, accurate prediction of storm surge height depends on the strength, path and track speed of typhoons. The information given in this previous chapter provides a good example of the effectiveness of the JMA forecasting system operating in the north-western Pacific region.

### 7.1.2 South-western Pacific

Australia operates three Tropical Cyclone Warning Centres (TCWCs) located in Perth (Western Region), Darwin (Northern Region) and Brisbane (Eastern Region). The regions of responsibility are shown in Figure 7.4. The procedures followed to forecast storm surge generated by tropical cyclones differ slightly in each of the three regions. Those used in the Eastern Region are described in this section while the Northern and Western Region procedures are described in 7.1.5.

In the absence of reliable forecasts for atmospheric fields associated with tropical cyclones, a commonly used alternative is synthetic wind fields based on a parametric representation of the cyclone forcing. This representation normally relies on a small set of parameters that can be estimated from available observations (satellite imagery, surface observations and radar). One commonly employed empirical parameterization is based on Holland (1980), which served as the basis for forcing-field parameters in the 1990s.

In the Australian Eastern Region, the primary method for forecasting surges is based on nomograms such as the Jelesnianski-Taylor nomogram shown in Figure 7.5. This requires two cyclone parameters:

- (a) The radius of maximum winds (an indicator of cyclone size);
- (b) The pressure drop (the ambient pressure surrounding the tropical cyclone minus the central pressure).

The system does not explicitly use the Jelesnianski-Taylor nomogram for cyclones of category one, two or three. This is because the solid lines representing intensity are nearly horizontal for these weaker cyclones. A preliminary surge value (in metres) for

**Table 7.2. Tide predictions by HA and the performance of RTSM during the passage of Typhoon *Maemi* on 12 September 2003 (centimetres)**

Source: Seo et al., 2006

| Station   | Maximum observed sea level | Predicted tide (HA) | Storm surge |       |
|-----------|----------------------------|---------------------|-------------|-------|
|           |                            |                     | Observation | Model |
| SEOGWIPO  | 150                        | 106.34              | 43.66       | 51.49 |
| JEJU      | 162                        | 120.99              | 41.01       | 51.01 |
| WANDO     | 131                        | 65.00               | 66.00       | 54.70 |
| YEOSU     | 393                        | 259.67              | 133.33      | 78.27 |
| TONGYOUNG | 426                        | 256.05              | 169.95      | 68.41 |
| MASAN     | 363                        | 197.77              | 162.23      | 62.75 |
| BUSAN     | 211                        | 130.96              | 80.04       | 47.61 |
| ULSAN     | 116                        | 53.02               | 65.98       | 42.26 |

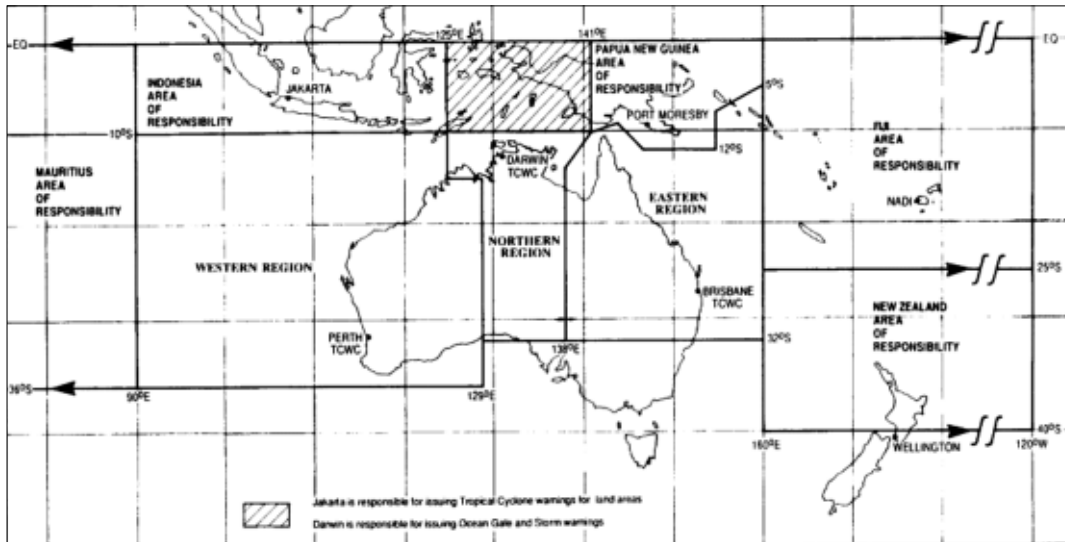


Figure 7.4. Areas of responsibility of the Australian TCWCs

less intense cyclones is conveniently obtained by dividing the pressure drop by 15. Whatever the preliminary surge height is computed to be, it has been derived for standard motion across a standard basin. This preliminary height has to be adjusted for actual motion and bathymetry.

For non-standard cyclone motion, the nomogram in Figure 7.6 corrects the preliminary surge value for any angle of attack to the coast at any speed of

motion. It is known that nomograms of this nature do not work well with strongly curved coasts (that is, if the coastal radius of curvature is smaller than the radius of maximum winds).

Although numerical models provide the best approach to computing surges, several computer model runs may be required to cover the range of potential tracks, intensities and sizes that are possible for a single scenario. During a real-time situation this can overload computer facilities and personnel, and require time-consuming analysis of the output that may be unacceptable.

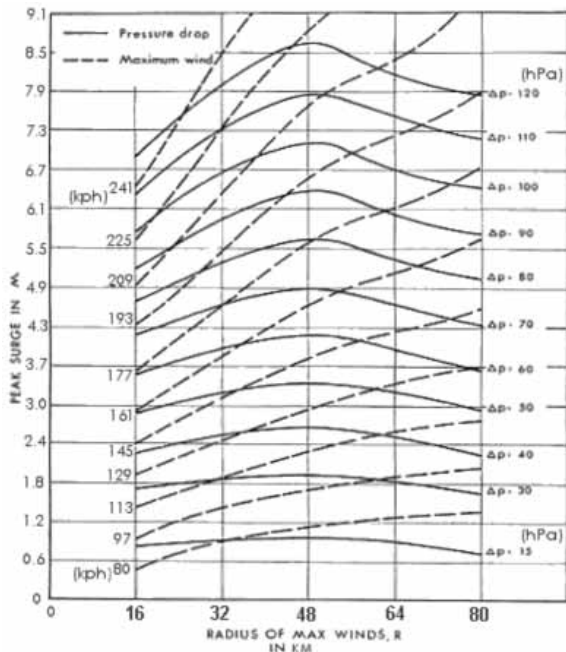


Figure 7.5. Jelesnianski-Taylor nomogram for peak surge on the open coast. Entering arguments are pressure drop and radius of maximum winds. The maximum winds are valid for 10 minutes average at 10 metres elevation for a stationary cyclone over water.

A new storm surge modelling system has been developed by the Australian Bureau of Meteorology Research Centre (BMRC) that uses the atmospheric fields from the Bureau’s tropical cyclone numerical prediction model (Tropical Cyclone Limited Area Prediction System: TC-LAPS) as forcing. It is intended to be deployed in regional offices on a PC that would run the model using TC-LAPS forecasts downloaded from a central server. The model uses a novel approach to address the potential errors in TC-LAPS forecasts by creating an ensemble of tropical cyclones with modified parameters and analysing the responses of the sea level to those cyclones (Entel et al., 2005).

Recent efforts have concentrated on using “storm surge atlases” that consist of a database of pre-computed storm surges for a particular basin. To generate the database, recourse is made to tropical cyclone climatology. The family of tracks account for alternate landfall points for a given direction along a coastal area of interest. Because the generated surge is strongly dependent on the angle that the track makes with the coast several hours before

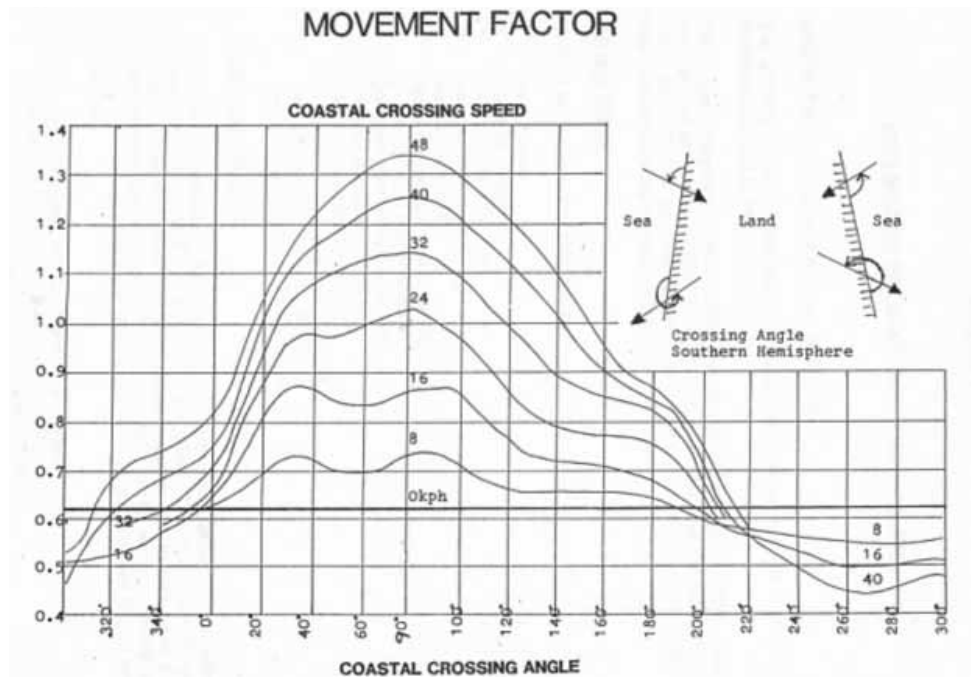


Figure 7.6. Nomogram of correction factors against the vector motion of tropical cyclones. The factor corrects for non-standard tropical cyclone motion and the inset orientates the cyclone track angle relative to a coast.

and after landfall, the remaining track segments affect the surge only mildly. Thus, although the location of a tropical cyclone far out to sea and its landfall point may be significantly in error, the family or families representing the broad approach to land can be used to estimate the likely surge consequences.

### 7.1.3 The Gulf of Mexico and United States Caribbean coastline

The material in this section is adapted from Dube et al. (2010).

There is a wide range of storm surge modelling systems in use for predicting the impact of tropical cyclones, covering a range of numerical methods, model domains, forcing and boundary conditions, and purposes. However, in the United States there are two primary surge models, SLOSH (see 4.3.1.1) and the Advanced Circulation (ADCIRC) model. While sometimes used for similar tasks, they are quite different in approach, have different strengths and weaknesses, and each is likely to be better suited to a particular application. There are, of course, many other models in use and a survey of some notable approaches is also provided below.

#### SLOSH

This model was developed by NWS (Jarvinen and Lawrence, 1985; Jelesnianski et al., 1992). It is based on a linearized form of the governing shallow-water

equations; the advective terms in the equations are discarded. The SLOSH model is a finite difference model that employs an orthogonal curvilinear grid. Such grids have been constructed for all vulnerable areas of the United States by NWS for use in emergency management (see: <http://www.weather.gov/tdl/marine/Basin.htm>). The structure of a SLOSH grid results in the finest resolution near the pole of the grid (which is placed near the area of interest). These grids are limited in domain size and their boundaries at the open ocean are located on the shelf. The model is able to simulate wetting and drying as well as parameterize features on a sub-grid scale, such as one-dimensional channel flow with contractions and expansions, vertical obstructions to flow with overtopping (levees, roads, and banks that include cuts) and increased friction drag in heavily vegetated areas. However, it is not able to account for inflow, rainfall or tides.

Within SLOSH a parametric tropical cyclone wind model is incorporated that is used for forcing both forecast and hypothetical storm simulations. The tropical cyclone track, central pressure deficit and radius of maximum winds are used as input to create wind and pressure fields that are interpolated onto the grid. A wind drag coefficient that is constant with respect to wind speed is applied, although this is modified according to vegetation over land.

The SLOSH model has been used by NWS for nearly four decades. An extensive skill assessment found

peak surge errors to be less than 0.6 metres for nearly 80 per cent of evaluations (Jarvinen and Lawrence, 1985). However, despite its merits the model does have limitations. At present it cannot provide astronomical-tide forcing or river inflow. It is a linearized model subject to error in locations where advection is important, such as in the vicinity of tidal inlets and similar constrictions. Furthermore, a SLOSH grid is generally limited to the coastal shelf surrounding the area being studied. Two issues arise from this limited-domain strategy. First, the use of a structured grid limits the capability to provide localized refinement. While SLOSH grids do have increased refinement at their centre, it is not always possible to resolve additional features that may be elsewhere (for example, an inlet along the coastline that is away from the centre of the grid). Conversely, the semi-annular structure of the grid also leads to over-resolution in regions outside the area of interest (for example, in areas inland beyond the flood plain). Second, during storm surge events the shelf-based, regional nature of a SLOSH domain limits accurate specification of boundary conditions because of lack of knowledge of set-up at the open boundary. This prevents dynamic coupling to larger basins.

In the United States, flood-prone areas are usually determined by using the SLOSH model with input parameters from thousands of hypothetical hurricanes. These model runs are used to create atlases of potential surge, which guide emergency managers in creating evacuation plans (Jarvinen and Lawrence, 1985). The NWS National Hurricane Center (NHC) also runs SLOSH for the prediction of storm surge from potentially landfalling tropical cyclones. The storm's parameters (track, size and intensity) are provided by the official hurricane forecast. These forecasts are distributed in real time to the forecast and emergency management community as Geographic Information System (GIS) products. Due to the limitations of accuracy of the storm forecasts, these only begin when a storm is within 24 hours of landfall. Therefore, they are only used to augment the pre-computed atlases of surge potential, which form the basis for emergency management activities. A probabilistic component based on the official NHC track forecast has been developed that forecasts the likelihood of surge as a function of the historical range of track error (see: <http://www.weather.gov/mdl/psurge/>).

#### ADCIRC

The ADCIRC model was originally developed for the United States Army Corps of Engineers for high-resolution coastal ocean modelling (Luettich et al., 1992). It has since been used by federal agencies, academic researchers and private companies for a wide range of modelling applications, including

storm surge, basin-scale tidal modelling and tidal inlet circulation studies. The ADCIRC model solves the shallow-water equations discretized in space using the finite element method, which allows for highly flexible, unstructured grids. All non-linear terms have been retained in these equations. The model can be run either in two-dimensional depth-integrated (2DDI) mode, or in three-dimensional mode. In either case, elevation is obtained from the solution of the depth-integrated continuity equation in generalized wave continuity equation (GWCE) form. The GWCE form is applied to prevent the generation of spurious oscillations. However, it replaces the continuity equation with its time derivative, so that continuity is not satisfied and mass balance errors exist. Velocity is obtained from the solution of either the 2DDI or three-dimensional momentum equations. The model requires input of wind and pressure fields to consider the effect of storm surge. These fields are developed by meteorological models independent of ADCIRC. For further description of the model implementation, see the ADCIRC theory report (Luettich and Westerink, 2004).

In order to simulate storm surge accurately, several features have been included within ADCIRC. These include modelling of the wetting and drying of inundated areas, representation of obstructions at sub-grid scale to flow as weirs, and application of the transfer of momentum from breaking wind waves as surface radiation stresses. Most importantly, the unstructured grid methodology allows for very high refinement of coastal regions (successfully modelled at scales of less than 50 metres). These highly refined coastal regions are built into basin-scale domains by smoothly varying element size. However, the high resolution of inundation regions and the small time steps required by the semi-explicit solution scheme is accompanied by high computational cost. The model can be run on a single processor, but most often it is run in parallel on high-performance computing systems with hundreds of processors using the message-passing interface (MPI).

The ADCIRC model is presently widely used in the United States by federal agencies for storm surge modelling. Following Hurricane *Katrina* in 2005, the United States Army Corps of Engineers partnered with other federal agencies and academic and private institutions to extend an existing ADCIRC storm surge application for southern Louisiana (Westerink et al., 2008). The extension of the model built for studying the hurricane protection system for Louisiana was to conduct an extremely large and refined forensic study of *Katrina's* disastrous storm surge. As part of the Inter-agency Performance Evaluation Task Force, this project applies very high resolutions of 50 to 100 metres across coastal

Louisiana and Mississippi, resulting in grids exceeding 1 million nodes. This model was adopted by the Federal Emergency Management Association (FEMA) to produce flood insurance-rate maps for the Gulf Coast. Furthermore, both NOAA and the United States Navy have been applying ADCIRC as a storm surge model for specific research and development projects.

#### Coupled hydraulic and storm surge models

Most of the studies that have been reviewed address models that forecast either storm surge or river flow, but few studies have described the coupling of both inland flood and storm surge models for forecasting purposes. In most cases surge and river flooding occur separately, with storm surge occurring at the time of landfall and river flooding occurring later. However, there are situations when both effects might coexist and result in severe flooding. This occurred in 1999, when Hurricane *Floyd* affected the East Coast of the United States. At the time when *Floyd's* storm surge was affecting coastal areas of North Carolina, it was also raining torrentially in an area that had been hit a few weeks earlier by Hurricane *Dennis*. Rivers were already in flood by the time *Floyd* made landfall. In the United States, coupled systems using one-dimensional models are operational for several coastal rivers and some of them were utilized in pilot projects for the generation of inundation mapping in real time. Reed and Stucky (2005) described the application of the NWS Dynamic Wave Operational Model (DWOPER) on the lower Ohio and Mississippi Rivers to the Gulf of Mexico. This model uses SLOSH water-level forecasts as the downstream boundary. Brown et al. (2007) recently described "the first attempt to model storm surge flooding of an urban area with a two-dimensional hydraulic model and to explore the uncertainties associated with model predictions" for Canvey Island, United Kingdom.

To reproduce accurately the passage of a flood wave through a river reach, the responses (water level, flow, velocity) are simulated using unsteady-state hydraulic models. Many hydraulic models are available to simulate water levels and river flow, but the characteristics of the local site might require specific model capabilities. Low-lying coastal estuaries are complex hydrodynamic systems that often require two-dimensional models for accurate simulation and the one-dimensional approach may not be appropriate. The resolution of computational grids sometimes requires issues to be addressed during the coupling process. For example, if the downstream boundary of the one-dimensional hydraulic model includes multiple computational cells from the surge model, then averaging of surge elevation

across this boundary may be required. Likewise, in the case of a two-dimensional depth-averaged hydraulic river model, the downstream boundary will likely include multiple river cells that must be linked with one or more surge model computational cells, again requiring some averaging or smoothing across the boundary. The Tar River example discussed in the following paragraph illustrates this issue.

The Tar River, North Carolina, was modelled using the NWS one-dimensional hydraulic model named Flood Wave (FLDWAV) coupled with a tidal model, a project developed by NWS and Riverside Technology, Inc. (Riverside). Riverside developed and calibrated a model for the reach of the Tar River between Tarboro and the Atlantic Ocean. The lower reach of the Tar River is described as follows:

The Tar River drains into the Pamlico Sound, which also receives flow from several other rivers in North Carolina. Pamlico Sound is protected by a series of barrier islands with a number of inlets through which tidal influences are transmitted and hydrologic inflows drain to the Atlantic Ocean. Tidal influences predominate in the determination of water levels in the Pamlico Sound and have a strong influence on stages in the Tar River as far upstream as Greenville under normal flow conditions and as far as Rock Springs under very low flow conditions.

This is an example in which the use of a one-dimensional hydraulic model might be inadequate for simulating conditions, a two-dimensional model being perhaps more appropriate for simulating flood and storm surge in the estuary. However, because of operational constraints it was modelled using a one-dimensional model.

Following selection of the hydraulic and tidal models, the general approach for simulating the coupled response of the river system to surge and inland flooding includes:

- (a) Selection of river reach boundaries, type and location;
- (b) Collection of geometries of the cross-section to build the channel and of the flood plain for the hydraulic model;
- (c) Determination of local flows using data or previously developed hydrologic models.

The upstream boundary of the model reach is usually defined by a time series of flow. The time series of water level for the downstream boundary will be provided by the surge model. This rather simplistic approach might become cumbersome when considering operational implementation. Demand for data for research and model development is usually confined to historical data for



calibration. Real-time operations require either observed or forecast information on rainfall, a forecast inflow hydrograph and forecast surge elevations derived from a surge model driven by meteorological forecast.

The following issues need to be considered for the coupling of the hydraulic and tidal components:

- The calibration period should be selected to ensure there is enough data for all the time series required by the model system. In addition, the period selected should include a wide range of river flows (low, medium and high) and minor, medium and major surge effects.
- The forecast window for individual models (including the hydrologic and meteorologic models) must be examined to define the window for the coupling system and to ensure that data from each model are available as needed by the dependent models.
- The time interval for the system coupling must be selected based on the minimum that is allowed to describe the process while maintaining feasibility of model execution for forecasting purposes. For example, in the United States most of the operational models used to forecast river flow are performed for incremental periods of between one and six hours. Storm surge models can produce output for time increments on the order of a few minutes. However, because the forecast-system architecture might be too rigid and because of operational limitations to the execution of the hydraulic models, the coupling is performed in hourly increments.
- Consistency of reference datums is essential for the accuracy of results. This includes vertical and horizontal datums for cross sections, water levels and tide gauges.
- Consistency of boundary conditions must be maintained for situations in which multiple-river computational cells (two-dimensional hydraulic models) coincide with a single surge-model cell. Multiple iterations between the hydraulic and estuarine models might be required.
- Continuous execution of the coupled system ensures that the models are initialized correctly. However, this might not be possible for a situation in which a surge model is not run continuously and no downstream real-time tidal data are available.

A coupled system for St. Johns River, Florida, has been in operation since 2001 (Figure 7.7). The NWS Southeast River Forecast Center (SERFC) currently forecasts water levels in the lower end of this river near Jacksonville using FLDWAV. The model is executed for a 300-mile reach. The



**Figure 7.7. St. Johns River, Florida. The river flows from south to north. The positions of three river-level monitoring stations are indicated.**

Source: Dube et al., 2010

upstream boundary (flow hydrograph) as well as the local inflows from tributaries is derived from the hydrological model Sacramento Soil Moisture Accounting. The downstream boundary selected is the tide gauge located at Mayport at the mouth of the river near Jacksonville. A forecast window of five days is used. The time series for the water level at the downstream boundary are composed of the observed water levels up to the forecast time. For the forecast period, the data on astronomical tides provided by the National Ocean Service (NOS) are combined with the output from the SLOSH model. Blending techniques have been developed by NWS to correct the downstream water level once observational data become available.

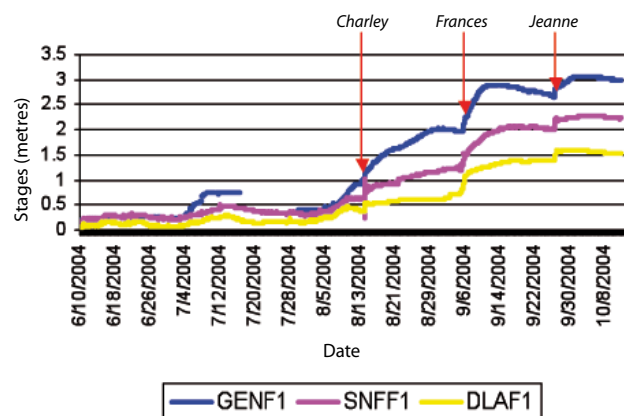


**Figure 7.8. Water levels in St. Johns River during the 2004 hurricane season monitored by the stations Geneva (GEN1), Sanford (SNFF1) and Deland (DLA1). Periods of impact for the hurricanes Charley (August), Frances and Jeanne (both in September) are indicated.**

Source: Dube et al., 2010

The 2004 hurricane season provided insight into the performance of the hydraulic model discussed above. During the period, three hurricanes affected the area – *Charley*, *Frances*, and *Jeanne* (Figure 7.8). Rainfall produced by these systems affected the water levels in the St. Johns River. Water levels were low at the beginning of August and the rainfall associated with Hurricane *Charley* produced a significant rise, but it wasn't until the passage of Hurricane *Frances* in September that the rises reached flood stage, above which levels remained until the beginning of November.

During the operational performance of the system, the wind acting on the river reach was observed to influence greatly the propagation of the surge and the forecasts of water levels. The jump in water levels due to wind effects was more noticeable at the station of Deland (DLAF1) when *Charley* affected the area and the river was at low levels (Figure 7.8). The FLDWAV model has the capability to incorporate wind direction and magnitude as a single value for the whole reach,

but this is not practical for the entire 300 miles. As a result, wind effects on the river are not included in the coupled system. NWS is in the process of incorporating this variable into the hydraulic modelling.

#### 7.1.4 French Caribbean

Météo-France uses a depth-averaged numerical model to provide a stand-alone system for forecasting storm surges provoked by tropical cyclones in the French Antilles, New Caledonia, the French Polynesia and in La Reunion. The model is driven by wind stress and atmospheric pressure gradients. It solves the non-linear shallow-water equations in a spherical coordinate system. Wind and pressure fields are inferred from an analytical-empirical cyclone model (Holland, 1980) that requires inputs for only cyclone position, intensity and size. The surface-wind stress components are computed using a quadratic relationship, with a drag coefficient derived from the Smith and Banke (1975)

**Table 7.3. Comparison between observed storm surges and those obtained from the Météo-France model for the French Antilles (centimetres)**

Source: Daniel, 1996, 1997

| <i>Location</i>              | <i>Cyclone</i>        | <i>Observed elevation</i> | <i>Model elevation</i> |
|------------------------------|-----------------------|---------------------------|------------------------|
| Pointe-à-Pitre               | <i>Hugo</i> 1989      | 150                       | 148                    |
| Baie Mahault                 | <i>Hugo</i> 1989      | 250                       | 248                    |
| Saint François               | <i>Hugo</i> 1989      | 150                       | 141                    |
| Pointe Fouillole             | <i>David</i> 1979     | 37                        | 25                     |
| Le Robert                    | <i>Allen</i> 1980     | 59                        | 53                     |
| Pointe Fouillole             | <i>Marilyn</i> 1995   | 40                        | 34                     |
| Nouméa                       | <i>Delilah</i> 1989   | 11                        | 11                     |
| Nouméa                       | <i>Lili</i> 1989      | 8                         | 16                     |
| Nouméa                       | <i>Theodore</i> 1994  | 22                        | 22                     |
| Papeete                      | <i>Emma</i> 1970      | 22                        | 9                      |
| Papeete                      | <i>Diana</i> 1978     | 15                        | 9                      |
| Papeete                      | <i>Tahmar</i> 1981    | 45                        | 16                     |
| Papeete                      | <i>Fran</i> 1981      | 15                        | 4                      |
| Papeete                      | <i>Lisa</i> 1982      | 20                        | 14                     |
| Papeete                      | <i>Orama</i> 1983     | 30                        | 14                     |
| Papeete                      | <i>Reva</i> 1983      | 22                        | 19                     |
| Papeete                      | <i>Veena</i> 1983     | 30                        | 30                     |
| Papeete                      | <i>Ima</i> 1986       | 18                        | 13                     |
| Papeete                      | <i>Wasa</i> 1991      | 45                        | 18                     |
| Rikitéa                      | <i>Nano</i> 1983      | 27                        | 24                     |
| Rikitéa                      | <i>William</i> 1983   | 25                        | 27                     |
| Rikitéa                      | <i>Cliff</i> 1992     | 18                        | 18                     |
| Port de la Pointe des Galets | <i>Hyacinthe</i> 1980 | 36                        | 32                     |

formulation. At open boundaries, the sea surface elevation is given by the inverted barometer effect. Tides are not modelled in this application since the forecast required is for surge heights above local tides (surge–tide interaction is negligible in this area). The model has been adapted to run on a personal workstation in a few minutes.

We may firstly consider results from hindcasts of tropical cyclones, which have given significant surges over the French overseas territories during the last 15 years. Table 7.3 lists model performance at a number of sites in the French Antilles, a full description of which can be found in Daniel (1996, 1997). The model was tested for each island for which observations were available for the last 15 years, and model simulations were compared with visual observations or tide-gauge measurements. Along coastlines without coral reefs and in large lagoons, such as the southern part of New Caledonia and Tuamotu atolls, the model compares well with the observations. The quality of the storm surge forecast is closely related to that of the atmospheric forcing quality, especially the cyclone trajectory.

The Météo-France model has been operating in the Caribbean since 1994. In 1995 the hurricane season was very active and two events produced significant surges. Hurricane *Luis* struck the islands of St. Barthelemy and San Marteen at the beginning of September. Two-metre surges were observed and also forecast by the model, but unfortunately no

tide-gauge data are available on these islands. Hurricane *Marilyn* produced a surge on Guadeloupe that corresponded well with that recorded by the Pointe Fouillole tide gauge.

Operationally, the model can be used in two different ways – either in real-time mode during the approach of a tropical cyclone to an island, or in climatological mode using a database of pre-computed surges. Due to the low accuracy of tropical cyclone trajectory forecasts, the climatological mode is currently the best way to use the model. In real-time mode, the user must provide hurricane positions, central pressures and radii of winds at any time (typically every three hours). A temporal interpolation is then made to provide hurricane parameters at each time step. The hurricane and surge models are then run for the required forecast period. The outputs consist of hourly forecasts of sea levels (Figure 7.9), current fields (not shown) and a maximum surge field (Figure 7.10). Time series with resolutions of one minute can be output for specific locations.

Because the accuracy of tropical cyclone trajectory forecasts is low, the average error for a forecast 24 hours ahead is approximately 200 kilometres. When a hurricane is crossing an island, a small error in the trajectory forecast results in a large error in the spatial distribution of the surge. An alternative procedure is to prepare an atlas of pre-computed surges based on hurricane climatology. Perret et al. (1996) performed more than

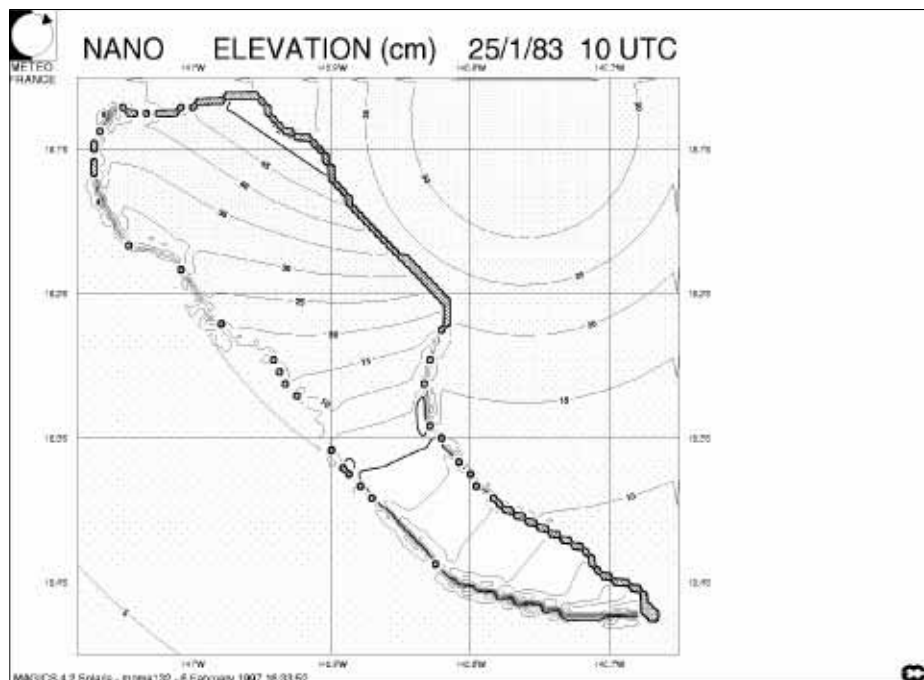


Figure 7.9. Tropical Cyclone *Nano* over Hao atoll (French Polynesia) showing modelled sea surface elevation (centimetres) on 25 January 1983 at 1000 coordinated universal time (UTC)

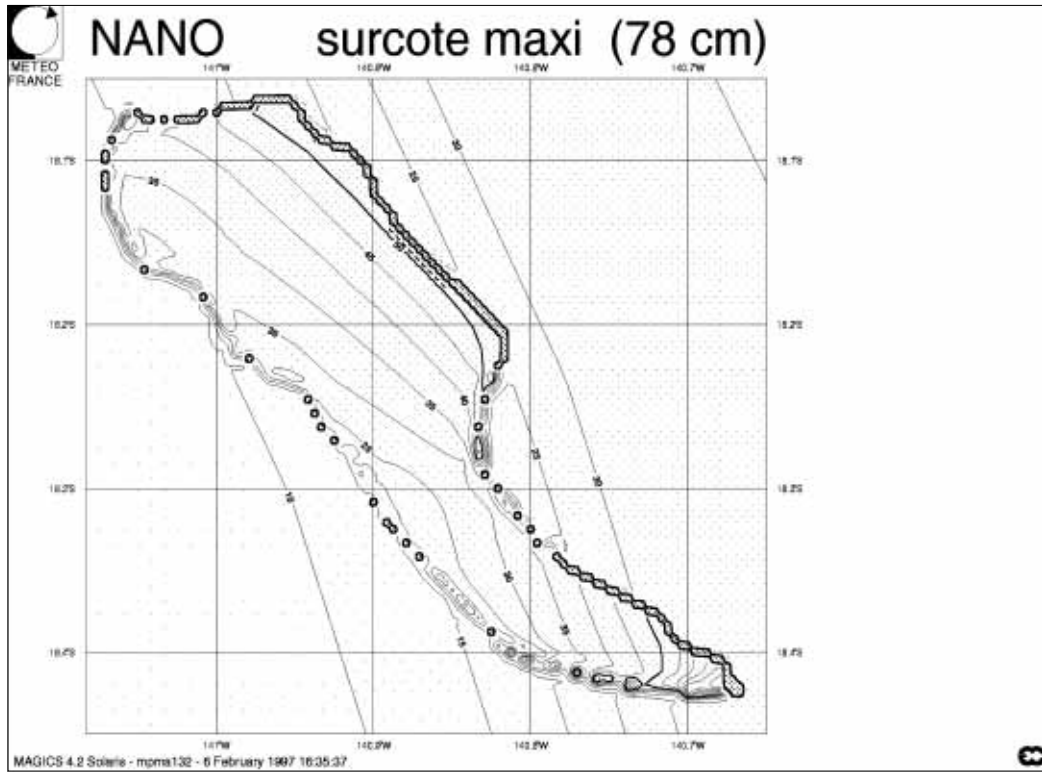


Figure 7.10. Tropical Cyclone *Nano* over Hao atoll (French Polynesia) detailing maximum surge (centimetres) predicted by the Météo-France model

1 000 model runs for islands in the Caribbean. Different impact points, intensity, size, direction and speed were tested. The results are compiled in a database that is displayed graphically (an example is shown in Figure 7.11) and forecasters have immediate access to the possible storm surges. As

each run gives an envelope of highest water around the island, it is simple to compile an ensemble of all the runs for any one class of intensity. The resulting risk map determines the highest possible surge along the coastline for a given hurricane intensity.

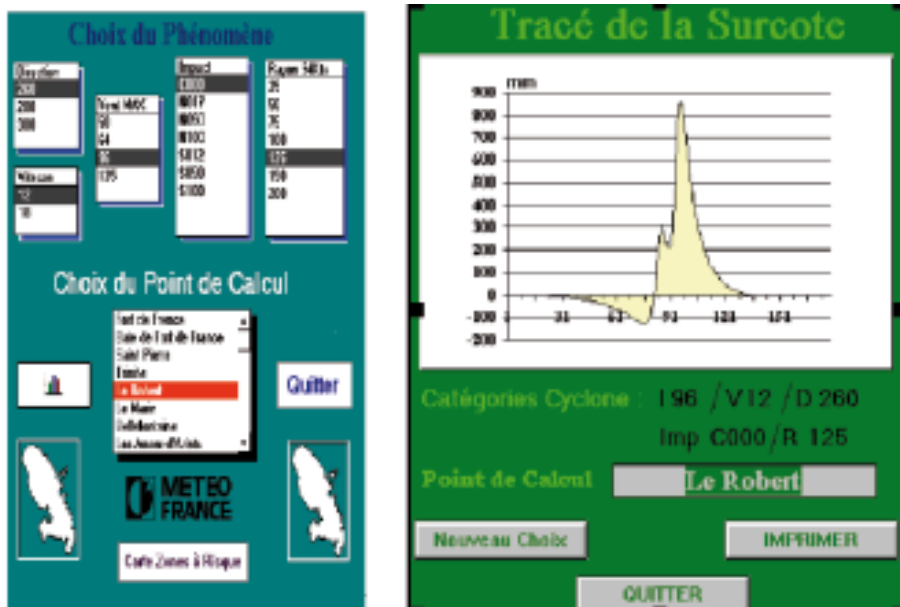


Figure 7.11. Main screen of the Martinique storm surge database (Météo-France) and an example of storm surge plotting for the specified location

### 7.1.5 Western and Northern Australia

In Darwin (Northern Region) the principle method for calculating storm surges associated with tropical cyclones has been historically the manual technique based on Jelesnianski (1972). More recently, a system based on the SEAtide model (Harper et al., 1978) and a database of possible scenarios has been implemented. This system was tested in the 2004–2005 season during Tropical Cyclone Ingrid and brought into operation in the season 2005–2006 with the occurrence of Tropical Cyclone Monica. This system is expected to be the primary storm-tide forecasting method used in Darwin TCWC for the foreseeable future. The system uses parameters of cyclone intensity, size, speed and track to produce an empirical prediction of the potential magnitude, location and duration of the total abnormal water level (storm plus tide) based on many numerical model runs. These models have been established over seven geographical regions, starting from the Queensland border and covering westerly areas to the Kimberley coast of Western Australia. Thousands of potential tropical cyclone scenarios have been constructed in order to determine the storm-tide response as a function of the incident storm parameters. The possibility that the characteristics of the tropical cyclone may be outside those observed in any finite period is acknowledged. To constrain cyclone parameters beyond those observed remains a challenge for statistical models.

A statistical analysis of historical tropical cyclone activity assigns the more likely scenarios a higher probability, but low-probability events are also included (for example tropical cyclones that reach their maximum intensity in the region). This probabilistic system enables forecasters to make allowance both for variability in the forecast storm parameters and also uncertainty in the prediction of the storm tide. Decision makers can then use the full range of predictions, including the maximum predicted inundation level if necessary, to decide the level of warnings and the appropriate emergency response. A comprehensive listing of coastal and near-coastal localities across the coastline of Northern Australia has been assembled, with special attention to those that are likely to be inhabited either permanently or occasionally by indigenous communities. The predictive system reports storm-tide estimates together with the locality names thought to be at risk.

Perth TCWC (Western Australia) uses a surge model based on Hubbert et al. (1990), developed to function on a personal computer, with a grid of 5 kilometres and incorporating coastal inundation. It has been used to generate tables of storm surge

elevations resulting from varying values of cyclone parameters at strategic locations such as Broome, Port Hedland, Karratha, Dampier, Onslow and Exmouth. For simplification, it has been assumed that the cyclone translational speed, central pressure and size remains constant along the track. The generating model runs have been based on:

- (a) Central pressures at 10-hectopascal intervals between 900 and 990 hectopascals;
- (b) Translation speeds at intervals of 5 kilometres per hour between 5 and 35 kilometres per hour;
- (c) Radii of maximum winds of 15 and 30 kilometres;
- (d) Angles of approach at 15-degree intervals from 285 to 75 degrees (west-north-west to east-north-east).

As described in 7.2.2, consideration is being given to the implementation of the new interactive storm surge modelling system based on TC-LAPS. For the 2002–2003 summer, when the new model was tested, there were no available measurements of cyclone-related surges. To illustrate the performance of the new model, TC-LAPS was run in hindcast mode to produce atmospheric forecasts for two past cyclones where reliable estimates of the surges were available. The results of these trials, based on data for Tropical Cyclones *Chris* and *Vance*, are described below.

Tropical Cyclone *Chris* was close to maximum intensity as it crossed the coast at 0400 UTC on 6 February 2002, approximately 160 kilometres north-east of Port Hedland. Forecasts from TC-LAPS for track and intensity are presented in Figure 7.12. Figure 7.12 also displays time series for the track errors and observed central pressure and forecast central pressure. The forecast for track was good (error 110–130 kilometres at landfall), while the strength of the cyclone was underpredicted by approximately 28 hectopascals.

Using a Dvorak diagram it is possible to calculate that this error resulted in the forecast maximum winds being weaker by a factor of 1.25. Using this correction coefficient for the strength of the wind, and shifting the track by 0.2 degrees northward and 0.7 degrees eastward, the surge model then produced the elevations presented in Figure 7.13. The maximum surge is 3.4 metres at a point approximately 40 kilometres to the east of the point of landfall. A survey of the area affected was conducted shortly after the passage of the cyclone. Allowing for wave run-up, the still-water elevation (storm surge) was estimated to have been 3–3.5 metres, which is in very good agreement with the output of the model.

Tropical Cyclone *Vance* provided a relatively rare opportunity when detailed measurements of the

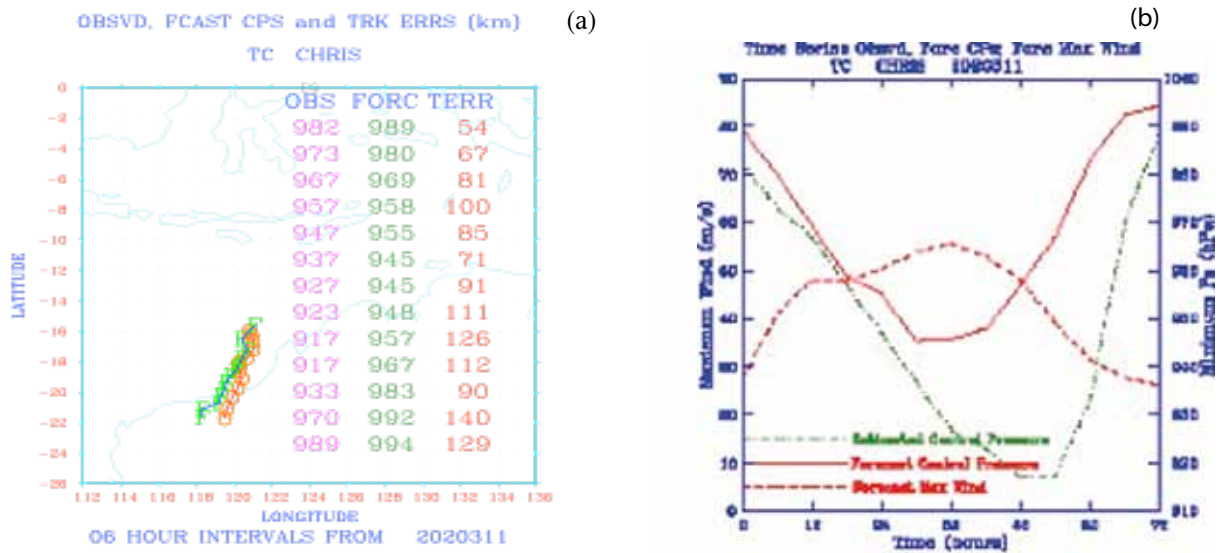


Figure 7.12. (a) Observed (orange symbols) and forecast (green symbols) track for Tropical Cyclone *Chris* (basetime 1100 UTC, 3 February 2003) – data columns present time series for observed and forecast central pressure and track error. (b) Estimates for central pressure and TC-LAPS forecast for central pressure and maximum wind

corresponding ocean surge were available. Figure 7.14 illustrates observed and forecast track and central pressures for *Vance* from basetime 1100 UTC, 19 March 1999. The maximum track error was in the range 150–180 kilometres, but almost half of the error was due to the faster speed of forward propagation in the forecast compared to the real track. The strength of the cyclone as it approached the coast was somewhat overpredicted, and an adjustment value of 0.85 for the strength of the wind was adopted in the simulations. Figure 7.15 shows the forecast maximum surge for a cyclone displaced roughly in accordance with the observations, which made it pass directly over Exmouth

Gulf. This led to a surge of 9.47 metres at the base of the Gulf (caused by the dynamics of the surge in the locality).

The surge at Exmouth due to Tropical Cyclone *Vance* (where severe erosion of the marina and inundation of the beachfront occurred) was measured to be 3.6 metres and the time series of both observed and modelled surges are shown in Figure 7.16. The maximum magnitude modelled was 3.35 metres. While there is a very good match between both the maximum value and the qualitative behaviour of the surge, the forecast peak is somewhat wider. It is interesting to note that both the measured and forecast surge reached their corresponding maximums after the eye of the storm passed the closest point to Exmouth. The observed delay was approximately 2.5 hours while for the forecast it was approximately 4 hours.

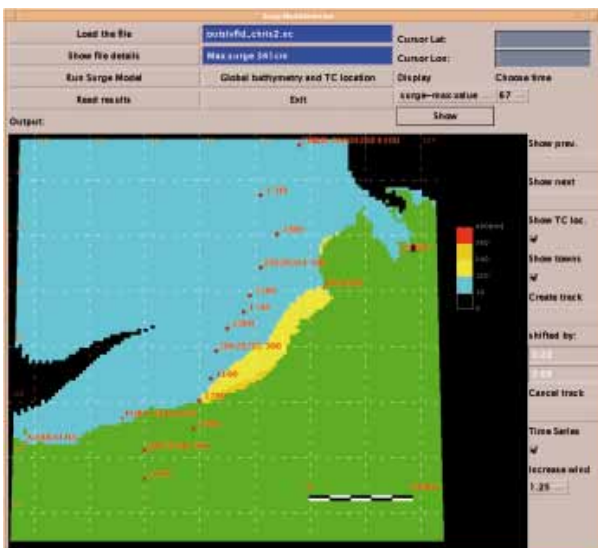


Figure 7.13. Estimates for the surge magnitude produced by Tropical Cyclone *Chris*

### 7.1.6 Bay of Bengal and Arabian Sea

The Bay of Bengal is one of the regions of the world the most affected by storm surges generated by tropical cyclones. The frequency of storm surges in the Arabian Sea is considerably less. The destruction due to the storm surge flooding is a serious problem along the coastal regions of India, Bangladesh, Myanmar, Pakistan, Sri Lanka and Oman. Storm surges cause significant loss of life and damage to property and agriculture in these countries. Approximately 300 000 lives were lost in one of the most severe cyclones to hit Bangladesh (then East Pakistan) in November 1970. More recently, the Chittagong cyclone of April 1991

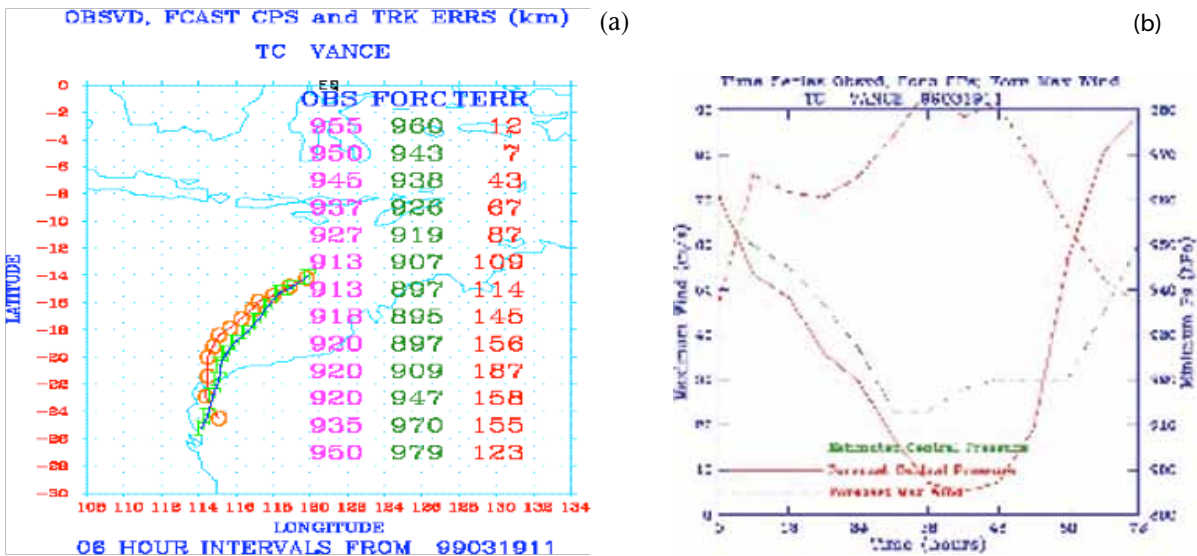


Figure 7.14. (a) Observed (orange symbols) and forecast (green symbols) tracks for Tropical Cyclone Vance (basetime 1100 UTC, 19 March 1999); data columns present time series for observed and forecast central pressure and track error. (b) Estimates for central pressure and TC-LAPS forecast for central pressure and maximum wind

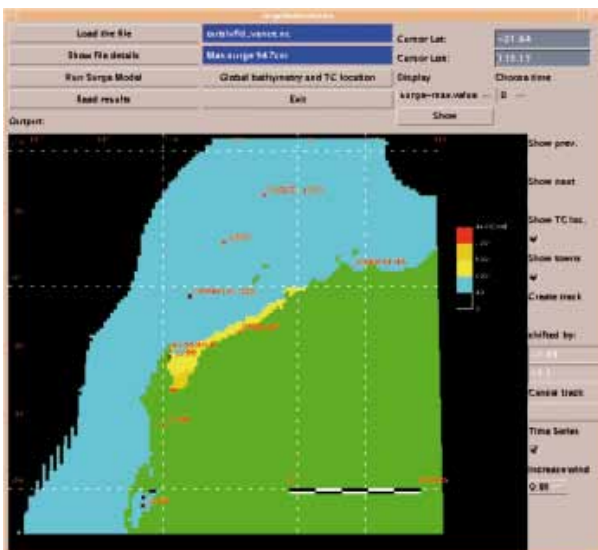


Figure 7.15. Predicted surge magnitude provoked by Tropical Cyclone Vance obtained using a corrected TC-LAPS forecast

killed 140 000 people in Bangladesh. The Orissa coast of India was affected by a severe storm in October 1999, killing in excess of 15 000 people and causing huge damage to property in the region. Many good reviews of storm surges in the Bay of Bengal can be consulted (see, for example, Murty et al., 1986; Dube et al., 1997). This section begins with a compendium (Tables 7.4–7.10) of important surge events in the area, organized geographically from east to west, beginning with Myanmar (Table 7.4).

Of all the countries surrounding the Bay of Bengal, Bangladesh is the most affected by storm surges (see Table 7.5).

In comparison to Bangladesh, the coastal regions of the Indian state of West Bengal experience less storm surge activity. In India, the two states that are most affected by storm surges are Orissa and Andhra Pradesh (Tables 7.6 and 7.7).

Table 7.4. Notable storm surges generated by tropical cyclones in Myanmar

| Date                                 | Location of landfall | Radius of maximum winds (km) | Pressure drop (hPa) | Surge maxima (m)      |
|--------------------------------------|----------------------|------------------------------|---------------------|-----------------------|
| 7 May 1975                           | North of Patheingyi  | 20                           | 22                  | 1.2 (near Patheingyi) |
| 4 May 1982                           | Near Gwa             | 30                           | 55                  | 4 (at Gwa)            |
| 19 May 1992                          | North of Sandoway    | 20                           | 25                  | 1.4 (near Sandoway)   |
| 2 May 1994                           | Near Sittwe          | 30                           | 50                  | 3.7 (at Sittwe)       |
| 29 April 2006                        | Gwa                  | 40                           | 48                  | 9                     |
| 2 May 2008 (Tropical Cyclone Nargis) | Bogale               | 25                           | 60                  | 4.5                   |

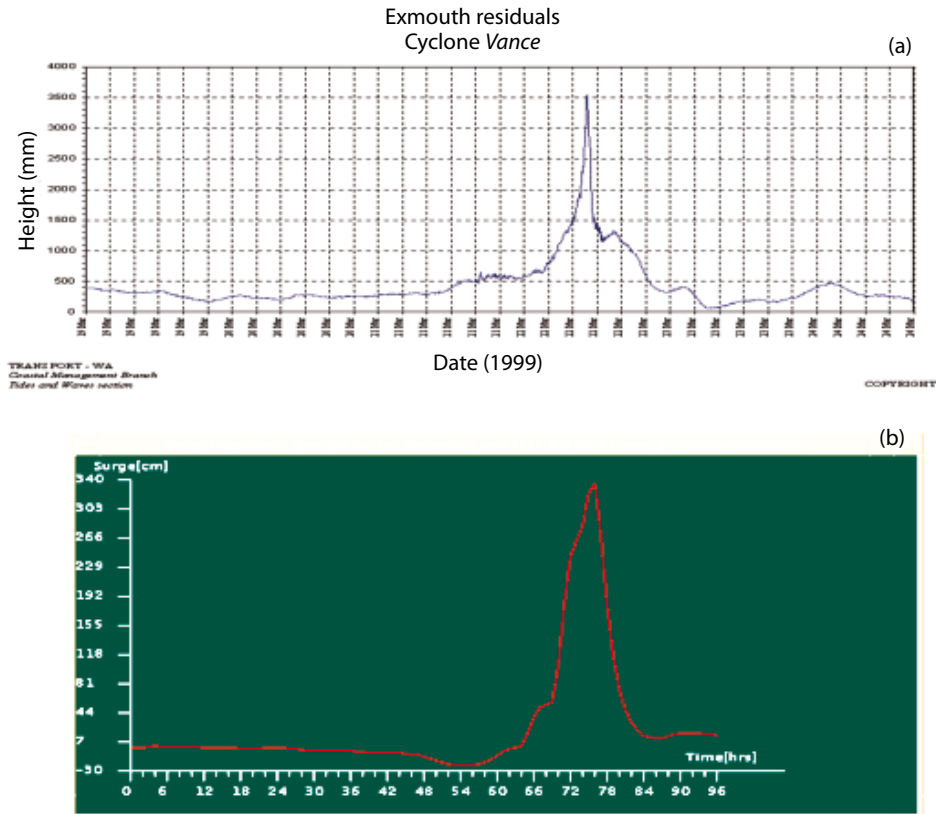


Figure 7.16. Observed (a) and modelled (b) time series of the surge magnitude at Exmouth (Western Australia) during Tropical Cyclone Vance

Compared to Orissa and Andhra Pradesh, the impact of storm surges on the coast of Tamil Nadu, on the south-east tip of India, is somewhat less, although the consequent impacts are better recorded in many cases (Table 7.8).

In the case of Sri Lanka, four important surge events have occurred in the twentieth century, listed in Table 7.9.

The State of Gujarat on the Arabian Sea coast of India has experienced three major surge events since 1982, as detailed in Table 7.10.

The National Meteorological and Hydrological Services of countries surrounding the north Indian Ocean have achieved some success in the provision of storm surge warnings and in the implementation of improved models. This has been achieved within the framework and guidance of the Tropical Cyclone Programme (TCP) of WMO. TCP supports technology transfer from the Indian Institute of Technology (IIT) to run and make operational storm surge models for other countries in the region. Real-time storm surge prediction systems for the coastal regions of India have been developed by Dube et al. (1994), Dube and Gaur (1995)

Table 7.5. Notable storm surges impacting the coast of Bangladesh since 1974

| Date             | Location of landfall            | Radius of maximum winds (km) | Pressure drop (hPa) | Surge maxima (m)                              |
|------------------|---------------------------------|------------------------------|---------------------|---|
| 15 August 1974   | Near Contai, West Bengal        | 25                           | 40                  | 2.5–3.5 (near Sagar Island)                   |
| 25 May 1985      | Near Hatia, Bangladesh          | 30                           | 42                  | 1.8 (at Chittagong)                           |
| 29 November 1988 | Near Khulna, Bangladesh         | 30                           | 45                  | 6.8 (in Mongal estuary)                       |
| 29 April 1991    | North of Chittagong, Bangladesh | 40                           | 65                  | 5.8 (at Chittagong);<br>3.8 (at Cox's Bazaar) |
| 2 May 1994       | Near Tecnaf, Bangladesh         | 30                           | 50                  | 3.8 (at Akyab)                                |



and Chittibabu et al. (2000). Based on these models, operational systems have also been created for Bangladesh, Myanmar, Pakistan, Sri Lanka and Oman (see, for example, Dube et al., 2004; Chittibabu et al., 2002).

**Table 7.6. Modelled surge maxima at various locations on the coast of Orissa for three different cyclones (metres)**

| <i>Location</i> | <i>Tropical cyclone surge maxima</i> |      |      |
|-----------------|--------------------------------------|------|------|
|                 | 1971                                 | 1982 | 1999 |
| Goplapur        | 0                                    | 0.12 |      |
| Puri            | 0.22                                 | 0.25 | 2.0  |
| Konark          | 0.32                                 | 0.58 | 4.6  |
| Paradip         | 3.49                                 | 3.74 | 7.8  |
| False Point     | 4.65                                 | 4.93 | 7.5  |
| Chandbali       | 1.80                                 | 1.60 | 7.5  |
| Balasore        | 0.87                                 | 0.81 | 2.0  |

**Table 7.8. Notable storm surges for Tamil Nadu**

| <i>Date</i>             | <i>Location</i>                        | <i>Observations</i>  |
|-------------------------|--|--|
| 13–23 May 1943          | South of Madras                        | Extensive damage; low-lying areas inundated  |
| 30 Nov. 1952            | South of Nagapatnam                    | 1.2-m surge penetrated 8 km inland; 400 deaths                                     |
| 28 November–2 Dec. 1955 | Tanjavore District                     | Surges up to 5 m penetrated 16 km inland; 500 deaths                               |
| 21 Oct. 1963            | Cuddalore                              | Surge almost 7 m   |
| 3–8 Nov. 1964           | Madras                                 | Low-lying areas of Madras flooded  |
| 20–23 Dec. 1964         | Tondi                                  | Surges of 3–6 m; 1 000 deaths  |
| 20–28 Dec. 1968         | Nagapatnam                             | Moderate surge; 7 deaths   |
| 24 Nov. 1978            | Between Killakkari and Rosemary Island | 3–5-m surges on the coasts of Tamil Nadu and Sri Lanka; extensive damage           |
| 11–17 Nov. 1992         | Sri Lanka and Tuticorin                | 1–2-m surge in Tuticorin; 170 deaths, 160 missing                                  |
| 1–4 Dec. 1993           | Near Karikal                           | 1–1.5-m surge; 111 deaths  |
| 29–31 Oct. 1994         | Madras                                 | 1–2-m surge; 304 deaths; 100 000 huts damaged and 60 000 hectares of crops damaged |

**Table 7.7. Modelled surge maxima at locations in Andhra Pradesh for the cyclones of November 1977 and May 1990 (metres)**

| <i>Location</i> | <i>Tropical cyclone surge maxima</i> |      |
|-----------------|--------------------------------------|------|
|                 | 1977                                 | 1990 |
| Krishnapatnam   | 0.35                                 | 0.6  |
| Ramayapatnam    | 0.54                                 | 1.0  |
| Nizampatnam     | 2.27                                 | 4.47 |
| Divi            | 5.95                                 | 5.88 |
| Machilipatnam   | 5.87                                 | 5.4  |
| Narsapur Point  | 3.51                                 | 2.64 |
| Sacramento      | 1.83                                 | 1.49 |
| Kakinada        | 1.91                                 | 1.87 |
| Visakhapatnam   | 0.7                                  | 0.9  |
| Santapalli      | 0.52                                 | 0.48 |

**Table 7.9. Damaging storm surges that have affected Sri Lanka in the twentieth century**

| <i>Date</i>     | <i>Location</i>            | <i>Observations</i>   |
|-----------------|----------------------------|---|
| 8–10 March 1907 | Eastern Coast of Sri Lanka | Not available   |
| 17–24 Dec. 1964 | Near Trincomalee           | Not available   |
| 17–24 Nov. 1978 | Near Batticaloa            | 2-m surge; 913 deaths; 100 000 houses damaged. At Kaikudah, the sea penetrated 1.5 km inland. |
| 11–17 Nov. 1992 | Eastern Coast of Sri Lanka | 4 deaths; 29 116 houses damaged   |

**Table 7.10. Maximum surge amplitudes at various locations for three cyclones in Gujarat (metres)**

| <i>Location</i> | <i>Tropical cyclone surge amplitudes</i> |      |                                    |
|-----------------|--|------|------------------------------------|
|                 | 1982                                     | 1996 | 1998                               |
| Mahua           |  | 2.5  |                                    |
| Jalana          |  | 3.7  |                                    |
| Diu             | 2.4                                      | 3.2  |                                    |
| Veraval         | 2.6                                      |      |                                    |
| Porbandar       |  |      | 3.5                                |
| Dwaraka         |  |      | 2.0                                |
| Kandha          |  |      | 3 (in addition to a tide of 6.6 m) |

In addition to these regional examples, local high-resolution systems based on the same model have been developed for the Indian coastal states of

Andhra Pradesh, Orissa, Tamil Nadu and Gujarat and also for Bangladesh, Myanmar, Pakistan, Sri Lanka, and Oman. The local systems all have accurate and detailed bathymetry for the offshore waters. It is well known that the development of cyclone surges is very sensitive to the coastal geometry and offshore bathymetry at the landfall of the cyclone. The models are two-dimensional and depth-averaged, and fully non-linear. A semi-explicit finite difference scheme is used for the numerical solutions. With a finely resolved grid of  $3.7 \times 3.7$  kilometres, computational stability is achieved with a time step of 80 seconds. Bathymetry for the models is derived from the 2-Minute Gridded Global Relief Data (ETOPO2) dataset, obtained from the United States National Geophysical Data Center (NGDC) database. A simple drying scheme is included to prevent instability during strong negative surges. Full details of the modelling system can be found in the papers cited in the previous paragraph. Surface-wind fields are based on the dynamic storm model of Jelesnianski and Taylor (1973). This model uses as input the radius of maximum wind and the drop in pressure. The other main components of the storm model are a trajectory model and a wind speed profile approximation.

A number of validation experiments have been performed to apply these location-specific models to cyclonic storms in the Bay of Bengal and the Arabian Sea. Modelled elevations of the sea surface are compared to any available observations from local tide gauges. Brief details of two such validations are now presented. On 29 April 1991, a severe cyclone crossed the Bangladesh coast north of Chittagong at 2000 UTC. This cyclone was one of the most catastrophic in

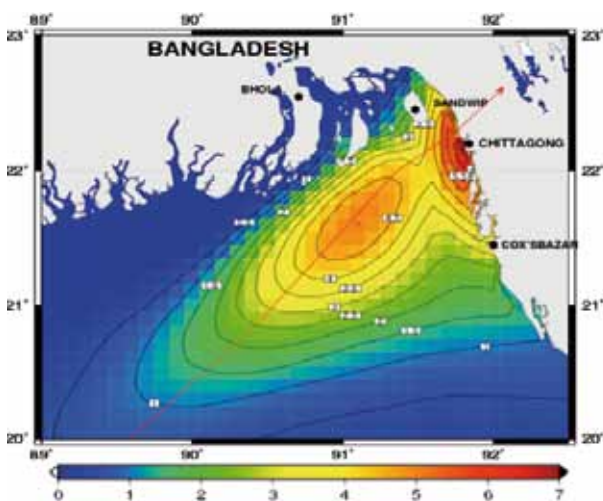


**Figure 7.17. Sea level (metres) associated with the 1991 Chittagong cyclone**

Source: Dube et al., 2004

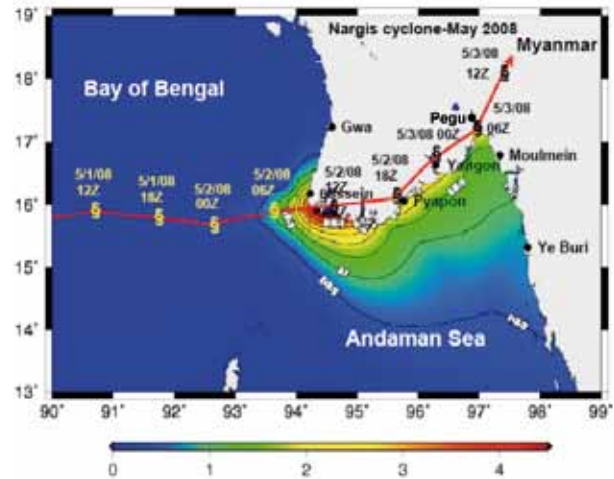


**Figure 7.18. Simulated peak surge contours (metres) for the 2008 Cyclone Nargis**

history. The estimated maximum wind speed was 235 kilometres per hour and surges of up to 7.6 metres were reported. Surges of 6 metres or more swept a coastal stretch of nearly 240 kilometres. Figure 7.17 shows the result of numerical experiments carried out using a pressure drop of 70 hectopascals and a radius of maximum winds of 40 kilometres. The computed surge values at Chittagong and Cox's Bazar were 5.8 and 3.8 metres, respectively. The astronomical tide at the time of landfall was approximately 1.5 metres, thus the total water level at Chittagong was approximately 7.3 metres, which compares well with the observational reports.

In the last week of April 2008, an area of low pressure was detected over the Bay of Bengal approximately 1 150 kilometres east-south-east of Chennai, India. At 0300 UTC on 27 April, the India Meteorological Department (IMD) classified the system as a depression and nine hours later the system intensified into a deep depression. At 0000 UTC on 28 April, the system became Tropical Cyclone *Nargis*, while it was located approximately 550 kilometres east of Chennai. During the first few hours of 28 April, *Nargis* became nearly stationary while located between ridges to its north-west and south-east. The system gained further strength to become a severe cyclonic storm by 0600 UTC. By 1 May, after turning nearly due east, the system had continued to gain strength and on 2 May at 0600 UTC it attained a maximum wind speed of 59 metres per second (212.4 kilometres per hour) as it approached the coast of Myanmar. Around 1200 UTC on 2 May, Cyclone *Nargis* made landfall in the Ayeyarwady Division of Myanmar. Early on 3 May, it quickly weakened after turning to the north-east towards rugged terrain near the Myanmar–Thailand border.

The model has been integrated with a pressure drop of 65 hectopascals and a maximum wind radius of 25 kilometres. The computed surge contours along the coast of Myanmar are shown in Figure 7.18. It can be seen that a maximum surge of 4.5 metres is computed close to the landfall point. The Deltaic region of Ayeyarwady is affected by computed surges of between 2.5–4 metres. The Myanmar coast from Pyapon to Yangon is flooded with a surge of more than 2 metres. The computed surge values at Pegu and Moulmein are 2.5 and 1.5 metres, respectively. During this cyclone a surge of more than 4 metres was reported. The Department of Meteorology and Hydrology at Yangon also reported a surge of approximately 4 metres at the Deltaic region of Ayeyarwady. This is in good agreement with the simulated sea-level elevations.

## 7.2 STORM SURGES GENERATED BY EXTRA-TROPICAL CYCLONES (MID-LATITUDE DEPRESSIONS)

This section presents a review of operational forecasting systems for subtly different physical domains where extra-tropical storm surges are common. Areas covered include the North Sea, which is a typical shelf sea adjacent to the relatively wide north-west European continental shelf. Following this, a system from Argentina has been chosen, which focuses on smaller-scale estuarine forecasting. Finally, the surge forecasting system in the virtually tideless and almost totally enclosed Baltic Sea is discussed.

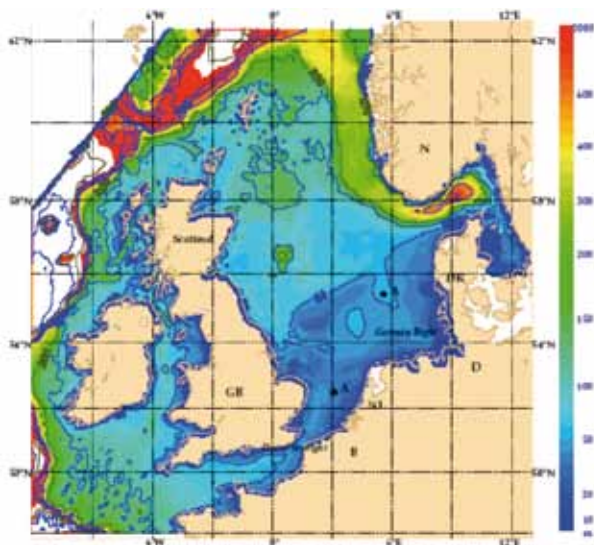


Figure 7.19. Bathymetry of the North Sea as used in the Dutch Continental Shelf Model (DCSM)

### 7.2.1 North Sea (a typical mid-latitude shelf sea)

The North Sea is largely surrounded by six highly developed countries: the United Kingdom, Belgium, the Netherlands, Germany, Denmark and Norway. Several of these have low-lying regions that can be threatened by extreme storm surges. The North Sea is also one of the most crowded seas in the world. With several of the largest ports in the world around it, the entrance to the Baltic and exploitable oil and gas reserves, shipping traffic is heavy. Due to these factors the North Sea is one of the most intensively monitored seas in the world and there is a large demand for high-quality forecasts for states of the weather and sea.

From the point of view of storm surges and water movement, the North Sea can be divided into three parts (Figure 7.19): the shallow southern part with depths of up to 50 metres, the northern part with depths to 200 metres and the deep trench along the Norwegian coast. The tide enters the North Sea along the Scottish coast and travels down the British coast as a Kelvin wave. The amplitude of the tide in the North Sea is typically of the order of 1 to 3 metres. The dominant tidal constituent is M2, but interaction between M2 and S2 gives a considerable spring-/neap-tide cycle with a period of about 14 days. Non-linear effects in the coastal zone generate higher harmonics (“overtides”).

Although the astronomical tide dominates sea-level variability, in the winter extra-tropical depressions can cause surges that are comparable to the tides. The characteristics of the basin (see, for example, de Vries et al., 1995) make the wind the dominant driving force of the storm surges, with atmospheric pressure gradients contributing approximately 20–30 per cent of the total (Pugh, 1987). Storm surge forecasts are issued by either the National Meteorological Services (United Kingdom, the Netherlands, Denmark, Norway) or the National Maritime Services (Belgium, the Netherlands, Germany) of the countries bordering the North Sea. All countries are members of the North West European Shelf Operational Oceanographic System (NOOS) and exchange their basic forecasts for a number of standard locations for comparison and ensemble forecasting. The United Kingdom and the Netherlands coastal flood warning systems were both established following the disastrous North Sea storm surge of 1953. During the night of 31 January on that year, coastal flooding caused the loss of 307 lives in the United Kingdom and 1 795 fatalities in the Netherlands (McRobie et al., 2005). The United Kingdom operational warning system that was created is now called United Kingdom Coastal Monitoring and Forecasting (UKCMF) and is shown schematically in Figure 7.20.

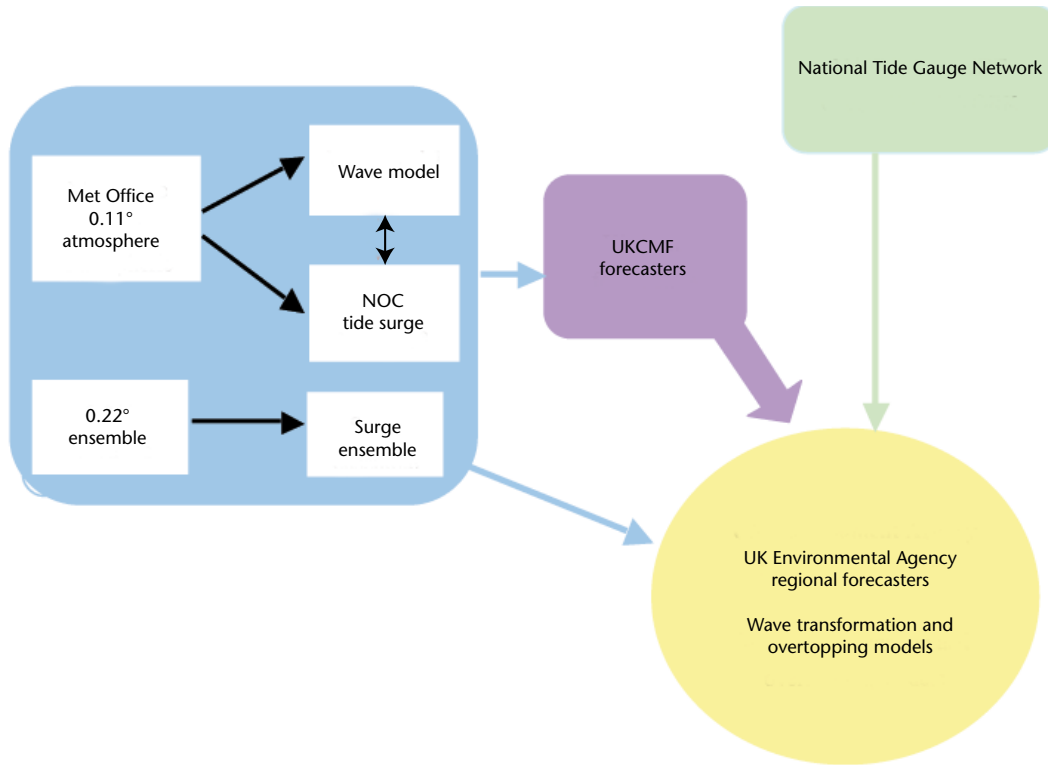


Figure 7.20. Components of United Kingdom Coastal Monitoring and Forecasting (UKCMF)

Meteorological forcing is taken from regional atmospheric models that have resolutions in the order of 10–20 kilometres. The United Kingdom and Germany have their own models Belgium uses the results from the United Kingdom model and the other countries are members of the Hirlam consortium and run their own version of the Hirlam model. The storm surge models used are both two- and three-dimensional and come in a variety of resolutions, covering either the whole of the north-west

European continental shelf, or being nested in the bigger models for local detail. For example, the current United Kingdom operational surge model covers the entire north-west European continental shelf at 12-kilometre horizontal resolution. The conditions for the surface boundaries of this model are the sea-level pressure and 10-metre wind fields from the Met Office North Atlantic and European (NAE) atmospheric model, at a similar spatial resolution (0.11 degrees longitude by 0.11 degrees

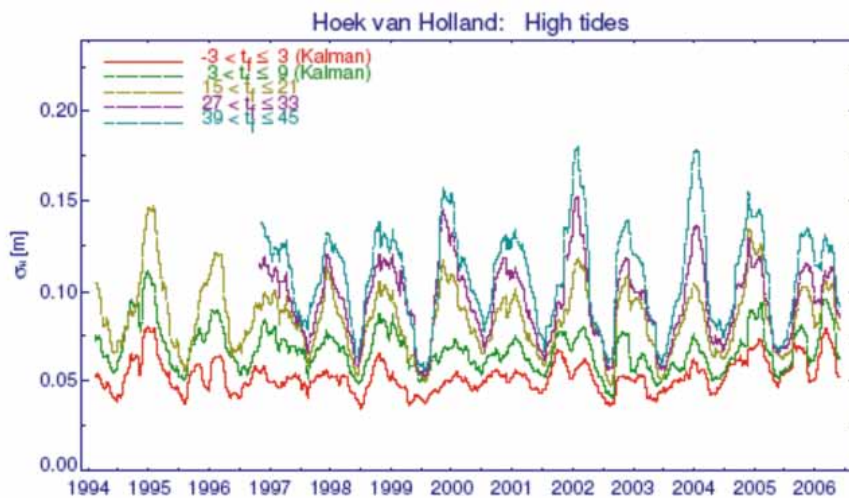


Figure 7.21. Running three-month standard deviation for high-tide surge forecasts for Hoek van Holland (Netherlands) from the Netherlands Hirlam and DCSM models. Data assimilation is applied for forecast lead times ( $t_f$ ) of up to 15 hours ahead (datasets labelled Kalman).

latitude). Tidal input at the model open boundaries consists of the largest 26 constituents. Models of finer resolution are nested within this outer domain. The model suite runs four times each day and simulations consist of a six-hour hindcast portion (where the model is forced with meteorological analysis) followed by a 48-hour forecast. The modelled surge is derived by subtracting a tidal model run from one forced by both tide and atmosphere. A study by de Vries et al. (1995) showed that differences between the storm surge models are small, and that the main source of errors in the forecasts is the meteorological input and the air–sea interaction.

The non-linearity of both meteorological and ocean models means that any deterministic forecast is strongly affected by the initial conditions, as well as choices for those parameters used to describe unresolved physical processes (for example, bed friction in hydrodynamic models). The United Kingdom has recently developed an ensemble-based surge forecasting system that has been validated over the

period 2006–2008 (Flowerdew et al., 2009; Flowerdew et al., 2010). Ensemble forecasting quantifies the uncertainty by making many numerical simulations using different choices of initial states and key parameters. The meteorological perturbations are generated using ETKF. This scheme uses estimates of the observation error to scale and mix differences between the ensemble mean and individual perturbations taken from the T+12 state of the previous forecast cycle (Bishop et al., 2001). The system gives confidence to those responsible for emergency responses because it provides an estimation of uncertainty at all future times in a forecast period.

The numerical models used for operational surge forecasting are non-linear and include the astronomical tide as well as the meteorological effect on the water level. However, tidal heights for coastal forecasts are derived from tide tables generated using harmonic analysis, since even at the finest resolution numerical models do not give comparable accuracy (see, for example, Jones and Davies, 1996). In practice, the astronomical tide from the model is replaced by the results of a more accurate harmonic analysis to provide a time series of water level upon which wave effects are then added.

The performance of the storm surge models is seasonally dependent. As an example, Figure 7.21 shows the running three-month standard deviation of the surge forecasts from the Netherlands two-dimensional model DCSM for high tides from 1994 to 2006 for different forecast lead times ( $t_f$ ). For forecasts up to  $t_f=15$  hours, data assimilation is applied. In the summer season, with generally little surge, the errors are of the order of the observational error, but in winter errors increase with lead time. Errors in individual forecasts for more extreme surges can be significantly larger, but as these occur less frequently a standard deviation for such errors is less meaningful. Validation of the United Kingdom models is performed monthly by comparison with observed sea-level data from the National Tide Gauge Network (see: <http://www.pol.ac.uk/ntslf/surgemonthlyplots/>). Typical monthly mean RMSEs are of the order of 10 centimetres, but maximum instantaneous errors can be as large as 50 centimetres, although these are very rare. Figure 7.22 shows a typical monthly validation plot from the United Kingdom operational modelling system.

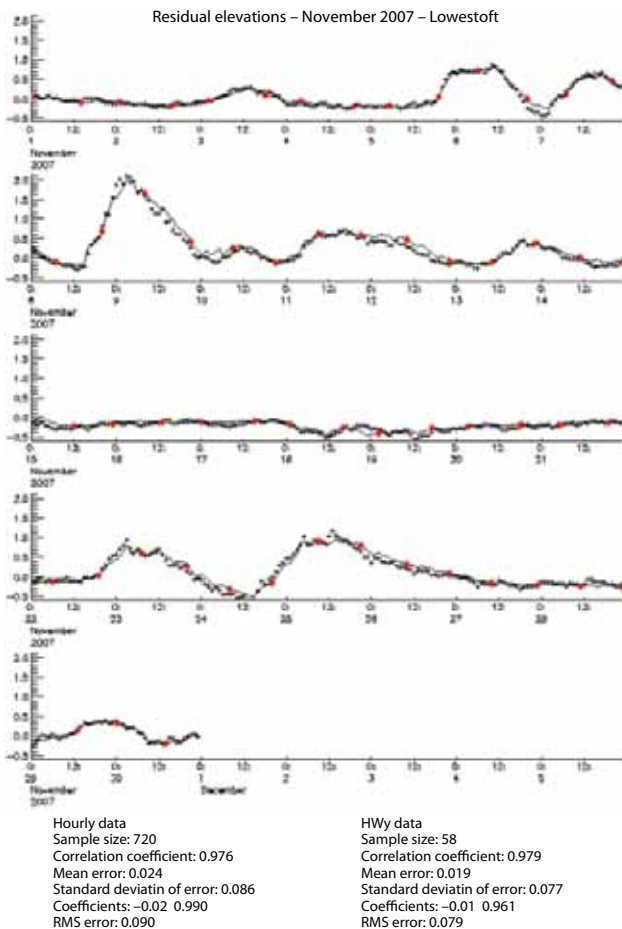
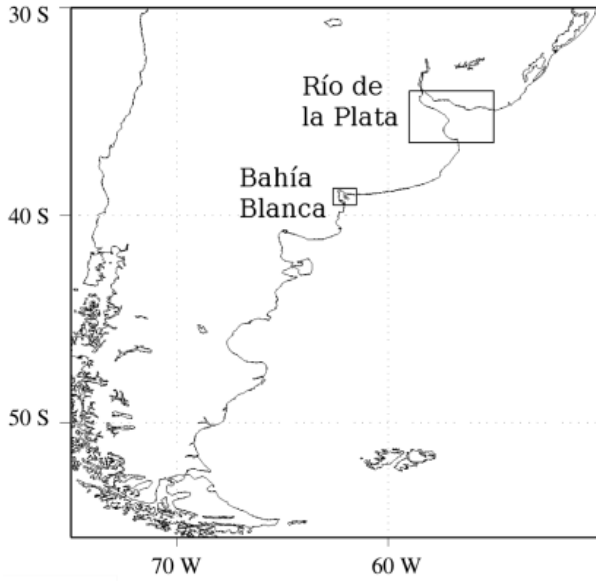


Figure 7.22. Validation plot from the United Kingdom operational modelling system for November 2007 at the Lowestoft tide gauge in the North Sea. The modelled sea-level residual (metres) is indicated by the solid line; crosses indicate observations.

### 7.2.2 Argentina – an example of smaller-scale estuarine forecasting

The Argentinean shelf sea is located by the south-east coast of South America (Figure 7.23). The topography of the region is characterized by a wide continental shelf extended along the Patagonian



**Figure 7.23. The Argentinean shelf sea and location of Río de la Plata and Bahía Blanca estuaries**

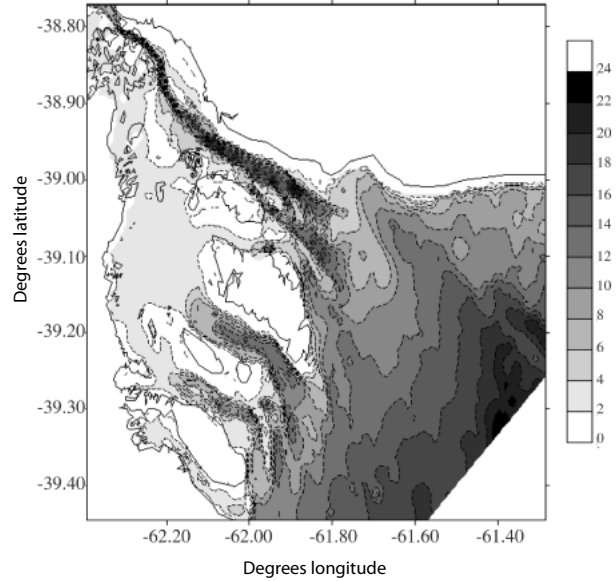


**Figure 7.24. Model bathymetry (metres) for Bahía Blanca**

coast. Its role is determinant in the deformation of the tidal wave from the South Atlantic Ocean and in the generation of storm surges on its shallow waters, before reaching the South American coast. The regional and local character of perturbations in water level requires accurate forecasting of the atmospheric and hydrodynamic variables over a range of scales.

Río de la Plata is the gateway to a densely populated and economically active area. Being 320 kilometres long and 230 kilometres wide at its mouth, its extent and limited depth are its most particular features. The semi-diurnal tidal constituents almost complete a whole wavelength from the mouth to the head, so that at certain times currents may be reversed at different locations. Furthermore, the storm surge travel time from the Atlantic coast into Río de la Plata makes it a suitable case for data assimilation.

The Bahía Blanca estuary (Figure 7.24) is an old delta formation with several channels orientated north-west to south-east, separated by large shallow marshes and intertidal flat areas. It contains the major port activity in this region. Its complex topography and circulation define the resolution needed in any storm surge simulation. This review of the region is focused on the non-linear aspects of surge modification within the estuary due to its highly non-linear behaviour.

Three two-dimensional depth-averaged models are used for storm surge prediction. The spatial resolution of the outer-shelf model is 20 minutes of latitude and 20 minutes longitude. Tidal harmonic constants at the open boundaries are taken from a

global model (Schwidderki, 1978). The model for Río de la Plata is nested with a resolution of three minutes latitude and three minutes longitude. Tidal constants at the boundary for the latter are interpolated from stations located at the mouth on both shores, following a Kelvin wave shape. The Bahía Blanca estuary is treated with a similar model, adapted to moving boundaries due to flooding and drying, at a resolution of 20 seconds latitude and 30 seconds longitude. An oceanographic station located at the mouth provides the tidal information required. The three models have been tuned to the most significant tidal constants from available analyses. Results for M2 tides are illustrated in Figure 7.25. In this figure, the left panels illustrate data for the outer-shelf model. The figure also illustrates that it is possible to obtain good representation of limited-area dynamics with higher resolutions and refined parameterizations (centre and right panels).

The principle calibration parameter used for this modelling is the Chèzy coefficient,  $C$ , for bottom friction. The final expressions for  $C$  obtained following the calibration process are shown in Table

**Table 7.11. Values obtained for the Chèzy coefficient ( $C$ ) following calibration for each model, where  $D$  is local depth (metres)**

| <i>Shelf sea (Argentinean Sea)</i>  | <i>Río de la Plata estuary</i>       | <i>Bahía Blanca estuary</i>   |
|---|--------------------------------------|---|
| $C = \begin{cases} 73 & D \leq 50 \\ 93 - \frac{2}{5}D & 50 < D \leq 80 \\ 61 & D > 80 \end{cases}$ | $C = 83 \text{ (depth-independent)}$ | $C = \begin{cases} 187 & D \leq 1.5 \\ 220 - 22D & 1.5 < D \leq 5 \\ 110 & D > 5 \end{cases}$ |

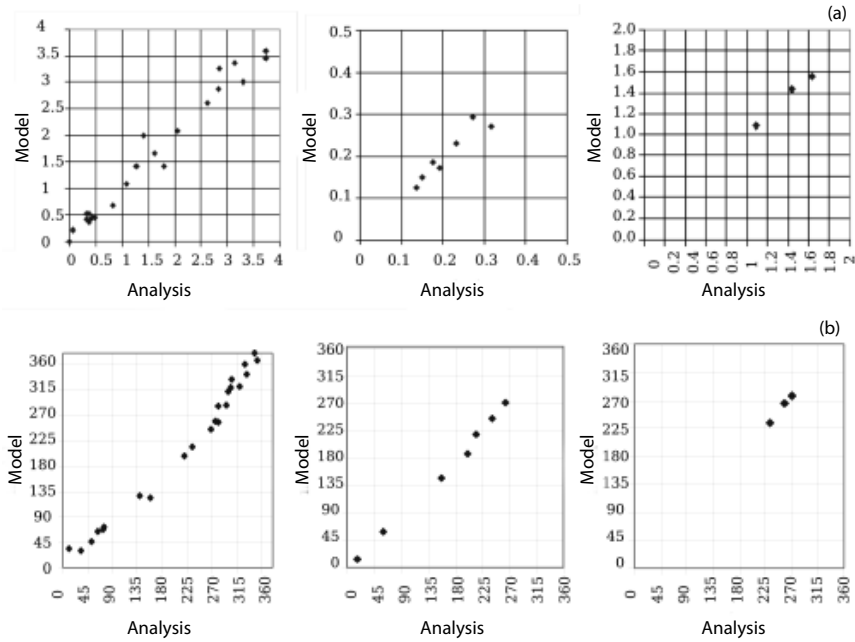


**Figure 7.25. (a) M2 tide amplitudes (metres), model and harmonic analyses at (left panel) the Atlantic coastline and islands, (centre panel) Rio de la Plata, (right panel) Bahia Blanca. (b) As for (a) but for phases (degrees)**

7.11. In the case of tides entering the shelf model, particularly through the southern boundary, modifications were applied to values provided by the global model. Differences were found among various bathymetric sources for the continental shelf, which altered the tidal propagation in the model. Topography was adjusted to represent shelf dynamics correctly. Additional calibration was necessary in Bahia Blanca for parameters in the wetting–drying process to properly represent the effect of the strong ebb currents in the navigable channels.

The shallow waters of the northern continental shelf, including Rio de la Plata and Bahia Blanca estuaries, are located in an area of strong meteorological cyclogenesis. A typical feature of this region

is the presence of upper-level troughs associated with frontal systems moving from south-west to north-east. These systems interact with the subtropical air masses to the north-east of Argentina, north of Uruguay and south-west of Brazil, and may lead to strong winds onshore and along the estuaries, resulting in disastrous flooding (Framiñan et al., 1999). Strong and persistent alongshore winds on the shelf, typically in winter, may also result in some coastal flooding of smaller magnitude, even in the inner estuaries. The more exposed, open coasts of Uruguay suffer the main damage with the combined effect of ocean waves.

The typical set-up of a storm surge in Rio de la Plata during a south-westerly wind event is illustrated in Figure 7.26. Figure 7.27 illustrates a hindcast

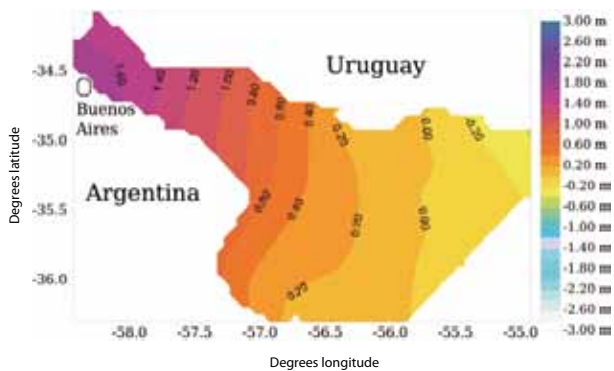


**Figure 7.26. Typical set-up of a storm surge in Rio de la Plata estuary during a south-westerly wind event**

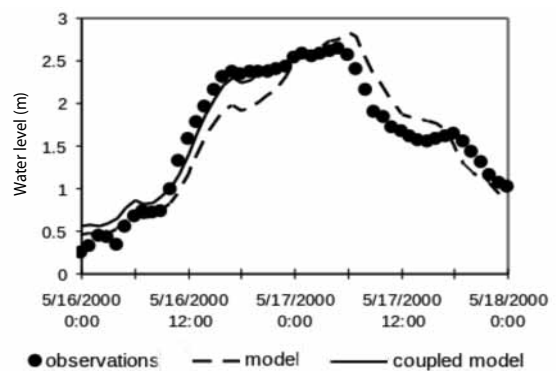


**Figure 7.27. Water level at Buenos Aires due to the storm surge of 16–17 May 2000. Model data are hindcast**

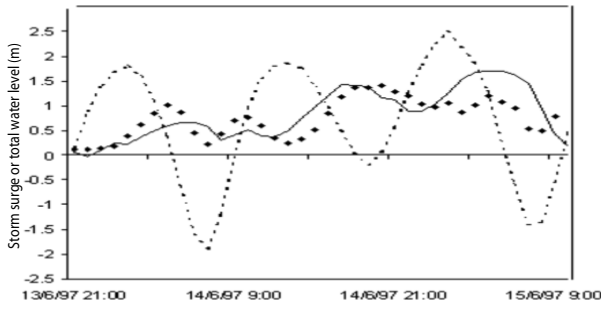


**Figure 7.28. Storm surge at upper-mid estuary in Bahia Blanca. Modelled (full), observed (dotted) and observed total water level (dashed)**

(dashed line) compared to hourly observations (dotted line) at Buenos Aires for the extreme case of 16–17 May 2000. The temporal and spatial scale of the phenomena allows surge–wave interaction to occur. Coupling with a wave model through roughness parameters improves the growth of the storm surge at its early stage (full line), as expected from theory (Komen et al., 1994).

Bahia Blanca presents a different situation to that described for Rio de la Plata. Due to the relatively deep channels and short length of the estuary, the storm surge wave is fast and quickly modifies the usual tidal pattern of flooding and drying. The speed of the process represents a serious danger to human life. The surge is distorted along the estuary due to tide–surge interaction. Currents and friction are the main cause for interaction in deep channels,



**Figure 7.29. The Baltic Sea and Gulf of Finland**

Source: The Baltic Sea Portal

while shallow-water effects are dominant in the large shallow areas. A phase shift of the storm surge is then produced between the shallow and deep areas. High resolution and accuracy in the currents is needed to reproduce correctly the frictional interaction. In such a scenario, the relative phase between the meteorological forcing and the tide can shift the peak of the storm surge several hours. A typical case of surge due to south-easterly winds produced by a storm extending over the adjacent shelf sea is shown in Figure 7.28. The numerical model (full line) is able to reproduce the modulation of the surge by its interaction with the tide.

**7.2.3 Baltic Sea (enclosed sea with low tidal range)**

Storm surges in the eastern part of the Gulf of Finland (Figure 7.29) are well known and have caused floods in Saint Petersburg with disastrous effects. During such floods, the water level in the Neva River has risen considerably and the central part of the city has been submerged under water depths of over 2 metres. The 10 most severe floods recorded in the history of the city are listed in Table 7.12.

The rise in the height of the water in the Neva is determined relative to a datum at the Kronshtadt foot gauge (corresponding to the average water level of the Baltic Sea near Kronshtadt). Flooding in Saint Petersburg tends to occur when the water rise is 160 centimetres over this datum. All the heights in the above table are cited relative to this datum. Flooding is categorized as dangerous (161–210 centimetres), specially dangerous (211–299 centimetres) and catastrophic (300 centimetres and higher). Of 299 recorded events,

**Table 7.12. The 10 highest recorded floods at Saint Petersburg (centimetres)**

Source: Pomeranets, 1998

| Date              | Height |
|-------------------|--------|
| 19 November 1824  | 421    |
| 23 September 1924 | 380    |
| 21 September 1777 | 321    |
| 15 October 1955   | 293    |
| 29 September 1975 | 281    |
| 2 November 1752   | 280    |
| 13 October 1723   | 272    |
| 12 November 1726  | 270    |
| 25 November 1903  | 269    |
| 16 November 1721  | 265    |
| 20 September 1706 | 262    |
| 30 November 1999  | 262    |



**Table 7.13. Domains of the nested three-level Baltic model**

| Parameter                 | Level of the model |                     |                                     |
|---------------------------|--------------------|---------------------|-------------------------------------|
|                           | The Baltic Sea     | The Gulf of Finland | Eastern part of the Gulf of Finland |
| Line number               | 53                 | 38                  | 123                                 |
| Column number             | 27                 | 80                  | 127                                 |
| Grid size (km)            | 30                 | 5                   | 1                                   |
| Integration time step (s) | 480                | 120                 | 30                                  |
| Maximum depth (m)         | 199                | 88                  | 60                                  |

228 were dangerous, 66 specially dangerous and 3 catastrophic. Most flooding occurs in the autumn (184 of the 299 recorded were autumn floods, and out of these 135 were dangerous, 46 specially dangerous and 3 were catastrophic – the totality of this latter category). The last flood occurred on 15 November 2005 with a height of 178 centimetres.

The hydrological conditions of the Gulf of Finland are dominated by the area's complicated, enclosed

morphology, high numbers of active weather systems, the presence of significant fluvial input and the appearance and disappearance of seasonal ice cover. Numerical modelling methods are preferred for hydrological forecasting in this region. A numerical model of joint water–ice dynamics for the Gulf of Finland has been developed and operated at the Arctic and Antarctic State Scientific Research Institute (AARI) (Russian Federation). The model is two-dimensional and depth-averaged and includes parameterization of ice friction in water. It is described fully in 7.4.

The operational system for the Baltic consists of three nested models whose domains are summarized in Table 7.13. In this application, ice thickness is considered to be constant both in time and in space and equal to 50 centimetres.

Verification is carried out for sea level and the drift of ice cover. Validation of water-level fluctuations compared with field observation data at a number of stations in the Gulf of Finland (Figure 7.30) demonstrates the effectiveness of the model: mean absolute error is 10–20 centimetres, mean squared error is 15–25 centimetres and the correlation coefficient ranges from 0.7 to 0.9 over the five locations.

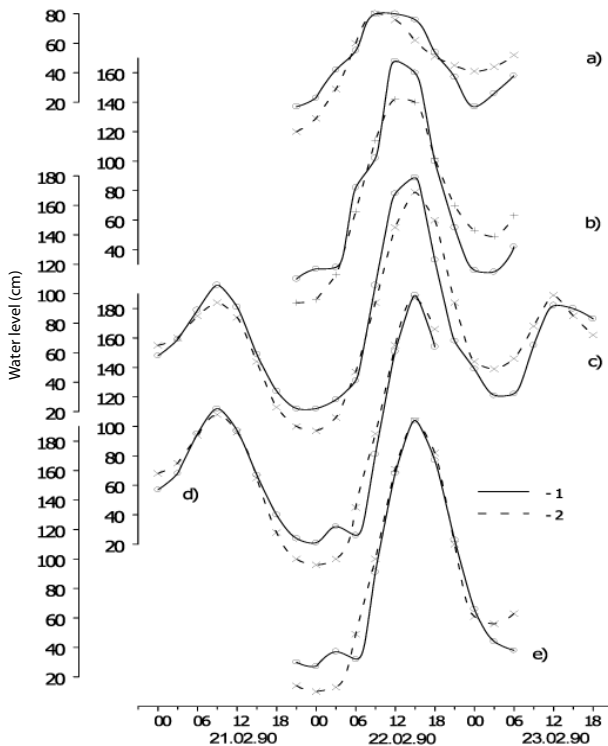


**Figure 7.30. Fluctuations in water level (centimetres) in the Gulf of Finland for the period 21–23 February 1990. Legend: 1 (solid line) actual; 2 (dashed line) estimated. Data are for the stations (a) Tallin, (b) Ust'-Neva, (c) Kronshtadt, (d) Strelna, (e) Institute of Mines**

### 7.3 STORM SURGES IN THE ARCTIC SEAS AND SEAS COVERED BY ICE

Arctic seas are complex and play a considerable role in the economy of the region. There is an increasing interest in the potential of the main thoroughfare of the Arctic, the Northern Sea Route. The bulk of settlements in the Arctic are located on the coasts or at the mouths of rivers. The Arctic shelf is rich in minerals, oil and gas. Hydrometeorological conditions in the Arctic seas, therefore, influence many aspects of the region's economic activity.

Numerical forecasts of non-cyclic sea-level oscillations on the Arctic shelf have been run on a regular basis since 1987. The earliest model was a depth-averaged two-dimensional surge model of the Arctic Ocean with a grid size of 30 nautical miles. In this first-generation model, the influence of ice cover on water mass dynamics was not taken into consideration, and therefore it was only used in the summer and autumn periods each year. From 1992, the effects of ice cover were included in a second-generation model. Since this time sea-level forecasts have been available for the entire year. The methods developed have now been used in the practical work of the AARI Ice and Hydrometeorological Information Centre for nearly 20 years. The current model grid and domain is shown in Figure 7.31.

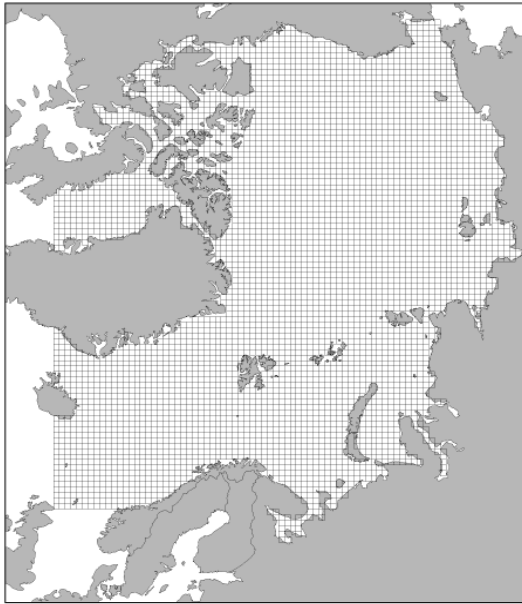


Figure 7.31. Domain of the AARI Arctic Ocean model

At the heart of the system is a joint water-ice dynamics model coupled to a two-dimensional storm surge model that accounts for ice friction in water. The numerical scheme employed is forward in time and centred in space. Quadratic formulations are used for both bed friction and the ice-water interface. Friction on the ice itself is taken to be equal to the friction on the water surface and estimated using an exponential function of the square of wind speed. A zero-flow condition is applied at solid lateral boundaries, and a radiation condition is used at open boundaries. An initial function for close ice is specified and ice thickness is taken to be constant at 2 metres. Estimation of ice redistribution is carried out on the basis of the transfer analysis method with flow corrections. A quiescent state is taken as the initial condition for water and ice.

Surface atmospheric pressure and information about the distribution of fast ice and close drift ice in the defined area of water provide the initial

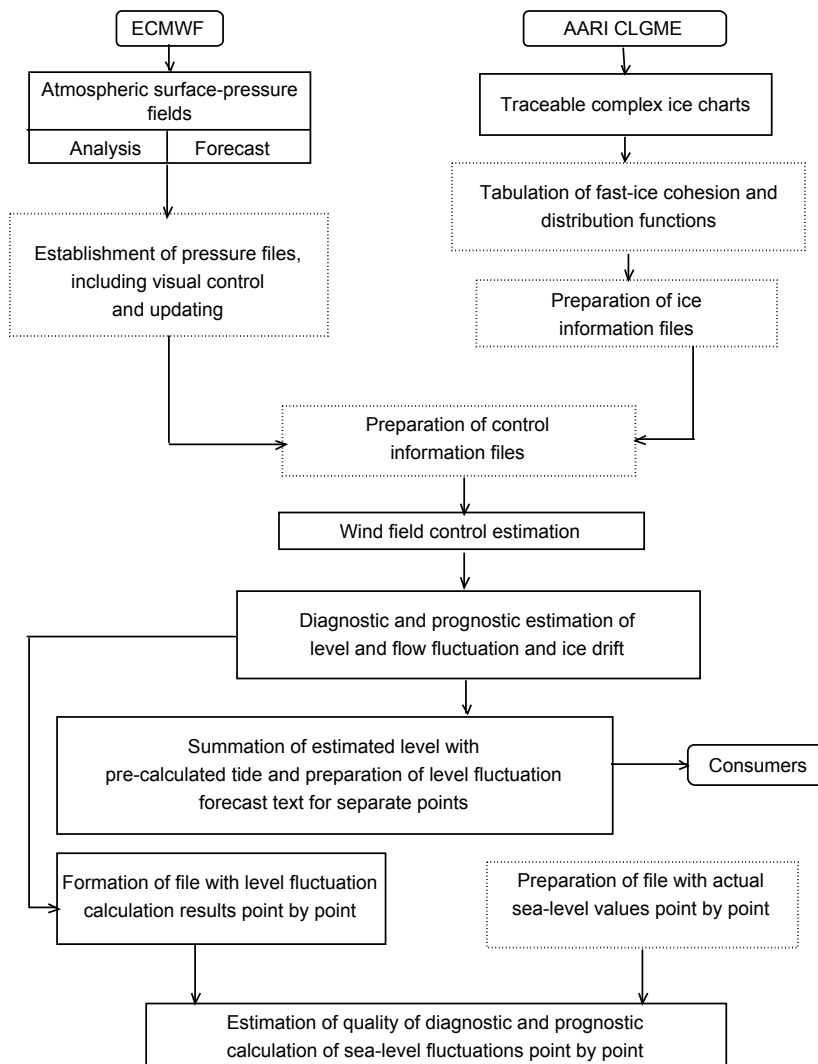


Figure 7.32. Flow diagram of the AARI sea-level fluctuation forecasting system in the Arctic seas that takes ice cover into account

information for calculations. Ice charts are compiled from data obtained from coastal stations, ships and satellites. Fields for surface pressure are supplied by ECMWF at 24-hour intervals and transmitted in gridded binary (GRIB) code on a five-degree geographic grid. The poor temporal resolution (24 hours) of the forcing atmospheric pressure field has a negative effect on the quality of calculations. It is impossible to reproduce accurately rapidly developing surge events where the event lasts less than 24 hours. Storm surge

situations that develop for 48 or more hours are better reproduced. From the hydrodynamic model various ice parameters can be calculated including close ice, ice drift speed and direction, pressing force, ice-speed divergence (ice rarefaction), sea-level fluctuation and the speed and direction of flows.

A flow diagram depicting the numerical forecast method for sea-level oscillations in the Arctic seas is shown in Figure 7.32.

---



## CHAPTER 8

# INUNDATION MAPPING

The material in this section is adapted from Dube et al. (2010). Several countries are working on projects involving potential inundation mapping. In China, the production of flood maps has been in practice since 1986. The current objective is that all available flood-hazard mapping will be available on the Internet (see the United Nations Economic and Social Commission for Asia and the Pacific (ESCAP)–WMO report, 2007). A pilot project in the Philippines produced a preliminary flood-hazard map of flood-prone areas in the San Juan River Basin. Flood maps have also been produced for Kuala Lumpur in Malaysia, including maps showing minimum, moderate and severe flooding for the River Gombak basin. Most of these mapping projects have involved steady-state models for the generation of static-map libraries of inundated areas at different water levels. Maps from these libraries are then called up for application based on forecast flood heights.

### 8.1 DEVELOPMENTS IN THE UNITED STATES

Inundation maps are based on predictions of water levels along the river reach and on the corresponding state of the terrain. The whole process of determining inundation mapping in coastal areas due to tropical cyclones involves meteorological forecasting (of storm track and intensity, and total precipitation), oceanographic, estuarine, and riverine hydrodynamic modelling (including wave

effects), watershed modelling of storm runoff and spatial mapping of inundation (Figure 8.1).

In addition to the normal forecasts of surge timing and height, flood inundation maps are increasingly being requested by emergency managers and decision makers. Maps are needed not only of coastal storm surge, but also of inland flooding resulting from high rainfall associated with cyclones. In the United States, since NWS instituted a programme to model tropical cyclone storm surge, more fatalities occur from inland flooding resulting from tropical cyclones than from storm surge (not including statistics from Hurricane *Katrina*), although this is not the case in all areas of the world. Flood inundation maps are useful for advance planning, as well as for response during events and for assessment following their occurrence.

Following Hurricane *Floyd* (1999), the State of North Carolina in the United States began a project to generate maps depicting inundated areas. This was the first NWS project involving the generation of libraries of inundation maps (Figure 8.2). The maps are based on steady-state hydraulic modelling of water surface elevations for incremented discharges.

The alternative to the use of the steady-flow assumption and development of such map libraries is to estimate inundated areas in real time during, or immediately prior to, a flood, so that the particular characteristics of the rainfall and flood hydrograph

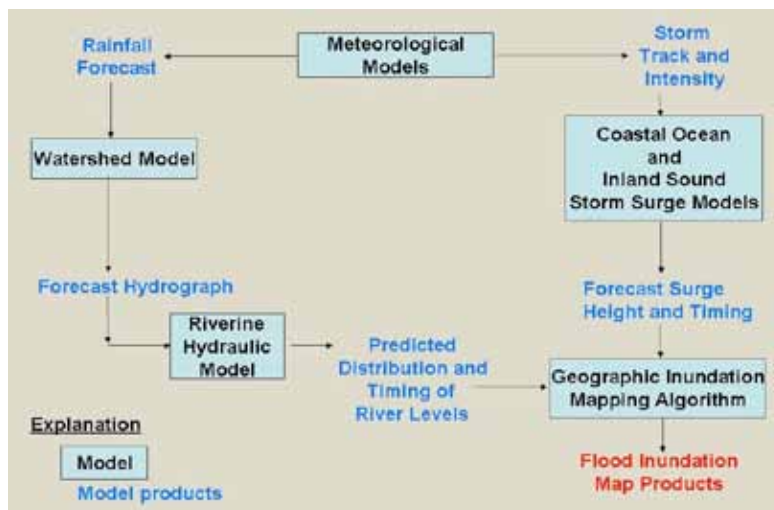
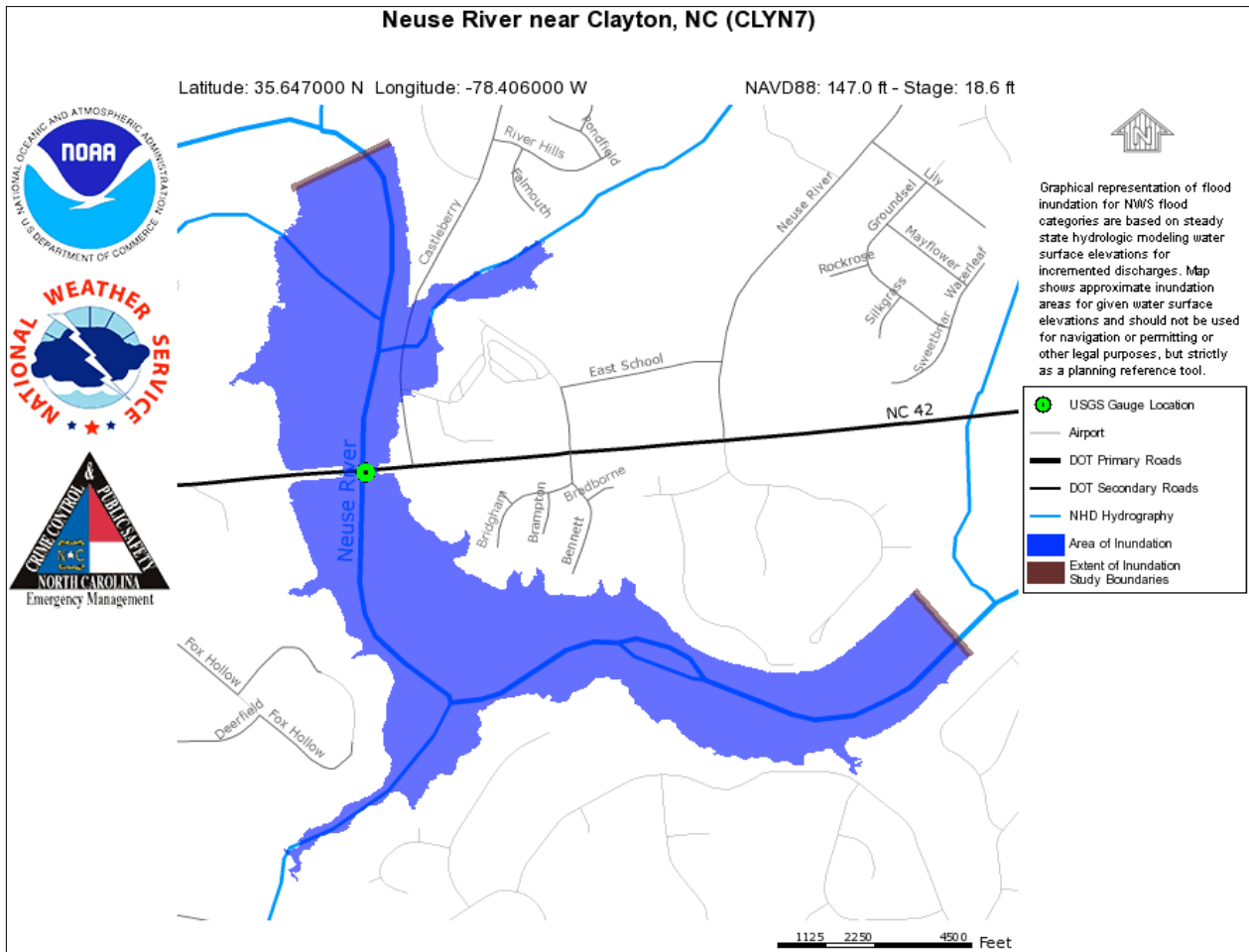


Figure 8.1. The suite of models required to simulate inundation from storm tides and upland flooding



**Figure 8.2. An example of an inundation map for the Neuse River near Clayton, North Carolina, United States**

Source: <http://water.weather.gov/ahps2/inundation/inundation.php?wfo=rah&gage=clyn7>

are well represented in the hydraulic modelling. The limitations of this approach are that the models must be run operationally in real time for each event and that the results must be distributed quickly to emergency management officials and all other interested parties. Moreover, there will be some uncertainty in the forecast flows for which the inundation modelling is to be conducted. A recent pilot project in the United States to test and evaluate dynamic mapping concluded that ongoing efforts in static mapping should be fully tested and evaluated before embracing the implementation of operational, real-time (dynamic) inundation mapping (NWS, 2008a, b).

Several different approaches have been taken to develop inundation maps. These include:

- (a) Making the assumption that a storm surge of a given height will inundate or impact up to the corresponding land contour of the same height;
- (b) Pre-generating a library of maps for a range of water levels (static maps);

- (c) Generating inundation maps from real-time forecasts of water level (dynamic maps) based on unique features of a given event.

Although dynamic mapping might seem the best option, implementation can be difficult and costly.

Examples of static maps are presented by Bales et al. (2007). These authors generated a set of profiles of the levels of the water surface at 0.305-metre (1-foot) increments for a reach of the Tar River. Based on these profiles, a water-level elevation was assigned to each cross section in the reach; the water was assumed to be level over the cross section, which is consistent with the one-dimensional modelling approach. Water-level elevations between cross sections were estimated using a spline interpolation. Inundated areas were identified by subtracting, for each grid cell, the elevation of the water surface from that of the land. An automated procedure was developed to identify all inundated cells that were

hydraulically connected to the cell at the downstream-most gauge in the model domain. This process resulted in a set of inundation-map libraries for each modelled reach. Inundation polygons were merged with a variety of other geospatial data to provide information for flood mitigation and emergency response.

At the time of writing, NWS does not use two-dimensional hydraulic models for operational purposes, so tests and pilot projects developed for dynamic maps have mainly focused on areas for which the one-dimensional approach is valid or can be approximated. However, in the pilot project for St. Johns River, Florida, there was an opportunity to test the coupling by using the one-dimensional hydraulic model to generate flow outputs that were used in turn as inputs for a two-dimensional estuarine model. The estuarine model was also used to forecast salinity and temperature.

Currently, the strategy within the United States is to develop static maps for flood-prone areas and gradually develop hydrodynamic models for estuaries to provide real-time flood maps. The increased demand for probabilistic inundation maps by emergency managers is being recognized, but still remaining is the need to develop operational procedures, including priorities for addressing mapping uncertainty.

## 8.2 A CASE STUDY: THE INDIAN COAST AT ANDHRA PRADESH

The remaining sections of this chapter provide an example of a case study of the Indian coast at Andhra Pradesh (Rao et al., 2007). Rao (1968) classified the Indian coastline into three categories based on combined storm surges and wind waves. According to this classification, the Andhra coast of India from 14 to 16.5 degrees north falls principally into the B-category (2- to 5-metre surges), with a short C-category belt (greater than 5-metre surges) near Nizampatnam Bay. According to an analysis of historical records by Jayanthi (Jayanthi, N., 1999: oral presentation – Storm Surge and its Risk Assessments over the Coastal Areas of Bay of Bengal and Arabian Sea, at: National Conference on Tropical Meteorology (Tropmet 99), Chennai, India, 16–19 February 1999), the Andhra coast is prone to be high risk with a small very high-risk zone near Nizampatnam Bay. The disastrous storm surges that occurred during 1977 and 1990 near Machilipatnam further support this categorization of the dangers of this coastline. In recent years, there has been considerable concern regarding the vulnerability of coasts due to cyclones and associated surges in view

of projected rises of sea level due to global warming. In this section, we have undertaken, as a case study, the development of a disaster management plan for cyclones and associated storm surges in the nine coastal districts of the State of Andhra Pradesh.

Based on historical cyclone data, through a simple statistical analysis, delta  $P$  (the atmospheric pressure deficit) was determined for cyclones making landfall on the Andhra Pradesh coast for return periods of 2, 5, 10, 25 and 50 years. The storm surge model developed by IIT–Delhi was run with the data values for a set of synthetic tracks, which were developed by compositing actual tracks, ensuring that each coastal district was covered. The results of the computer simulations, calibrated with observed surge data for each region of the coast, provided maximum probable surge amplitudes at the mandal level, which is the administrative unit immediately below the district level.

A generally accepted procedure when determining the extent of land inundation by a storm surge is to assume that a water level of 5 metres at the coastline would have an impact up to the 5-metre land contour, and similarly for other depths. This is a standard approach when very detailed orographic information is not available, although it might somewhat overestimate the extent of inundation. It is an acceptable approach for coastal zone storm-mitigation planning purposes.

In summary, the approach to determine the physical vulnerability is as follows:

- (a) A database of tropical cyclone-generated storm surges impacting the Andhra Pradesh coast was constructed from data from IMD and from several other national and international sources.
- (b) Because of climate change, projections into the future were limited to 50 years. All the available cyclone tracks for Andhra Pradesh were synthesized into composite tracks to cover each of the coastal districts of the state.
- (c) Making use of the projected pressure drop, the IIT–Delhi storm surge model was applied using the synthetic tracks to determine the maximum possible storm surge amplitude, during a 50-year period, at various locations along the Andhra Pradesh coast.
- (d) The total water-level envelope (TWLE) was determined by superimposing the tidal amplitudes and the set-up of wind waves on the surge amplitudes.
- (e) The determined water levels were then projected onto the coastal land using data on onshore topography to demarcate the horizontal extent of inundation.

(f) Maps of regions subjected to possible wind damage from cyclones were also prepared.

This conservative approach may slightly overestimate the extent of inundation, but it is appropriate for hazard mitigation and for coastal zone management, and is widely used around the world.

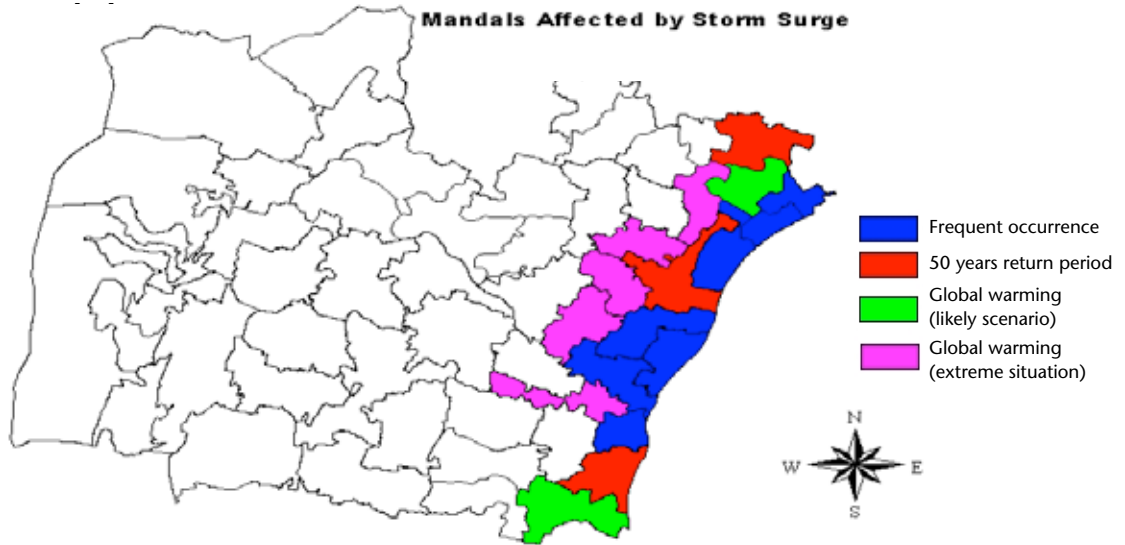
**8.2.1 Maps of physical vulnerability for the coastal districts**

Mapping of inundation by storm surge and of regions subjected to wind damage was performed for the districts of Prakasham

(Figure 8.3) and Guntur (Figure 8.4) of coastal Andhra Pradesh. The maps of physical vulnerability were prepared for four scenarios – (a) frequent (10 per cent annual recurrence interval), (b) infrequent (2 per cent annual recurrence interval), (c) a future climate scenario resulting in an intensification of the pressure field by 5 per cent and (d) a more extreme case of intensification of 7 per cent.

The three large rivers in Andhra Pradesh, Godavari, Krishna and Pennar, are subject to storm surge penetration. The extent of this was determined by projecting the surge water levels into the rivers. For this, it was assumed that, for a river with many meanders, the storm surge would

(a) Guntar District land inundation map Mandals affected by storm surge



(b) Guntar District wind map Mandals affected by strong winds >64 knots

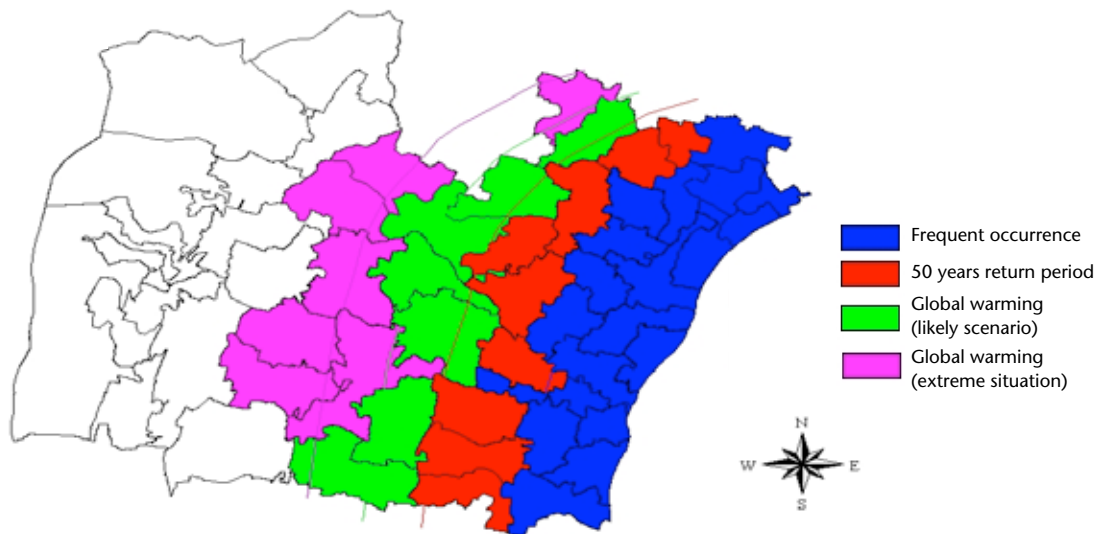


**Figure 8.3. (a) Map of land inundation by storm surge, and (b) regions affected by cyclonic winds for Prakasham District, Andhra Pradesh, India**



penetrate 10 per cent further than on land, and for a river with few meanders the penetration would be 15 per cent more. These assumptions are based on actual observations of storm surge penetration through these rivers (Murty, 1984). Physical-vulnerability maps for storm surge penetration up the rivers were then prepared (Figure 8.5 illustrates the estimation for the Krishna River).

8.2.2 Social vulnerability

Social vulnerability was estimated for physically vulnerable mandals. By using the available data on population and other factors, along with the physical-vulnerability maps, overall index maps of cyclone vulnerability were developed. Figure 8.6 shows the map for one of the districts of coastal Andhra Pradesh.

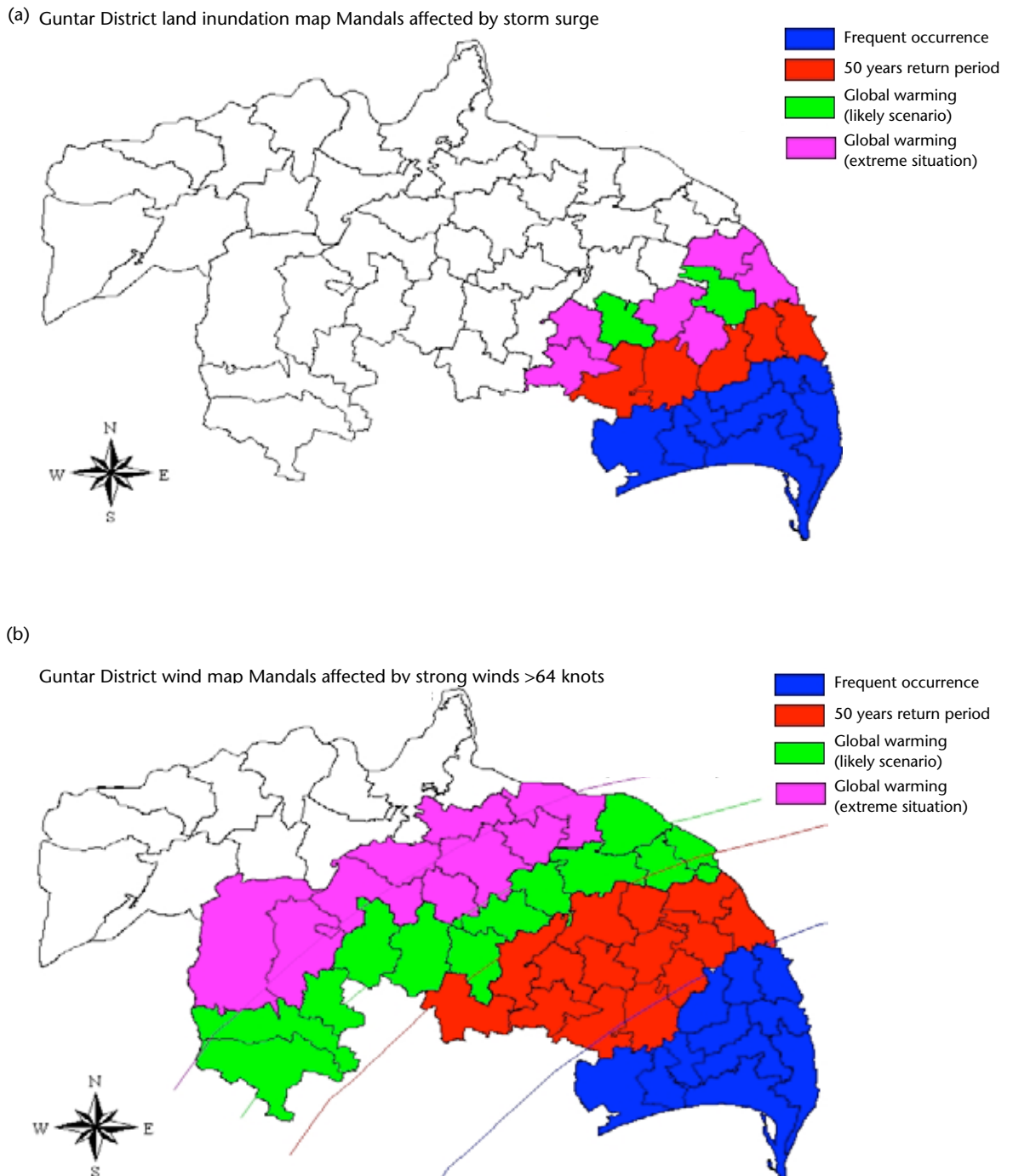


Figure 8.4. (a) Map of land inundation by storm surge, and (b) regions affected by cyclonic winds for Guntur District, Andhra Pradesh, India

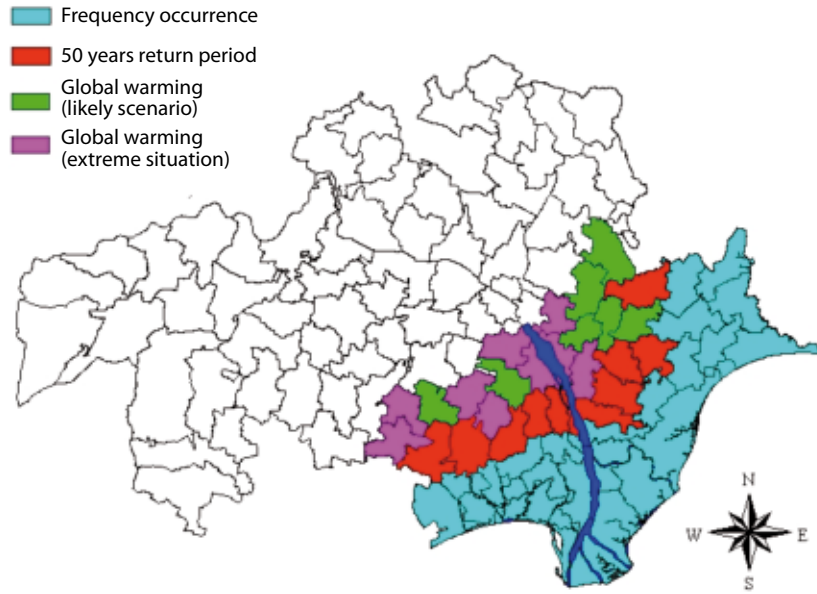


Figure 8.5. Estimated storm surge penetration through the Krishna River system

Note:

- 1. Missing data  
Children below 6 years  
Children between 6 to 14 years
- 2. Missing weightage points  
9 points

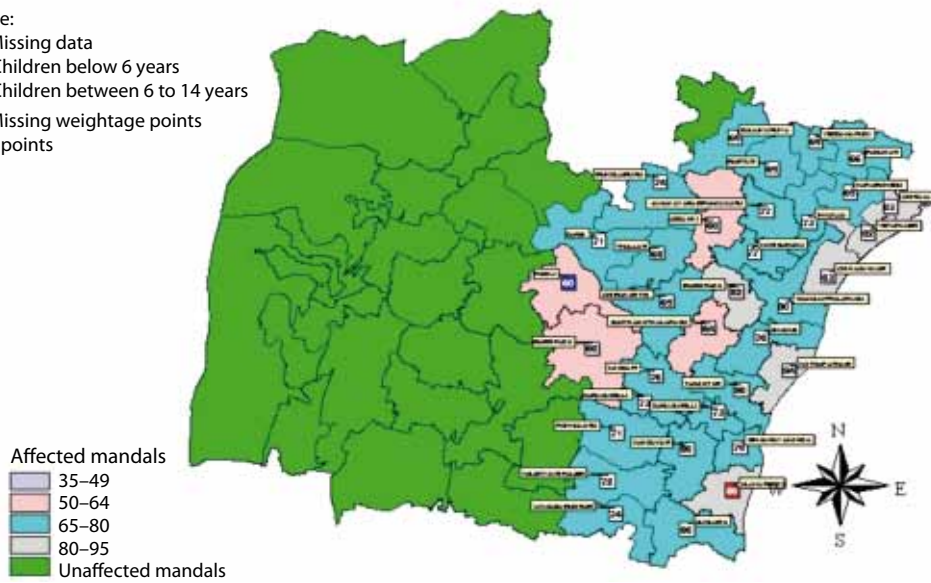


Figure 8.6. Map of overall cyclone vulnerability for Prakasham District, Andhra Pradesh, India

## STORM DISASTER PREPAREDNESS: FINDINGS OF THE JCOMM ETWS SURVEY OF NATIONAL AGENCIES

### 9.1 INTRODUCTION

Following the JCOMM-I mandate to assess the state of the art in operational storm surge numerical models and existing basic information sources, ETWS conducted a survey among Members and through IOC contact points. For the first time, an overview of operational practice regarding storm surge prediction has been documented. The compilation of the results is intended to enrich the group's expertise and provide a reference point of guidance for Members.

The information provided in this chapter is exclusively based on the 20 responses that were received to the questionnaire. Figure 9.1 illustrates the geographical areas covered by the survey, including the distribution of areas prone to storm surges and those covered by observations and operational or pre-operational storm surge models, as reported in the responses. Half of the responses answered all sections completely, that is, section A on data records and section B and C on operational forecasting systems. In five cases there is no operational

model or forecast, although observations are supported. In another five cases, details on instruments and data have not been provided.

### 9.2 BASIC INFORMATION ON STORM SURGES

#### 9.2.1 Observational data

The results of the enquiry on basic data sources confirm that measurements of sea level are extensive but regular measurements of current are still rare and limited to the most advanced countries and institutions. Digital sea-level records have been available since the 1950s, although a major change in technology is widely noted in the 1990s. Nevertheless, a few analog instruments in operational use are still reported.

The meteorological offices running storm surge models do not usually manage sea-level data on their own. Data are shared among institutions, in

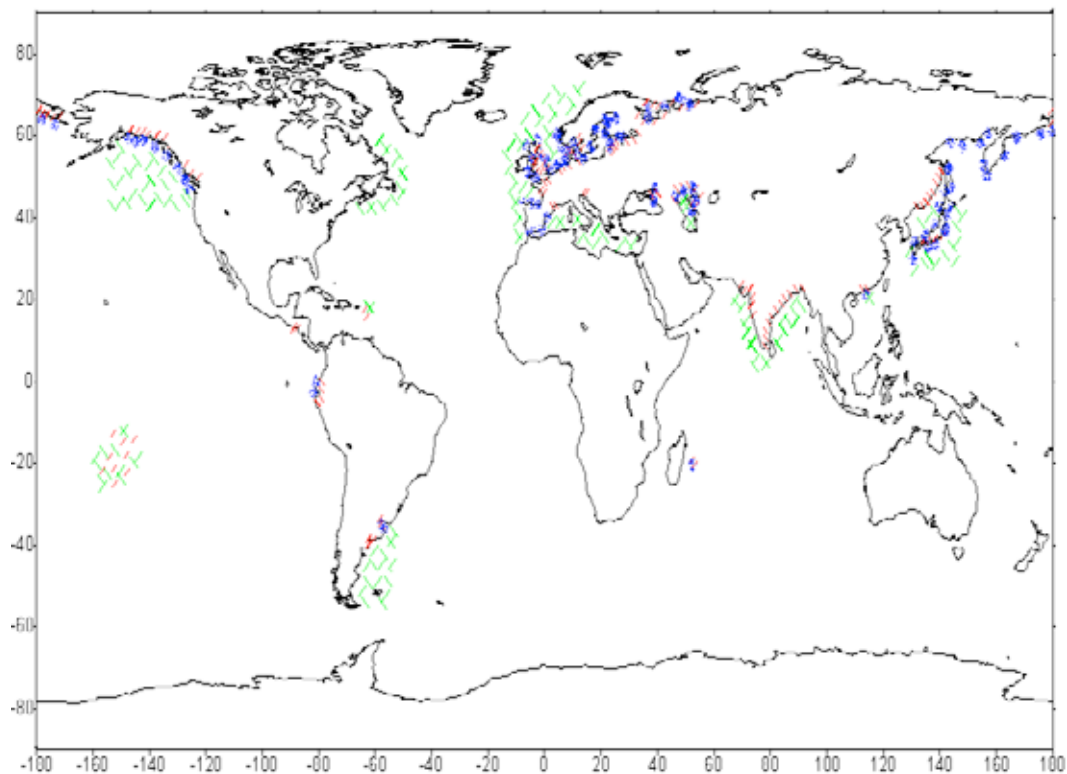


Figure 9.1. Geographical areas from which responses were received to the ETWS survey. Red dashes indicate areas prone to storm surges. Blue dots indicate areas covered by observations. Green dashes indicate areas covered by operational or pre-operational storm surge models.

most cases in real time. About half of the responses reflect the use of metadata, in some cases well documented. Other agencies in the countries surveyed did not respond, probably not being responsible for the data management. Climatological analysis of extreme values is done on these databases in most cases. Table 9.1 summarizes the responses concerning basic information on storm surges.

### 9.2.2 Hindcast databases

The number of different ways of creating hindcast databases on storm surges are revealed by the survey. Databases maintained from operational runs, whose records depend on the period of operation of the models, are not very extensive, with eight years of data being reported at most. Case studies of extreme events are almost always carried out after the event, usually to assess the model – these kinds of studies do not (and are not intended to) ensure completeness for the climatology of extreme events. Except for a few cases, the models used are the same as the operational ones. However, extensive hindcast databases are reported as the outcomes of two European projects and also projects from Hong Kong, China and the Russian Federation (see Table 9.2).

## 9.3 OPERATIONAL AND PRE-OPERATIONAL NUMERICAL MODELS

Only 5 of the 20 responses to the survey received reported not running an operational or pre-operational storm surge model. The information collected on storm surge models in use is detailed in Tables 9.3–9.6. A wide variety of uses of sea-level observations in real time in conjunction with numerical prediction is indicated, for example, correction of forecast bias, assimilation of initial conditions, blending in of bulletins with the forecasts, application of regression and empirical methods, and model validation.

### 9.3.1 Model characteristics

Approximately 75 per cent of the applications use two-dimensional models and some use finer nested grids. Resolution ranges from 10 to 20 kilometres for regional models to 1 kilometre or finer for nested grids in the coastal regions. Two-dimensional models are especially suitable for ensemble

forecasting. Table 9.3 compiles the information received concerning the model features.

### 9.3.2 External forcing

Most of the applications are forced by the most significant tidal constituents at the open boundaries, with a boundary definition for storm surge estimated from atmospheric pressure (inverted barometer). Extra-tropical storm surge models use forcing winds from high-resolution national NWP, whereas tropical cyclone surge models derive winds from parametric models of storm track and intensity (Table 9.4).

### 9.3.3 Products and dissemination

The forecast ranges of most of the operational applications are from 36 to 72 hours, although a forecast range as long as 120 hours has been reported. The predictions of surges generated by tropical cyclones have shorter ranges, usually under 12 hours. Products derived from the numerical models are diverse and include time-varying sea-level (surge) forecasts at specified locations and also charts, including local peaks and maxima charts, outputs for flooded areas, currents, and oil spill drift and spread. One report was received of the application of a statistically derived scale of risk for set-up (floods) as well as for abatement (navigation risk). Responses of the community to the enquiry about additional requirements from predictive models include increased information on flooded areas, the evolution of oil spills and surface currents (Table 9.5).

### 9.3.4 Verification procedures

The performance of operational and pre-operational storm surge models is monitored, in most cases, on a continuous basis (see Table 9.6). The sea-level products considered for the validation are either complete time series, peak levels or levels at selected times (such as high and low waters). The statistical parameters obtained, usually for different forecast ranges, are varied. The bias, RMS, standard deviation, average percentage error, linear regression (correlation coefficient) and the relation of standard error to mean square deviation are chosen by the different services. Statistics are provided either with a monthly or yearly frequency or may be related to the occurrence of major storms. The reader is referred to Chapter 6 for a more detailed treatment of verification procedures.

**Table 9.1. Basic information on storm surges (SL: sea level; ADCP: acoustic Doppler current profiler)**

| <i>Stations</i>  | <i>Parameter</i> | <i>Period</i>  | <i>Instrument</i>  | <i>Digital/<br/>analog</i> | <i>Metadata</i>   | <i>Climatology</i>  | <i>Country</i>    |
|--|------------------|--|--|----------------------------|---|---|-------------------|
| 2  | SL               | 1986–present   | Stevens type A   | D/A                        |   | Yes   | Mauritius         |
| 21. Further information: <a href="http://www.puertos.es">http://www.puertos.es</a> | SL               | 1992–present   | 15 acoustic, 7 pressure                                      | D                          | Sensors, units, models  | Trends, extremes, main regimes                                | Spain             |
| North Sea, Baltic, Skagerrak coasts  | SL, current      | Nineteenth century–present (SL), 1990s (current)                         | Pressure, buoy   | D                          | Yes: Web-based. Further information: <a href="http://www.edios.org/">http://www.edios.org/</a>    | Yes   | Denmark           |
|  | SL               | ISDM gauge   |  | D                          |   |   | Canada            |
| 66   | SL               | 1960–present   | 53 float gauges with stilling wells, 12 acoustic, 1 pressure | D                          | Location, datum versus ground elevation   | Maxima  | Japan             |
| 25   | SL               | 1970–present   | 22 well-type tide gauges, 3 radar-type                       | D                          | Yes: Web-based  | Maximum SL return periods                                     | Republic of Korea |
| 170  | SL, current      | Analog since 1845, digital since 1950                                    | Tide gauges, vector-averaging current meters, ADCP           | D                          | SL: other institutes. Currents: position, depth, start and end date, interval types of instrument | Extreme value analysis, return periods                        | Germany           |
| 7  | SL               | Earliest 1921, 3 new   | Staff gauge  | D                          | None  | River inflow, evaporation, precipitation, ice cover for model | Kazakhstan        |
| 18   | SL               | Early 1900   | Well-type  | D                          |   |   | Sweden            |
| North-east coasts. Other services  | SL               | 10 years or more   | Various  |                            |   |   | Netherlands       |
| Other services   |                  |  |  |                            |   | Risk-areas mapping. Extreme heights for sensitive areas       | France            |
|  | SL               | SL: hourly 1954–1987. Since 1988, 1-minute SL maximum. Events, 1906–1953 |  | D (all)                    | Station name, location, type of instrument, data period and availability (%)                      | Maximum SL return periods                                     | Hong Kong, China  |
|  | SL               | Since 1992   | Staff gauges, float and pressure recorders                   | D since late 1990s         | Location, start date, programme, type of instrument, accuracy                                     | Frequency over threshold. Maxima, 1961–2000                   | Latvia            |

| <i>Stations</i> | <i>Parameter</i> | <i>Period</i>                                     | <i>Instrument</i>   | <i>Digital/<br/>analog</i> | <i>Metadata</i>  | <i>Climatology</i>   | <i>Country</i>     |
|-----------------|------------------|---|---------------------|----------------------------|--|--|--------------------|
| 1               | Current          | Since December 2002                               | ADCP                | D                          | Documents  |  | Slovenia           |
|                 | SL, current      | Up to early nineteenth century, field experiments | Tide gauges, others | D/A                        |  | Positive and negative surge, averaged maximum, different periods | Russian Federation |
|                 | SL               | Since 1980  | Tide gauge, Stevens | D/A                        | Date and location  | SL monthly means   | Ecuador            |
|                 | SL               | Since 1582  | Analysed            |                            | Surge peak, extent of damage (number of people), inland inundation (km)                              | Analysis of maxima, return periods                               | India              |
| 44              | SL               | Hourly  | Tide gauges         | D                          | Documented. Further information: <a href="http://www.pol.ac.uk/ntslf">http://www.pol.ac.uk/ntslf</a> |  | United Kingdom     |

**Table 9.2. Hindcast databases on storm surges**

| <i>Source</i>  | <i>Model</i>                               | <i>Period</i>           | <i>Country</i>     |
|--|--|-------------------------|--------------------|
| EU HIPOCAS project, operational  | HAMSOM, Nivmar                             | 1958–2002, 1998–present | Spain              |
| EU STOWASUS-2100 project. See: <a href="http://web.dmi.dk/pub/STOWASUS-2100/">http://web.dmi.dk/pub/STOWASUS-2100/</a> | Climate storm surge model, non-operational | 1958–2002               | Denmark            |
| Events, case studies   | Operational                                | 1998–present. Events    | Japan              |
| Case studies   | Operational                                | 1997–present            | Republic of Korea  |
| Continuous and case studies  | Operational                                | 2002–2004, 2005–present | Argentina          |
| Case studies   | Operational                                | 1962–1999               | Germany            |
| Case studies. Simulations  | Operational                                | 1940–2004               | Kazakhstan         |
| Case studies   | Operational                                | 1999                    | France             |
| Extensive  | Operational                                | 1947–2004               | Hong Kong, China   |
| Extensive and case studies   | Operational                                | 1948–2004               | Russian Federation |
| Maximum envelope of surge water  |  |                         | India              |
| EU STOWASUS-2100 project   | Operational                                | 1958–2002, 1992–present | United Kingdom     |

**Table 9.3. Features of operational and pre-operational storm surge models (nmi: nautical miles)**

| <i>Model</i>   | <i>Area</i>   | <i>Type</i>   | <i>Grid</i>   | <i>Country</i>       |
|--|---|---|---|----------------------|
| HAMSOM,<br>Nivmar  | Mediterranean Sea<br>and Iberian Peninsula  | Vertically integrated<br>barotropic   | 10 minutes  | Spain                |
| Mike 21<br>pre-operational<br>3-D<br><br>2-D finite element<br>MOG2D | North Sea, Baltic Sea   | 2-D hydrodynamic  | Finite difference 9 nmi, 3 nmi,<br>1 nmi, 1/3 nmi   | Denmark              |
| Coupled ice-<br>ocean<br><br>NPAC                                    | Grand Banks,<br>Newfoundland,<br>Labrador<br><br>NE Pacific,<br>120°W–160°W,<br>40°N–62°N   | 3-D circulation based<br>on the Princeton Ocean<br>Model                        | Approximately 20 km x<br>20 km<br><br>Finite difference curvilinear<br>C-grid 1/8 degree  | Canada               |
| JMA Storm Surge  | 23.5°N–46.5°N,<br>122.5°E–146.5°E   | 2-D linearized shallow<br>water   | Staggered Arakawa C-grid.<br>1 minute latitude/longitude  | Japan                |
| KMA Storm Surge  | 20°N–50°N,<br>115°E–150°E   | 2-D barotropic surge and<br>tidal current based on the<br>Princeton Ocean Model | Approximately 8 km x 8 km,<br>finite difference curvilinear<br>C-grid 1/12 degree   | Republic of<br>Korea |
| NIVELMAR   | Portuguese mainland<br>coastal  | Shallow water   | 1 minute latitude x 1 minute<br>longitude   | Portugal             |
| SMARA storm<br>surge   | Shelf sea 32°S–55°S,<br>51°W–70°W.<br><br>Rio de la Plata   | 2-D depth-averaged  | Geographical Arakawa C-grid,<br>1/3 degree latitude x<br>1/3 degree longitude<br><br>1/20 degree latitude x 1/20<br>degree longitude                | Argentina            |
| BSH circulation<br>(BSHcmod)<br><br>BSH surge<br>(BSHsmod)           | North-east Atlantic,<br>North Sea, Baltic   | 3-D hydrostatic circulation<br><br>2-D barotropic surge                         | Regional spherical, North Sea,<br>Baltic 6 nmi, German Bight<br><br>Western Baltic, 1 nmi, surge<br>North Sea, 6 nmi, north-east<br>Atlantic 24 nmi | Germany              |
| Caspian Storm<br>Surge   | Caspian Sea<br>36°N–48.5°N,<br>45°E–58°E<br><br>North Caspian<br>Sea 44.2°N–48°N,<br>46.5°E–55.1°E  | 2-D hydrodynamic, based<br>on MIKE 21 (DHI Water &<br>Environment)              | 10 km x 2 km  | Kazakhstan           |
| HIROMB/NOAA  | North-east Atlantic,<br>Baltic  | 3-D baroclinic  | C-grid, 24 nmi  | Sweden               |
| WAQUA-in-<br>Simona/DCSM98   | Continental shelf<br>48°N–62°N, 12°E–<br>13°E   | 2-D shallow water, ADI<br>method, Kalman filter data<br>assimilation            | 1/8 degree longitude x 1/12<br>degree latitude  | Netherlands          |
| Derived from<br>MOTHY oil spill<br>drifts model                      | Near-Europe Atlantic<br>(Bay of Biscay,<br>Channel and North<br>Sea) 8.5°E–10°E,<br>43°N–59°N<br><br>West Mediterranean<br>basin (from the Strait<br>of Gibraltar to Sicily)<br><br>Restricted area in<br>overseas departments<br>and territories | Shallow-water equations   | Arakawa C-grid<br><br><br>5' of latitude x 5' of longitude<br><br><br>Finer meshes  | France               |
| SLOSH  | Sea area south of<br>Hong Kong within<br>130 km   | Finite difference   | Polar, 1 km near to 7 km,<br>South China Sea  | Hong Kong,<br>China  |

| <i>Model</i>                              | <i>Area</i>   | <i>Type</i>   | <i>Grid</i>  | <i>Country</i>     |
|---|---|---|--|--------------------|
| Short-term sea-level and current forecast | Caspian Sea and near-shore low-lying zones              | 3-D hydrodynamic baroclinic                         | 3 nmi horizontal, 19 levels  | Russian Federation |
| IIT-Delhi, IIT-Chennai, NIOT-Chennai      | East and west coasts of India and high-resolution areas | Non-linear, finite element, explicit finite element | For example, for inundation model average spacing of 12.8 km offshore direction and 18.42 km along shore | India              |
| CS3 tide surge                            | North-west European shelf waters                        | Finite difference, vertically averaged              | C-grid 12 km, nested finer resolution  | United Kingdom     |

**Table 9.4. External forcing provided to operational or pre-operational applications**

| <i>Wind</i>   |  |  | <i>Open boundaries</i>  |  | <i>Country</i>    |
|---|--|--|---|--|-------------------|
| <i>Source</i>   | <i>Update</i>  | <i>Spatial resolution</i>  | <i>Surge</i>  | <i>Tides</i>   |                   |
| INM (HIRLAM)  | Twice daily, input every 3 hours                                     | 0.2 degrees  | Inverse barometer   | MOG2D model  | Spain             |
| DMI HIRLAM  | 6 hours, hourly input  | 5 km   | Air pressure, atmospheric effects   | North bound: <i>Obeskommando der kiriegsmarine</i> (Naval High Command, Germany, 1943), 10 constituents<br><br>South bound: Admiralty Tsales, 4 constituents | Denmark           |
| MSC United States Navy COAMPS                                     | Input every 3 hours, daily. Daily 48-hour forecasts, 6-hourly        | Approximately 24 km x 24 km  | Fixed seasonal conditions. Radiation  | Tide model<br>Topex altimeter inverse model  | Canada            |
|   |  |  | Radiation, zero flow normal to sea-land interface   | Harmonic analysis of tide-gauge data   | Japan             |
| KMA mesoscale model (MMS)   | Input every 3 hours, daily<br><br>Daily 48-hour forecasts, 12-hourly | Approximately 30 km x 30 km  | Air pressure, atmospheric effects   | Tide model and harmonic analysis of tide-gauge data  | Republic of Korea |
| ECMWF 10-m wind   |  | 1 degree latitude x 1 degree longitude   |   |  | Portugal          |
| NCEP GFS (analyses)<br><br>SMN (Argentina) Eta model (forecasts)  | Every 6 hours<br><br>Every 3 hours                                   | Approximately 0.47 degrees latitude x 0.47 degrees longitude<br><br>1/3 degree latitude x 1/3 degree longitude |   | Schwidderky atlases, 5 constituents open sea Kelvin wave interpolation from stations at mouth of estuary   | Argentina         |
| DWD (German Weather Service): global GME<br><br>Local LM (Europe) | Twice daily  | Approximately 40 km<br><br>Approximately 7 km  | Circulation: two-way nesting, monthly climatological temperature and salinity inflow through buffer layer<br><br>Circulation and surge: radiation, surge from north-east Atlantic model | North Sea 14 constituents  | Germany           |



| <i>Wind</i>                                 |                                  |  | <i>Open boundaries</i>  |   | <i>Country</i>     |
|---|----------------------------------|--|---|---|--------------------|
| <i>Source</i>                               | <i>Update</i>                    | <i>Spatial resolution</i>                    | <i>Surge</i>  | <i>Tides</i>                                |                    |
| ECMWF global                                | 120 hours every 6 hours          | 1.5 degrees latitude x 1.5 degrees longitude | Closed boundaries (coarse). Nesting   |   | Kazakhstan         |
| HIRLAM                                      | Hourly                           | 22 km  |   | Calculated tidal components                 | Sweden             |
| HIRLAM (NL-KNMI)                            | Update 6 hours, 1 hour           | 0.2 degrees                                  |   | 10 tidal components tuned from ocean models | Netherlands        |
| IFS   | 6 hours                          | 0.5 degrees                                  | Inverted barometric radiation for current, normal zero at coastline                                       | Tide components from past observations      | France             |
| ARPEGE                                      | 3 hours                          | 0.25 degrees                                 |   |   |                    |
| ALADIN                                      | 3 hours                          | 0.1 degrees                                  |   |   |                    |
|   |                                  |  | Tropical cyclone track, size and intensity  | Predicted astronomical tides                | Hong Kong, China   |
| LAAM  | Twice daily, input every 6 hours | 75 km  | River runoff. Ice conditions  |   | Russian Federation |
| Objective analyses of synoptic observations |                                  |  | Pressure drop<br>Radius of maximum wind<br>Maximum wind speed<br>Forecast landfall<br>Motion of the storm |   | India              |
| United Kingdom mesoscale model              |                                  |  | Inverse barometer   | Larger-scale model                          | United Kingdom     |

**Table 9.5. Products and dissemination of operational storm surge numerical predictions**

| <i>Model output</i>   | <i>Range/time interval</i>        | <i>Real-time data use (routine)</i>                     | <i>Applications</i>                  | <i>Country</i>   |
|---|-----------------------------------|---|--------------------------------------|--|
| Storm surge   | 72 hours                          | Assimilation  | Water-level forecast                 | Spain:<br><a href="http://www.puertos.es">http://www.puertos.es</a>  |
| Water level and currents  | 54 hours, hourly, 4 times per day | Remove bias of local forecast.<br>Autoregressive filter | Water level, oil drift calculations  | Denmark:<br><a href="http://www.dhi.dk">http://www.dhi.dk</a>  |
| Water level at locations.<br>Surface height anomaly.<br>Local time series | 2 days 48 hours, 6-hourly         | Real-time height anomalies from gauges, comparisons     | Water level, surface currents, drift | Canada:<br><a href="http://www.mar.dfo-mpo.gc.ca/science/ocean/icemodel/ice_ocean_forecast.html">http://www.mar.dfo-mpo.gc.ca/science/ocean/icemodel/ice_ocean_forecast.html</a> |
| Time series of sea level and surges                                       | 33 hours                          | Under development                                       | Time series of sea level and surges  | Japan  |
| Time series of sea level  | 2 days. 48 hours, 12-hourly       | Empirical methods combine model and real-time data.     | Time series of sea level             | Republic of Korea  |
| Sea level and currents  | 120 hours                         |   | Sea level and currents               | Portugal   |
| Water level and mean current, surge                                       | 48 hours                          |   | Water-level forecasts                | Argentina  |

| <i>Model output</i>   | <i>Range/time interval</i>  | <i>Real-time data use (routine)</i>                 | <i>Applications</i>  | <i>Country</i>     |
|---|---|---|--|--------------------|
| Currents, water level, temperature, salinity, ice thickness and compactness | Circulation: 72 hours, starting from 12 hour meteorological forecast once a day<br><br>Surge: 2 per day, 84 hours water level | Empirical methods combine model and real-time data. | Water-level and current forecasts. Drift, oil-spreading calculations | Germany            |
| Current and water level, maps of water depth, P and Q fluxes, time series   |   | Initial conditions with empirical methods           | Local predictions. Weekly bulletins                                  | Kazakhstan         |
| Sea-level maps, time series, Web presentations for internal use             |   | Comparisons, internal use                           | Water-level forecasts, drift calculations, currents                  | Sweden             |
| Sea-level maps and selected locations                                       | 48 hours, maps every 3 hours, 10 minutes at selected points   | Data assimilation                                   | Water-level/surge forecasts for the coast                            | Netherland         |
| GRIB and BUFR data files  | 48 hours, fields hourly, 5 minutes $t$ ports  |   | Water-level forecasts  | France             |
| Maximum sea level and tides at locations, table of hourly sea levels        | 18 hours before and 12 hours after the closest approach of the cyclone  | Combination in bulletins                            | Storm surge forecasting  | Hong Kong, China   |
| Sea level, 3-D currents, flooded areas                                      | 48 hours, 1 hour  | Forecast regression-based positive/negative surge   | Water-level forecasts, flooding, others                              | Russian Federation |
| Peak surge and inundation   | 48 hours, 3 hours   |   | Forecasts for the case of tropical cyclones                          | India              |
| STFS  | 36 hours  | Validation  | Hindcast, forecasts  | United Kingdom     |
|   |   |   | Bulletins, marine forecasts  | El Salvador        |

**Table 9.6. Verification of operational and pre-operational storm surge models (sea level)**

| <i>Method</i>   | <i>Time period/frequency</i>   | <i>Country</i>     |
|---|--|--------------------|
| Case studies, comparisons with observations   | 15 years of tropical cyclone events overseas   | France             |
| Events, hindcast peak surges, biases and RMSE, collocations.<br>Time series   | Continuous   | Japan              |
| Events, hindcast peak surges, biases and RMSE.<br>Time series, water level at selected stations   | Monthly  | Republic of Korea  |
| Full range of statistics  | Monthly  | United Kingdom     |
| Research mode   |  | India              |
| RMS, others   | Pre-operational validation   | Russian Federation |
| See: <a href="http://www.puertos.es">http://www.puertos.es</a>  | Real time  | Spain              |
| Mean absolute percentage error on the 3 highest high waters at a set of predefined stations as a function of forecast range every 6 hours. Running means are applied for 12 months and averaged for the 18 stations. Refer to Section 7.2.1 | Continuous: see: <a href="http://ocean.dmi.dk/validations/surges/background.uk.php">http://ocean.dmi.dk/validations/surges/background.uk.php</a> | Denmark            |
| Water level at selected stations  |  | Canada             |
| 0-hour forecast at stations   | Not continuous   | Portugal           |
| Storm surge case studies and continuous at selected locations   | Monthly  | Argentina          |
| Statistics of deviations from measured data. Forecasts within 12 hours, corresponding to high or low waters. 0-hour not done. Additional parameters. Refer to Section 7.2.1   | Yearly   | Germany            |
| Peak storm surge height, linear regression  | 1947–1998  | Hong Kong, China   |
| Parameters according to pre-established norms, mainly relation of standard error to mean square deviation   |  | Kazakhstan         |
| Comparison with observations and specific campaigns   |  | Sweden             |
| RMS, bias, standard deviation, for main locations   | Since 1994   | Netherlands        |



## APPENDIX I

### REFERENCES

- Abbott, M.B., A. Danesgaard and G.S. Rodenhuis, 1973: System 21, Jupiter: a design system for two-dimensional nearly-horizontal flow. *J. Hydraul. Res.*, 11:1–28.
- Abramovich, G.N., 1960: *Theory of Turbulent Currents*. Moscow, Physmatgiz Publishing House.
- Akamatsu, H., 1982: On seiches in Nagasaki Bay. *Pap. Meteor. Geophys.*, 33:95–115.
- Arakawa, A., 1966: Computational design for long-term numerical integration of the equations of fluid motion: Two-dimensional incompressible flow. Part 1. *J. Comput. Phys.*, 1:119–143.
- Arakawa, A. and V.R. Lamb, 1977: Computational design of the UCLA general circulation model. *Meth. Comput. Phys.*, 17:173–265.
- Ashik, I.M., 1995: Numerical prediction of sea surges and ice conditions in the Laptev and the East Siberian seas. In: *Russian–German Cooperation: Laptev Sea System* (H. Kassens, D. Piepenburg, J. Thiede, L. Timokhov, H.-W. Hubberten and S.M. Priamikov, eds). *Ber. Polarforsch.*, 176:47–54.
- Ashik, I.M. and G.A. Larionova, 2003: Sea hydrological forecasts in the defined areas of water in Arctic Ocean. *Proceedings on Hydrography*, 259:48–57.
- Baba, M., 2005: Occurrence of “Swell Waves” along the south-west coast of India from southern Indian Ocean storm. *J. Geol. Soc. India*, 66:248–249.
- Backhaus, J., 1976: *Zur Hydrodynamik im Flachwassergebiet, ein numerisches Modell* [Hydrodynamics in shallow water areas, a numerical model]. *Dtsch. Hydrogr. Z.*, 29:222–238 (in German).
- Bales, J.D., C.R. Wagner, K.C. Tighe and S. Terziotti, 2007: *LiDAR-derived Flood-inundation Maps for Real-time Flood-mapping Applications, Tar River Basin, North Carolina*. United States Geological Survey Scientific Investigations Report 2007-5032. pubs.usgs.gov/sir/2007/5032/pdf/SIR2007-5032.pdf.
- Belsky, N.I., 1954: Synoptic conditions of Leningrad floods. *Works of the State Oceanographic Institute (GOIN)*, 27(39):43–80 (in Russian).
- Birchfield, G.E. and T.S. Murty, 1974: A numerical model for wind-driven circulation in Lakes Michigan and Huron. *Mon. Weather Rev.*, 102(2):157–165.
- Bishop, C.H., B.J. Etherton and S.J. Majumdar, 2001: Adaptive sampling with the ensemble transform Kalman filter. Part 1: Theoretical aspects. *Mon. Weather Rev.*, 129:420–436.
- Bode, L. and T.A. Hardy, 1997: Progress and recent developments in storm surge modelling. *J. Hydraul. Eng.-ASCE*, 123(4):315–331.
- Bogden, P.S., P. Malanotte-Rizzoli and R.P. Signell, 1996: Open-ocean boundary conditions from interior data: Local and remote forcing of Massachusetts Bay. *J. Geophys. Res.*, 101:6487–6500.
- Bolzano, A., 1998: Evaluation of methods for numerical simulation of wetting and drying in shallow water flow models. *Coast. Eng.*, 34:83–107.
- Borishansky, L.S., 1958: Salinity distribution in sea for-mouth area. *Works of the State Oceanographic Institute (GOIN)*, 42:121–141 (in Russian).
- Borishansky, L.S., 1964: Calculation of water salinity distribution in sea for-mouth area for rivers with wide mouth using the Neva River as example. *Works of the State Oceanographic Institute (GOIN)*, 72:5–18 (in Russian).
- Bowler, N.E., A. Arribas, K. Mylne and K. Robertson, 2007a: *Met Office Global and Regional Ensemble Prediction System (MOGREPS). Part I: System description*. NWP Technical Report 497. Exeter, The Met Office.
- , 2007b: *Met Office Global and Regional Ensemble Prediction System (MOGREPS). Part II: Case Studies, Performance and Verification*. NWP Technical Report 498. Exeter, The Met Office.
- Brebbia, C.A. and P.W. Partridge, 1976: Finite element simulation of water circulation in the North Sea. *Appl. Math. Model.*, 1:101–107.
- Bretschneider, C.L., 1966: Engineering aspects of hurricane surge. In: *Estuary and Coastline Hydrodynamics* (A.T. Ippen, ed.). New York, McGraw-Hill.
- Brown, J.D., T. Spencer and I. Moeller, 2007: Modelling storm surge flooding of an urban area with particular reference to modelling uncertainties: A case study of Canvey Island, United Kingdom. *Water Resour. Res.*, 43(6):1–22.
- Brown, J.M., R. Bolaños and J. Wolf, 2011: Impact assessment of advanced coupling features in a tide-surge-wave model, POLCOMS-WAM, in a shallow water application. *J. Marine Syst.*, 87(1):13–24.
- Canizares, R., A.W. Heemink and H.J. Vested, 1998: Application of advanced data assimilation methods for the initialization of storm surge models. *J. Hydraul. Res.*, 36:655–674.
- Chapman, D.C. and G.S. Giese, 1990: A model for the generation of coastal seiches by deep-sea internal waves. *J. Phys. Oceanogr.*, 20:1459–1467.
- Charnock, H., 1955: Wind stress on a water surface. *Quart. J. Roy. Meteorol. Soc.*, 81:639–640.
- Chittibabu, P., S.K. Dube, A.D. Rao, P.C. Sinha and T.S. Murty, 2000: Numerical simulation of extreme sea levels using location specific high-resolution model for Gujarat coast of India. *Mar. Geod.*, 23:133–142.
- Chittibabu, P., S.K. Dube, P.C. Sinha, A.D. Rao and T.S. Murty, 2002: Numerical simulation of extreme sea levels for the Tamilnadu (India) and Sri Lanka coasts. *Mar. Geod.*, 25(3):235–244.

- Connor, J.J. and C.A. Brebbia, 1976: *Finite Elements for Fluid Flow*. London, Butterworths.
- Crean, P.B., 1978: A numerical model of barotropic mixed tides between Vancouver Island and the mainland and its relation to studies of the estuarine circulation. In: *Hydrodynamics of Estuaries and Fjords, Proceedings of the 9th International Liège Colloquium on Ocean Hydrodynamics*, Liège, Belgium, 1977 (J.C.J. Nihoul, ed.). Amsterdam, Elsevier.
- Cressman, G.P., 1959: An operational objective analysis system. *Mon. Weather Rev.*, 87:367–374.
- Daniel, P., 1996: A real-time system for forecasting hurricane storm surges over the French Antilles. In: *Small Islands: Marine Science and Sustainable Development, Coastal and Estuarine Studies* (G.A. Maul, ed.). Washington, AGU.
- , 1997: Forecasting tropical cyclone storm surges at Météo-France. In: *Computer Modelling of Seas and Coastal Regions III* (J.R. Acinas and C.A. Brebbia, eds). Southampton, Computational Mechanics Publications.
- Davies, A.M. and R.A. Flather, 1978: *Application of Numerical Models of the North-west European Continental Shelf and the North Sea to the Computation of the Storm Surges of November to December 1973*. Deutsche hydrographische Zeitschrift 14. Hamburg, Deutsches Hydrographisches Institut (in German, summary in English).
- Deacon, E.L., 1962: Aerodynamic roughness of the sea. *J. Geophys. Res.*, 67(8):3167–3172.
- Deacon, E.L. and E.K. Webb, 1962: Small scale interactions. In: *The Sea, Volume 1* (M.N. Hill, ed.). New York, Interscience Publishers/John Wiley and Sons.
- de Vries, H., M. Breton, T. de Mulder, Y. Krestenitis, J. Ozer, R. Proctor, K. Ruddick, J.C. Salomon and A. Voorrips, 1995: A comparison of 2D storm surge models applied to three shallow European seas. *Environ. Softw.*, 10(1):23–42.
- Donelan, M.A., F.W. Dobson, S.D. Smith and R.J. Anderson, 1993: On the dependence of sea surface roughness on wave development. *J. Phys. Oceanogr.*, 23(9):2143–2149.
- Drabkin, V.V. and K.S. Pomeranets, 1978: “Winter” floods in Leningrad and their researches by empirical and hydrodynamic methods. *Bulletin of Leningrad State University, Ser. Geol.–Geogr.*, 12:69–75.
- Dube, S.K., P. Chittibabu, P.C. Sinha, A.D. Rao and T.S. Murty, 2004: Numerical modelling of storm surges in the head Bay of Bengal using location specific model. *Nat. Hazards*, 31:437–453.
- Dube, S.K. and V.K. Gaur, 1995: Real-time storm surge prediction system for the Bay of Bengal. *Curr. Sci.*, 68:103–113.
- Dube S.K, T.S. Murty, J.C. Feyen, R. Cabrera, B.A. Harper, J.D. Bales and S. Amer, 2010: Storm surge modeling and applications in coastal areas. In: *Global Perspectives on Tropical Cyclones* (J. Chan and J. Kepert, eds). Singapore, World Scientific.
- Dube, S.K., A.D. Rao, P.C. Sinha and P. Chittibabu, 1994: A real-time storm surge prediction system: An application to the east coast of India. *Proc. Indian Natl. Sci. Acad.*, 60:157–170.
- Dube, S.K., A.D. Rao, P.C. Sinha, T.S. Murty and N. Bahulayan, 1997: Storm surge in the Bay of Bengal and Arabian Sea: The problem and its prediction. *Mausam*, 48:283–304.
- Eliassen, A., 1956: *A Procedure for Numerical Integration of the Primitive Equations of the Two-parameter Model of the Atmosphere*. Scientific Report No. 4. Department of Meteorology, University of California at Los Angeles.
- Entel, M.B., N.R. Smith, N.E. Davidson, G.R. Warren and B.N. Hanstrum, 2005: *Enhancements to the Bureau of Meteorology’s Ocean Surge Forecasting System Using Operational TC-LAPS*. BMRC Research Report No. 114. Bureau of Meteorology of Australia.
- Eremeev, G.V., 1974: On calculating non-stationary currents and levels in shallow sea. *Works of the State Oceanographic Institute (GOIN)*, 121:32–43 (in Russian).
- Filippov, Y.G., 1974: Some problems of impurity distribution in sea. *Works of the State Oceanographic Institute (GOIN)*, 121:107–113 (in Russian).
- Flather, R.A. and N.S. Heaps, 1975: Tidal computations for Morecambe Bay. *Geophys. J. R. Astron. Soc.*, 42:489–518.
- Flather, R.A. and K.P. Huppert, 1990: Tide and surge models for shallow water – Morecambe Bay revisited. In: *Modelling Marine Systems Volume 1* (A.M. Davies, ed.). Boca Raton, Florida, CRC Press.
- Flather, R.A., R. Proctor and J. Wolf, 1991: Oceanographic forecast models. In: *Computer Modelling in the Environmental Sciences* (D.G. Farmer and M.J. Rycroft, eds). Oxford, Clarendon Press.
- Flowerdew, J., K.J. Horsburgh and K. Mylne, 2009: Ensemble forecasting of storm surges. *Mar. Geod.*, 32:91–99, DOI:10.1080/01490410902869151.
- Flowerdew, J., K.J. Horsburgh, C. Wilson and K. Mylne, 2010: Development and evaluation of an ensemble forecasting system for coastal storm surges. *Q. J. R. Meteorol. Soc.*, 136:1444–1456, DOI:10.1002/qj.648.
- Foreman, M.G.G., 1979: *Manual for Tidal Heights Analysis and Prediction*. Pacific Marine Science Report 77–10. Victoria, B.C., Institute of Ocean Sciences.
- Framiñan, M.B., M.P. Etala, E.M. Acha, R.A. Guerrero, C.A. Lasta and O.B. Brown, 1999: Physical characteristics and processes of the Rio de la Plata estuary. In: *Estuaries of South America, their Geomorphology and Dynamics* (G.M. Perillo, M.C. Piccolo and M. Pino, eds). Berlin, Springer-Verlag.
- Freidson, A.I., N.I. Belsky and A.A. Popkov, 1960: Calculation methods of water level rise in Neva mouth. *Works of the State Oceanographic Institute (GOIN)*, 56:65–79 (in Russian).
- Fujita, T., 1952: Pressure distribution within typhoon. *Geophys. Mag.*, 23(4):437–451.
- George, D.L. and R.J. Le Veque, 2006: Finite volume methods and adaptive refinement for global tsunami propagation and local inundation. *Sci. Tsunami Haz.*, 24(5):319–328.

- Ghil, M. and P. Malanotte-Rizzoli, 1991: Data assimilation in meteorology and oceanography. *Adv. Geophys.*, 33:141–266.
- Giese, G.S., D.C. Chapman, P.G. Black and J.A. Fornshell, 1990: Causation of large-amplitude coastal seiches in the Caribbean coast of Puerto Rico. *J. Phys. Oceanogr.*, 20(9):1449–1458.
- Gill, A.E., 1982: *Atmosphere–Ocean Dynamics*. International Geophysics Series No. 30. New York and London, Academic Press.
- Gomis, D., S. Monserrat and J. Tintore, 1993: Pressure-forced seiches of large amplitude in inlets of the Balearic Islands. *J. Geophys. Res.*, 98(C8):14437–14445.
- Gönnert, G., S.K. Dube, T. Murty and W. Siefert, 2001: *Global Storm Surges: Theory, Observations and Applications*. Holstein, Die Kueste 63.
- Greenberg, D.A., 1979: A numerical model investigation of tidal phenomena in the Bay of Fundy and Gulf of Maine. *Mar. Geod.*, 2(2):161–187.
- Gudkovich, Z.M. and A.Y. Proshutinsky, 1988: Modelling of wind-forced sea level variations under ice cover. *Works of AARI*, 413:85–95 (in Russian).
- Hansen, W., 1962: Hydrodynamical methods applied to oceanographic problems. In: *Proceedings of the Symposium on Mathematical-hydrodynamical Methods of Physical Oceanography*, Hamburg, Germany, September 1961. Institute of Oceanography, University of Hamburg.
- Harper B.A., R.J. Sobey and K.P. Stark, 1978: Sensitivity analysis of a tropical cyclone surge model. In: *Proceedings of Numerical Simulation of Fluid Motion: International Conference on Numerical Simulation of Fluid Dynamic Systems*, Melbourne, Australia, 1976 (B.J. Noye, ed.). Monash University, Amsterdam/New York, North-Holland Publishers.
- Harris, D.L., 1962: The equivalence between certain statistical prediction methods and linearized dynamical methods. *Mon. Weather Rev.*, 90:331–340.
- Hastie, T., R. Tibshirani and J. Friedman, 2001: *The Elements of Statistical Learning: Data Mining, Inference and Prediction*. Springer Series in Statistics. New York, Springer.
- Heaps, N. S., 1969: A two-dimensional numerical sea model. *Phil. Trans. R. Soc. A*, 265:93–137.
- , 1974: Development of a three-dimensional numerical model of the Irish Sea. *Rapp. P.-V. Reun. – Cons. Int. Explor. Mer*, 167:147–162.
- , 1976: On the numerical solution of the three-dimensional hydrodynamical equations for tides and storm surges. *Met. Soc. R. Sci. Liege, Collect. 6°*, 2:143–180.
- Heemink, A.W., K. Bolding and M. Verlaan, 1997: Storm surge forecasting using Kalman filtering. *J. Meteorol. Soc. Jpn.*, 75(1B):305–318.
- Henry, R.F., 1975: *Storm Surges*. Technical Report No. 19, Beaufort Sea Project. Sidney, B.C., Department of the Environment.
- Henry, R.F. and N.S. Heaps, 1976: Storm surges in the southern Beaufort Sea. *J. Fish. Res. Board Can.*, 33:2362–2376.
- Hibiya, T. and K. Kajiura, 1982: Origin of the Abiki phenomenon (a kind of seiche) in Nagasaki Bay. *J. Oceanogr. Soc. Jpn.*, 38(3):172–182.
- Holland, G.J., 1980: An analytic model of the wind and pressure profiles in hurricanes. *Mon. Weather Rev.*, 108:1212–1218.
- Holthuijsen, L.H., 2007: *Waves in Oceanic and Coastal Waters*. Cambridge, Cambridge University Press.
- Horsburgh, K.J. and C. Wilson, 2007: Tide surge interaction and its role in the distribution of surge residuals in the North Sea. *J. Geophys. Res. (Oceans)*, 112:C08003, DOI:10.1029/2006JC004033.
- Howard, T., J. Lowe and K.J. Horsburgh, 2010: Interpreting century-scale changes in North Sea storm surge climate derived from coupled model simulations. *J. Clim.*, 23:6234–6247.
- Hubbert, G.D., L.M. Leslie and M.J. Manton, 1990: A storm surge model for the Australian region. *Q. J. R. Meteorol. Soc.*, 116:1005–1020, DOI:10.1002/qj.49711649411.
- Jansa, A., 1986: Marine response to mesoscale-meteorological disturbances: the June 21, 1984, event in Ciutadella (Menorca). *Rev. Meteorol.*, 7:5–29 (in Spanish).
- Jansa, A., S. Monserrat and D. Gomis, 2007: The rissaga of 15 June 2006 in Ciutadella (Menorca), a meteorological tsunami. *Adv. Geosci.*, 12:1–4.
- Janssen, P.A.E.M. and J.R. Bidlot, 2003: *IFS Documentation – Part VII – ECMWF Wave Model (CY25R1)*. IFS Documentation Cycle CY25r1. Reading, ECMWF.
- Jarvinen, B. and M. Lawrence, 1985: An evaluation of the SLOSH storm-surge model. *Bull. Am. Meteorol. Soc.*, 66(11):1408–1411.
- Jelesnianski, C.P., 1972: *SPLASH I: Landfall Storms*. NOAA Technical Memorandum NWS-TDL 46. Silver Spring, Maryland, NWS Systems Development Office.
- Jelesnianski, C.P., J. Chen and W.A. Shaffer, 1992: *SLOSH: Sea, Lake, and Overland Surges from Hurricanes*. NOAA Technical Report NWS 48. Silver Spring, Maryland, NWS Systems Development Office.
- Jelesnianski, C.P. and A.D. Taylor, 1973: *A Preliminary View of Storm Surges Before and After Storm Modifications*. NOAA Technical Memorandum ERL WMPO-3. Boulder, Weather Modification Program Office.
- Johnson, H.K., J. Højstrup, H.J. Vested and S.E. Larsen, 1998: On the dependence of sea surface roughness on wind waves. *J. Phys. Oceanogr.*, 28:1702–1716.
- Johnson, W.R. and Z. Kowalik, 1986: Modelling of storm surges in the Bering Sea and Norton Sound. *J. Geophys. Res. C: Oceans Atmos.*, 91(C4):5119–5128.
- Jones, J.E. and A.M. Davies, 1996: A high resolution three dimensional model of the  $M_{2s}$ ,  $M_{4s}$ ,  $M_{6s}$ ,  $S_{2s}$ ,  $N_{2s}$ ,  $K_1$  and  $O_1$  tides in the eastern Irish Sea. *Estuarine, Coastal Shelf Sci.*, 42:311–346.
- Kazakov, O.V., 1976: About one modification of bottom friction law and its use at storm surge modelling in the northern part of Caspian Sea. *Meteorology and Hydrology*, 10:58–67.

- Komen, G.J., L. Cavalieri, M. Donelan, K. Hasselmann, S. Hasselmann and P.A.E.M. Janssen, 1994: *Dynamics and Modelling of Ocean Waves*. Cambridge, Cambridge University Press.
- Kondo, H., K. Saito, Y. Mamiya and M. Hara, 1982: On the conservation of the energy of low-frequency waves in iterative time integration schemes. *J. Meteorol. Soc. Jpn.*, 60(2):824–829.
- Kowalik, Z., 1984: Storm surges in the Beaufort and Chukchi Seas. *J. Geophys. Res.*, 89(C6):10570–10578.
- Kuprianova, N.G. and A.I. Freidson, 1977: About forecasting of seiche water level rise in Neva mouth. *Collected Works of Leningrad Hydrometeorological Organization*, 9:146–153.
- Kuprianova, N.G. and A.I. Freidson, 1981: Influence of ice conditions in the Gulf of Finland on water-level height rise in Neva mouth. *Collected Works of Leningrad Hydrometeorological Organization*, 12:95–101.
- Kuprianova, N.G. and A.P. Tretyakova, 1981: Correlation between water level rises in Western and Eastern parts of Neva inlet. *Collected Works of Leningrad Hydrometeorological Organization*, 12:109–111.
- Kurian, N.P., N. Nirupama, M. Baba and K.V. Thomas, 2009: Coastal flooding due to synoptic scale, meso-scale and remote forcings. *Nat. Hazards*, 48:259–273.
- Labzovsky, N.A., 1971: *Non-periodic Sea Level Oscillations*. St. Petersburg, Hydrometeoizdat Publishing House (in Russian).
- Lauwerier, H.A., 1962: Some recent work of the Amsterdam Mathematical Centre on the hydrodynamics of the North Sea. In: *Proceedings of the Symposium On Mathematical Hydrodynamical Methods of Physical Oceanography*, Hamburg, Germany, 18–27 September 1961. University of Hamburg.
- Lax, P.D. and B. Wendroff, 1960: Systems of conservation laws. *Commun. Pur. Appl. Math.*, 13(2):217–237.
- Lee, T.L., 2004: Back-propagation neural network for the long-term tidal predictions. *Ocean Eng.*, 31(2):225–238.
- , 2006: Neural network prediction of a storm surge. *Ocean Eng.*, 33(3–4):483–494.
- , 2008: Back-propagation neural network for the prediction of the short-term storm surge in Taichung harbor, Taiwan. *Eng. Appl. Artif. Intel.*, 21(1):63–72.
- Lee, T.L. and D.S. Jeng, 2002: Application of artificial neural networks in tide forecasting. *Ocean Eng.*, 29(9):1003–1022.
- Lee, D.U., H. Lee, J.W. Seo, S.H. You and Y.H. Youn, 2005: Storm surge prediction using artificial neural networks. *J. Korean Meteorol. Soc.*, 41:661–670.
- Leendertse, J.J., 1970: *A Water Quality Simulation Model for Well Mixed Estuaries and Coastal Seas. Volume I: Principles of Computation*. Rand Corporation Report RM-6230-RC. Santa Monica, Rand Corporation.
- Leendertse, J.J. and E.C. Gritton, 1971: *A Water Quality Simulation Model for Well Mixed Estuaries and Coastal Seas. Volume II: Computational Procedures*. Rand Corporation Report R-708-NYC. Santa Monica, Rand Corporation.
- Leith, C.E., 1965: Numerical simulation of the earth's atmosphere. *Meth. Comput. Phys.*, 4:1–28.
- Liland, D.M., 1971: *Surges in Ice Covered Channels*. M.Sc. thesis. Department of Civil and Environmental Engineering, University of Alberta.
- Lilly, D.K., 1961: A proposed staggered grid system for numerical integration of dynamic equations. *Commun. Pur. Appl. Math.*, 9:267–293.
- Lisitzin, E., 1973: Sea level variations in the Gulf of Bothnia. *Nord. Hydrol.*, 4(1):41–53.
- , 1974: *Sea Level Changes*. Elsevier Oceanographic Series No. 8. Amsterdam, Elsevier.
- Longuet-Higgins, M.S. and R.W. Stewart, 1961: The changes in amplitude of short gravity waves on steady non-uniform currents. *J. Fluid Mech.*, 10:529–549.
- , 1963: A note on wave set-up. *J. Mar. Res.*, 21:4–10.
- Luettich, R., Jr. and J.J. Westerink, 2004: *Formulation and Numerical Implementation of the 2D/3D ADCIRC Finite Element Model Version 44.XX*. ADCIRC Theory Report: [http://adcirc.org/adcirc\\_theory\\_2004\\_12\\_08.pdf](http://adcirc.org/adcirc_theory_2004_12_08.pdf).
- Luettich, R., Jr., J.J. Westerink and N. Scheffner, 1992: *ADCIRC: An Advanced Three-dimensional Circulation Model for Shelves, Coasts and Estuaries. Report 1: Theory and Methodology of ADCIRC-2DDI and ADCIRC-3DL*. Dredging Research Program Technical Report DRP-92-6. Vicksburg, United States Army Corps of Engineers Waterways Experiment Station.
- Luick, J.L., R.F. Henry and T.S. Murty, 1997: Storm surges in the Pacific Forum Region. In: *Recent Advances in Marine Science and Technology-96, Proceedings of the Seventh Pacific Congress on Marine Science and Technology (PACON)*, Honolulu, United States, 17–20 June 1996 (N.K. Saxena, ed.). Honolulu, PACON International.
- Lynch, D.R. and A.M. Davies (eds), 1995: *Quantitative Skill Assessment for Coastal Ocean Models*. Coastal and Estuarine Studies Series Volume 47. Washington, American Geophysical Union.
- Makin, V.K., 2003: A note on a parameterization of the sea drag. *Bound.-Lay. Meteorol.*, 106:593–600.
- Mastenbroek, C., G. Burgers and P.A.E.M. Janssen, 1993: The dynamical coupling of a wave model and a storm surge model through the atmospheric boundary layer. *J. Phys. Oceanogr.*, 23:1856–1867.
- McRobie, A., T. Spencer and H. Gerritsen, 2005: The Big Flood: North Sea storm surge. *Phil. Trans. R. Soc. A*, 363(1831):1263–1270.
- Mesinger, F. and A. Arakawa, 1976: *Numerical Methods Used in Atmospheric Models, Volume 1*. GARP Publication Series No. 17. Geneva, WMO.
- Miles, J. and W. Munk, 1961: Harbour paradox. *J. Waterw. Harbors Div.-ASCE*, 87:111–130.
- Molchanov, V.N., 1976: Numerical model of water circulation in mouth coastal waters taking into account liquid, thermal and ionic runoff effects. *Works of AARI*, 314:36–43 (in Russian).



- Morey, S.L., S. Baig, M.A. Bourassa, D.S. Dukhovskoy and J.J. O'Brien, 2006: Remote forcing contribution to storm-induced sea level rise during Hurricane Dennis. *Geophys. Res. Lett.*, 33:L19603, DOI:10.1029/2006GL027021.
- Monserrat, S., A. Ibbetson and A.J. Thorpe, 1991: Atmospheric gravity waves and the 'Rissaga' phenomenon. *Q. J. Roy. Meteor. Soc.*, 117(499):553–570, DOI:10.1002/qj.49711749907.
- Moon, L.-J., I.S. Oh, T. Murty and Y.-H. Youn, 2003: Causes of the unusual coastal flooding generated by Typhoon Winnie on the west coast of Korea. *Nat. Hazards*, 29:485–500.
- Murty, T.S., 1977: *Seismic Sea Waves – Tsunamis*. Bulletin of the Fisheries Research Board of Canada 198. Oslo, Unipub.
- , 1984: *Storm Surges – Meteorological Ocean Tides*. Canadian Bulletin of Fisheries and Aquatic Sciences 212. Ottawa, Department of Fisheries and Oceans.
- Murty, T.S., M.I. El-Sabh and J.M. Briand, 1981: Statistics of extreme storm surges in eastern Canadian water bodies. In: *Proceedings of Oceans 81*, Boston, United States, 16–18 September 1981. Piscataway, IEEE, DOI:10.1109/OCEANS.1981.1151532.
- Murty, T.S., R.A. Flather and R.F. Henry, 1986: The storm surge problem in the Bay of Bengal. *Prog. Oceanogr.*, 16:195–233.
- Murty, T.S. and G. Holloway, 1985: Influence of marginal ice cover on storm surges. *J. Waterw. Port Coastal Ocean Eng.*, 11(2):329–336.
- Murty, T.S. and N.P. Kurian, 2006: A possible explanation for the flooding several times in 2005 on the coast of Kerala and Tamil Nadu. *J. Geol. Soc. India*, 67:535–536.
- Murty, T.S. and R.J. Polavarapu, 1979: Influence of an ice layer on the propagation of long waves. *Mar. Geod.*, 2(2):99–125.
- Mustafin, N.F., 1970: *O faktorakh, formiruyuschikh sgonno-nagonnye kolebaniya urovnya arkticheskikh morey* [On factors forming storm surges sea-level oscillations in the arctic seas]. *Problemy Arktiki i Antarktiki*, 34:5–12 (in Russian).
- Myers, V.A., 1954: *Characteristics of United States Hurricanes Pertinent to Levee Design for Lake Okechobee, Florida*. Hydrometeorologic Reports 32. Government Printing Office No. C30.70:32, United States Weather Bureau.
- Narayana, A.C. and R. Tatavarti, 2005: High wave activity on the Kerala coast. *J. Geol. Soc. India*, 66:249–250.
- NWS, 2008a: Flood forecasting mapping. <http://www.weather.gov/oh/hrl/hymb/hydraulics/mapping.html>.
- , 2008b: *Real-time (Dynamic) Inundation Mapping Evaluation (R-Time) Team Report*. [http://www.weather.gov/oh/rfcdev/docs/Final\\_Document\\_inundation\\_mapping\\_011508rev.doc](http://www.weather.gov/oh/rfcdev/docs/Final_Document_inundation_mapping_011508rev.doc).
- Obukhov, A.M., 1957: *O tochnosti predvychisleniya advektivnykh izmeneniy polei pri chislenom prognoze pogody* [About the accuracy of precomputation of advective changes of the fields for numerical weather prediction]. *Izv. Akad. Nauk S.S.S.R., Ser. Geofiz.*, 9:1133–1141 (in Russian).
- Parker, G., 1975: Sediment inertia as cause of river antidunes. *J. Hydraul. Div.-ASCE*, 101:211–221.
- Perret, G., L. Feuillatre and P. Frayssinet, 1996: *Estimations du Risque Lié aux Marées de Tempête en Guadeloupe. Etudes et Développement No.2* [Estimations of Risk Associated with Storm Tides in Guadeloupe. Studies and Development No. 2]. Fort-de-France, Météo-France, Direction Interrégionale Antilles-Guyane (in French).
- Platzman, G.W., 1958: The lattice structure of the finite-difference primitive and vorticity equations. *Mon. Weather Rev.*, 86:285–292.
- , 1963: *The Dynamic Prediction of Wind Tides on Lake Erie*. Meteorological Monographs, Volume 4 No. 26. Boston, American Meteorological Society.
- POL, 2007: Maintenance and development of operational tide-surge models. <http://www.pol.ac.uk/ntslf/model.html>.
- Pomeranets, K., 1998: Two floods separated by 100 years. "Neva", No. 7 (in Russian).
- Powell, M.D., P.J. Vickery and T.A. Reinhold, 2003: Reduced drag coefficient for high wind speeds in tropical cyclones. *Nature*, 422:279–283.
- Proctor, R. and A. Flather, 1989: Storm surge prediction in the Bristol Channel – the floods of 13 December 1981. *Cont. Shelf Res.*, 9:889–918.
- Proshutinsky, A.Y., 1993: *Arctic Ocean Sea Level Variability*. St. Petersburg, Hydrometeoizdat Publishing House (in Russian).
- Proshutinsky, A.Y. and E.I. Uranov, 1985: Complex forecasting methods of surge/unsurge level oscillations in Yenisei mouth seaside in winter period with 2–3 days and nights advance time. *Works of AARI*, 389:78–85 (in Russian).
- Proudman, J., 1953: *Dynamical Oceanography*. London, Methuen.
- Pugh, D.T., 1987: *Tides, Surges and Mean Sea Level: A Handbook for Engineers and Scientists*. Winchester, John Wiley and Sons.
- Rabinovich, A.B., 1993: *Long Ocean Gravity Waves: Trapping, Resonance and Leaking*. St. Petersburg, Hydrometeoizdat Publishing House (in Russian).
- Rabinovich, A.B. and S. Monserrat, 1996: Meteorological tsunamis near the Balearic and Kuril Islands: Descriptive and statistical analysis. *Nat. Hazards*, 13:55–90.
- Ramming, H.G., 1972: Reproduction of physical processes in coastal areas. In: *Proceedings of the 13th International Conference on Coastal Engineering*, Vancouver, Canada, 10–14 July 1972. New York, ASCE.
- Rao, N.S.B., 1968: *On Some Aspects of Local and Tropical Storms in India*. PhD thesis. University of Jadavapur.
- Rao, A.D., P. Chittibabau, T.S. Murty, S.K. Dube and U.C. Mohanty, 2007: Vulnerability from storm surges and cyclone wind fields on the coast of Andhra Pradesh, India. *Nat. Hazards*, 41:515–529.

- Rao, N.S.B. and S. Mazumdar, 1966: A technique for forecasting storm waves. *Indian J. Meteorol. Geophys.*, 17:333–346.
- Reed, D.B. and B.E. Stucky, 2005: Forecasting hurricane storm surge on the Mississippi River. In: *Proceedings of Solutions to Coastal Disasters*, Charleston, United States, 8–11 May 2005 (L. Wallendorf, L. Ewing, S. Rogers and C. Jones, eds). New York, ASCE, DOI:10.1061/40774(176)6.
- Reid, R.O., 1956: *Approximate Response of Water Level on a Sloping Shelf to a Wind Fetch Which Moves Towards Shore*. Beach Erosion Board Technical Memorandum No. 83. Washington, United States Army Corps of Engineers.
- Reid, R.O. and B.R. Bodine, 1968: Numerical model for storm surges in Galveston Bay. *J. Waterw. Harbors Div.-ASCE*, 94(WW1):33–57.
- Reid, R.O., A.C. Vastano and T.J. Reid, 1977: *Development of Surge II Program With Application to the Sabine-Calcasieu Area for Hurricane Carla and Design Hurricanes*. Technical Paper No. 77-13. Fort Belvoir, United States Army Corps of Engineers Coastal Engineering Research Center.
- Richtmeyer, R.D. and K.W. Morton, 1963: *A Survey of Difference Methods for Non-steady Fluid Dynamics*. NCAR Technical Notes 63-2. Boulder, National Center for Atmospheric Research.
- Roll, H.U., 1968: *Physics of the Marine Atmosphere*. New York and London, Academic Press.
- Runchal, A.K., 1975: Numerical model for storm surge and tidal run-up studies. In: *Proceedings of Modeling '75, ASCE Symposium on Modeling Techniques*, San Francisco, United States, 3–9 September 1975. New York, ASCE.
- Sasaki, Y.K., 1958: An objective analysis based on the variational method. *J. Meteorol. Soc. Jpn.*, 36:77–88.
- Scheffner, N.W., D.J. Mark, C.A. Blain, J.J. Westerink and R.A. Luettich, 1994: *ADCIRC: An Advance Three-dimensional Circulation Model for Shelves, Coasts and Estuaries. Report 5: A Tropical Storm Data Base for the East and Gulf of Mexico Coasts of the United States*. Dredging Research Program Technical Report DRP-92-6. Vicksburg, United States Army Corps of Engineers Waterways Experiment Station.
- Schureman, P., 1958: *Manual of Harmonic Analysis and Prediction of Tides*. United States Department of Commerce, Coast and Geodetic Survey Special Publication No. 98. Washington, United States Government Printing Office.
- Schwiderski, E.W., 1978: *Global Ocean Tides, Part I: A Detailed Hydrodynamical Interpolation Model*, NSWC/DL TR-3866. Silver Spring, Naval Surface Weapons Center.
- Seo, J.W., Y.S. Chang, D.U. Lee, S.H. You, J.G. Park, Y.G. Kim and J.H. Jeong, 2005: *The Detectible Technique Development of Marine Meteorological Variation (III)*. Report MR043M10 2002M-004-00. Seoul, Korea Meteorological Administration.
- Seo, J.W., S.H. You, D.U. Lee, H.J. Lee, J.G. Park, G.T. Son, Y.G. Kim, J.H. Jeong and J.H. Kwun, 2006: *The Detectible Technique Development of Marine Meteorological Variation (IV)*. Report MR053M16 2002M-004-00. Seoul, Korea Meteorological Administration.
- Sheng, Y.P. and W.J. Lick, 1972: *The Wind Driven Currents in a Partially Ice Covered Lake*. School of Engineering Report FTAS/TR. Cleveland, Case Western Reserve University.
- Shkudova, G.Y., 1974: Distribution and dispersion of polluting substances in the sea (calculation model). *Works of the State Oceanographic Institute (GOIN)*, 121:96–106 (in Russian).
- Sielecki, A. and M.C. Wurtele, 1970: The numerical integration of the non-linear shallow water equations with sloping boundaries. *J. Comput. Phys.*, 6:219–236.
- Silvester, R., 1971: Computation of storm surge. In: *Proceedings of the 12th Conference on Coastal Engineering*, Washington, United States, 13–18 September 1970. New York, ASCE.
- Simons, T.J., 1980: *Circulation Models of Lakes and Inland Seas*. Canadian Bulletin of Fisheries and Aquatic Sciences 203. Ottawa, Department of Fisheries and Oceans.
- Skandrani, C. and P. Daniel, 2001: Atmospheric forcing impact study in MOTHY oil drift model. In: *Coastal Engineering V. Computer Modelling of Seas and Coastal Regions* (C.A. Brebbia, ed.). Southampton, WIT Press.
- Skriptunov, N.A. and G.N. Gan, 1964: Penetration of short-term sea level oscillations into Neva mouth. *Works of the State Oceanographic Institute (GOIN)*, 78:40–62 (in Russian).
- Smith, S. and E. Banke, 1975: Variation of the sea surface drag coefficient with wind speed. *Q. J. Roy. Meteor. Soc.*, 101:665–673.
- Stelling, G.S., 1984: *On the Construction of Computational Methods for Shallow Water Flow Problems*. Rijkswaterstaat Communications No. 35. The Hague, Rijkswaterstaat.
- Sztobryn, M., 2003: Forecasting of storm surge by means of artificial neural networks. *J. Sea Res.*, 49:317–322.
- Talagrand, O., 1981: A study on the dynamics of four-dimensional data assimilation. *Tellus*, 33:43–60, DOI:10.1111/j.2153-3490.1981.tb01729.x.
- Tang, Y.M., R. Grimshaw, B. Sanderson and G. Holland, 1996: A numerical study of storm surges and tides, with application to the north Queensland coast. *J. Phys. Oceanogr.*, 26:2700–2711.
- Tintore, J., D. Gomis, S. Alonso and D.P. Wang, 1988: A theoretical study of large sea level oscillations in the western Mediterranean. *J. Geophys. Res.*, 93(C9):10797–10803.
- Tissot, P.E., D.T. Cox and P.R. Michaud, 2003: Optimization and performance of a neural network model forecasting water levels for the Corpus Christi, Texas, Estuary. In: *Proceedings of the 3rd Conference on the Applications of Artificial Intelligence to Environmental Science*, Long Beach, United States, 9–13 February 2003. Boston, The American Meteorological Society.

- Tsai, C.P. and T.L. Lee, 1999: Back-propagation neural network in tidal-level forecasting. *J. Waterw. Port Coast. Ocean Eng.-ASCE*, 12(4):195–202.
- Tolman, H.L., 2002: *User Manual and System Documentation of WAVEWATCH-III Version 2.22*. MMAB Technical Note No. 222. Washington, NOAA/NWS/NCEP.
- United Nations Economic and Social Commission for Asia and the Pacific–World Meteorological Organization, 2007: *Report of the Fortieth Session of the Typhoon Committee, Macao, China, 21–26 November 2007*. <http://www.wmo.int/pages/prog/www/tcp/documents/TC40FinalReport.pdf>.
- Venkatesh, S., 1974: *The Development of Manual Techniques for the Real-time Prediction of Storm Surges on the Great Lakes*. Report prepared for the Canadian Centre for Inland Waters under contract No. OS3-0248. Unpublished.
- Verkaik, J.W., 2006: *On Wind and Roughness Over Land*. PhD thesis. University of Wageningen.
- Verkaik, J.W., A.B.C. Tijn and A.J.M. Jacobs, 2003: Refinement of numerical wind forecasts using a high-resolution roughness map. Poster presentation in: *European Wind Energy Conference and Exhibition*, Madrid, Spain, 16–19 June 2003. European Wind Energy Association. <http://www.knmi.nl/publications/fulltexts/poster3.pdf>.
- Vulis, I.L. and Y.V. Masalov, 1972: To the calculation of salinity and temperature in sea's for-mouth area. *Oceanology*, 12(1):158–161.
- Wang, X., K. Li, Z. Yu and J. Wu, 1987: Statistical characteristics of seiches in Longkou Harbor. *J. Phys. Oceanogr.*, 17:1063–1065.
- Wanstrath, J.J., 1977: *Near Shore Numerical Storm Surge and Tidal Simulation*. Technical Report H-77-17. Vicksburg, United States Army Corps of Engineers Waterways Experiment Station.
- , 1978: An open coast storm surge model with inland flooding. In: *Proceedings of the Eleventh Technical Conference on Hurricanes and Tropical Meteorology*, Miami Beach, United States, 13–16 December 1977. Boston, American Meteorological Society.
- Welander, P., 1961: Numerical prediction of storm surges. In: *Advances in Geophysics Volume 8* (H.E. Landsberg and J. van Miegham, eds). New York and London, Academic Press.
- Wessel, P. and W.H.F. Smith, 1996: A global, self-consistent, hierarchical, high-resolution shoreline database. *J. Geophys. Res.*, 101(B4):8741–8743, DOI:10.1029/96JB00104.
- Westerink, J.J., R.A. Luetlich, J.C. Feyen, J.H. Atkinson, C.N. Dawson, H.J. Roberts, M.D. Powell, J.P. Dunion, E.J. Kubatko and H. Pourtaheri, 2008: A basin- to channel-scale unstructured grid hurricane storm surge model applied to southern Louisiana. *Mon. Weather Rev.*, 136:833–864.
- Wilson, B.W., 1972: Seiches. In: *Advances in Hydrosience Volume 8* (V.T. Chow, ed.). New York and London, Academic Press.
- Wolzinger, N.E. and R.V. Pyaskovsky, 1968: *Main Oceanological Problems of Shallow Water Equations*. St. Petersburg, Hydrometeoizdat Publishing House (in Russian).
- , 1977: *Shallow Water Theory*. St. Petersburg, Hydrometeoizdat Publishing House (in Russian).
- Yeh, G.T. and F.K. Chou, 1979: Moving boundary numerical surge model. *J. Waterw. Port Coast. Ocean Eng.-ASCE*, 105(WW3):247–263.
- Young, J.A., 1968: Comparative properties of some time differencing schemes for linear and non-linear oscillations. *Mon. Weather Rev.*, 96:357–364.
- Zubov, N.N., 1947: *Dynamic Oceanology*. St. Petersburg, Hydrometeoizdat Publishing House (in Russian).



## APPENDIX II

### ACRONYMS

|             |   |         |   |
|-------------|---|---------|---|
| 2DDI        | two-dimensional depth-integrated  | HIPOCAS | Hindcast of Dynamic Processes of the Ocean and Coastal Areas of Europe (funded by the Energy, Environment and Sustainable Development Programme of the European Commission) |
| 3Dvar       | three-dimensional variational   |         |   |
| 4Dvar       | four-dimensional variational  |         |   |
| AARI        | Arctic and Antarctic State Scientific Research Institute (Russian Federation) |         |   |
| AARI CLGME  | AARI Ice and Hydrometeorological Information Centre                           | ICSU    | International Council for Science (formerly International Council of Scientific Unions)   |
| ADCIRC      | Advanced Circulation Model (United States)                                    | IFS     | integrated forecasting system   |
| ADCP        | acoustic Doppler current profiler   | IHO     | International Hydrographic Organization   |
| ADI         | alternate direction implicit  | IIT     | Indian Institute of Technology  |
| ANN         | artificial neural network   | IMD     | India Meteorological Department   |
| BMRC        | Bureau of Meteorology Research Centre (Australia)                             | IOC     | Intergovernmental Oceanographic Commission  |
| BODC        | British Oceanographic Data Centre   | JCOMM   | Joint Technical Commission for Oceanography and Marine Meteorology  |
| CFL         | Courant-Friedrichs-Levy   | JMA     | Japanese Meteorological Association   |
| CLGME       | Ice and Hydrometeorological Information Centre (Russian Federation AARI)      | JST     | Japan Standard Time   |
| DCSM        | Dutch Continental Shelf Model   | KMA     | Republic of Korea Meteorological Administration   |
| DHI         | Danish Hydraulic Institute  | KNMI    | Royal Netherlands Meteorological Institute  |
| DMI         | Danish Meteorological Institute   | LAM     | limited area model/local area model   |
| DOI         | digital object identifier   | MLP     | multilayer perception   |
| DWOPER      | Dynamic Wave Operational Model (United States NWS)                            | MM5–KMA | Mesoscale Model 5 (Republic of Korea KMA)   |
| ECMWF       | European Centre for Medium-Range Weather Forecasts                            | MOGREPS | Met Office Global and Regional Ensemble Prediction System   |
| EPS         | Ensemble Prediction System (ECMWF)  | MPI     | message-passing interface   |
| ESCAP       | Economic and Social Commission for Asia and the Pacific                       | NAE     | North Atlantic and European atmospheric model (United Kingdom Met Office)   |
| ETKF        | ensemble transform Kalman filter  | NCEP    | National Centers for Environmental Protection (United States NWS)   |
| ETOPO2      | 2-Minute Gridded Global Relief Data (United States NGDC)                      | NGDC    | National Geophysical Data Center (United States NOAA)   |
| ETWS        | Expert Team on Wind Waves and Storm Surges (JCOMM)                            | NHC     | National Hurricane Center (United States NWS)   |
| EU HIPOCAS  | see HIPOCAS   | NOAA    | National Oceanic and Atmospheric Administration (United States)   |
| EU STOWASUS | see STOWASUS  | NOC     | National Oceanography Centre (United Kingdom)   |
| FEMA        | Federal Emergency Management Association (United States)                      | NOOS    | North West European Shelf Operational Oceanographic System  |
| FLDWAV      | Flood Wave (one-dimensional hydraulic model, United States NWS)               | NORI    | National Oceanographic Research Institute (Republic of Korea)   |
| GARP        | Global Atmospheric Research Programme (WMO–ICSU)                              | NOS     | National Ocean Service (United States NOAA)   |
| GEBCO       | General Bathymetric Chart of the Oceans                                       | NWP     | numerical weather prediction  |
| GFS         | global forecast system  | POL     | Proudman Oceanic Laboratory   |
| GIS         | Geographical Information System   | RBF     | radial basis function   |
| GMT         | Greenwich mean time   | RDAPS   | Regional Data Assimilation and Prediction System (Republic of Korea KMA)  |
| GRIB        | gridded binary code   |         |   |
| GSHHS       | Global Self-consistent, Hierarchical, High-resolution Shoreline Database      |         |   |
| GTS         | Global Telecommunications System  |         |   |
| GWCE        | generalized wave continuity equation  |         |   |
| HA          | harmonic analysis   |         |   |

|          |  |                |  |
|----------|--|----------------|--|
| RMS      | root mean square   |                | by the Environment and Climate                                 |
| RMSE     | root mean square error   |                | Research Programme of the European                             |
| RSMC     | Regional Specialized Meteorological<br>Centre  |                | Commission)  |
| RTSM     | Regional Tide/Storm Model (Republic of<br>Korea KMA)                                   | TC-LAPS        | Tropical Cyclone Limited Area Prediction<br>System (Australia) |
| SERFC    | Southeast River Forecast Center (United<br>States NWS)                                 | TCP            | Tropical Cyclone Programme (WMO)                               |
| SLOSH    | Sea, Lake and Overland Surges from<br>Hurricanes model (United States NOAA)            | TCWC           | Tropical Cyclone Warning Centre<br>(Australia)                 |
| SMN      | <i>Servicio Meteorológico Nacional</i> (Argentina)                                     | t <sub>f</sub> | forecast lead time   |
| SPLASH   | Special Program to List Amplitudes of<br>Surges from Hurricanes (United States<br>NWS) | TWLE           | total water-level envelope                                     |
| STOWASUS | Regional Storm, Wave and Surge<br>Scenarios for the 2100 Century (funded               | UKCMF          | United Kingdom Coastal Monitoring and<br>Forecasting           |
|          |  | UKMO           | United Kingdom Met Office                                      |
|          |  | UT             | Universal Time   |
|          |  | UTC            | Coordinated Universal Time                                     |
|          |  | WMO            | World Meteorological Organization                              |

---



[www.wmo.int](http://www.wmo.int)

P-WDS\_11671